



**HAL**  
open science

# Uranium isotopes as proxies for investigating land-to-sea sediment transfer response to Late Quaternary climate changes

Maude Thollon

► **To cite this version:**

Maude Thollon. Uranium isotopes as proxies for investigating land-to-sea sediment transfer response to Late Quaternary climate changes. Earth Sciences. Université de Bretagne occidentale - Brest; University of Wollongong (Wollongong, Australie), 2020. English. NNT: 2020BRES0077. tel-03617304

**HAL Id: tel-03617304**

**<https://theses.hal.science/tel-03617304v1>**

Submitted on 23 Mar 2022

**HAL** is a multi-disciplinary open access archive for the deposit and dissemination of scientific research documents, whether they are published or not. The documents may come from teaching and research institutions in France or abroad, or from public or private research centers.

L'archive ouverte pluridisciplinaire **HAL**, est destinée au dépôt et à la diffusion de documents scientifiques de niveau recherche, publiés ou non, émanant des établissements d'enseignement et de recherche français ou étrangers, des laboratoires publics ou privés.

## THESE DE DOCTORAT EN CO-TUTELLE DE

L'UNIVERSITE DE BRETAGNE OCCIDENTALE

ECOLE DOCTORALE N° 598

*Sciences de la Mer et du littoral*

Spécialité : Géosciences Marines

AVEC L'UNIVERSITE DE WOLLONGONG

Par

**Maude THOLLON**

**Evolution des temps de transfert sédimentaire océan-continent au regard de la variabilité climatique quaternaire : Apports des isotopes de l'Uranium**

Thèse présentée et soutenue à l'Institut Universitaire Européen de la Mer, Technopôle Brest-Iroise, Rue Dumont d'Urville, 29280 Plouzané, le 10 Décembre 2020

Unité de recherche : Géosciences marines (IFREMER)

Et Wollongong Isotopes Geochronology Laboratory

### Rapporteurs avant soutenance :

Hella WITTMANN

Docteure, GFZ German Research Centre for Geosciences–Germany

Lin MA

Professeur, Univ. Texas – USA

### Composition du Jury :

Marina RABINEAU

Directrice de recherches, UBO / Présidente du jury

Hella WITTMANN

Docteure, GFZ German Research Centre for Geosciences–Germany / Rapporteuse

Lin MA

Professeur, Univ. Texas – USA / Rapporteur

François CHABAUX

Professeur, Univ. De Strasbourg / Examinateur

Jean-Alix BARRAT

Professeur, UBO / Directeur de thèse

### Invités

Samuel TOUCANNE

Docteur, Ifremer / Encadrant

Germain BAYON

Docteur, Ifremer / Encadrant

**Ifremer**





# REMERCIEMENTS - ACKNOWLEDGEMENTS

---

Une thèse ne pourrait se faire sans encadrement. C'est pour cela que je tiens dans un premier temps à remercier Jean Alix Barrat. Merci pour m'avoir présenté cette opportunité et suivi l'évolution du projet. Je remercie ensuite énormément Samuel Toucanne, Germain Bayon et Tony Dosseto de m'avoir accordé leur confiance pour la réalisation de cette thèse. Merci à tous les trois de m'avoir encadrée durant ces trois années, pour vos conseils et soutient quand il y avait besoin. Je suis reconnaissante de d'avoir eu la possibilité de découvrir et travailler dans deux unités de recherche, entre Brest et Wollongong.

J'en profite pour remercier également Nathalie Vigier et Stefan Lalonde pour avoir suivi mon projet. Merci pour l'intérêt porté au sujet, et d'avoir été toujours si enthousiaste au sujet des résultats. Merci également pour les suggestions et conseils apportés au cours du projet.

Au cours de ma thèse, de nombreuses personnes m'ont accompagnées et aidées. Je tiens à remercier en particulier à l'Ifremer Yoann Germain et Anne Trinquier pour m'avoir initiée aux rudiments de la spectrométrie de masse. Je remercie aussi Audrey Boissier et Sandrine Cheron pour les conseils portant de la préparation des échantillons à l'interprétation de résultats de la mineralogie des échantillons. Je tiens à remercier tous les membres de GM à l'Ifremer qui ont interagi avec le projet. Un merci particulier à toutes les personnes qui ont récoltés les échantillons, tant sur terre qu'en mer, sans qui la thèse n'aurait été possible.

At the university of Wollongong, I would like to particularly thanks Alex Francke, for having introducing to me its samples preparation that save me a lot of time. I also thanks him for being always so enthusiastic about uranium isotopes conversations. I thanks Tibi codilean, for his help on the strategy to adopt on the GIS analysis. I also thanks Heidi Brown for helping me with ArcGIS with such enthusiasm. I am thankful to Christopher Richardson for his help while I was doing IQ analyses and Alan Champion for his availability and helps.

A joint supervision between two countries is not always easy and I thanks Samuel T., Sylvia Baronne, Denise Alsop, both faculties and Studies up (Anne-Sophie) for the different kind of help to handle the administrative part.

Ce travail a bénéficié d'une aide de l'Etat gérée par l'Agence Nationale de la Recherche au

titre du programme «Investissements d'avenir» portant la référence ANR-17-EURE-0015. Je remercie Isblue pour l'attribution de cette aide qui a facilité la co-tutelle.

I would also thank all the members of the Jury for having accepted to be part of it. I thank Marina Rabineau for chairing the jury during the defence. I thank Hella Witmann and Lin Ma for being the reviewers of my manuscript, and François Chabaux for being part of the jury. I thank all of you for your constructive remarks during my defence.

Une aventure de trois ans ne se résumant pas seulement au travail, je tiens à remercier l'équipe d'étudiants de l'Ifremer et en particulier Arthur, Aurélien et Vincent.

At Wollongong I sincerely thank all the PhD team. I thank the Wigals, for the great, friendly and supportive working environment, a particular thanks to Holly, Dafne, Alex and Sally. A huge thanks to Holly for introducing me to the Australian's life and I should mention it, for supporting me emotionally.

A huge thanks to Maria for being such a great flatmate. Also, thanks to Meagan and Nick for having welcomed me in their home.

Je tiens à remercier tous les amis de Beauvais, pour m'avoir accompagnée de loin dans ce projet, pour tous les agréables moments qui ont permis de mettre la thèse de côté le temps d'un week-end. Un énorme merci à Cécile, pour tout et notamment le temps accordé durant ces trois années. Un très gros merci à Sophie aussi, dont la compréhension de la vie de doctorante a été très utile.

Je voudrais aussi en profiter pour remercier ma famille. Merci d'avoir été d'un tel soutien tout au long de la thèse et de m'avoir permis d'aller jusqu'au bout.

Et enfin, un immense merci à Sam.

# TABLE OF CONTENTS

---

<b>Remerciements - Acknowledgements</b>	<b>3</b>
<b>Introduction</b>	<b>15</b>
General background . . . . .	15
Objectives of this thesis . . . . .	16
<b>Introduction</b>	<b>19</b>
Généralités . . . . .	19
Objectifs de la thèse . . . . .	20
<b>1 Literature Review</b>	<b>25</b>
1.1 From source to sink: the sediment's life . . . . .	26
1.1.1 Concept . . . . .	26
1.1.2 Environmental signal propagation in sedimentary systems . . . . .	31
1.1.3 Soil: the origin of the sediment . . . . .	41
1.2 Uranium isotopes . . . . .	45
1.2.1 Background . . . . .	45
1.2.2 Radioactive disequilibrium . . . . .	45
1.2.3 Secular equilibrium . . . . .	47
1.2.4 Uranium abundances in rock forming minerals and the fractionation of ( $^{234}\text{U}/^{238}\text{U}$ ) in sedimentary systems . . . . .	48
1.2.5 The concept of comminution age . . . . .	53
1.3 Uranium at Earth's surface . . . . .	59
1.3.1 From bedrock to soil: weathering processes . . . . .	59
1.3.2 Uranium isotopes to infer timescale of sedimentary processes and its control . . . . .	61
1.3.3 Uncertainties based on the comminution age method . . . . .	62
<b>2 Methodology</b>	<b>65</b>
2.1 Samples collection . . . . .	66
2.1.1 Sediments from world rivers . . . . .	66
2.1.2 Var sediments . . . . .	66
2.2 Samples preparation . . . . .	71
2.2.1 Reagent and labware . . . . .	71
2.2.2 Grain-size separation . . . . .	71

2.2.3	Leaching . . . . .	72
2.2.4	Sediments dissolution . . . . .	76
2.3	Ion exchange chromatography . . . . .	78
2.3.1	Ifremer method . . . . .	78
2.3.2	UOW method . . . . .	80
2.4	Uranium analyses . . . . .	82
2.4.1	Isotopic measurement of Uranium isotopes . . . . .	82
2.4.2	Concentration . . . . .	83
2.4.3	Accuracy and precision of the data . . . . .	84
2.5	Specific surface analyses . . . . .	87
2.6	Geographic Information System analyses . . . . .	89
2.6.1	Basin and sub-basin delineation . . . . .	89
2.6.2	Extraction of the geomorphologic characteristics . . . . .	89
<b>3</b>	<b>The distribution of (<math>^{234}\text{U}/^{238}\text{U}</math>) activity ratios in river sediments</b>	<b>91</b>
3.1	Introduction . . . . .	93
3.2	Methods . . . . .	95
3.2.1	Samples . . . . .	95
3.2.2	Analytical procedures . . . . .	97
3.3	Results . . . . .	98
3.3.1	Leaching experiments . . . . .	98
3.3.2	Uranium in river sediments . . . . .	100
3.4	Discussion . . . . .	102
3.4.1	Influence of grain size on ( $^{234}\text{U}/^{238}\text{U}$ ) ratios of detrital sediments . .	102
3.4.2	The effect of weathering, climate and erosion on $^{234}\text{U}$ - $^{238}\text{U}$ fractionation . . . . .	102
3.4.3	The role of lithology . . . . .	109
3.4.4	The role of catchment size and sediment residence time on ( $^{234}\text{U}/^{238}\text{U}$ ) sedimentary ratio . . . . .	111
3.4.5	Complex interactions of environmental controls on sediment residence time . . . . .	114
3.5	Conclusion . . . . .	115
3.6	Acknowledgments . . . . .	116
<b>4</b>	<b>The Var sediment routing system: spatial residence time variation</b>	<b>117</b>
4.1	Study site: the Var basin . . . . .	118
4.1.1	Environmental setting . . . . .	118
4.1.2	A source to sink system . . . . .	120
4.2	Controls on the regolith residence time in an Alpine river catchment . . . .	124
4.3	Introduction . . . . .	125

4.4	Study site . . . . .	126
4.5	Materials and Methods . . . . .	127
4.6	Results . . . . .	129
4.7	Discussion . . . . .	131
4.7.1	Assessing the role of lithology and weathering regimes on the U isotope ratio . . . . .	131
4.7.2	Geomorphologic control on ( $^{234}\text{U}/^{238}\text{U}$ ) ratios . . . . .	133
4.7.3	Quantification of regolith residence times in the Var River catchment	135
4.7.4	Geomorphic controls on regolith residence time . . . . .	139
4.8	Conclusion and perspectives . . . . .	140
<b>5</b>	<b>The Var sediment routing system: paleo-residence time variations</b>	<b>143</b>
5.1	The climatic cyclicity during the Quaternary . . . . .	144
5.1.1	Long terms climatic cycles . . . . .	144
5.1.2	Millennial-scale climate changes . . . . .	145
5.1.3	The climatic context in the Alps during the Quaternary . . . . .	147
5.2	Temporal sediment residence time variations . . . . .	149
5.2.1	Stratigraphy of the Var sedimentary ridge . . . . .	149
5.2.2	Methods . . . . .	151
5.2.3	Uranium variations over time - Results . . . . .	153
5.2.4	Interpretation . . . . .	157
5.2.5	Conclusion . . . . .	165
	<b>Conclusions and perspectives</b>	<b>167</b>
	Rationale and objectives of this thesis . . . . .	167
	The variation of U-fractionation . . . . .	168
	Spatial variation of the sediment residence time in a mountainous river basin . .	169
	Linking paleo-sediment residence time to paleo-erosional processes . . . . .	170
	Perspectives . . . . .	172
	<b>Conclusions et perspectives</b>	<b>175</b>
	Rappel des objectifs de la thèse . . . . .	175
	La distribution spatiale de ( $^{234}\text{U}/^{238}\text{U}$ ) . . . . .	176
	Variation spatiale du temps de résidence sédimentaire dans un bassin montagneux	178
	Lier les temps de résidence aux événements passés . . . . .	179
	Perspectives . . . . .	181
	<b>Appendix</b>	<b>183</b>
	<b>References</b>	<b>203</b>



# LIST OF FIGURES

---

1	Conceptual representation of the sediment residence time. . . . .	17
1	Représentation conceptuelle du temps de résidence sédimentaire. . . . .	21
1.1	Representation of a source to sink system. . . . .	27
1.2	Schema of weathering profile. . . . .	28
1.3	Schema of the bedrock weathering into soil. . . . .	29
1.4	Parameters influencing the source to sink system . . . . .	32
1.5	Weathering series of both silicate and non silicate minerals . . . . .	34
1.6	Parameters influencing the source to sink system . . . . .	34
1.7	Denudation rate as function of the hillslope curvature. . . . .	35
1.8	Erosion rate depending on the vegetation cover. . . . .	37
1.9	Representation of the sediment supply signal propagation inside a basin. . . . .	38
1.10	Summary of the sedimentary signal propagation from source to sink . . . . .	40
1.11	Schematic representation of the Critical Zone . . . . .	41
1.12	Models of the soil depth production . . . . .	43
1.13	Decay of the U series . . . . .	46
1.14	Evolution of daughter-parents isotopes activity ratio to return to secular equilibrium. . . . .	47
1.15	Eh–pH diagram representing the stability of the most common U species . . . . .	50
1.16	Diagram of thoranite solubility . . . . .	51
1.17	Schematic representation of the recoil process . . . . .	52
1.18	Secular equilibrium . . . . .	57
1.19	U mobility in weathering profile . . . . .	60
2.1	Map of the world rivers sediments location . . . . .	67
2.2	Location of the sediments from the Var River and its tributaries. . . . .	68
2.3	Map of the cores location. . . . .	69
2.4	Sedimentary facies observed in the studied turbiditic cores. . . . .	70
2.5	Pictures of the turbiditic cores . . . . .	74
2.6	Evolution of ( $^{234}\text{U}/^{238}\text{U}$ ) during the leaching . . . . .	74
2.7	Elution profile before improvement of the method . . . . .	79
2.8	Elution profile after improvement of the method . . . . .	80
2.9	Uranium concentration and ( $^{234}\text{U}/^{238}\text{U}$ ) for the standard BCR-2 . . . . .	85
2.10	Evolution of ( $^{234}\text{U}/^{238}\text{U}$ ) obtained for the standard U005A . . . . .	86

2.11	Evolution of U (ppm) obtained for the standard 71A measured on the iCAP Q-ICP MS . . . . .	86
2.12	Adsorption-desorption isotherms . . . . .	87
3.1	World River sediments location . . . . .	96
3.2	Evolution of ( $^{234}\text{U}/^{238}\text{U}$ ) trough the leaching steps. . . . .	99
3.3	U concentration and ( $^{234}\text{U}/^{238}\text{U}$ ) histogram. . . . .	100
3.4	Variation of ( $^{234}\text{U}/^{238}\text{U}$ ) depending on weathering. . . . .	104
3.5	Variation of ( $^{234}\text{U}/^{238}\text{U}$ ) depending on climate. . . . .	106
3.6	Variation of ( $^{234}\text{U}/^{238}\text{U}$ ) depending on the maximum elevation of the catchment. . . . .	107
3.7	Variation of ( $^{234}\text{U}/^{238}\text{U}$ ) depending on the area of the basin. . . . .	110
3.8	Variation of ( $^{234}\text{U}/^{238}\text{U}$ ) depending on the depth to bedrock. . . . .	113
3.9	Model of ( $^{234}\text{U}/^{238}\text{U}$ ) evolution depending on the area of the basin. . . . .	114
3.10	Evolution of ( $^{234}\text{U}/^{238}\text{U}$ ) depending on multi-parameters. . . . .	115
4.1	Elevation model of the Var basin . . . . .	118
4.2	Geological map of the Var basin . . . . .	119
4.3	Variation of the denudation rates inside the Var basin. . . . .	121
4.4	Pictures of the Vesubie before and after the tempete Alex (2020) . . . . .	122
4.5	Picture of the Var delta just after the tempete Alex . . . . .	122
4.6	Localisation of the samples on elevation model of the Var basin. . . . .	126
4.7	Variation of ( $^{234}\text{U}/^{238}\text{U}$ ) depending on lithologic and weathering proxies. . . . .	131
4.8	( $^{234}\text{U}/^{238}\text{U}$ ) depending on morphologic parameters . . . . .	134
4.9	Variation on U-derived sediment residence time depending on the spatial analysis-derived sediment residence time. . . . .	137
4.10	Variation of regolith residence time depending on morphologic parameters. . . . .	139
4.11	Variation of calculated regolith residence time as function of the predict regolith residence time . . . . .	140
5.1	Millenial climatic variations in the Northern Hemisphere. . . . .	146
5.2	Location of the cores along the Var canyon and the Var Sedimentary Ridge . . . . .	149
5.3	Composite $\delta^{18}\text{O}$ (VPDB) and $\delta^{18}\text{O}$ (NGRIP) variations. . . . .	150
5.4	Results . . . . .	154
5.5	( $^{234}\text{U}/^{238}\text{U}$ ) in function of the concentration for the Var sediments . . . . .	155
5.6	( $^{234}\text{U}/^{238}\text{U}$ ) in function of U-derived sediment residence time. . . . .	157
5.7	( $^{234}\text{U}/^{238}\text{U}$ ) and sediment residence time variation over the last 75 ka in the Var basin. . . . .	158
5.8	Spatial variation of ( $^{234}\text{U}/^{238}\text{U}$ ) and $\varepsilon_{Nd}$ in the Var basin. . . . .	159
5.9	$\varepsilon_{Nd}$ and denudation rate variation over the last 75 ka in the Var. . . . .	161

5.10 ( $^{234}\text{U}/^{238}\text{U}$ ) compared to climatic and vegetation parameters. . . . .	163
5.11 ( $^{234}\text{U}/^{238}\text{U}$ ) variations in correlation with the sea surface temperature over the last 75 ka. . . . .	164



# LIST OF TABLES

---

1.1	Relative abundance (% Area) of outcropping rocks in Central Europe (Geo-LiM) and associated mean and standard elevation and slope (from Donnini et al. 2020). . . . .	33
2.1	Location of the cores from the Var . . . . .	69
2.2	Composition of the tracer-solution used at Ifremer and WIGL . . . . .	77
2.3	U and Th separation protocol (adapted from Edwards et al., 1986) . . . . .	78
2.4	Purification protocol of the U-fraction . . . . .	80
2.5	Purification protocol of the U-fraction at WIGL . . . . .	81
2.6	Values of BCR-2 obtained during the thesis compared with the referenced value. . . . .	84
2.7	Quantity of uranium obtained in the blank during the thesis. . . . .	85
2.8	Reference Material BCR-173 measured and certified values . . . . .	88
2.9	Precision of the specific surface area measurement access using two aliquot of the Var River sample EST-05 . . . . .	88
3.1	U isotopic compositions of reference materials. . . . .	98
3.2	U concentration and activity ratio for silt and clay of Loire River Sediments. . . . .	99
3.3	Uranium concentration and activity ratio of silt and clay size fractions in river sediments and corresponding basin parameters . . . . .	101
3.4	Characteristics of the studied samples and their sedimentary system . . . . .	108
4.1	BCR-2 standard values measured during the Var River sediments study. . . . .	129
4.2	Table of U concentration, ( $^{234}\text{U}/^{238}\text{U}$ ) and $S_{BET}$ measured in Var River sediments. . . . .	130
4.3	Sediment residence time derived from ( $^{234}\text{U}/^{238}\text{U}$ ) . . . . .	138
5.1	BCR-2 standard values measured during the Var cores sediments study. . . . .	152



# INTRODUCTION

---

## General background

The landscape morphology of the Earth's surface is greatly diversified. It results from complex interactions between climate, weathering and tectonic processes. Over the last decades, one of the major societal challenges has been the comprehension of these interactions, with the aim to investigate the impact they may have on the global carbon cycle and atmospheric CO<sub>2</sub> concentrations, which is a significant concern in the context of the current global warming. Briefly, the process of chemical weathering of silicate rocks uses carbonic acid resulting in the formation of secondary clay minerals in soils and releasing dissolved carbonate ions (HCO<sub>3</sub>) that act as a net sink for atmospheric CO<sub>2</sub> (Holland 1978, Berner 1990). Some researchers consider that the main control on weathering is tectonics (Koppes & Montgomery 2009, Willenbring & Jerolmack 2016) and that the long-term Cenozoic global cooling is the result of weathering-driven enhanced atmospheric CO<sub>2</sub> storage in response to the uplift of the Himalaya-Tibetan plateau (Walker et al. 1981, Molnar & England 1990, Raymo & Ruddiman 1992). In contrast, other researchers have argued that climate represents the main driver of continental weathering (Peizhen et al. 2001, Herman & Champagnac 2016). To date, this “chicken-and-egg theory” still remains debated (Molnar & England 1990).

Additional questions relate to the control of climate, weathering and tectonic on landscape morphology. The complex interactions between both internal (e.g. tectonic, weathering) and external (e.g. climate, biological activity) processes shape the morphology of continental surfaces, resulting in a thin soil interface also referred to as Critical Zone (van Breemen & Buurman 2002, Chorover et al. 2007, Brantley et al. 2007, Amundson et al. 2007). While tectonics generate reliefs at the Earth surface, through mountain uplift for example, the combination of erosion and weathering processes result in their progressive destruction over time. The climate may accentuate or not these processes. Over geological timescale, the presence of glaciers acting as efficient erosional agents in mountain ranges increases denudation rates (Hallet et al. 1996, Hinderer 2001, Herman & Champagnac 2016). At shorter time scale, precipitation also enhances the denudation of the relief for example, which is attenuated by the development of vegetation (e.g. temperate forest) that stabilize soils (Löbmann et al. 2020). All these processes affect the formation of the soil cover at the surface of the continents, and its subsequent export via the source to sink sedimentary system.

While the global inter-correlations between weathering, climate, and tectonics are nowadays accepted and relatively well understood, some issues are yet to be settled. One of them is the nature of the variability of erosion and weathering processes over glacial-interglacial timescales (Foster & Vance 2006, Vance et al. 2009, Lupker et al. 2012, von Blanckenburg et al. 2015, Cogež et al. 2015). Another one is the timescale of the sedimentary cycle: from the soil production to its erosion and transportation until its final deposition. This latter point is particularly important because the duration of these processes strongly influence the emergence of a sedimentary signal, i.e. the landscape response to perturbations of environmental variables, such as climate and tectonic, and its transmission until its deposition and preservation in the depositional environment (Romans et al. 2016). While erosive processes can be efficiently measured at present, it still remains challenging to determine the time elapsed from the formation of the sediment until its final storage in the deposition area of the sedimentary basin.

## Objectives of this thesis

The temporal evolution of the Earth surface and landscape morphology is complex. In order to unravel it, it is important to clearly understand which parameters (e.g. climate, weathering, tectonic) are involved in the formation of land surfaces and how these various factors may interact with each other. This issue is important since our humanity is directly dependent on this Critical Zone., which represents the interface between the atmosphere and the upper continental crust, including the bedrock, the soil, and the vegetation. Soil thickness is a fundamental variable in many Earth science disciplines due to its critical role in many hydrological (e.g. runoff, water residence) and ecological processes, but it is difficult to predict. Soil thickness is highly variable spatially and difficult to practically measure even for a small watershed Dietrich et al. (1995). Inside the soil profile, sediments are formed and can be stored depending on the sedimentary system, before being exported until they reach their final deposition site. The time spent by the sediment from its formation until its final deposition can be estimated using U-series and one of their characteristics: i.e. the so-called recoil effect. This method is very efficient and can provide estimates of sediment residence time but requires various assumptions and careful sample preparation in order to analyse selectively the pure detrital fraction of the fine ( $<63 \mu\text{m}$ ) fraction sediment.

**The focus of this PhD thesis is the timescale of sedimentary processes on the continents, investigated here using geochemical tools that aim at determining the sediment residence time in river catchments.** The sediment residence time is the time elapsed since the formation of the sediment as part of the regolith, and its transfer until its final deposit (Fig. 1). The sediment residence time - by indicating the

time spent by the sediment inside the basin, can 1. give information about denudation processes (e.g. potential storage of sediments, soil stability); 2. help to understand the timing of the response of sedimentary systems to any environmental variations.

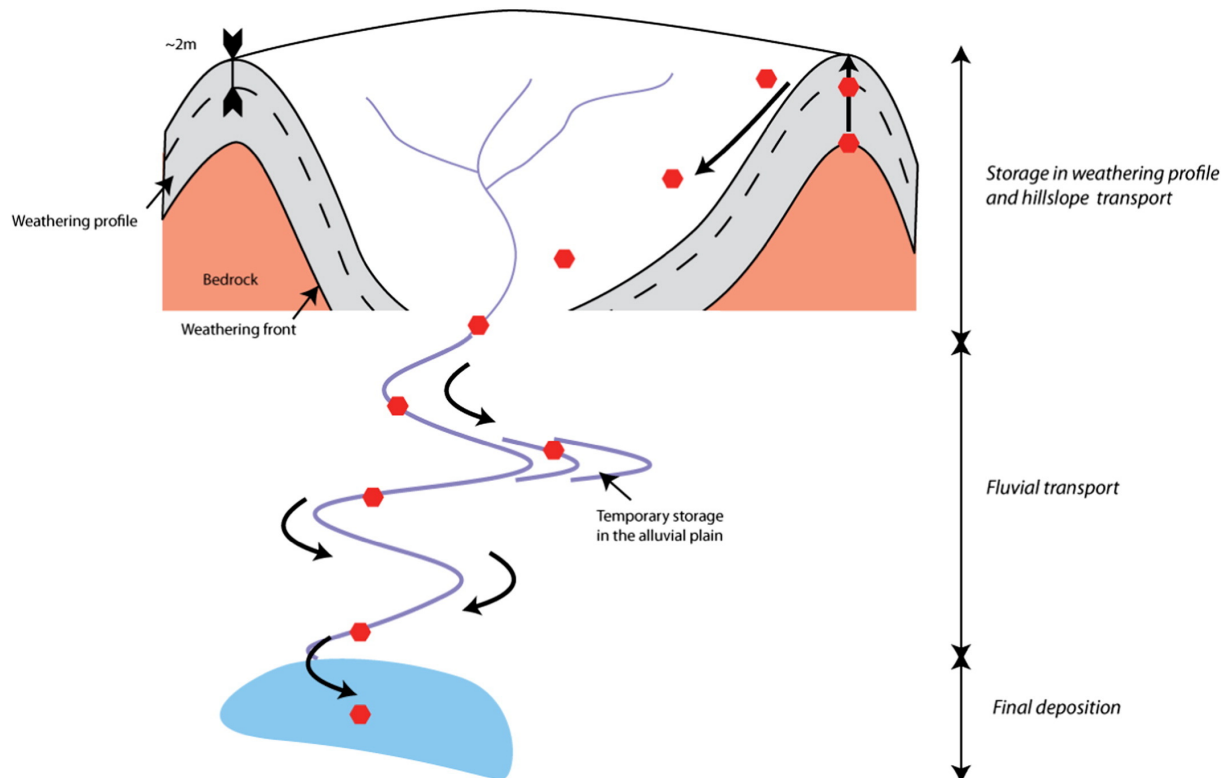


Figure 1 – Conceptual representation of the regolith (red polygone) transport from source to sink  
 Dosseto & Schaller (2016).

The manuscript is divided into 6 chapters, as defined hereafter:

**Chapter 1** provide a brief literature review of what is currently known to measure the transport and storage time of sediment from source to site of deposition, divided in three parts.

The first one describes the source-to-sink concept and associated sedimentary processes, which are the main object of this study. Particular attention is given to the formation of soils and their evolution as major sediment storage, and to the transmission of the environmental signals; a subject that remains highly debated mainly because of the difficulties to have quantitative constraints about it.

The second part is dedicated to the general description of the uranium-series; the geochemical tracers that have been used in this work. The properties of thorium isotopes are also briefly presented as they have been also investigated during the course of this thesis, despite of various limitations which led us to focus exclusively on uranium (U) isotopes (see method chapter). The second part ends with a description of the ‘comminution age’ dating technique, which is used here to calculate sediment residence time. The third part

is a summary of the previous applications of U-series for investigating weathering processes or providing constraints on the timescale of sediment transport.

In **chapter 2**, the methodology used during this thesis is detailed, from the sieving of the bulk sediment to the analysis of uranium isotope ratios. A particular attention is given to the leaching protocols used at both Ifremer and UOW laboratory and their careful evaluation for U isotope studies.

In **chapter 3**, we focused on the uranium fractionation inside sediments. For this purpose, the influence of external parameters, such as climate, lithology, weathering, and internal parameters, such as grain size, on the degree of fractionation of uranium isotopes in river sediments are discussed. This discussion is based on the measurement of ( $^{234}\text{U}/^{238}\text{U}$ ) in two grain-size fractions from various world river sediments. This large data set allowed us to draw general conclusions about the main factors influencing the distribution of ( $^{234}\text{U}/^{238}\text{U}$ ) ratios in river sediments.

In **chapter 4**, we present the result of a spatial investigation of sediment residence times inside a small mountainous river system (Var, S-E France) and compare the observed ( $^{234}\text{U}/^{238}\text{U}$ ) intra-basin variability with the morphology of each sub-basins. On the basis of these results, we further assess the potential of using sediment residence time to constrain erosion processes. Conjointly, we also discuss about the validity of U-based sediment residence time by comparing them with regolith residence time, which we calculate using denudation rates and soil thickness estimates.

In **chapter 5** we finally investigate past variations in sediment residence time in the Var River basin, over the last 75 kyr, on the basis of the results presented in chapter 4. We discuss on the obtained ( $^{234}\text{U}/^{238}\text{U}$ ) cyclicity and inferred changes in sediment residence time, through comparison with various parameters including climate, denudation rate, sediment source, vegetation, to further understand which factors control long-term changes of erosion.

The **chapter 6** concludes with the work conducted during the course of this PhD thesis, and outlines a few perspectives of research for future work.

# INTRODUCTION

---

## Généralités

La morphologie des paysages à la surface de la Terre est très diversifiée. Elle résulte d'interactions complexes entre le climat, l'altération et les processus tectoniques. Au cours des dernières décennies, l'un des principaux défis scientifiques a été la compréhension de ces interactions, afin de connaître l'impact qu'elles peuvent avoir sur le cycle global du carbone et les concentrations atmosphériques de CO<sub>2</sub>. Il s'agit d'une préoccupation importante dans le contexte du réchauffement climatique actuel. Succinctement, le processus d'altération chimique des roches silicatées utilise l'acide carbonique, ce qui engendre la formation de minéraux argileux secondaires dans les sols et libère des ions carbonate dissous (HCO<sub>3</sub>). Ceux-ci agissent comme un piège pour le CO<sub>2</sub> atmosphérique (Holland 1978, Berner 1990). Certains scientifiques considèrent que l'altération est principalement contrôlée par les processus tectoniques (Koppes & Montgomery 2009, Willenbring & Jerolmack 2016) et que le refroidissement global sur le long terme depuis le Pléistocène est le résultat de la capture du CO<sub>2</sub> atmosphérique (Walker et al. 1981, Molnar & England 1990, Raymo & Ruddiman 1992). En opposition, d'autres estiment que le climat a une influence plus prédominante (Peizhen et al. 2001, Herman & Champagnac 2016). C'est la "théorie de l'œuf et de la poule" qui reste débattue (Molnar & England 1990).

D'autres préoccupations concernent l'impact du climat, de l'altération et de la tectonique sur la morphologie du paysage. Les interactions complexes entre les processus internes (e.g. tectonique, altération) et externes (e.g. climat, activité biologique) façonnent la morphologie des surfaces continentales, ce qui se traduit par une interface sol mince également appelée zone critique (van Breemen & Buurman 2002, Chorover et al. 2007, Brantley et al. 2007, Amundson et al. 2007). Alors que la tectonique génère les reliefs à la surface de la Terre, à travers le soulèvement des montagnes par exemple, la combinaison des processus d'érosion et d'altération entraîne leur destruction progressive au fil du temps. Le climat peut accentuer ou non ces processus. Sur une échelle de temps géologique, la présence de glaciers, connue pour être un agent d'érosion efficace lors de la déglaciation, dans les chaînes de montagnes augmente les taux de dénudation (Hallet et al. 1996, Hinderer 2001, Herman & Champagnac 2016). À plus petite échelle de temps, les précipitations favorisent la dénudation du relief, atténuée par le développement de la végétation (comme la forêt tempérée) qui stabilise les sols (Löbmann et al. 2020). Tous ces processus affectent la formation de la couverture du sol à la surface des continents, et son exportation ultérieure

pour former le système sédimentaire.

L'intercorrélation globale entre l'altération, le climat et la tectonique est aujourd'hui acceptée et relativement bien comprise, mais certaines questions restent encore en suspens. L'une d'elles est la nature de la variabilité des processus d'érosion et d'altération sur l'échelle de temps glaciaire-interglaciaire (Foster & Vance 2006, Vance et al. 2009, Lupker et al. 2012, von Blanckenburg et al. 2015, Cogež et al. 2015). Une autre est l'échelle de temps du cycle sédimentaire : de la production du sol à son érosion et son transport jusqu'à son dépôt final. Ce dernier point est particulièrement important car la durée de ces processus influence fortement l'émergence d'un signal sédimentaire, c'est-à-dire la réponse du paysage aux perturbations des variables environnementales, telles que le climat et la tectonique, et sa transmission jusqu'à son dépôt et sa préservation dans le dépôt (Romans et al. 2016). Si les processus érosifs peuvent être efficacement mesurés à l'heure actuelle, il reste encore difficile de déterminer le temps écoulé entre la formation du sédiment et son stockage final dans la zone de dépôt du bassin sédimentaire.

Cette thèse porte sur les temps des processus sédimentaires sur les continents, étudiés ici à l'aide d'outils géochimiques dans le but d'estimer le temps de résidence sédimentaire dans différents bassins versants. Celui-ci peut donner des informations sur l'efficacité des processus de dénudation (par exemple la possibilité de stockage temporaire des sédiments, la stabilité du sol, etc.) et aider à déterminer le temps de réaction du système sédimentaire à s'adapter aux variations environnementales.

## **Objectifs de la thèse**

L'évolution de la surface terrestre et ainsi de la morphologie du paysage est complexe. Afin de mieux l'appréhender, il est important de saisir clairement quels paramètres (par exemple, le climat, l'altération atmosphérique, la tectonique) sont impliqués dans le modelage des surfaces terrestres et comment ces différents facteurs peuvent interagir. Cette question est importante car l'humanité dépend directement de cette zone critique, avec l'utilisation des surfaces terrestres, notamment pour l'agriculture. Cette zone, qui représente l'interface entre l'atmosphère et la croûte continentale supérieure, comprend le substratum rocheux, le sol au-dessus de celui-ci et la végétation. L'épaisseur du sol est une variable fondamentale dans de nombreuses disciplines des sciences de la Terre en raison de son rôle critique dans de nombreux processus hydrologiques (par exemple, le ruissellement, l'adsorption de l'eau) et écologiques. Elle est très variable dans l'espace et difficile à mesurer dans la pratique, même pour un petit bassin hydrographique Dietrich et al. (1995). À l'intérieur du profil du sol, les sédiments sont formés et peuvent être

stockés en fonction du système sédimentaire, avant d'être exportés jusqu'à leur site de dépôt final. Le temps passé par les sédiments depuis leur formation jusqu'à leur dépôt final peut être estimé à l'aide de séries isotopiques de l'uranium grâce à l'une de leurs caractéristiques : l'effet dit de recul. Cette méthode est très efficace et peut fournir des estimations de temps de résidence sédimentaires. Cependant elle nécessite divers postulats et une préparation minutieuse des échantillons afin d'analyser seulement la fraction détritique de la fraction fine ( $<63 \mu\text{m}$ ) des sédiments.

**L'intérêt de cette thèse porte sur l'échelle des temps des processus sédimentaires à la surface de la Terre. Pour cela, des outils géochimiques sont utilisés dans l'objectif de déterminer les temps de résidences sédimentaires.** Ce temps de résidence sédimentaire est le temps passé entre la formation des sédiments dans le régolite jusqu'à son dépôt final (Fig. 1). Le temps de résidence sédimentaire en indiquant le temps passé par le sédiment au sein du bassin peut 1. donner des informations sur les processus de dénudations et le stockage sédimentaire temporaire); 2. aider à comprendre le temps de réponse des systèmes sédimentaires face aux variations environnementales.

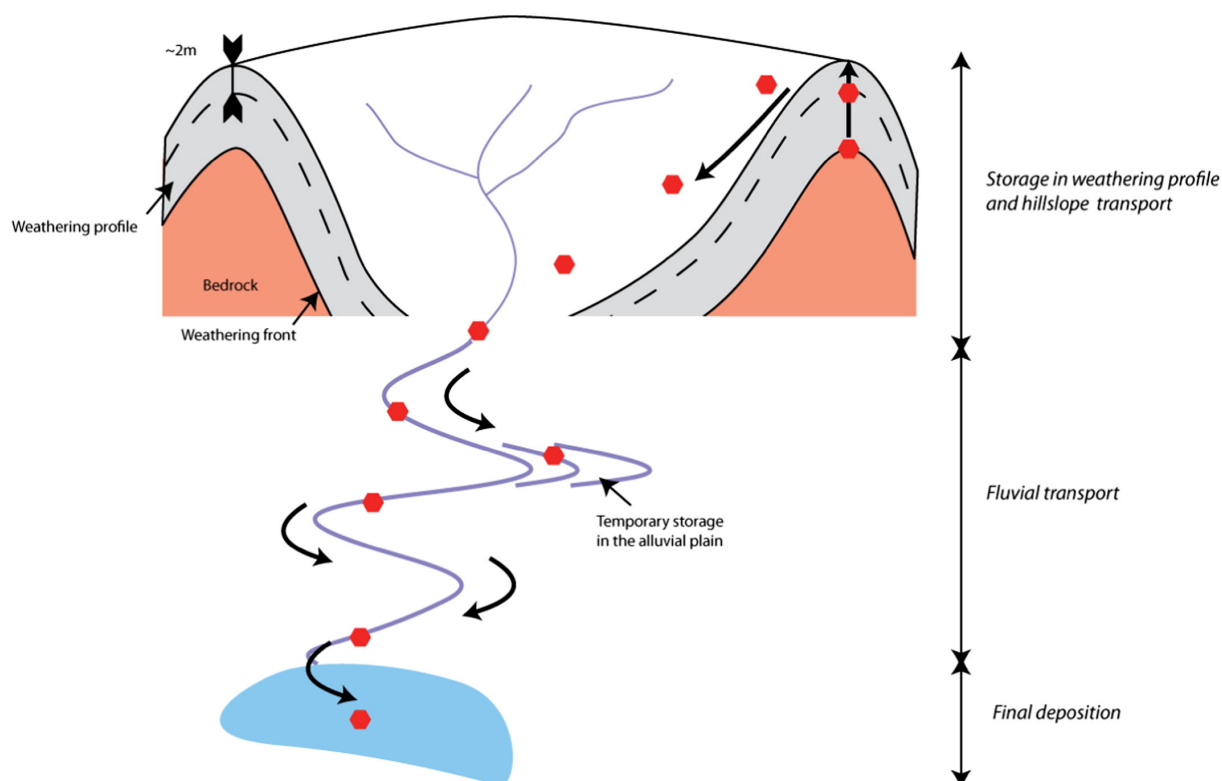


Figure 1 – Représentation conceptuel du transport du régolithe depuis sa source jusqu'à son dépôt final. Dosseto & Schaller (2016).

Le manuscrit de thèse est divisé en 6 chapitres, comme défini ici:

Le **chapitre 1** est consacré à une brève revue de la littérature concernant les connaissances actuelles pour mesurer les temps de transport des sédiments et de leurs stockages temporaires entre leur source et leur zone de dépôt finale. Le chapitre est divisé en trois parties.

La première décrit le concept de source-au-puit et les processus sédimentaires qui s'y déroulent. Ceux-ci sont l'objet principal de cette étude. Une attention particulière est accordée à la formation des sols et à leur évolution en tant que stockage majeur de sédiments, ainsi qu'à la transmission des signaux environnementaux. Ce sujet reste très débattu, principalement en raison des difficultés à avoir des contraintes quantitatives.

La deuxième partie est consacrée à la description générale des isotopes des séries d'uranium, traceurs géochimiques utilisés dans ce travail. Les propriétés des isotopes du thorium sont également présentées, car elles ont aussi été étudiées au cours de cette thèse, malgré diverses limitations qui nous ont amenés à nous concentrer exclusivement sur les isotopes U (voir le chapitre sur la méthode). Cette partie se termine par une explication sur la technique de datation de « l'âge de comminution », utilisée dans le calcul du temps de résidence sédimentaire.

La troisième partie est un résumé des applications antérieures de la série U soit pour l'étude des processus d'altération soit pour fournir des contraintes sur l'échelle de temps du transport des sédiments.

Le **chapitre 2** détaille la méthodologie utilisée au cours de cette thèse. Du tamisage des sédiments en vrac aux analyses des isotopes de l'uranium, l'ensemble du processus est présenté. Une attention particulière est portée sur les protocoles de lessivage utilisés à l'Ifremer et au laboratoire WIGL et sur les tests réalisés pour les valider, en raison de l'importance d'étudier seulement la fraction détritique des sédiments.

Dans le **chapitre 3** est examinée l'influence des paramètres externes, tels que le climat, la lithologie, l'altération et les paramètres internes (par exemple la taille des grains) sur le fractionnement des isotopes d'uranium dans les sédiments fluviaux. Cette étude est basée sur la mesure de ( $^{234}\text{U}/^{238}\text{U}$ ) dans deux fractions granulométriques de sédiments fluviaux du monde (par exemple Amazone, Nil, Fraser, Lule). Ce vaste ensemble de données nous a permis d'obtenir une bonne représentativité de la variabilité de ( $^{234}\text{U}/^{238}\text{U}$ ) dans les systèmes sédimentaires à la surface de la Terre.

Dans le **chapitre 4**, nous présentons les résultats portant sur les variations spatiales et actuelles du temps de résidence des sédiments à l'intérieur d'un petit système sédimentaire (Var, S-E France) et nous comparons la variation avec la morphologie du bassin. Sur la base de ces résultats, nous évaluons la possibilité d'utiliser le temps de résidence des sédiments pour déduire les processus d'érosion. Conjointement, nous discutons de la

précision du temps de résidence des sédiments en les comparant avec le temps de résidence au sein du régolite, que nous estimons avec le taux de dénudation et une prédiction de l'épaisseur du sol provenant d'une base de données.

Sur la base des résultats présentés au chapitre 4, nous avons étudié la variation du temps de résidence sédimentaire au cours des 75 derniers ka. Dans le **chapitre 5**, nous abordons la cyclicité observée du temps de résidence sédimentaire et nous l'étudions en fonction parallèle à divers paramètres tels que les variations climatiques, les taux de dénudation, un traceur de source, etc. pour comprendre ce qui contrôle les processus d'érosion et, ce qui contraint les périodes de stockage des sédiments.

Le **chapitre 6** conclut sur les travaux réalisés dans le cadre de cette thèse et définit des perspectives de recherche intéressantes qui en découlent.



# LITERATURE REVIEW

---

## Contents

---

<b>1.1</b>	<b>From source to sink: the sediment's life</b>	<b>26</b>
1.1.1	Concept	26
1.1.2	Environmental signal propagation in sedimentary systems	31
1.1.3	Soil: the origin of the sediment	41
<b>1.2</b>	<b>Uranium isotopes</b>	<b>45</b>
1.2.1	Background	45
1.2.2	Radioactive disequilibrium	45
1.2.3	Secular equilibrium	47
1.2.4	Uranium abundances in rock forming minerals and the fractionation of ( $^{234}\text{U}/^{238}\text{U}$ ) in sedimentary systems	48
1.2.5	The concept of comminution age	53
<b>1.3</b>	<b>Uranium at Earth's surface</b>	<b>59</b>
1.3.1	From bedrock to soil: weathering processes	59
1.3.2	Uranium isotopes to infer timescale of sedimentary processes and its control	61
1.3.3	Uncertainties based on the comminution age method	62

---

## 1.1 From source to sink: the sediment's life

The framework of this thesis is to better understand the timescale of the processes occurring inside a sedimentary basin through the study of sediments. In this regard, it is important first to describe the conceptual nature of the source-to-sink principle, and to introduce the various processes that can affect the sediment's life.

### 1.1.1 Concept

A sedimentary system, also called *sediment-routing system* (Allen 1997) is defined as a “integrated dynamical system connecting erosion in mountain catchments to downstream deposition” (see Romans et al. 2016 for a thorough review). It is the combination of various topographic units (and bathymetric units if the system is connected to the ocean) where sediments are formed, transported, and deposited. In order to simplify natural sediment-routing systems, Schumm (1977) idealized the system by identifying three distinct zones (Fig. 1.1) at the lithosphere-atmosphere interface (Castelltort & Van Den Driessche 2003). These 3 zones (i.e. the source area, the transfer pathways, and the depositional area) are connected to each other and are characterized by a distinctive behavior of the sediment fluxes (Schumm 1977, Allen 1997, Castelltort & Van Den Driessche 2003):

- **The source area:** the elevated part of the basin is the location of erosional processes principally dominated by the denudation of hillslopes and to a lesser extent by fluvial incision (Hovius 1998, Castelltort & Van Den Driessche 2003).
- **The transfer pathways:** a sector predominantly dominated by sediment transport processes. This zone can be absent depending on the sediment-routing system being considered, in particular in those watersheds where the source region is directly connected to the depositional basin, such as in small mountain basins for example. Alternatively, this region can extend over several thousand of kilometers in the case of the largest river systems (Castelltort & Van Den Driessche 2003).
- **Deposition zone:** the ultimate location of sediment deposition, which can be continental and/or marine and can include deep turbiditic system (e.g. Amazon, Congo, Indus).

Several processes occur at different temporal and spatial scales in sediment-routing systems. For example, the variability of climate can be expressed over relatively short, seasonal, timescales to much longer geological periods (e.g. Swift et al. 2002, Holmgren et al. 2003, Mayewski et al. 2004, Covault & Graham 2010). Additionally, tectonics can also influence sediment-routing systems over drastically different timescales: from daily (earthquakes; e.g. Lin et al. 2008, West et al. 2014, Marc et al. 2015) to million-year periods (mountain uplifts; e.g. Allen 2008a, Sømme et al. 2009, Whitchurch et al. 2011, Allen & Heller 2012). For this reason, the study of each of the three sub-systems is necessary,

taking into account all their distinctive morphological, sedimentary, geochemical and hydrological characteristics in order to fully comprehend the nature of the interactions that are at play.

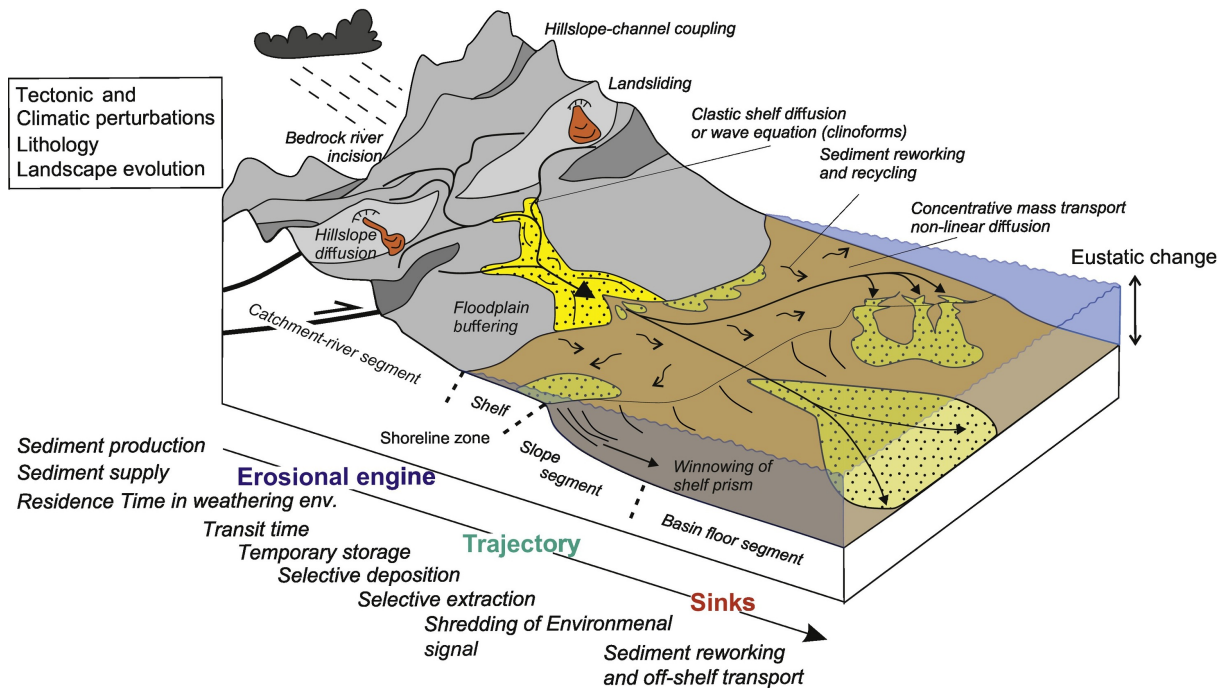


Figure 1.1 – Schematic representation of the three units (from left to right: source represented as Erosional engine, the trajectory is the transfer pathways, and deposition zone delimited by the sinks area) of a sedimentary routing system with the main external forcing (e.g. climate, tectonic) (from Caracciolo 2020).

Below, each part of the sediment-routing system is described to introduce the various processes occurred within it and to explain how each of these three parts are correlated to each other.

### Source: weathering processes

Sediments are formed in the source area of the sediment-routing system. In this area, two main processes are involved in the disintegration of the bedrock into fine-grained sediments: weathering and denudation.

The alteration of rock-forming minerals combines various chemical, physical and biological processes. Chemical weathering achieves partial dissolution of bulk rocks by modifying their initial mineralogical and chemical characteristics, resulting in products such as secondary clays and iron oxides that are more stable at the Earth's surface. In soils, the intensity of chemical weathering depends on various physico-chemical characteristics such as pH and  $\text{CO}_2$ , which represents the main weathering agent (Drever 1994). In parallel to chemical weathering, physical weathering also strongly affects the physical properties

of the initial rocks (e.g. shape of the grains, size, etc.) through the effect of freeze thaw action or grinding for example. The combination of both chemical and physical weathering operates to transform the pristine bedrock into saprolite (i.e. the immobile part of the weathering profile; Fig. 1.2). The evolution of bedrock into soil by weathering is enhanced by biological action caused by the vegetation (e.g. which promotes efficient rock fracturing with roots) or by any living organisms that interact with the soil profile.

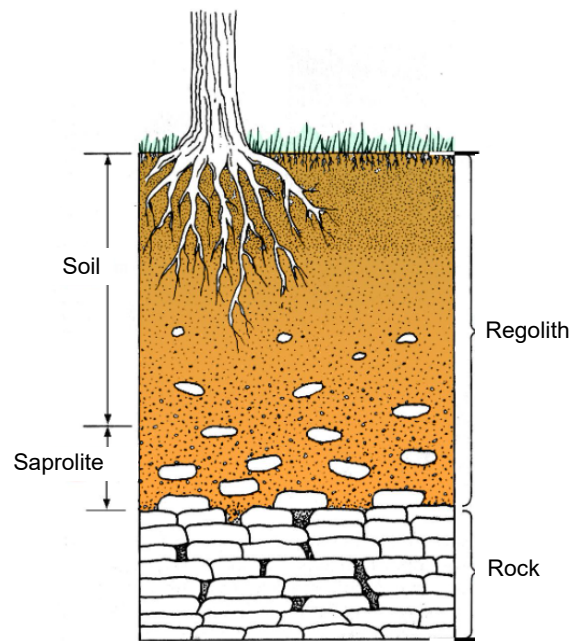


Figure 1.2 – Weathering profile identifying soil (mobile) and saprolite (immobile) fractions which represent the regolith, i.e. the unconsolidated layer above the bedrock (Adapted from Juilleret et al. 2014).

Chemical and physical weathering are intertwined with erosional processes which altogether result in the formation and regulation of soil (Stallard & Edmond 1983, Gaillardet et al. 1999, Millot et al. 2002, Riebe et al. 2001, Riotte et al. 2003, Ferrier & Kirchner 2008, West 2012). On one hand, chemical weathering, by modifying the initial mineralogy of pristine rocks, also change its strength, increasing its vulnerability to further erosion. On the other hand, the removal of regolith by erosion results in the exposition of fresh rock and mineral surfaces available to chemical and physical weathering. This interrelationship regulates the development of soils and ultimately shapes the land surfaces. However, the balance between each of these two processes, while being of utmost importance for land use management and landscape evolution (Anderson & Humphrey 1989, Riebe et al. 2001), remains difficult to quantify and can vary spatially depending on the system.

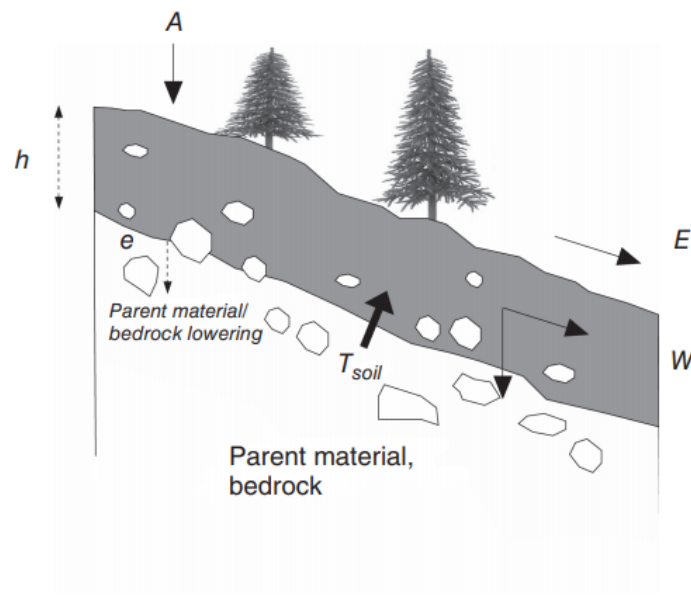


Figure 1.3 – Representation of the soil profile formed by weathering (W) of the parent material with  $T_{soil}$  corresponding to the formation rate; the evolution of the interface bedrock - soil (e) get deeper as soils increased (h). Atmospheric (A) input can be involved in the process, such as erosional processes (E) (from Egli et al. 2014).

The export of sediments formed by weathering from their source region results in the levelling of the continental surfaces (Ahnert 1967). The rate of sediments removed from the soil is referred as denudation rate. It represents the sum of chemical weathering rates and physical erosion rates without taking into account any possible sediment storage along the system. Thus, in river systems having a large storage capacity (e.g. Amazon; Gaillardet et al. 1997), temporary trapping of sediments is important and reduces denudation rates (Slaymaker 2003). The estimation of the volume of sediment deposited in sedimentary basins is used instead (e.g. Hinderer 2001, Kuhlemann et al. 2002, Calvès et al. 2013): an approach that was subsequently improved through the development of quantitative geomorphologic methods (e.g. Anderson & Anderson 2010). Recently, various geochronological techniques such as cosmogenic nuclides (e.g.  $^{10}\text{Be}$ ,  $^{26}\text{Al}$ ) have been developed to improve the quality of measured denudation rates (e.g. Brown et al. 2009, Wittmann et al. 2009, Hippe et al. 2012, Lupker et al. 2012).

### Sediment transfer

Once the sediments have been exported from the catchment source region, they are transported to the deposition site by fluvial fluxes or, alternatively, by aeolian transport. The transfer zone directly connects the source region, dominated by weathering and erosion processes, to the sink, which corresponds to the deposition zone. The sediment connectivity is a concept used to study the processes across multiple scales involved in the transfer of sediments from the source to the sink (Bracken et al. 2015). It combines

the influence of the structure of the catchment (i.e. morphology) and the action of the sediment (i.e. flow, transport of materials), which conjointly impact the long-term behavior of the sediment flux (Preston & Schmidt 2003, Turnbull et al. 2008, Bracken et al. 2015). Therefore, the sediment connectivity concept includes all the aspects (e.g. spatial and temporal scale, frequency and magnitude of the processes; Bracken et al. 2015) of any source-to-sink system (Preston & Schmidt 2003, Sandercock & Hooke 2011). In systems with an efficient connectivity, which leads to rapid landscape response to any environmental change, the basin is referred as *reactive routing system* (Allen 2008b, Covault & Graham 2010, Covault et al. 2013). Conversely, when the connectivity is less efficient, because of sediment storage for example, the system is referred to as a *buffered routing system* as a significant lag is created between the disturbance and the system's response (Allen 2008b).

For any given sediment-routing system, reactive or buffered, the principle of mass conservation applies. From a basic perspective, the amount of sediment input is balanced by the sum of storage and output. Slaymaker (2003) expressed this using the following equation:

$$I_s = \Delta S_s + O_s \quad (1.1)$$

where  $I$  represents the input,  $S$  the storage,  $O$  the output and the subscript letters refer to the type of transported matter, i.e. sediments.

The principle of mass conservation implies that the amount of sediment being produced in the source region should be equal to the amount of sediment that is deposited along or at the end of the sediment-routing system. Exceptions are the case of marine sediment deposits, which can be subject to intense winnowing effects (e.g. Mozambican channel; Miramontes et al. 2019, Fierens et al. 2019). In these systems, the amount of sediments produced is higher than the amount of sediment reaching the final marine deposit. When the sedimentary contribution from the source is higher than the capacity of transport of the fluvial system, a temporary storage operates in the river channel (Kirkby 1971). Conversely, when the sedimentary supply is lower than the transport capacity, the river channel is eroded (Whipple & Tucker 1999, Blum & Törnqvist 2000). Hence, this process of sediments regulation can result in an increase or a decrease of the time spent by the sediment to reach the ultimate sink, causing a dephasing between the source and the sink.

Previous studies have aimed at quantifying sedimentary fluxes (which represent the quantity of sediment exported from the transfer zone by units of time; Slaymaker 2003) to investigate their variability in river systems. The sedimentary flux is usually expressed in tons per years (t/y) or cubic meters per years ( $\text{m}^3/\text{y}$ ). To compare sediment-routing systems amongst each other, the specific sediment yield is generally used, which normal-

izes measured sedimentary fluxes to the catchment area (e.g. Milliman & Syvitski 1992, Syvitski et al. 2005, de Vente et al. 2007). Milliman & Syvitski (1992) pointed out that the river systems displaying extensive sedimentary transfer zones typically exhibit lower specific sedimentary fluxes (e.g. Amur River, Russia: 28 t/km<sup>2</sup>/years) than smaller rivers (e.g. Lamone River, Italy: 2400 t/km<sup>2</sup>/years). In other words, small mountainous rivers are expected to be reactive by adapting themselves rapidly to any environmental change, which affect the sediment flux and the quantity of sediments reaching the deposition zone (Covault & Graham 2010, Bonneau et al. 2014).

## Deposition and storage

The depositional zone is where the sediment is stored. It can be either continental or marine (Schumm 1977). All sediments formed in the catchment source area do not reach the ocean, especially in the case of endorheic basins. During the transport, sediment grains can transit via lakes or other inland water bodies, where deposition can occur. Along the river paths, sediments can also be trapped in alluvial fans, channel deposits *etc.*, or, for the sediments that ultimately reach the ocean, within estuaries or subaerial deltas. Once the sediments have reached the depositional zone, some disturbance can occur (e.g. displacement or destruction; Milliman et al. 2007), which affect the conservation of sediments stored. These processes are detailed thereafter, as part of the environmental signal preservation.

### 1.1.2 Environmental signal propagation in sedimentary systems

Any environmental disturbance (e.g. climate, morphology, anthropogenic presence) results in a modification of the sediment routing system. This adaptation induces a change into the sediment cycle (sediments production, transport or deposition) and the variation of the sedimentary flux is then referred to as an environmental signal (Romans et al. 2016). The signal can then propagate within the sediment routing system until it reaches the depositional zone (Allen 2008*a*). However, the signal can also be trapped or destroyed depending on the characteristic of the signal and the catchment (Castelltort & Van Den Driessche 2003, Jerolmack & Paola 2010). This section aims to present the parameters that can create signals when they are subject to a change, but also the elements to take into consideration for a good signal propagation and preservation.

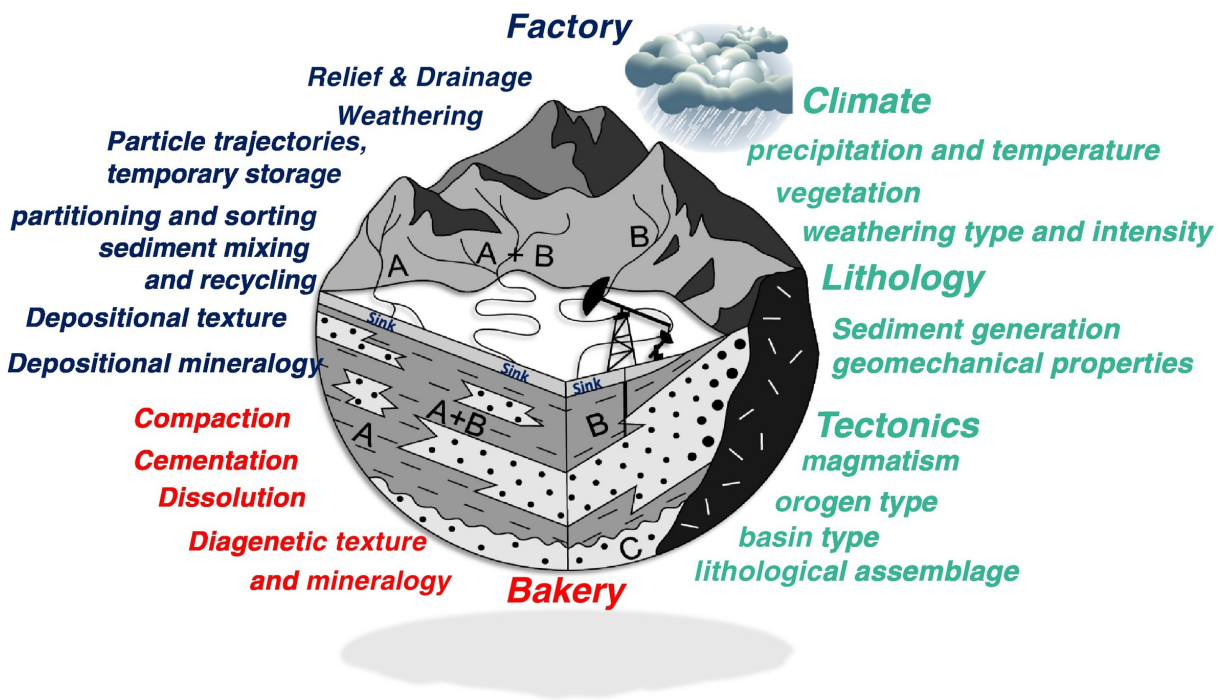


Figure 1.4 – Schematic representation of a sediment routing system with the summary of the internal and external forcing parameters (from Caracciolo 2020 after Johnsson & Basu 1993, Weltje & von Eynatten 2004).

### Factors involved in the sediment's life cycle

In natural conditions, drastic modifications of sedimentary systems can occur as a result of environmental perturbations related to climate, vegetation, weathering, or non-natural conditions changes. These factors can be separated into two groups: 1. intrinsic characteristics including lithology (e.g. Johnsson & Basu 1993, Caracciolo et al. 2012), morphology (Montgomery & Brandon 2002, Riebe et al. 2015) and the size of the basin (e.g. Milliman & Syvitski 1992); 2. external parameters: the climate (e.g. Syvitski et al. 2003, Burbank & Anderson 2011), the anthropogenic influence (Wilkinson & McElroy 2007, Milliman & Farnsworth 2013) on the sedimentary system. This section details these two groups and how all these different parameters may affect the sediment life from their formation to their transport and deposition.

#### *The influence of intrinsic properties of the system*

The characteristics intrinsic to the sedimentary routing system (e.g. lithology, morphology) are presented here. This section also introduces the influence internal parameters have on the formation, transfer, and deposition of the sediment grains.

The lithology of the catchment area exerts a strong influence on sedimentary processes, depending on the cohesion of the bedrock. The bedrock can be composed of loose material

such as loess or unconsolidated clastic sediments, which are more prone to generate high amount of sediments.

Table 1.1 – Relative abundance (% Area) of outcropping rocks in Central Europe (Geo-LiM) and associated mean and standard elevation and slope (from Donnini et al. 2020).

Rock type	% Area	Elevation (m. asl)		Slope (°)	
		mean	sd	mean	sd
Sandstone	30.57	246.6	329.4	3.7	5.9
Mixed carbonate	26.73	441.1	457.7	7.5	8.6
Claystone	15.55	449.5	621.6	7.3	9.8
Pure carbonate	14.04	572.1	581.1	10.5	11.8
Acid rocks	7.93	735.3	645.7	10.9	10.9
Mafic rocks	1.65	889.9	693.8	12.2	11.4
Metamorphic rocks	1.42	807.3	638.0	10.9	10.8
Peat	1.18	90.2	169.1	1.1	1.4
Water (lakes and glaciers)	0.52	1448.4	1330.6	10.7	14.1
Intermediate rocks	0.39	649.3	736.3	10.1	11.2
Gypsum evaporite	0.02	437.3	506.3	10.0	7.6

The lithology also influence the relief of the landscape due to the variation of strength and resistance of the rocks. For example in central Europe, igneous and metamorphic rocks mostly outcrops in high the relief (Table 1.1), which indicate their low weathering susceptibility. In basins draining these crystalline hard rocks, erosion is typically reduced so that less detrital grains are generated, resulting in relatively low sedimentary fluxes (Syvitski & Milliman 2007). Sedimentary rocks (siliclastic sedimentary rocks, limestones and dolostones) and volcanic rocks are generally more prone to weathering than plutonic and metamorphic rocks (e.g Arribas & Tortosa 2003, Caracciolo et al. 2012, von Eynatten & Dunkl 2012).

The susceptibility of the rock to weathering is also determined by rock-forming minerals (Fig. 1.5). The stability of the silicate minerals is generally considered as being the inverse of the so-called Bowen sequence: that is that the minerals crystallized at the highest temperature and pressure conditions (e.g. olivine, pyroxene) are altered more rapidly than those forming in the later stages of magmatic crystallization (e.g. muscovite, quartz; Jackson & Sherman 1953, Rai & Lindsay 1975, Stallard 1988, Nesbitt et al. 1997).

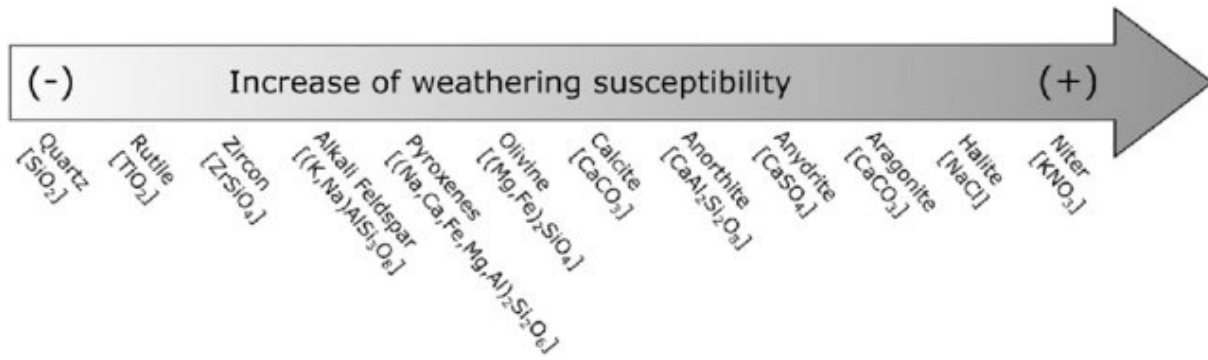


Figure 1.5 – Weathering series of both silicate and non silicate minerals (from Donnini et al. 2020).

The morphology of the basin also strongly impacts the sediment cycle in river systems. First, the morphology of the source region (i.e. slope, curvature, relief) plays a role in controlling the soil thickness and thus the sediment storage capacity, but also the transport of the sediment to the depositional areas. Culling (1960) conceptualized the relationship between sediment fluxes and hillslope gradients; which was further supported by several field studies (McKean et al. 1993, Small et al. 1999). The nonlinear relationship between the hillslope and sediment fluxes has also been used in landscape evolution models (Fig. 1.6; e.g Ahnert 1970, Dietrich et al. 1995, Howard 1997, Willgoose et al. 2008).

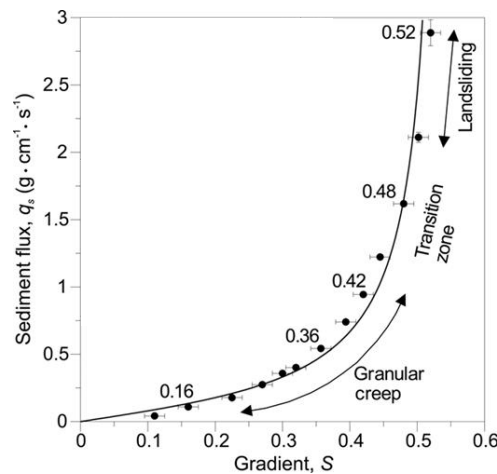


Figure 1.6 – Modelisation of the relation between sediment flux and the slope gradient in an experimental hillslope (from Roering et al. 2001).

Montgomery & Brandon (2002) highlighted the different geomorphological control on erosion rates between low- and high-topography reliefs. In landscapes with low hillslope gradient, the mean slopes or the local relief can be linearly correlated with the denudation rate (Fig. 1.7). In contrast, in high hillslope gradient landscapes, this relationship is nonlinear (Roering et al. 2001, Montgomery & Brandon 2002, Binnie et al. 2007, Dixon et al. 2016), as the result of the transition between diffusive to non-diffusive transport

dynamics above a threshold slope angle (Fig. 1.6; Roering et al. 2001, Montgomery & Brandon 2002, Binnie et al. 2007).

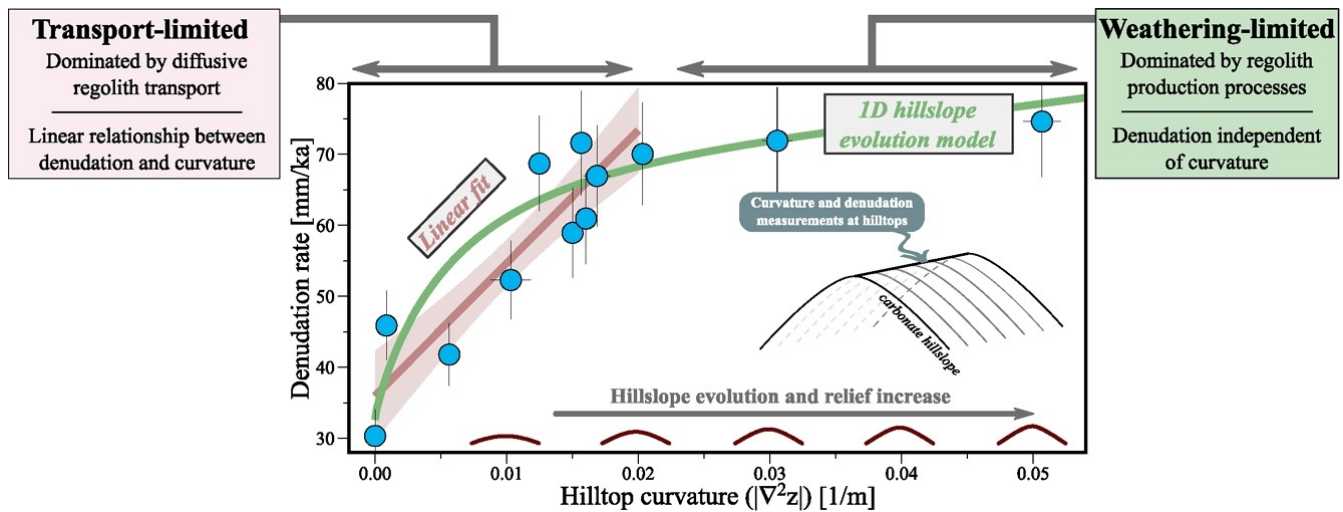


Figure 1.7 – Denudation rate as function of the hillslope curvature (from Godard et al. 2016).

The relief of the source region also determines the type of weathering regime (i.e. transport- or weathering-limited), and thus the sediment supply of the system. Under weathering-limited conditions, such as in areas of high-topography, the sediment is exported rapidly at a rate faster than the dissolution rate of silicate minerals (Stallard 1985, West et al. 2005). In contrast, in floodplains and other areas characterized by transport-limited weathering regimes, the increase of soil residence times is typically accompanied by more intense weathering reactions (West et al. 2005, Lupker et al. 2012), which results in the formation of thicker soil sequences. In addition elevation can also play a role in the sediment storage capacity. In high-elevation areas, soil production and sediment storage capacity are both limited, due to efficient sediment export (i.e. short sediment residence time). In contrast, in low-elevation regions, thicker soil sequences go in pair with enhanced storage capacity and longer sediment residence times.

Furthermore, the size of the draining area also greatly impacts the sediment residence time, in particular in those basins where the presence of extensive alluvial plains contributes to a large sediment storage capacity (Phillips 2003, Parsons et al. 2007), as this is the case for the Po basin (Italia; Amorosi et al. 2016). As a result, any increase in the size of the catchment area generally results in the decrease of the sediment connectivity.

These intrinsic properties of the basin (e.g. lithology, morphology) influence the transfer of sediments. Moreover, they can also be inter-correlated with the external properties of the system (e.g. climate, anthropogenic influence), which are presented below.

*The influence of the external parameters*

Here are presented the external conditions (e.g. climate, anthropogenic influence) to the sediment routing system that can impact the cycle of the sediments. The section also details the ways in which these external factors influence the formation and transfer of the sediment.

The influence of climate on weathering, erosion and sediment transfer in basins is mostly dependent on two variables: temperature and precipitation. Temperature impacts the kinetics and intensity of chemical weathering reactions, but also the vegetation patterns and on the development of glacier. Rainfall, on another side, can induce alluvial aggradation, incisions and controls the run-off (Romans et al. 2016, Covault et al. 2011). In addition, long-term climate change over glacial-interglacial timescales also results in sea-level variations, hence indirectly influencing sediment transport processes by modifying the morphology of the lower river course (e.g. river incision when the sea level lowered; Blum & Törnqvist 2000).

The vegetation and land cover patterns, which are directly dependent on the type of climate, also exert an important role in weathering (e.g. Egli et al. 2008) and other sedimentary processes within watersheds (Drever 1994, Ivory et al. 2014). For instance, in areas dominated by humid forests associated with extensive root systems, soils are generally stable, reducing the denudation capacity (e.g. Molina et al. 2009). Additionally, the presence of biological activity can increase weathering (Lucas 2001), promoting the sediment formation. In contrast, bare soils and other areas with limited vegetation cover will be more prone to considerable denudation rate as the newly formed soil will immediately be exported. Hence the increase in vegetation cover lead to a diminution of the erosion rate as represented in the Figure 1.8.

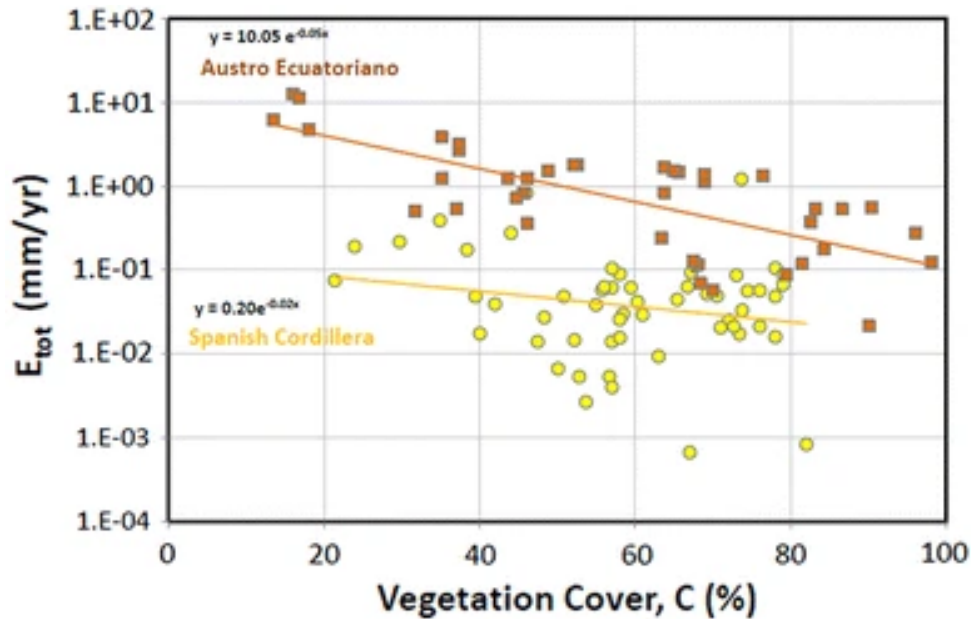


Figure 1.8 – Evolution of the erosion rate ( $E_{tot}$ ) depending on the vegetation cover in two different sites (from Vanacker et al. 2014).

Finally, anthropogenic activities also play a major role in the sedimentary cycle on continents. On one hand, they have a direct impact on the soil cover with agriculture and deforestation typically resulting in an increase of denudation rates and reduced sediment storage within the alluvial plain (Syvitski et al. 2003, Bayon et al. 2012, Costa et al. 2018). Proxy investigations of sedimentary records suggested links between erosion and the presence of agriculture back to 3000 yr ago in Central Africa (Bayon et al. 2012) and 3 500 yr ago in Greece (Rothacker et al. 2018). On the other hand, the urbanisation of river systems, in particular the presence of dams can severely reduce sedimentary fluxes and enhance sediment storage, thereby increasing sediment residence time within the watershed (Yang et al. 2018). Furthermore, human interventions in deltas steadily increase (Syvitski & Saito 2007, Syvitski & Kettner 2011) through trajectory controls (e.g. Po, Colorado), stabilization (Rhone, Fraser) or to attenuate the variations in sediment supply due to seasonal flooding (Mekong, Indus). As a consequence of the combined effects of human activities on river systems, in Oceania and Indonesia, where less dams have been constructed over the last decades, there has been an increase of 80 and 100 % of the sediment flux during the Anthropocene period (i.e. human dominated geological epoch; Lewis & Maslin 2015) respectively. Conversely, in Europe, Africa, and North America, sediment fluxes have decreased since the beginning of anthropization and the advent of agriculture during the course of the Holocene (Syvitski et al. 2005).

## Signal propagation

When a change in environmental conditions occurs, causing a sediment disturbance, a particular ‘sedimentary signal’ induced will be transferred and subsequently archived in the depositional record (Fig. 1.9). The generation of sedimentary signal depends of the capacity of the sedimentary routing system to produce sediments (Caracciolo 2020) that can record the signal. Some studies have shown that the transmission of ‘sedimentary signals’ can be buffered or delayed along the river system depending on various parameters such as the size of the basin (Bull 1991, Dearing & Jones 2003, Lane et al. 2011). Such river systems are considered being out of equilibrium (i.e. the sediment input is not equal to the sediment output at the river mouth; Ahnert 1994, Phillips 2003) or in a transient state (i.e. the relaxation time is larger than the recurrence time of events ; Brunsten & Thornes 1979) characterized by continuous aggradation or degradation. In addition, once the sediment has reached the depositional zone, it can be subject to further erosional processes, as for example sediments mixing, that can disturb the original environmental signal (e.g. Tofelde et al. 2019). All the above illustrates the potential limitations of sediment records for investigating past environmental changes (Jerolmack & Paola 2010).

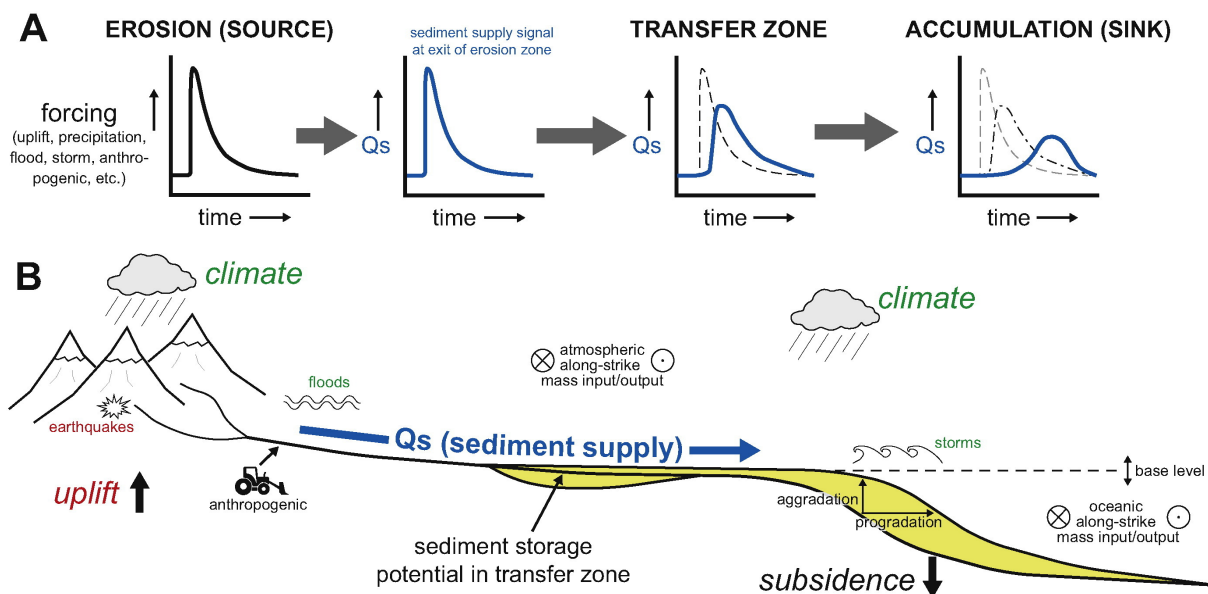


Figure 1.9 – Representation of the sediment supply signal propagation inside a basin (from Romans et al. 2016).

Romans et al. (2016) produced an overview of the environmental signal and its propagation along a sediment routing system (Fig. 1.10). They investigated the response of both uplift and climatic disturbances occurring in the erosion zone of a given watershed, and their transformation and propagation as sediment supply ( $Q_s$ ) signals in both the transfer and accumulation zones. In only a few cases environmental signals are faithfully

transmitted into the depositional zone and well preserved (gray shaded circles, Fig. 1.10). According to Simpson & Castelltort (2012) it mainly depends on the source of the external perturbation: climatic variations are more likely to be transmitted when it induces water discharge ( $Q_w$ ) variations rather than only sediment flux variations. The frequency and amplitude of the environmental disturbance are important in regard of the inherent sediment transfer cyclicity (Jerolmack & Paola 2010). Indeed, long alluvial rivers ( $>300$  km) buffer high-frequency ( $\leq 100$  kyr) disturbances in sediment input coming from the erosion subsystem (Castelltort & Van Den Driessche 2003). Finally, stratigraphic cyclicity and sediment supply rates may result from both changes in climate and erosions rates as well as from glacio-eustatic sea-level variations and up-system signal propagation driven by base level change (see Blum & Törnqvist 2000 for a thorough review).

Despite the significant progress achieved over the last decades in the comprehension of paleo-weathering processes (Lerman 1988, Muto & Steel 1992, Tucker & Slingerland 1997, Syvitski & Milliman 2007, Jerolmack & Paola 2010, Phillips & Jerolmack 2016, Romans et al. 2016), it remains difficult to directly link proxy records in sedimentary archives to corresponding environmental perturbations within any sediment routing system. Consequently, some experts are concerned about the accuracy of using landscape or sedimentary data to detect past environmental change (Wiel & Coulthard 2010, Phillips & Jerolmack 2016). However, marine stratigraphic record has shown evidence of sediment inputs correlated with long-term (e.g. Milankovitch-type) and short-term (e.g. Dansgaard-Oeschger) climate cycles (Vail et al. 1977, Van der Zwan 2002, Bonneau 2014). Some recent works have also shown evidence of efficient long-term (glacial-interglacial) signal propagation (Simpson & Castelltort 2012, Macklin et al. 2012, Blum et al. 2018, Watkins et al. 2019). Nevertheless, Watkins et al. (2019) suggested that signals are modified by sediment remobilization (see, e.g. Clift et al. 2008 and Clift et al. 2014 for the case of the Indus delta), which can delay, attenuate or emphasize the signals from the landscape adjustment. This emphasizes the necessity to quantify (i.e. measure) the transport and storage time of the sediment from source to sink (DePaolo et al. 2006) to be able to detect and quantify this signal phase shifts.

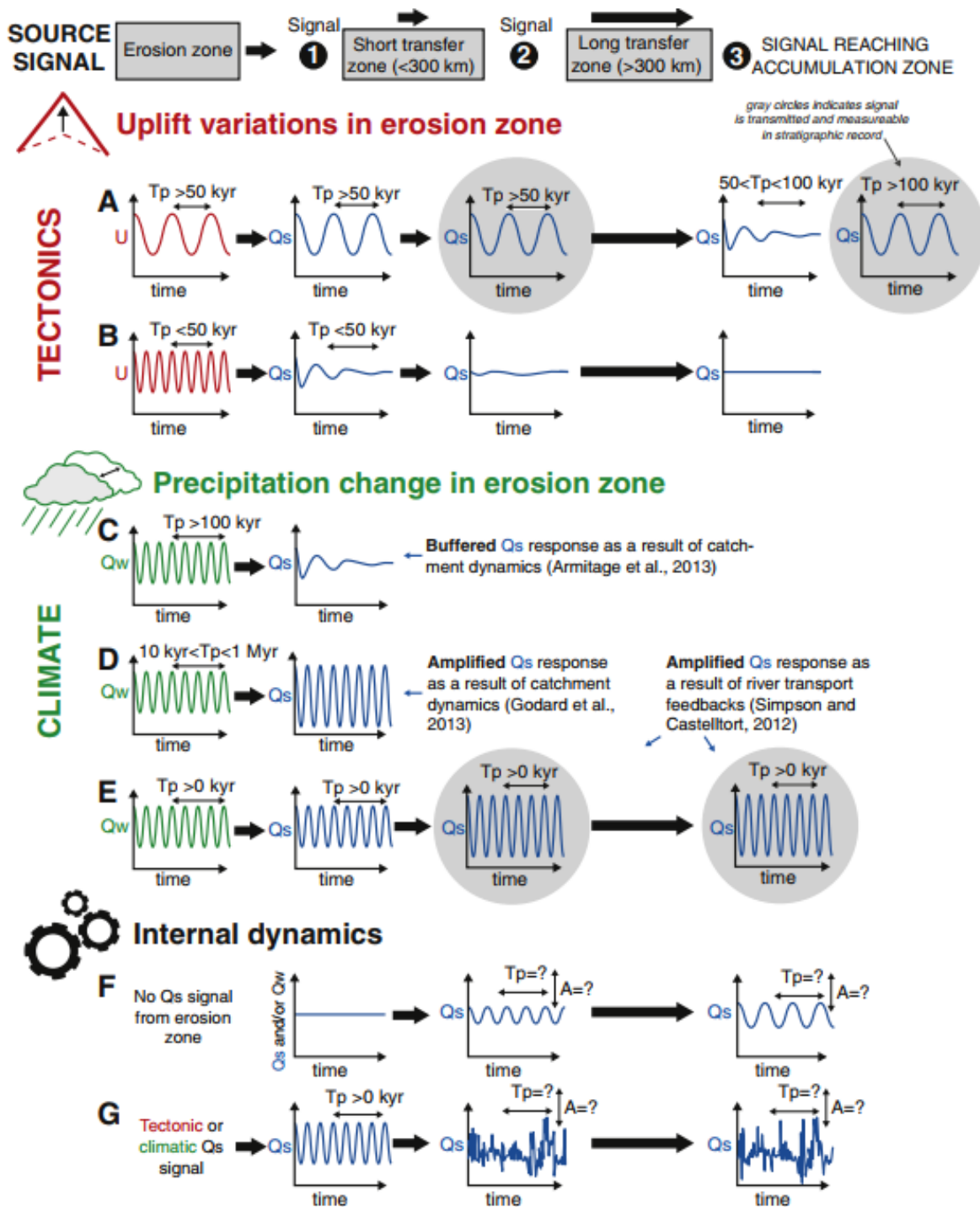


Figure 1.10 – Summary of the sedimentary signal propagation from source to sink at intermediate timescales ( $10^2$ - $10^6$  yr) (from Romans et al. 2016). Sedimentary signal initiated by tectonics variations are only transmitted when the period of these variations are  $>50$  kyr. When variation originate from climatic change, the signal is generally amplified. In addition, the internal dynamic of the sedimentary basin can greatly perturbed the signal.

### 1.1.3 Soil: the origin of the sediment

Sediments are the products of bedrock weathering and are part of the soil profile before their export down the system. The soil profile acts as an efficient sediment storage, representing in reactive systems a non-negligible part of the sediment residence time. As soils represent the main interface between atmosphere and bedrock, shaping the land surfaces, they have become of great interest to study the links between climate, weathering and White & Blum 1995, Riebe et al. 2001, Millot et al. 2002, von Blanckenburg 2006). Additionally, sediment residence times in small and reactive systems mainly represent the time spent by the sediments within the weathering profile, i.e. the soil. For these reasons, a particular attention is given to the soil in the following section to detail its structure and the factors that can control its thickness.

#### Structure of the Critical Zone

The Critical Zone (CZ ; National Reaserch Council Committee on Basic Reaserch Opportunities in the Earth Sciences 2001) refers to that layer at the Earth surface, which connects the deep zone (formed by rocks) and the atmosphere (providing the gas and meteoric waters required for weathering to proceed). The CZ is particularly important as it is where life occurs, supporting biodiversity and sustaining Humanity (Fig. 1.11; Chorover et al. 2007, Anderson et al. 2007). The evolution of the CZ depends on the interaction between physical, chemical, and biological processes (Brantley et al. 2007).

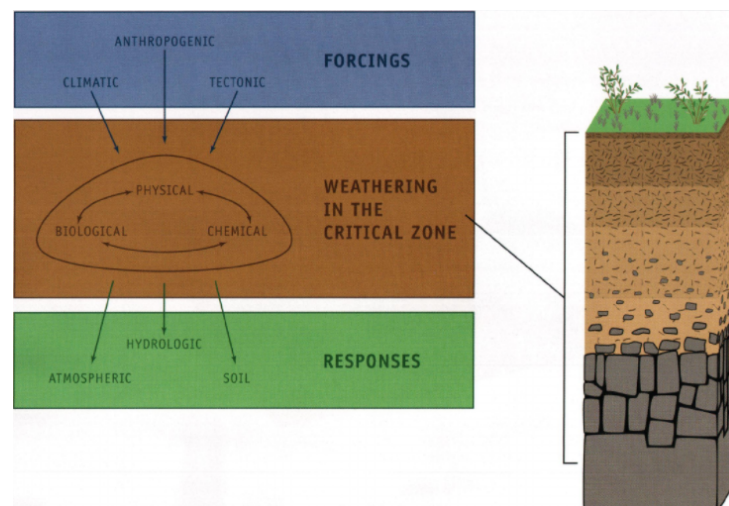


Figure 1.11 – Schematic representation of the Critical Zone and the major forcings influencing the weathering (from Anderson et al. 2004).

The soil is a complex structure above the bedrock, which can be defined differently depending on the discipline. For an engineering point of view, the soil gathers all uncon-

solidated material above bedrock (Bates & Jackson 1987) leaving no distinction between soil and unconsolidated sediments. To differentiate between these two components, Retallack (1984) defined the soil as the immobile part that forms in place, whereas sediments represent the mobile component that is transported beyond the place of its formation. The geomorphologists considered instead the soil as corresponding to the mobile particles within the weathering profile that are no longer binded to the parent rocks (Yoo & Mudd 2008). On the other hand, pedologists and geochemists define the soil as the entire vertical weathering sequence, including both the loose material available for erosion but also that portion of the bedrock that can be highly chemically weathered but still maintains its structural integrity (Yoo & Mudd 2008).

### **Soil thickness: balance between soil production and erosion**

On continents, the thickness of the mobile section of the weathering sequence strongly dependent on soil production and erosion processes. In a system in which soil production rates equals erosion rates, the soil thickness is considered as being at steady state (Carson & Kirkby 1972, Dietrich et al. 1995, Heimsath et al. 1997).

Catchment areas can be categorized into two weathering regimes: weathering- or transported-limited (Carson & Kirkby 1972). Under limited erosional rates, the soil thickens, and the system is referred to as being transport limited. In contrast, whenever soil erosion dominates over soil production, the thickness of the mobile soil sequence is reduced causing ultimately bedrock exposure. In such cases, the absence of soil cover profoundly modifies the landscape dynamics, impacting the hydrology, ecology, and even its anthropic use (Anderson et al. 2007). For this reason, it is important to be able to predict the evolution of the soil.

Over the years, various models have been designed to estimate soil production rates (e.g. Carson & Kirkby 1972, Dietrich et al. 1995, Pelletier & Rasmussen 2009, Catani et al. 2010, Patton et al. 2018). Humphreys & Wilkinson (2007) made an overview of the history on the soil production rate studies with the pioneered work of Gilbert (1877). His general idea later on revisited by Carson & Kirkby (1972) was that soil results from weathering and thus needs weathering agents such as water and frost. The water required for chemical weathering reactions and subsequent soil production need to be temporally stored in soils. Therefore, the soil thickness is important as soil itself is being essential to produce soil. However, when the soil profile is already thick, the weathering agents have difficulties to reach the bedrock, thereby limiting the weathering processes. This results in a soil production law defined as a "humped" function (Fig. 1.12; Cox 1980). However, this model shows limitation for hillslope profiles Davis (1892).

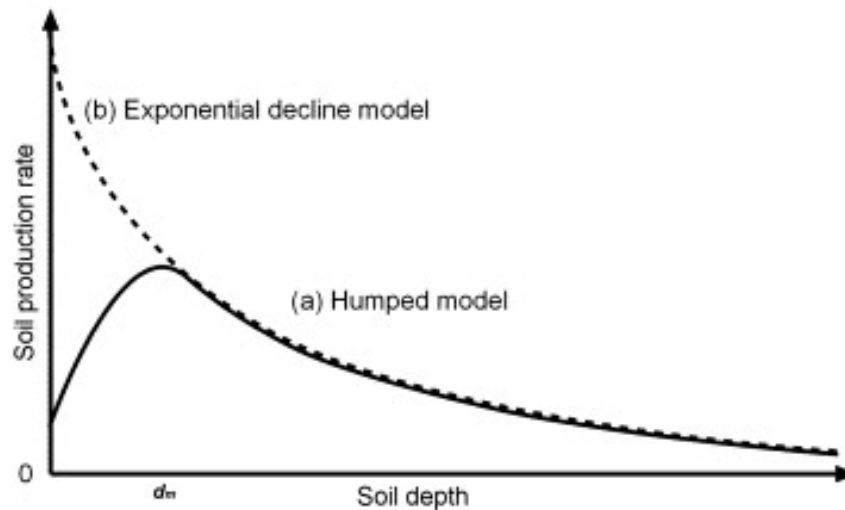


Figure 1.12 – Schematic representation the soil production models: (a) the humped function and (b) the exponential decline function (from Humphreys & Wilkinson 2007).

Davis (1899) presented early the idea that the soil production was inversely correlated to soil depth. Then, it is only during the 1960s that studies focusing on soil production truly emerged with the concept of mass balance (e.g. Ahnert 1967, 1976, Armstrong 1976, Kirkby 1976). It led to the development of a different soil production law from the "humped" function (Culling 1960) with the introduction of the exponential function (Fig 1.12, model b) (Dietrich et al. 1995). This model presented a better correlation with real-situation occurring on hillslope.

In parallel, the advent of several major geochronological tools (e.g.  $^{14}\text{C}$ ,  $^{10}\text{Be}$ ) progressively increased the possibility of providing quantitative constraints on soil production rates, using colluvial fills (Reneau et al. 1989, Reneau & Dietrich 1991, Monaghan et al. 1992, McKean et al. 1993). With the improvement of these analytical tools that subsequently allowed the use of smaller amounts of material, the measurement of in-situ produced cosmogenic nuclides resulted in significant advances in the field. The more recent studies have given arguments for using each of the two soil production laws: "humped" and exponential model without promoting one to the detriment of the other (Dietrich et al. 1995, Heimsath et al. 1997, 1999, Small et al. 1999, Heimsath et al. 2000, 2001a,b, Anderson et al. 2002, Wilkinson et al. 2005, Minasny & McBratney 2006).

During the process of developing soil production laws, the importance of other parameters have emerged: 1. the degree of the comminution of the weathering particles (Davis 1899), 2. transport law of sediment inside the soil (e.g. creep; Anderson et al. 2002), 3. morphology of the hillslope (e.g. slope), 4. climatic and lithologic variability inside the basin. Depending on the thickness of the soils on hillslopes, creep and bioturbation can lead to higher rates of sediment flux compared to thin soil (e.g. Gabet 2000, Heimsath et al. 2005). Therefore, biotic processes and appropriate transport models also need to be

considered (Corenblit & Steiger 2009, Reinhardt et al. 2010, Roering et al. 2010, Richter et al. 2020). Pelletier & Rasmussen (2009) determined a model based on nonlinear depth with slope dependent transport model to predict soil thicknesses in landscapes dominated by creep, bioturbation, and mass movements. The remaining limitation of all these models is the absence of consideration of the variation of weathering rate according to the lithology (Pelletier & Rasmussen 2009) and the vegetation cover, which influence the soil stabilization.

The quantification of the soil production rate is important to understand and predict its evolution through time. However, the quantification of the soil production rate remains challenging over large spatial scale (i.e. large sediment-routing system) because of the internal and external variability along the system (e.g. lithology, climate). In this context, the determination of sediment residence time can bring new perspectives in the soil production studies by quantifying the time spent by sediments inside the soil profile. This is precisely the aim of this thesis: the quantification of the sediment residence time, using the uranium series isotopes, to better understand erosive processes.

## 1.2 Uranium isotopes

Uranium isotope series are the central point of this thesis, as they are used as a tool to estimate sediment residence times in sediment routing systems. Consequently, after a brief history of the uranium isotopes application, the concept required to understand the application of U-series to sedimentary systems are detailed. Finally, this section presents the comminution age theory, applied to determine sediment residence time, and the method required to be able to use this model.

### 1.2.1 Background

The first investigations of the uranium-series began with the initial discovery of the radioactivity in 1896 by Becquerel and the first published version of the radioactive decay scheme by Marie Curie in 1903. The invention of mass spectrometry in 1918 then led to further development of isotope studies. At first, the domain of applications of the uranium (U) series mostly concerned geochronological studies dealing with deep magmatic processes (Newman et al. 1984, McKenzie 1985, Williams & Gill 1989, Hawkesworth et al. 1997, Bourdon & Sims 2003, Condomines et al. 2003), in parallel with investigations related to regolith formation (Rosholt et al. 1966, Megumi & Mamuro 1977) or the dating of carbonate (carbonate terraces: Sharp et al. 2003; marine carbonate: Edwards et al. 2003; corals: Broecker et al. 1968, Mesolella et al. 1969, Edwards et al. 1986, Muhs et al. 1994, Cheng et al. 2000).

The U geochemistry and isotopic composition of marine sediments have been investigated since several decades (Anderson 1982, Anderson & Humphrey 1989, Cochran 1992, Henderson & Anderson 2003). Over the last decades, significant improvements in analytical techniques such as the advent of thermal ionization mass spectrometry (TIMS) and, more recently, since the late 1990s, of multi-collector inductively coupled plasma mass spectrometry (MC-ICP-MS) have enabled the determination of U-series isotopic ratios with much improved precision and the analysis of samples with low U concentration. These analytical advances have made possible the use of U isotopic ratios for the investigation sedimentary processes in source to sink systems (e.g. DePaolo et al. 2006, Dosseto et al. 2008a).

### 1.2.2 Radioactive disequilibrium

In the natural environment, there are three series of radioactive decays that include uranium and thorium isotopes (Fig. 1.13), as a parent nuclide:  $^{238}\text{U}$ ;  $^{235}\text{U}$ , and  $^{232}\text{Th}$ . These three decay schemes end with a final stable isotope of lead:  $^{206}\text{Pb}$ ;  $^{207}\text{Pb}$ ;  $^{208}\text{Pb}$ , respectively. Uranium has three natural isotopes, with different abundance:  $^{238}\text{U}$  (99.27%),

$^{235}\text{U}$  (0.7%) and  $^{234}\text{U}$  (0.03%).

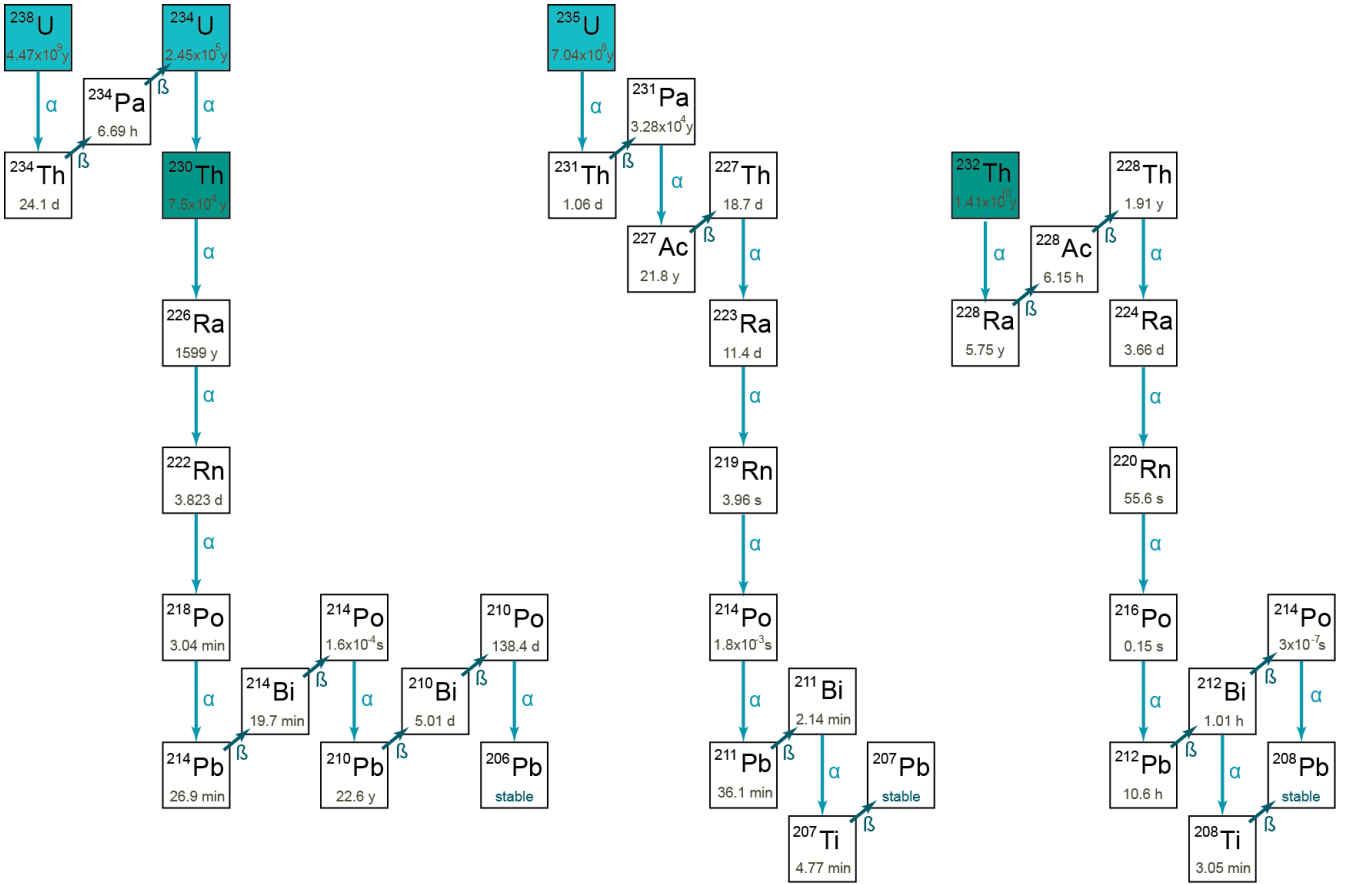


Figure 1.13 – Uranium and thorium natural decays (adapted from Bourdon et al. 2003).

Bateman (1910) was the first to mathematically describe the decay of a given number of atoms ( $N$ ), with the following formula, where  $N_0$  is the initial number of atoms of the nuclide;  $\lambda$  is the decay constant measured in  $\text{yr}^{-1}$ :

$$\frac{dN_1}{dt} = -\lambda N_1 \quad (1.2)$$

The period of radioactivity  $T$ , or the half-life time  $t_{1/2}$  is the time elapsed until the half of the radioactive nuclei initially present have decayed:

$$t_{1/2} = \frac{\ln 2}{\lambda} \quad (1.3)$$

This parameter does not depend on the environment but is linked to the considered radioactive nuclei. For intermediate nuclides of the decay chain  $N_i$  the corresponding equation is:

$$\frac{dN_i}{dt} = \lambda_{i-1} N_{i-1} - \lambda_i N_i \quad (1.4)$$

with  $N_{i-1}$  represents the number of atoms of parent nuclide of  $N_i$ .

For the case of open systems where the input and output of nuclides are not only controlled by the radioactive decay, such as for a given rock submitted to leaching, Latham & Schwarcz (1987) proposed the following equation:

$$\frac{dN_i}{dt} = \lambda_{i-1}N_{i-1} - (\lambda_i + k_i)N_i \quad (1.5)$$

with  $k_i$  being the leaching coefficient of the daughter nuclide (i.e. the portion of the nuclide put in solution by units of time).

### 1.2.3 Secular equilibrium

In a closed system, following an event that resulted in the fractionation of U and Th isotopes in the natural environment (e.g. precipitation of carbonate mineral phases, partial dissolution of silicate rocks), the ratio between the daughter and parent isotopes in the resulting material (e.g. carbonate, weathered sediment) will tend to naturally return to the secular equilibrium due to the radioactive decay (Fig. 1.14).

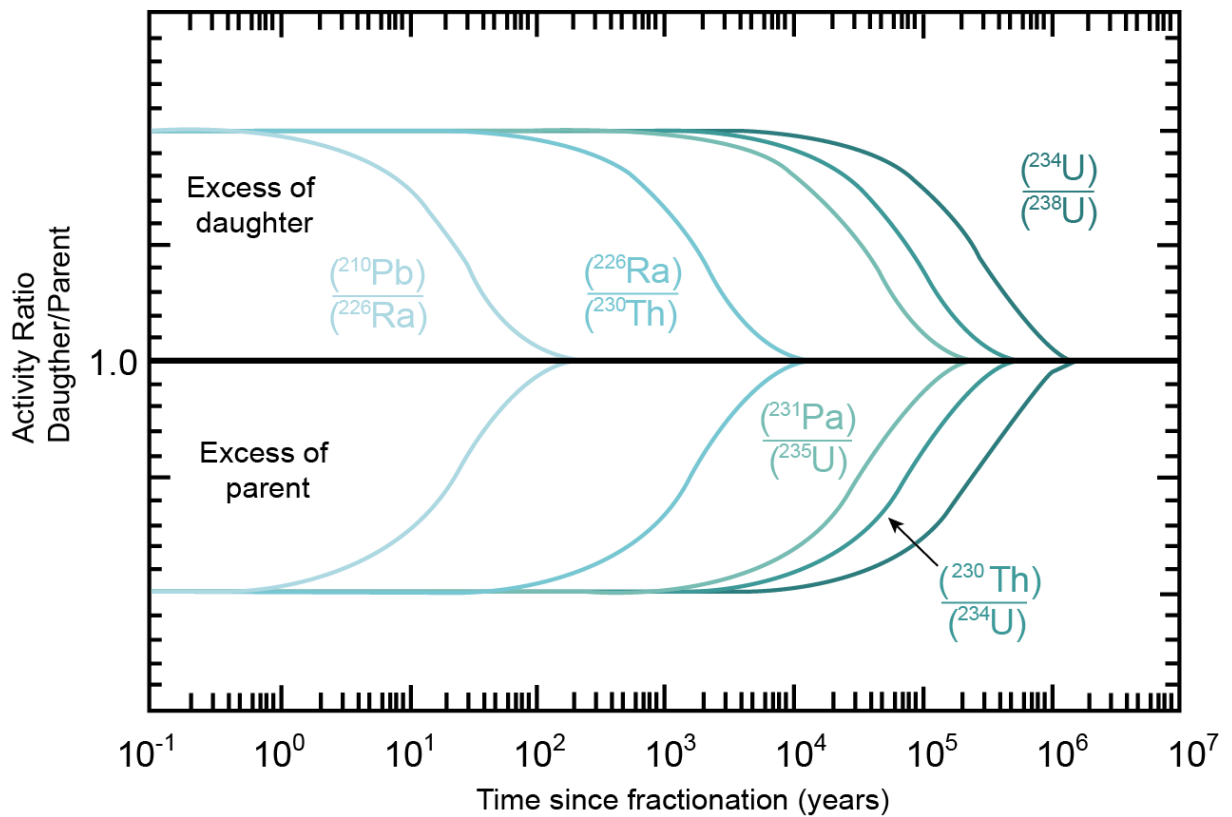


Figure 1.14 – Representation of the evolution of activity ratio of daughter-parents isotopes to return to secular equilibrium in a close system (adapted from Latham & Schwarcz 1987 ).

For the U-series investigations focused on sedimentary processes and associated timescales, the commonly used isotopes are  $^{238}\text{U}$ ,  $^{234}\text{U}$ ,  $^{232}\text{Th}$  and  $^{230}\text{Th}$ . Their half life are respectively  $4.47 \times 10^9$ ;  $2.45 \times 10^5$   $14.01 \times 10^9$  and  $7.5 \times 10^4$  years (Jaffey et al. 1971, Steiger &

Jager 1978, Cheng et al. 2000). In a closed system, which considers that there has been no interaction of U and Th isotopes with the surrounding environment, the time required for the activity ratio between two isotopes to reach the secular equilibrium is equivalent to five times of  $t_{1/2}$  of the daughter nuclide. For instance, for the case of the ( $^{234}\text{U}/^{238}\text{U}$ ) activity ratio, the time needed to reach the secular equilibrium, i.e. meaning ( $^{234}\text{U}/^{238}\text{U}$ ) being equal to 1, is five times  $t_{1/2}$  of  $^{234}\text{U}$ , hence approximately 1.2 Ma. For the ( $^{230}\text{Th}/^{234}\text{U}$ ) ratio, the time required to return to secular equilibrium will be approximately 300 kyr. The quantification of the U-series disequilibrium provides unique information on the timing of the initial U-Th fractionation and of the processes that initially disturbed the secular equilibrium. This approach is particularly useful for investigating processes that occurred at the timescale of the Quaternary period, especially using the following isotopes  $^{234}\text{U}$ ,  $^{230}\text{Th}$ ,  $^{226}\text{Ra}$ .

For clarity, the measurements of U-series isotopes are conventionally reported as ratios of their respective activity, which corresponds to the number of disintegrations per units of time (Bq), calculated as following:

$$(N_i) = \lambda_i N_i \quad (1.6)$$

The parent-daughter activity ratio is also commonly used to study two isotopes:

$$\frac{N_2}{N_1} = \frac{\lambda_2 N_2}{\lambda_1 N_1} \quad (1.7)$$

The delta notation ( $\delta^{234}\text{U}$ ) can also be used and is expressed as:

$$\delta^{234}\text{U} = \left( \frac{\lambda_2 N_2}{\lambda_1 N_1} - 1 \right) \times 1000 \quad (1.8)$$

but it is generally not used in the studies that focused on the timescales of sedimentary processes. For this thesis, the activity ratio notation is used.

#### 1.2.4 Uranium abundances in rock forming minerals and the fractionation of ( $^{234}\text{U}/^{238}\text{U}$ ) in sedimentary systems

Despite the relatively low abundance of uranium in most rocks outcropping at the Earth surface (Dahlkamp 1993), some rock-forming minerals do display higher concentrations than others (Taylor & McLennan 1995). For instance, this is the case for uraninite, which represents the main uranium ore on Earth, but also, to a lesser degree, for minerals such xenotime, monazite and allanite, which are also typically enriched in other trace elements (e.g. rare earth elements). Titanium-enriched minerals are also likely to display high relatively U concentrations, due to the similar ionic radii of Ti and U.

In sedimentary systems, disequilibrium between  $^{234}\text{U}$  -  $^{238}\text{U}$  mostly occurs during water-rock interactions associated with weathering and erosion processes, mostly caused by: 1) the preferential natural leaching of  $^{234}\text{U}$  within the minerals (DePaolo et al. 2006) enhanced by the preferential oxidation of  $^{234}\text{U}$  over  $^{238}\text{U}$ ; and 2) the recoil effect induced by nuclear decay reactions. As a result, all soils, sediments, and fresh waters exhibit uranium activity ratios ( $^{234}\text{U}/^{238}\text{U}$ ) that differ from 1. In the application of the comminution age theory to fine-grained sediments, the assumption is generally made that the recoil fraction is the only responsible for the fractionation of the U-isotopes and natural leaching is then not considered. However, some studies have considered that  $^{234}\text{U}$  leaching can occur and that this process could explain some of the high sediment residence times inferred in particular river basins (Dosseto et al. 2015, Dosseto & Schaller 2016, Martin et al. 2019). Therefore, both processes are briefly described in the section below.

### Chemical fractionation

The behavior of U and Th isotopes results from their own respective chemical properties. U-Th fractionation is controlled by environmental parameters and thermodynamic conditions such as temperature or the composition of the weathering solution (pH, redox potential, ionic strength). Here, a brief overview of the chemical properties of both U and Th is presented to understand their importance in low temperature U-Th fractionation (more detailed reviews of the U and Th characteristics can be found in: Murphy & Shock 1999, Bourdon et al. 2003, Chabaux et al. 2003b).

#### *Uranium*

In earth surface environments, U has two stable oxidation states, which are U(IV) and U(VI) (Fig. 1.15; Langmuir 1978). Under oxidizing conditions, most of the uranium in the natural environment is under its most mobile and stable state: the U(VI) state. In solution, U(VI) produces uranyl ions ( $\text{UO}_2^{2+}$ ), which can complex with carbonates, phosphates, hydroxides and organic ligands (Fig. 1.15; Langmuir 1978). In contrast, in reducing environments, uranium mostly occurs as U(IV), being immobile and precipitating into uranite minerals ( $\text{UO}_2$ ). The U mobility increases with the presence of ligands (e.g. fluorides) at low pH (Fig. 1.15).

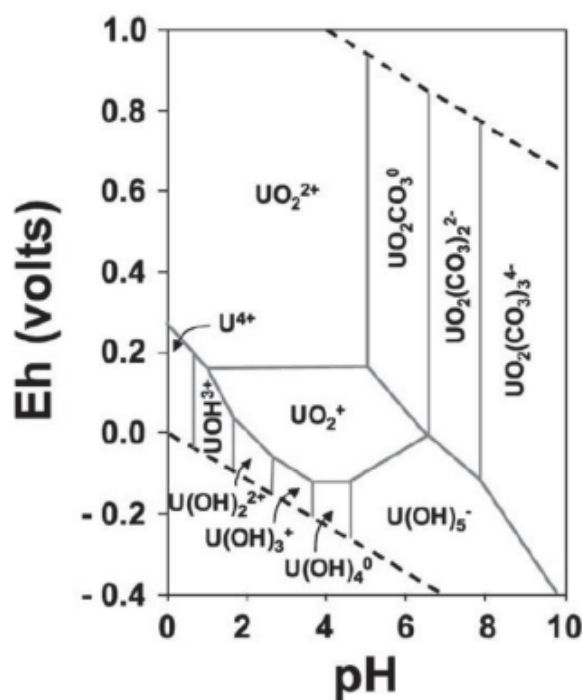


Figure 1.15 – A) Eh–pH diagram representing the stability of the most common U species under the following conditions:  $T = 25^{\circ}\text{C}$ ;  $\Sigma\text{U} = 1 \mu\text{mol/l}$ ;  $p\text{CO}_2 = 10^{-2} \text{ atm}$  (Langmuir, 1978).

In solution, minerals and organic matter can interact on the mobility and fractionation of uranium depending on the type of mineral and the physico-chemical properties of the aqueous solution. The pH of the solution plays an important role in the adsorption of U: a neutral pH will reinforce this process (Pabalan et al. 1996). On the contrary, any increase in temperature will limit the adsorption capacity of uranium (Ames et al. 1983). Uranium can be adsorbed at the mineral surfaces by complexation of the dissolved U phase (Sims et al. 1996), especially by Fe- and Mn-oxides and hydroxides, which are present under secondary particles, inclusions or mineral surface coating (Hsi & Langmuir 1985, Andersson et al. 1998, Blanco et al. 2004). Despite the small amount of U found in Fe- and Mn-oxides (Lee & Baik 2009, Suresh et al. 2014), the control of these secondary phases on uranium mobility is generally accepted (Plater et al. 1992, Blanco et al. 2004, Suresh et al. 2014). Moreover, uranium easily complexes with clays and organic colloids, which are then enriched in U (Dearlove et al. 1991, Porcelli et al. 1997, 2001, Riotte et al. 2003, Blanco et al. 2004, Campos et al. 2013, Suresh et al. 2014, Francke et al. 2018). In addition to having an influence on the mobility of uranium, clay minerals, organic matter and iron oxyhydroxide phases are generally enriched in U from surrounding waters. Thus they inherit their isotopic composition which is enriched in  $^{234}\text{U}$  (Plater et al. 1988, 1992, Andersson et al. 1998, Maher et al. 2006).

### Thorium

In natural environments, thorium exists as  $\text{Th}^{4+}$  oxidation state. It is generally assumed that Th is greatly immobile under neutral pH conditions in fresh waters, but its mobility increases as pH decreases ( $<4$ ). One of the most enriched Th-bearing mineral is thorianite ( $\text{ThO}_2$ ), which is soluble under acidic condition. The mobility of Th also raises in the presence of organic and inorganic ligands (Fig. 1.16; from Langmuir & Herman 1980).

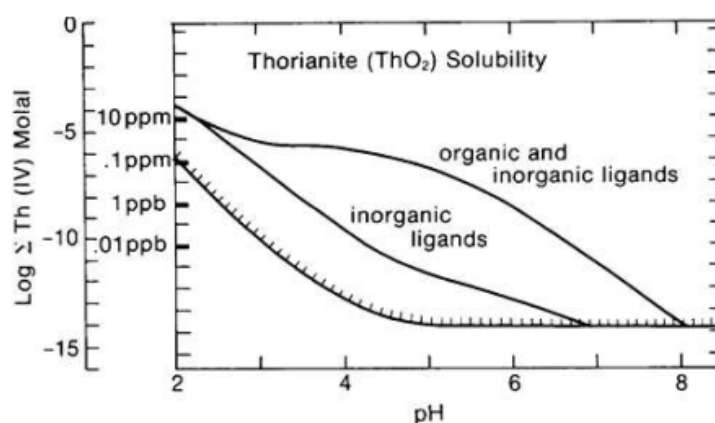


Figure 1.16 – Diagram of thorianite solubility depending of pH in pure water, with organic and inorganic ligands, at  $T = 25^\circ\text{C}$  (from Langmuir & Herman 1980).

As uranium, thorium can be, adsorbed into Fe-oxides and hydroxides (Andersson et al. 1998, Porcelli et al. 2001) and into carbonate minerals and clay minerals (Suresh et al. 2014). Despite its low mobility, dissolved Th concentrations natural waters can be quite significant, due to its complexation and/or adsorption by organic colloids (Fig. 1.16 ; Porcelli et al. 1997, Dupré et al. 1999, Riotte et al. 2003, Blanco et al. 2004, Rihs et al. 2011). Secondary phases, such as clays, and organic matter can be relatively enriched in  $^{230}\text{Th}$ . Indeed, same as for U, these phases are enriched in Th from surrounding waters thus inherit their isotopic compositions (Plater et al. 1992, Suresh et al. 2014). This enrichment is mainly represented in the Fe- and Mn-oxyhydroxides phases.

In conclusion, the particular chemical properties of uranium and thorium isotopes induce in Earth surface environments the preferential leaching of  $^{234}\text{U}$  embedded in recoil tracks (Fleischer 1980, 1982) when a solution fills the pore space (Fleischer 1980, Andersen et al. 2009). The  $^{234}\text{U}$ - $^{238}\text{U}$  fractionation can be enhanced by the preferential oxidation of  $^{234}\text{U}$  in comparison with  $^{238}\text{U}$ . The preferential oxidation is due to the highest probability in minerals with low concentration that  $^{234}\text{U}$  is close to oxygen atoms (Adloff & Roessler 1991) and would therefore be more prone to oxidation to the hexavalent state which is more mobile compared to  $^{238}\text{U}$  (Dosseto et al. 2015).

## Recoil effect

Significant U isotopic fractionation can occur in rocks and detrital sediments during the  $\alpha$ -decay of  $^{238}\text{U}$ , which results in the production of a daughter nuclide ( $^{234}\text{Th}$ ), together with an  $\alpha$  particle and a certain quantity of energy, that can lead to the displacement the daughter nuclide over tens of nanometers (Fig. 1.17). This phenomenon is called alpha-recoil (Kigoshi 1971).

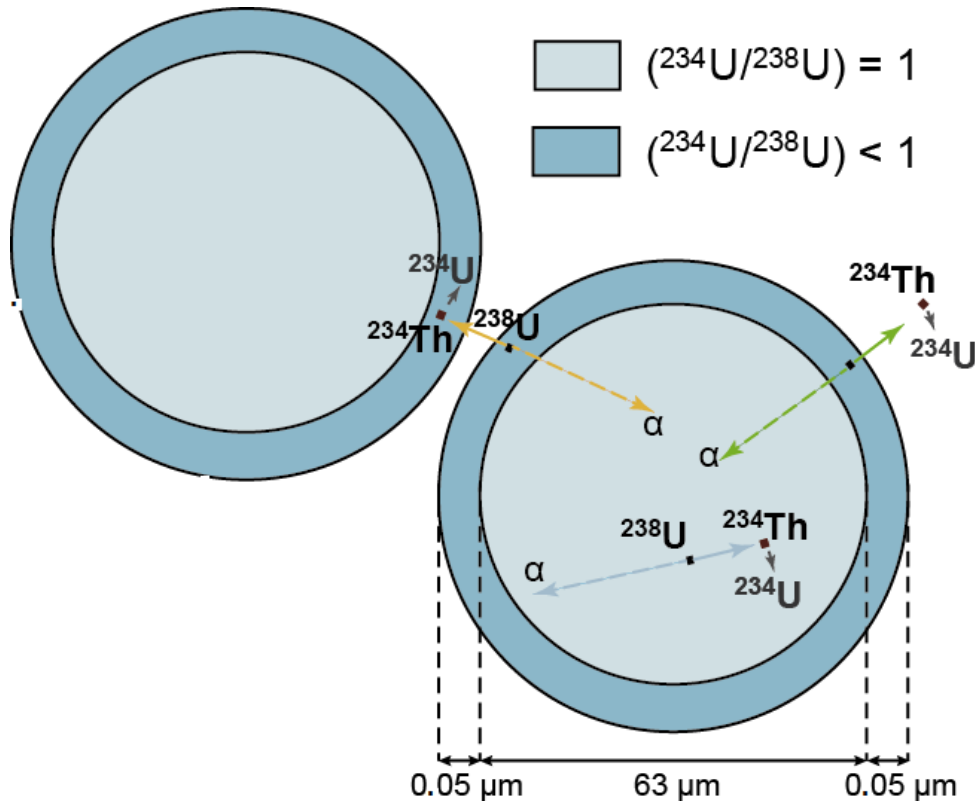


Figure 1.17 – Schematic representation of the recoil during the decay of  $^{238}\text{U}$  into  $^{234}\text{Th}$  (modified from DePaolo et al. (2006)).

The distance of recoil can vary according to the decay energy of the parents nuclide, but also on the density of the studied solid phase. Generally, the distance ranges from 20 to 60 nm (Kigoshi 1971, Bourdon et al. 2003, DePaolo et al. 2006, Chabaux et al. 2008) and is considered to be about 30 nm in most silicate minerals (Maher et al. 2006).

When decay occurs at the grain boundary, the ejected particles are lost from the mineral grain, resulting in an isotopic fractionation (open system), which depends on the distance and the angle of ejection, in relation with the grain surface (Fleischer & Raabe 1978). This capacity is restricted by some parameters such as: the size and the shape of the grains but also by the nature of the matrix (Fleischer 1982). The quantity of emitted nuclides and their half-life are also parameters to be considered. It has been shown that the rejected particles or the integrated nuclide are leached quicker (Fleischer 1988). To summarize, the combined association of the fractionation induced by chemical properties (e.g. preferential

leaching and oxidation of  $^{234}\text{U}$ ) and the recoil loss effect is responsible for the observed variations of U activity ratios measured at the Earth surface. As a result, the soil profiles are generally depleted in  $^{234}\text{U}$ , whereas pore waters and freshwaters in river systems are enriched in  $^{234}\text{U}$  compared to  $^{238}\text{U}$ .

## 1.2.5 The concept of comminution age

This section presents the concept of the comminution age, which represents the time elapsed since the formation of the fine sediment grains until their deposition. It also provides details on the methods required in order to obtain accurate comminution ages from sediments, with a particular focus on the specific surface area measurement.

### Concept

The *comminution age* dating method is based on the disequilibrium between  $^{234}\text{U}$  and  $^{238}\text{U}$  in fine-grained detrital minerals (DePaolo et al. 2006).

As mentioned above, following the disintegration of  $^{238}\text{U}$ , the daughter isotope  $^{234}\text{Th}$ , which rapidly decays into  $^{234}\text{Pa}$  and then  $^{234}\text{U}$ , recoils over a short distance ( $\sim 30$  nm). In the case where the reaction occurs at the edge of a detrital particle, the daughter isotopes are ejected out of the grain, inducing a disequilibrium in the  $^{234}\text{U}/^{238}\text{U}$  ratio. When the grain is small enough and displays a large surface area to volume ratio, the disequilibrium is significant enough to be measured. Following disequilibrium, it then takes about 1.2 Ma for the residual detrital grain to reach secular equilibrium, assuming no subsequent external disturbance. During this period, the measured disequilibrium indicates the time elapsed since the disequilibrium occurred, i.e. which corresponds to the time when the grain was first produced. This dating method is thus based on the  $\alpha$ -recoil effect. The comminution age  $t_{com}$  can be calculated using the equation determined by DePaolo et al. (2006):

$$t_{com} = \frac{-1}{\lambda_{234}} \ln \left[ \frac{A - (1 - f_{\alpha})}{A_0 - (1 - f_{\alpha})} \right] \quad (1.9)$$

with  $A$  is the measured ( $^{234}\text{U}/^{238}\text{U}$ ) activity ratio in any fine-grained sediment,  $A_0$  is the initial ( $^{234}\text{U}/^{238}\text{U}$ ) of the initial rock (i.e. the unaltered bedrock or the grains  $>63$   $\mu\text{m}$ ),  $\lambda_{234}$  is the decay constant of  $^{234}\text{U}$  (in  $\text{a}^{-1}$ ) and  $f_{\alpha}$  is the direct recoil of the fraction. This method considers that only the recoil effect process is important in the fractionation of  $^{234}\text{U}$  over  $^{238}\text{U}$ .

The degree  $^{234}\text{U}$  and  $^{238}\text{U}$  fractionation of can also be different before and after the deposition of the sediment. Therefore, Francke et al. (2018) compared two scenarios: one with no loss of  $^{234}\text{U}$  after deposition ( $f_{post}$ , i.e. the recoil loss factor post deposition =0) and the second with a continuous loss of  $^{234}\text{U}$  after deposition ( $f_{pre}$ , i.e. the recoil loss

factor pre deposition =  $f_{post}$ ), using the following equation:

$$t_{res} = \frac{-1}{\lambda_{234}} \ln \left[ \frac{[A - (1 - f_{post})] e^{-\lambda_{234} t_{dep}} + (1 - f_{post}) - (1 - f_{pre})}{A_0 - (1 - f_{pre})} \right] \quad (1.10)$$

with  $t_{dep}$  the deposition age (yr). Even though they obtained comparable sediment residence time with the two methods (within the error range of each other for the majority of the sample), they considered the second scenario as being the most probable because of the importance of the water content within the samples.

The preferential leaching of  $^{234}\text{U}$  could also have an influence on the degree of U isotope disequilibrium, due to preferential oxidation of  $^{234}\text{U}$  induced by the recoil effect (Adloff & Roessler 1991, Dosseto et al. 2015, Kolodny et al. 2017). To implement the preferential leaching of  $^{234}\text{U}$  processes in the comminution age method, Dosseto & Schaller (2016) modified the equation 1.9 as following:

$$t_{com} = \frac{-1}{\lambda_{234} + \left(\frac{w_{234}}{w_{238}} - 1\right) w_{238}} \ln \left[ \frac{A - \left(\frac{(1-f_{\alpha})\lambda_{234}}{\lambda_{234} + \left(\frac{w_{234}}{w_{238}} - 1\right) w_{238}}\right)}{A_0 - \left(\frac{(1-f_{\alpha})\lambda_{234}}{\lambda_{234} + \left(\frac{w_{234}}{w_{238}} - 1\right) w_{238}}\right)} \right] \quad (1.11)$$

with the leaching coefficients  $w_{234}$  and  $w_{238}$  for  $^{234}\text{U}$  and  $^{238}\text{U}$  (in  $\text{a}^{-1}$ ), respectively. Studies on leaching coefficients from both field and laboratory-based work determined  $w_{234}/w_{238}$  around  $1.2 \pm 0.2$  (Dequincey et al. 2002, Vigier et al. 2005, Dosseto et al. 2006a, 2014, Andersen et al. 2009). Martin et al. (2019) explored the influence of the leaching parameters on the calculated sediment residence time through a Monte Carlo simulation. They obtained younger ages when considering the leaching processes because the direct recoil is then less important. This study pointed out the importance in the determination of the leaching parameters as this effect can result in a bias of ( $^{234}\text{U}/^{238}\text{U}$ ) ratios. Using a similar approach as Francke et al. (2019) to infer the difference of fractionation pre- and post-deposition, Francke et al. (2020) implemented equation 5.1 to determine the  $^{234}\text{U}$  loss effect pre- and post-deposition on calculated sediment residence time. For this purpose, they combined equations 5.1 with 1.11 and proposed the two following equations to compare the obtained sediment residence time:

$$t_{res} = \frac{-1}{\lambda_{234}} \ln \left[ \frac{\left[ A - \left( \frac{(1-f_{post})\lambda_{234}}{\lambda_{234} + \left( \frac{w_{234post}}{w_{238post}} - 1 \right) w_{238}} \right) \right] e^{-\lambda_{234}t_{dep}} + \left( \frac{(1-f_{post})\lambda_{234}}{\lambda_{234} + \left( \frac{w_{234post}}{w_{238post}} - 1 \right) w_{238}} \right) - (1 - f_{pres})}{A_0 - (1 - f_{pre})} \right] \quad (1.12)$$

$$t_{res} = \frac{-1}{\lambda_{234} + \left( \frac{w_{234}}{w_{238}} - 1 \right) w_{238}} \ln \left[ \frac{\left[ A - (1 - f_{post}) \right] e^{-\lambda_{234}t_{dep}} + (1 - f_{post}) - \left( \frac{(1-f_{pre})\lambda_{234}}{\lambda_{234} + \left( \frac{w_{234pre}}{w_{238pre}} - 1 \right) w_{238pre}} \right)}{A_0 - \left( \frac{(1-f_{pre})\lambda_{234}}{\lambda_{234} + \left( \frac{w_{234pre}}{w_{238pre}} - 1 \right) w_{238pre}} \right)} \right] \quad (1.13)$$

The comparison of the sediment residence times calculated with the assumption of post depositional leaching using realistic and extreme leaching factors are in the same range of the sediment residence time obtained without any consideration of leaching processes from Francke et al. (2019). This suggests that the effect of preferential  $^{234}\text{U}$  leaching after the deposition has no real impact on the determination of sediment residence time. Conversely, assuming leaching processes pre-deposition, Francke et al. (2020) obtained lower sediment residence times. The correlation between sediment residence times and climatic parameters decrease with the consideration of  $^{234}\text{U}$  leaching in both modern and paleo sediment residence times (Martin et al. 2019, Francke et al. 2020). Li et al. (2016a) considered that leaching is only important for sediment with residence time  $< 10,000$  years because leaching is only high in young material with very high surface areas. The comminution age are obtained by resolving of one of the equation mentioned above by a Monte-Carlo inversion method. This method allows to simulate the distribution of possible comminution age.

## Method

### Sample treatment

In the natural environment, sediments are composed of a mixture of various detrital, authigenic and organic phases. One important requirement prior to applying the comminution age method to fine-grained sediments is to remove all non-detrital phases, which may strongly influence measured U isotopic ratios. This step is particularly important because any authigenic or organic phases formed from soil pore waters or river waters are likely to be enriched in  $^{234}\text{U}$  due to recoil effect (see section above), hence being characterized by  $(^{234}\text{U}/^{238}\text{U}) > 1$ . However, the isolation of the detrital fraction needs to be done carefully in order to prevent any partial dissolution of the surface of the grains (which

would otherwise induced subsequent recoil loss of  $^{234}\text{U}$  that would biased measured ratios; Martin et al. 2015, Suresh et al. 2014). For this purpose, various sequential leaching protocols have been developed (Lee et al. 2010) and improved over time (Martin et al. 2015, Francke et al. 2018).

### Surface area measurement

The comminution age is mainly based on the depletion of  $^{234}\text{U}$  by recoil ejection. In the ideal case of a spherical mineral grain, the fraction (noted  $f_\alpha$ ) of  $^{238}\text{U}$  decays that is supposed to be ejected by  $\alpha$ -decay of the daughter  $^{234}\text{Th}$  isotope can be estimated with the general geometric equation:

$$f_\alpha = \frac{3}{4} \left( \frac{L}{r} - \frac{L^3}{12r^2} \right) \quad (1.14)$$

with  $L$  being the recoil distance and  $r$  the grain radius. Because grains are not spherical in the natural environment, the recoil loss factor has been considered as function of the grain surface roughness (equation 1.10; Kigoshi 1971, Luo et al. 2000, Maher et al. 2006). It corresponds to the ratio between the specific surface areas of the sediments related to the geometric surface area of a sphere (Helgeson et al. 1984).

$$f_\alpha = \frac{1}{4} LS\rho \quad (1.15)$$

where  $S$  the surface area of the sediment ( $\text{m}^2/\text{g}$ ),  $\rho$  is the density of the solid (generally considered as  $2.6 \text{ g}\cdot\text{m}^{-3}$ ). Compared to the geometrical approaches, as seen in the previous section, this method is not based on assumptions of particles shapes or surface roughness. The surface roughness can be measured using gas sorption technics using Brunauer–Emmett–Teller (BET) theory ( $S_{BET}$ ) (Brunauer et al. 1938). It is based on the concept of adsorption to multiple molecular layers from Langmuir (1918) in order to correlate the adsorption phenomenon to physical properties (e.g. total surface area, pore-size distribution, micropore analysis, porosity) of solid. The surface area  $A$  of an adsorbent is measured using the faculty of an adsorbed gas to cover the monolayer as defined by Brunauer et al. (1938) and Sing (1985):

$$A_s = n_m^a L a_m \quad (1.16)$$

with  $n_m^a$  being the monolayer capacity,  $L$  is the Avogadro constant and  $a_m$  is the area of the adsorbed molecule. The specific surface area,  $a_s$ :

$$a_s = \frac{A_s}{m} \quad (1.17)$$

is the unit mass of adsorbent where  $m$  is the adsorbent mass.

The measurement of specific surface area using the gas sorption method is dependent of the adsorption-desorption isotherms. They can be classified into six groups (Fig. 1.18; Sing 1985). Briefly, the type I isotherms are typical from microporous grains that have small external surface area and large internal surface area. The type II isotherms are the results of non-porous or macroporous solids (the point B refers to the moment where monolayer coverage is done, and multilayer adsorption start). The type III isotherms are not common and are produced by adsorbate-adsorbent interactions. The type IV isotherms exhibit divergence between the adsorption and desorption isotherms, also named hysteresis. The type V isotherms are produced by weak adsorbent-adsorbate interactions and are rare. The last type isotherms VI are also not common and are related to multilayer adsorption in steps on a regular non-porous surface.

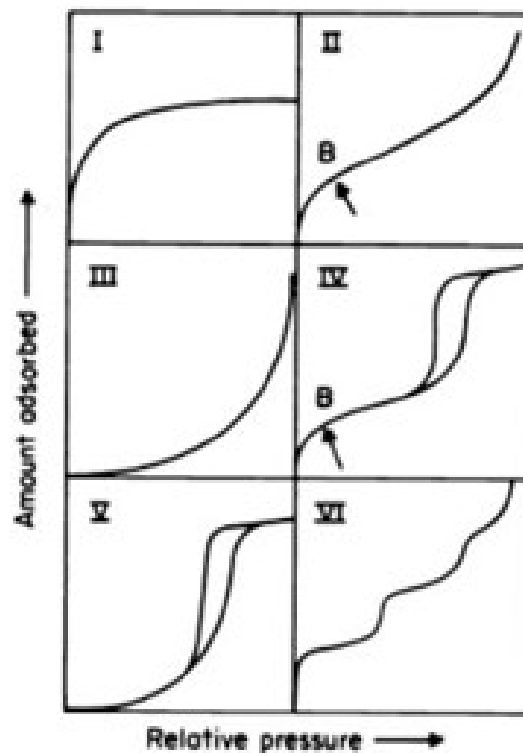


Figure 1.18 – The six types of adsorption-desorption isotherms (from Sing 1985).

The amount of gas adsorbed  $n_a$  at the specific partial pressure of  $P/P_0$  used to determine the surface area can be calculated with the BET equation:

where  $C$  is a constant dependent of the enthalpy of adsorption in the initially adsorbed layer. This equation is applied to the linear plot between  $V$  and  $P/P_0$ , with  $P/P_0$  range 0.05-0.30.

An overestimation of the specific surface area can occur with the BET model, because of the size of  $N_2$  molecule (approximately 0.3 nm) is about two order of magnitudes smaller than the length scale of alpha recoil (Hashimoto et al. 1985). It could overestimate the

recoil loss factor (Maher et al. 2006). In order to overcome this issue, Bourdon et al. (2009) suggested a correction inspired by the work of Semkow (1991) using the fractal dimension  $D$ . The corrected direct-recoil fraction is then calculated with:

$$f = \frac{1}{4} \left[ \frac{2^{D-1}}{4-D} \left( \frac{\alpha}{L} \right)^{D-2} \right] LS\rho \quad (1.18)$$

where  $\alpha$  is the adsorbate gas diameter (in m). The fractal dimension of the surface can be estimated with BET measurement and range from 2 (perfectly smooth surface) to 3 (complexes surface). This correction is only necessary for micro- (<2 nm) or mesoporous sediments (2 – 50 nm), in which the pore size is similar to the recoil length and increase the measured surface area without contributing to the loss of  $^{234}\text{U}$  (Francke et al. 2018).

## 1.3 Uranium at Earth's surface

In this section, I present the application of the uranium isotopes fractionation to study Earth's surface processes. Even if it is not the main focus of this thesis, the first section briefly reviews the main results of the applications of the uranium activity ratio in weathering-related studies, as the importance of soil production rates has already been demonstrated. The second part reviews the comminution age studies to demonstrate the progress in this field and to highlight its limitation.

### 1.3.1 From bedrock to soil: weathering processes

Uranium isotope series have been widely used to study weathering processes (e.g. timescale and regime) using soils (e.g. Mathieu et al. 1995, Dequincey et al. 2002, Dosseto et al. 2008b, 2012, Ma et al. 2010, Chabaux et al. 2013, Suresh et al. 2013), but also suspended and riverbank sediments and dissolved river loads (e.g. Vigier et al. 2001, 2005, 2006, Dosseto et al. 2006a,b, 2008a, Granet et al. 2007, 2010). Because all bedrocks older than 1 Ma are assumed to be at secular equilibrium, any source effect related to changing sediment or water provenance on measured ( $^{234}\text{U}/^{238}\text{U}$ ) ratios is expected to be negligible (Pogge von Strandmann et al. 2006).

The absence of any significant source effect on measured ( $^{234}\text{U}/^{238}\text{U}$ ) inside any river basin under investigation (e.g. Amazon river, Murrumbidgee river) generally indicates that U isotope fractionation during sediment transport can be considered as negligible (Dosseto et al. 2006b, Suresh et al. 2014). Therefore, the measured ( $^{234}\text{U}/^{238}\text{U}$ ) is mainly representative of the depletion occurring along the weathering profile and, with the assumption that weathering is constant at the timescale of soil formation,  $^{234}\text{U}$ - $^{238}\text{U}$  fractionation can be estimated using a continuous weathering model (e.g. Vigier et al. 2001, Dosseto et al. 2006a,b, Granet et al. 2007, 2010, Ma et al. 2010; Fig. 1.19). The model is based on the concentration of any given radioactive isotope as a function of its product by decay from the parent isotope, and loss through its own radioactive decay, in addition to the incorporation of the leaching parameter.

The presence of soil fraction with ( $^{234}\text{U}/^{238}\text{U}$ )  $>1$  within the weathering profile indicates that  $^{234}\text{U}$  can be implemented inside soils grains (e.g. Dequincey et al. 2002, Chabaux et al. 2003b, 2008, Pelt et al. 2008). Therefore, the weathering model has been implemented to consider the potential gain by secondary processes or external input (e.g. Dequincey et al. 2002, Chabaux et al. 2003b, Dosseto et al. 2008a,b, Ma et al. 2010, see Chabaux et al. 2011 for a detailed review).

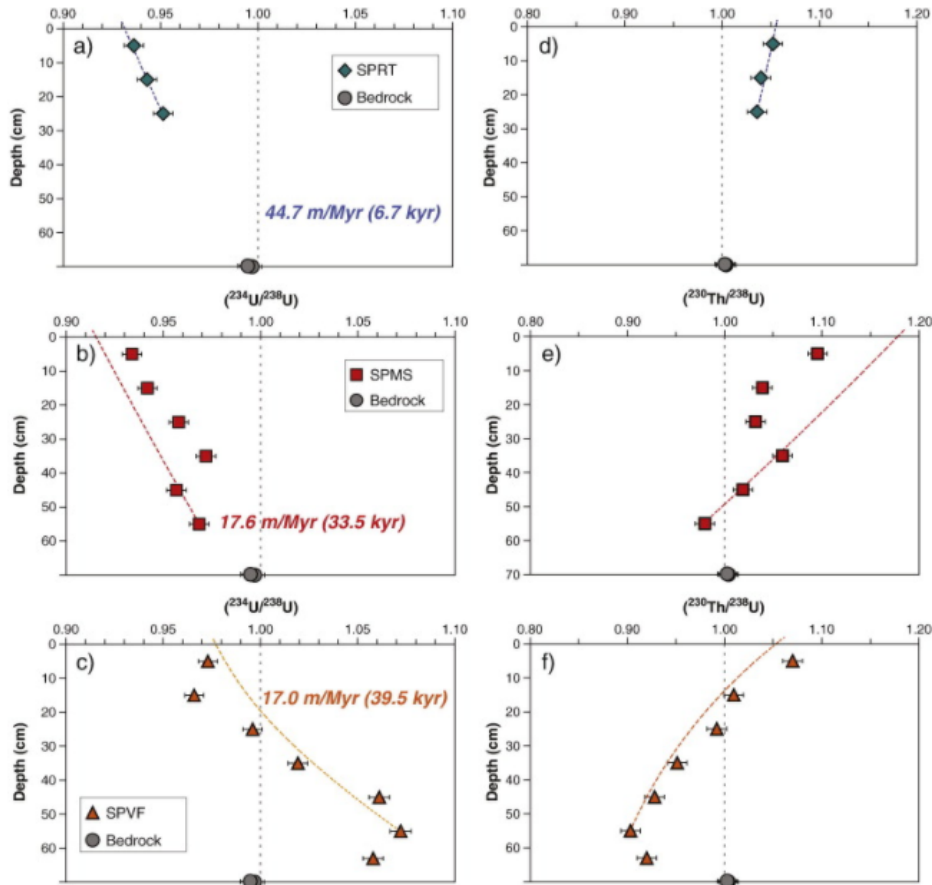


Figure 1.19 – Evolution of the U-series isotopes along weathering profile (Ma et al. 2010) caused by the decrease of mobility of  $^{234}\text{U} > ^{238}\text{U} > ^{230}\text{Th}$ .

The weathering regime can be inferred from the U-series disequilibrium (Moreira-Nordemann 1980, Vigier et al. 2001, Dosseto et al. 2006b) considering that erosion is at steady state, i.e. considering a balance between soil production and sediment export (Milliman & Meade 1983, Trimble 1983). Ackerer et al. (2016) applied this method to the Strengbach catchment (Vosges, France) in correlation with in-situ  $^{10}\text{Be}$  analysis. They identified the bedrock as the most suitable place to determine the soil production rate. They show low U concentrations and high  $(^{234}\text{U}/^{238}\text{U})$  in glacial rivers from Iceland whereas in non-glacial river U concentration are higher with lower  $(^{234}\text{U}/^{238}\text{U})$ . Pogge von Strandmann et al. (2006) attributed these results to the dilution of U in the river with glacial melting while important physical erosion of the soil due to the glacier caused high  $(^{234}\text{U}/^{238}\text{U})$ .

### 1.3.2 Uranium isotopes to infer timescale of sedimentary processes and its control

The comminution age is the time elapsed since the sediment has reached a particle size  $<63 \mu\text{m}$  due to the combination of weathering and physical erosion processes. In fine-grained sediments  $<63 \mu\text{m}$ , the fractionation between  $^{234}\text{U}$  and  $^{238}\text{U}$  is mostly caused by the recoil effect and preferential  $^{234}\text{U}$  leaching is then considered negligible (DePaolo et al. 2006). When this method is applied to alluvial sediments, the comminution age can be taken as representative of the sediment residence time. The comminution age method has been improved over the years in an attempt to address some inherent limitations (e.g. Lee et al. 2010, Handley et al. 2013a,b, Suresh et al. 2014, Martin et al. 2015, Bosia 2016, Francke et al. 2018).

DePaolo et al. (2006) first applied the comminution age method to core sediments from the North Atlantic Ocean. They revealed a correlation between ( $^{234}\text{U}/^{238}\text{U}$ ) and the glacial-interglacial variability inferred from the  $\delta^{18}\text{O}$  foraminiferal record. This cyclicity only applied for the three-last glacial cycles (sediments  $<300$  kyr). The obtained sediment transport times were more elevated during the glacial periods (up to 400 kyr), while being much lower during interglacial periods (within 10 kyr). The longer sediment transport times inferred for glacial periods were explained by the occurrence of sediment redistribution caused either by strong bottom current or glacier activity, which could have transported older sediments (i.e. causing sediment recycling).

In small river basins with high topography, generally characterized by the absence of any alluvial plain (hence with no alluvial storage capacity), the sediment residence time mainly refers to the time spent by the sediment inside the weathering profile and, as a consequence, can be referred to as the *weathering age* (Dosseto et al. 2014). However, Suresh et al. (2014) based on the work of Li et al. (2016a,b). The comparison of sediment residence times for river basins exhibiting markedly different catchment size indicates marked differences. Large sediment residence times (250-600 kyr) were calculated for a mainland China catchment (Yangtze) because of the large storage capacity. Conversely, the comminution age calculated for a small mountainous basin in Taiwan was much lower (110 kyr), due presumably to high denudation rates caused by tectonic uplift and sub-tropical climate conditions characterized by extreme rainfall events.

Dosseto et al. (2010) analysed sediments from various paleochannels with depositional ages ranging from  $15 \pm 2$  to  $100 \pm 9$  kyr in a tributary of the Murray river (SE Australia). They observed a decrease of sediment residence times from 400 to 27 kyr (between the time interval  $>100$  ka to 15 ka) with a sharp increase after 15 ka. These variations were at-

tributed to changes in the sediment source reservoir (upland soils versus alluvial deposits) due to shifts in vegetation patterns. The influence of the vegetation on sediment residence time has also been suggested by Martin et al. (2019), in a study that investigated seven catchments draining the Gulf of Carpentaria basin. This latter study highlighted the climatic influence on sediment residence time, showing a strong degree of correlation with mean annual precipitation ( $R^2 = 0.71$ ), but also with the percentage of vegetation cover, showing that an increase in Eucalyptus and Acacia woodland cover was accompanied by a decrease in the sediment residence time. These findings were also supported by Francke et al. (2019) in a study of a sediment core from the Ohrid lake (Greece), showing that shorter sediment residence times ( $34 \pm 7$  kyrs) occurred during wet periods, and vice versa. A transition occurred between the Early and the Mid-Holocene due to enhanced forest cover, resulting in the stabilization of soils on hillslopes (Francke et al. 2019). On this basis, Francke et al. (2019) considered that the control on sediment residence times switched from precipitation to vegetation cover during that transitional period.

The above-mentioned studies show that sediment residence times display a large variability in river catchments. The first and main control identified for the sediment residence time inside a sediment-routing system is its reactivity, which depends on the storage capacity along the river path and thus the size of the catchment. In small and reactive basins, the influence of tectonics (e.g. Li et al. 2016a), glacier coverage (e.g. DePaolo et al. 2006), climate (e.g. Dosseto et al. 2010) and the vegetation cover (e.g. Martin et al. 2019) have been shown to play an important role on the long-term evolution of sediment residence time. However, as detailed in the next section, this large sediment residence time variability could also partly reflect, at least to some extent, some uncertainties and inherent limitations associated with the sediment residence time estimation method.

### **1.3.3 Uncertainties based on the comminution age method**

The studies of the timescale of sediment processes (weathering, transport, deposition) are based on multiple assumptions. For this reason, it is important to mention all the uncertainties related to the comminution age method (for a more detailed overview see Handley et al. 2013b).

#### **Natural leaching effect and comminution**

The comminution age model is based on the comminution of the bedrock during the weathering. The theory to estimate the comminution age assumes that no further comminution processes occurs after the production of the fine-grained sediment (DePaolo et al. 2006). Therefore, if secondary episode of comminution happens, the inferred age is then considered as a minimal value (Dosseto et al. 2010).

## Bedrock equilibrium

One of the uncertainties in the comminution age method is related to the assumption that the bedrocks older 1.2 Ma are systematically at secular equilibrium (e.g. Dequincey et al. 1999, Dosseto et al. 2006a, Pelt et al. 2013, Suresh et al. 2014). However, ( $^{234}\text{U}/^{238}\text{U}$ ) measurements of bedrock samples are scarce in comminution age studies due to the inherent difficulties to accessing the pristine unweathered bedrock. A few studies have pointed out that some bedrocks could depart from secular equilibrium, corresponding generally to non-volcanic bedrock that otherwise looked pristine and unaltered (Rosholt 1983, Landstroem & Tullborg 2001, Bourdon et al. 2009, Handley et al. 2013b, Martin et al. 2019). While the causes for U-isotopes disequilibrium in pristine rocks remain unclear, this could be possibly related to issues related to porosity or grain-size, at least for the case of sedimentary rocks (DePaolo et al. 2006).

## Grain size and mineralogical effect

The influence of the grain size on measured ( $^{234}\text{U}/^{238}\text{U}$ ) ratios has already been mentioned by DePaolo et al. (2006), who model the sediment residence time decreased with decreasing grain size, in contrast to Dosseto et al. (2014), who reported instead a decrease of the uranium activity ratio with increasing grain size in suspended sediments from the Murray-Darling Basin (from  $<10\ \mu\text{m}$  to  $>25\ \mu\text{m}$ ). The influence of grain size has also been also demonstrated in the Ganges river basin, where coarse sediments exhibit residence times  $>100\ \text{kyr}$  while fine-grained sediments display residence time  $<25\ \text{kyr}$  (Granet et al. 2010). However, Chabaux et al. (2012) attributed this size-dependent ( $^{234}\text{U}/^{238}\text{U}$ ) variation to sample bias. In addition, Bosia (2016) pointed out the importance of the mineralogy in the determination of sediment residence time based on U isotopes. In addition, lithology could play an indirect role on measured sediment residence times, through differences in weathering susceptibility (Dosseto et al. 2014). In large river catchments, with high storage capacity, a particular attention must be also paid to the possibility of a return to secular equilibrium, which can alterate the interpretation of the measured ( $^{234}\text{U}/^{238}\text{U}$ ) (Chabaux et al. 2006, 2012, Granet et al. 2007, 2010).

## Methodologic limitation

Over time, the leaching protocols aimed at isolating the detrital fraction of the sediment have been developed and improved as seen in the section 1.2.5 (e.g. Handley et al. 2013a, Suresh et al. 2014, Martin et al. 2015, Francke et al. 2018). Furthermore, the measurement of the recoil loss is also difficult as seen in the section 1.2.5. As  $S_{BET}$  measurements are time and cost consuming, an estimated value for the recoil loss factor is usually used for calculating comminution ages, but this possibly results in significant uncertainties on calculated sediment residence time.

## **External input**

Finally, another parameter that is not often taking into account in communiton age studies is the possibility of an external contamination via atmospheric and/or anthropogenic (non-natural) detrital inputs (e.g. atmospheric, anthropogenic) (e.g. Pelt et al. 2013).

# METHODOLOGY

## Contents

<b>2.1</b>	<b>Samples collection . . . . .</b>	<b>66</b>
2.1.1	Sediments from world rivers . . . . .	66
2.1.2	Var sediments . . . . .	66
<b>2.2</b>	<b>Samples preparation . . . . .</b>	<b>71</b>
2.2.1	Reagent and labware . . . . .	71
2.2.2	Grain-size separation . . . . .	71
2.2.3	Leaching . . . . .	72
2.2.4	Sediments dissolution . . . . .	76
<b>2.3</b>	<b>Ion exchange chromatography . . . . .</b>	<b>78</b>
2.3.1	Ifremer method . . . . .	78
2.3.2	UOW method . . . . .	80
<b>2.4</b>	<b>Uranium analyses . . . . .</b>	<b>82</b>
2.4.1	Isotopic measurement of Uranium isotopes . . . . .	82
2.4.2	Concentration . . . . .	83
2.4.3	Accuracy and precision of the data . . . . .	84
<b>2.5</b>	<b>Specific surface analyses . . . . .</b>	<b>87</b>
<b>2.6</b>	<b>Geographic Information System analyses . . . . .</b>	<b>89</b>
2.6.1	Basin and sub-basin delineation . . . . .	89
2.6.2	Extraction of the geomorphologic characteristics . . . . .	89

## **2.1 Samples collection**

### **2.1.1 Sediments from world rivers**

The investigation of the ( $^{234}\text{U}/^{238}\text{U}$ ) variability in river sediments is based on a collection of sediment samples gathered at Ifremer over the past few years (e.g. Freslon et al. 2014, Bayon et al. 2015, 2018 ). This large collection includes samples from all around the world, in particular some of the longest rivers (e.g. Amazon, Nile), and other rivers draining particular lithological or climate settings. Most studied samples were collected from river watersheds (riverbank sediments, suspended loads), estuaries, or submarine deltas near the mouth of rivers (Fig. 2.1, Appendix A2.1). The same sediment samples have been previously used in other studies aiming at investigating the links between chemical proxies and environmental parameters, such as rare earth and neodymium isotopes variations (Bayon et al. 2015), Hf-Nd isotopic fractionation (Bayon et al. 2016), Si isotopic variations (Bayon et al. 2018), triple oxygen isotopes (Bindeman et al. 2019).

### **2.1.2 Var sediments**

#### **Modern Var sediments**

The fluvial sediments were collected from the bed of the Var River (S-E France) and its tributaries during two field-trips in June 2011 and September 2012 (Bonneau et al. 2014). The sampling sites were chosen according to the geological and lithological characteristics of each sub-basins. Sediments were also taken upstream and downstream of the main confluences. The location of the sampling sites (GPS source; Appendix A2.2) is shown in Figure 4.3. Fine-grained sediments were separated on-site by washing large quantities of sediments using a 125  $\mu\text{m}$  sieve.

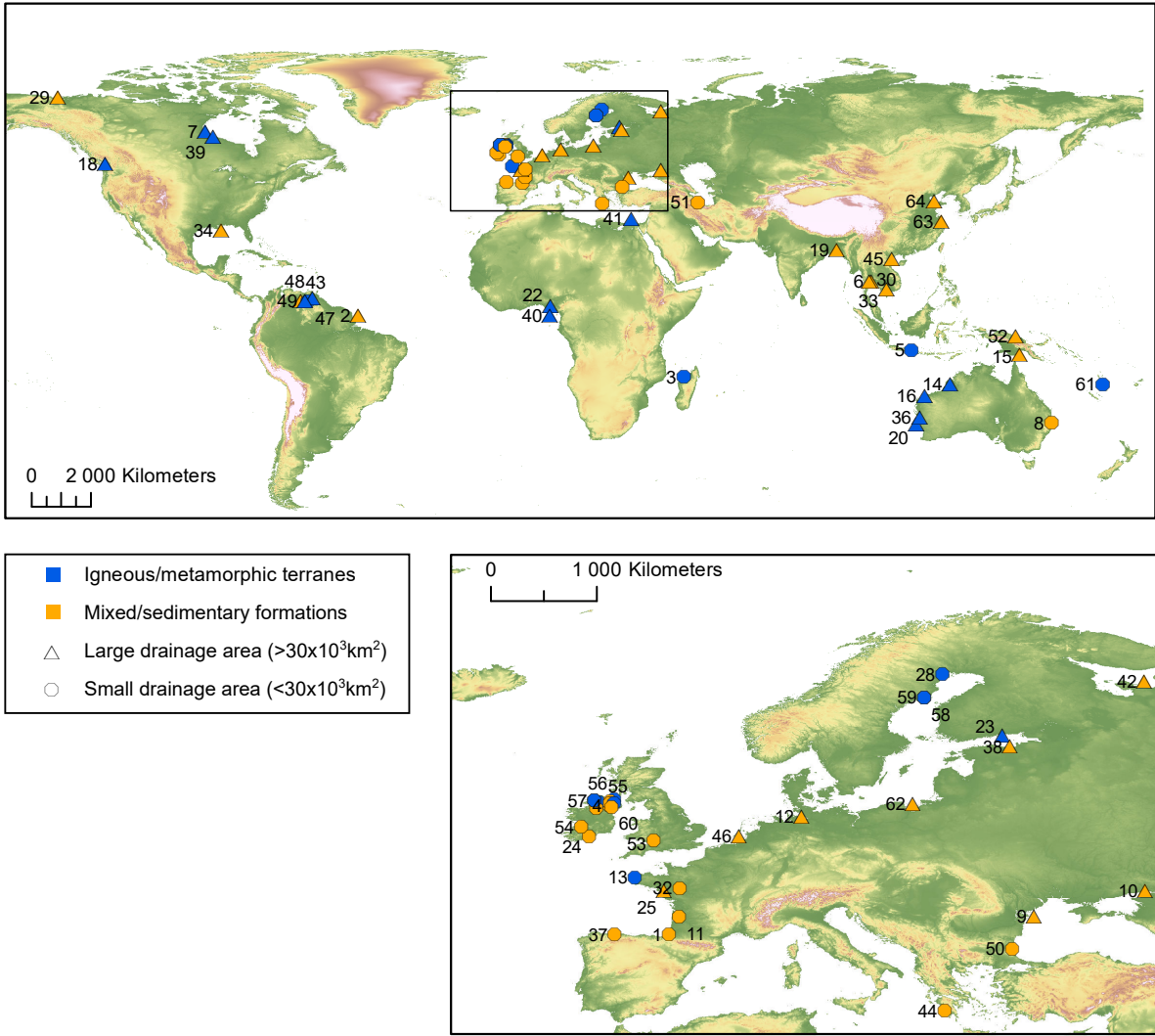


Figure 2.1 – World map with the location of studied sediment samples, the sediments derived from igneous & metamorphic rocks are in blue whereas those from sedimentary and mixed lithologies are in orange. The sediments from large catchments (>30 × 10<sup>3</sup>km<sup>2</sup>) are symbolised by a triangle and those from small basins (<30 × 10<sup>3</sup>km<sup>2</sup>) by a circle. The digital elevation model is derived from the ETOPO1 Global relief Model (<https://www.ngdc.noaa.gov/mgg/global/global.html>).

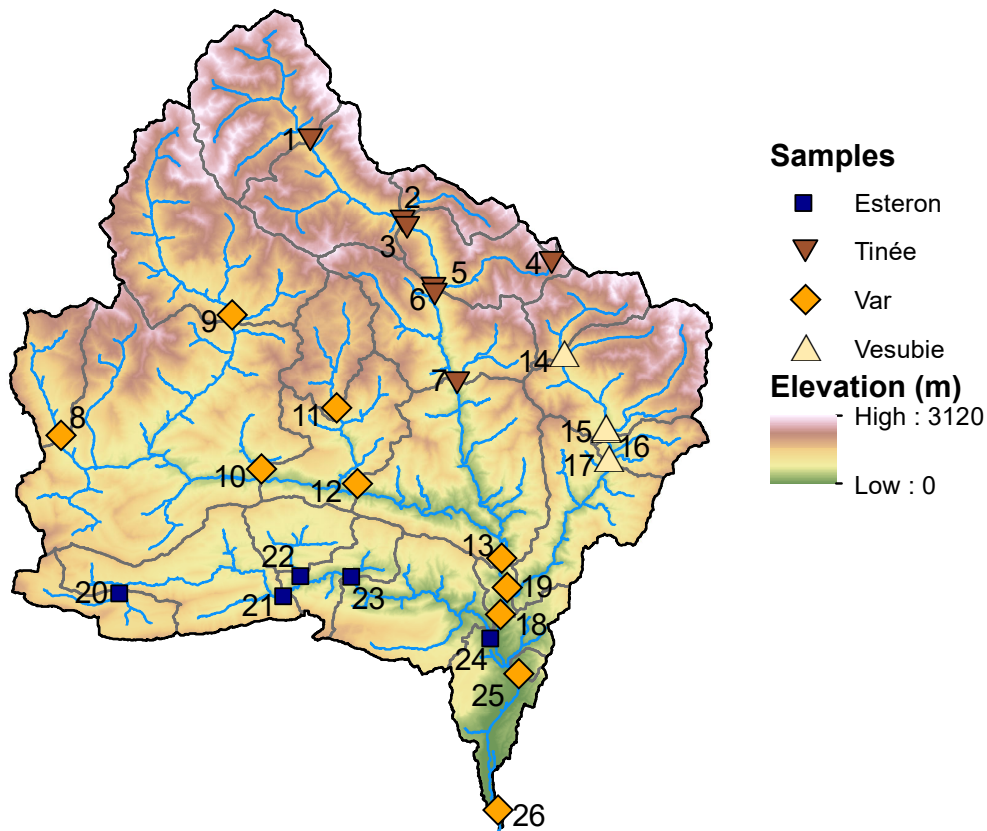


Figure 2.2 – Location of the sediments sampled along the Var River and its tributaries (blue square for the Esteron ;brown triangle for the Tinee ,yellow diamond for the Var and beige triangle for the Vesubie subcatchments) on the digital elevation model (from the French Institute National de l’Information Géographique et Forestière).

### Marine sediments cores

The marine sediment samples investigated during this thesis were collected during two oceanographic cruises. The first one was held in 2008 during the ESSDIV cruise on the *N/O Pourquoi pas?* (Lefort 2008) and allowed the sampling of two of the three marine sediments cores used here (ESSK08-CS01 and ESSK08- CS13). Core ESSK08-CS01 is located on the edge of the Var sedimentary ridge (VSR) whereas the ESSK08-CS13 has been sampled on the southern side of the VSR (Fig. 2.3). The third core (KESC9-14) was retrieved in 2008 during the ESSCAR-9 campaign on the *N/O Le Surort* (Woerther 2008). All these cores were stored at Ifremer (Brest).

Table 2.1 – Table summarising the information on the studied cores.

Core	Cruise	Latitude	Longitude	Water Depths	Length	Levee height
				(m)	(cm)	(m)
ESSK8-CS01	ESSDIV	N43°23.024	E07°44.181	2146	2212	130
ESSK8-CS13	ESSDIV	N43°23.022	E07°47.817	2473	2253	
KESC9-14	ESSCAR-9	N43°.32	E07°18	550	190	

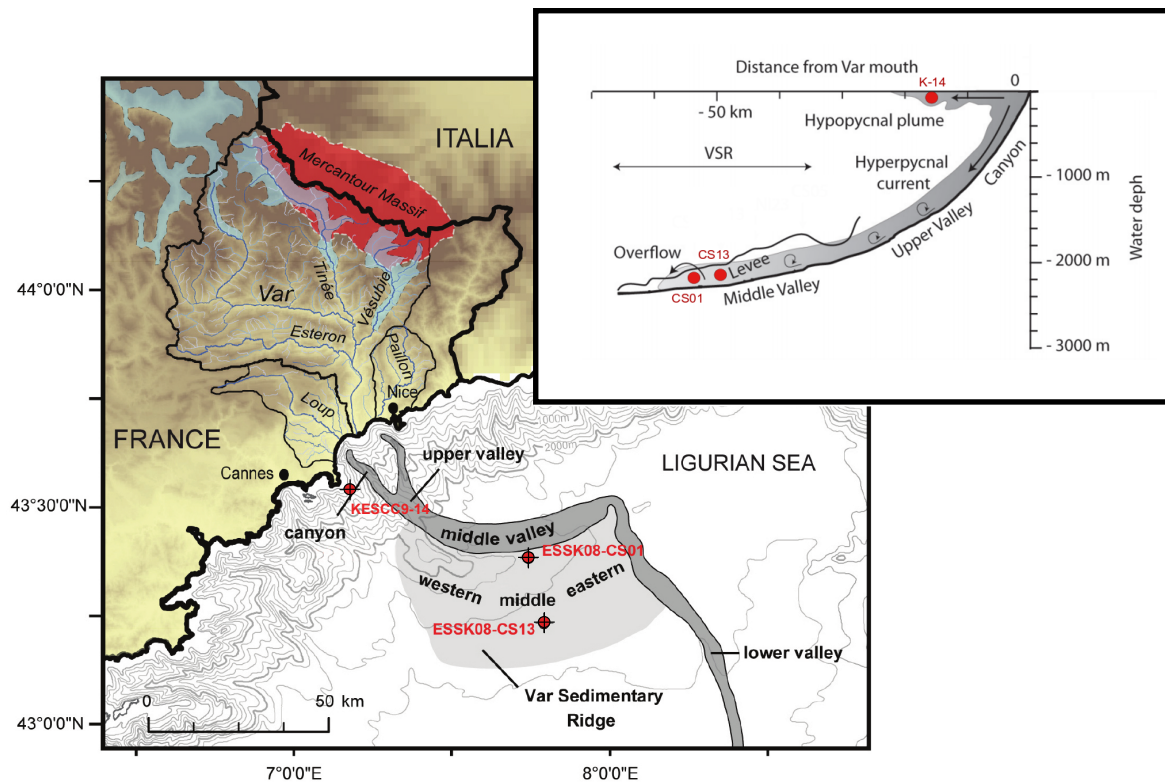


Figure 2.3 – Location of the three studied sites along the Var sediment-routing system with a schematic view of the deposition area of the Var routing system (Adapted from Bonneau et al. 2014).

The age models for cores are derived from ESSK08-CS01 and ESSK08-CS13, and KESC9-14, are derived from Bonneau et al. (2014) and Jalali et al. (2018); Le Houedec, (submitted), respectively. They have been already been exploited in the context of various studies focused of provenance studies Bonneau et al. (2017) and denudation rates (Mariotti et al., 2020). The age model of the three cores being well constrained, it allowed us to elaborate a sampling strategy aiming at analyzing a series of samples deposited during the Late Glacial Period and the Holocene in order to investigate the long-term variability of ( $^{234}\text{U}/^{238}\text{U}$ ) along a continuous composite sedimentary record (Appendix A2.3). It also permitted to study the shorter millennial timescale of the Dansgaard-Oeschger cycles, particularly during the Marine Isotopic Stage 3.

The location of the KESC9-14 core ensured that the studied sediment at this particular

site is derived from the hypopycnal plume, thereby exhibiting a constant and very fine grain size. Conversely, the ESKK08-CS01 and ESKK08-CS13 cores were sampled from the turbiditic levees of the Var Sedimentary Ridge (Fig. 2.4). To avoid any effect linked to grain-size effect in these turbiditic sediments, two different types of sediments were investigated in this study: hemipelagic sediments deposited above the turbidite layers (mainly composed of fine clays) and the uppermost part of the turbiditic sequences (mainly composed of silts).

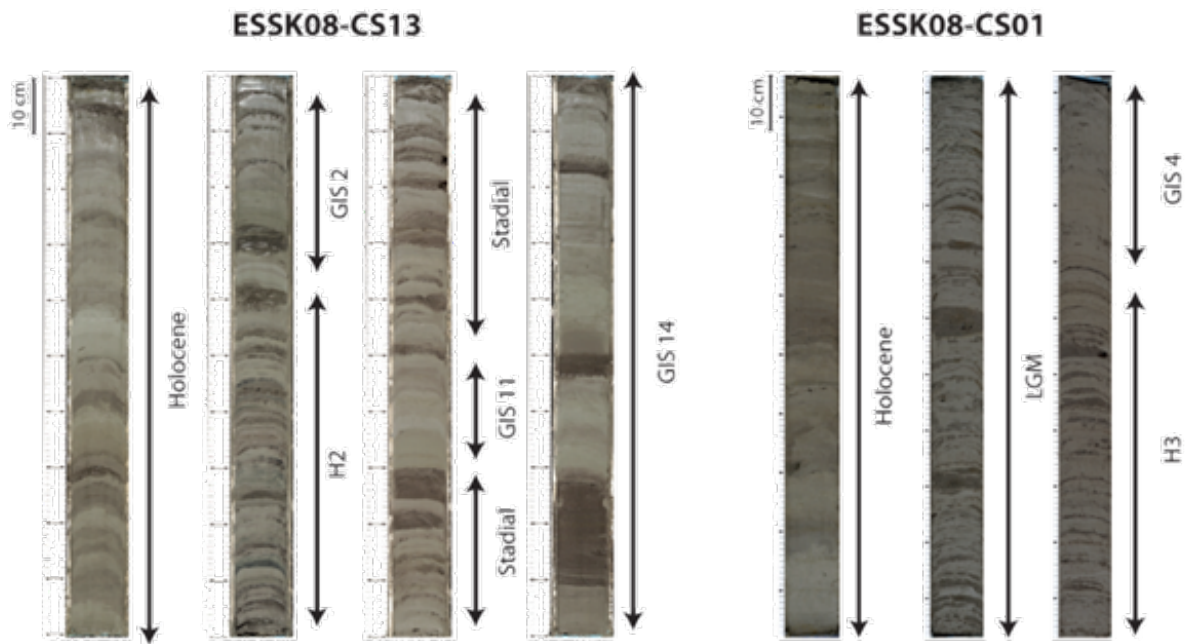


Figure 2.4 – Sedimentary facies observed in cores ESKK08-CS13 and ESKK08-CS01 with fine-grained hemipelagic deposits (light brown) alternating with silt-to sand deposits (dark brown) (from Bonneau 2014).

## 2.2 Samples preparation

### 2.2.1 Reagent and labware

The study dealing with the sediments from the world river systems was performed at Ifremer (Brest, France), with all chemical preparations including the separation and purification of uranium being conducted in a Class 1000 (ISO 6) clean laboratory.  $\text{HNO}_3$  and  $\text{HCl}$  solutions (commercial grade, Merck) were double distilled using a sub-boiling system. Hydrogen peroxide  $\text{H}_2\text{O}_2$  (Trace select, 30%), acetic acid and hydroxylamine from Fisher Scientific (Loughborough, UK) were also used. All diluted reagents were prepared using Millipore Milli-Q water ( $18.2 \text{ M}\Omega \cdot \text{cm}$  at  $25^\circ\text{C}$ ).

The Var sediments, including both fluvial and marine sediment samples, were prepared and analyzed in a Class 10 cleanroom at the Wollongong Isotopes Geochronology Laboratory from the University of Wollongong (Wollongong, Australia). Reagents used during the sequential extraction (acetic acid, hydroxylamine hydrochloride, hydrogen peroxide) and acid dissolution ( $\text{HF}$ ,  $\text{HCl}$ ,  $\text{HNO}_3$ ) were of Ultrapure grade. The reagents used for the column chromatography were of Suprapur grade.

### 2.2.2 Grain-size separation

Because grain size may play an important role in measured uranium activity ratio, an efficient and robust grain size separation method needs to be applied prior to the analyses, aiming at separating the fine  $<63 \mu\text{m}$  detrital fraction.

#### Ifremer methods

About 3 g of dry sediments were placed into 50 mL centrifuge tubes, filled with  $18.2 \text{ M}\Omega$  water and shaken manually. The suspended sediments were sieved at  $<63 \mu\text{m}$  using  $18.2 \text{ M}\Omega$  water.

#### UOW methods

Bulk sediments were first dry sieved in order to only keep the fraction  $<2 \text{ mm}$ . Approximately 10 g of the finest fraction was placed in a 50 mL centrifuge tube with  $\sim 0.25 \text{ g}$  of sodium hexametaphosphate. Each centrifuge tubes were then filled up with around 30 mL of dionized (DI) water and placed on a mixing wheel overnight. The sediments in suspension were then wet sieved using a  $63 \mu\text{m}$  sieve and DI water. The fraction  $<63 \mu\text{m}$  was transferred to a clean centrifuge tube, and the DI water was removed by centrifugation (15 min – 4000 rpm). The  $63\text{-}200 \mu\text{m}$  fraction was removed of the sieved using a clean

plastic spoon and transferred into a clean glass beaker in order to get dry and stored in sample bags.

### **2.2.3 Leaching**

The measurement of uranium isotopic ratios must be made on the detrital fraction of the fine-grained sediment (see section 1.2.5). This means that all bulk sediment samples had to be leached to remove all non-detrital components (e.g. carbonate minerals, Fe-Mn oxyhydroxide phases, and organic compounds) without attacking the specific surface area of the grain. Two different protocols were used during the course of this PhD: the Ifremer's one for the investigation of world river sediments, and that from UOW for all the Var sediments. Both methods are described below.

#### **Ifremer leaching method**

The leaching method used at Ifremer is adapted from Bayon et al. (2002). The same method was used in all previous studies on the same collection of world river sediments (e.g. Bayon et al. 2015, 2016, 2018, Bindeman et al. 2019).

The procedure starts with the separation of the fine fraction ( $<63 \mu\text{m}$ ) from about 3 g of bulk sediment, using ultrapure ( $18.2 \text{ M}\Omega$ )  $\text{H}_2\text{O}$  (see procedure described above) The sequential leaching procedure was then conducted in three steps:

- 1.** The carbonate fraction was extracted by placing the  $<63 \mu\text{m}$  bulk sediment in a 50 ml polypropylene (PP) tube together with 20 ml of 5% (v/v) acetic acid ( $\text{CH}_3\text{COOH}$ ). The tube was placed at room temperature on a mechanical shaker for 3 hours. The supernatant was then discarded by centrifugation.

- 2.** Iron and manganese oxides were removed of the residue left after step 1, by adding 20 mL of a mixture of 0.05M hydroxylamine hydrochloride ( $\text{HONH}_2 \cdot \text{HCl}$ ) in 15% (v/v) acetic acid solution. The tube was left on a mechanical shaker overnight. The supernatant was then removed by centrifugation.

- 3.** The organic fraction was extracted by addition of 20 mL 5% hydrogen peroxide ( $\text{H}_2\text{O}_2$ ). The samples were left on a mechanical shaker for two days. The solution was removed by centrifugation. Then, the silt ( $4\text{-}63 \mu\text{mm}$ ) and clay-rich ( $<4 \mu\text{mm}$ ) fractions were separated from the detrital residues by low-speed centrifugation (Bayon et al. 2015).

After the leaching process, the silt and clay sized fractions were separated by centrifugation following the protocol reported in Bayon et al. (2015). For this purpose, the detrital fractions of the sediment samples were first centrifuged at 1000 rpm for 2 min. The 25

ml supernatant was recovered in a cleaned polypropylene tube, which corresponds to the clay-rich fraction ( $<4 \mu\text{m}$ ). Another 25 mL of 18.2 M $\Omega$  water were then added to the residual detrital fraction, vigorously shake and centrifuged at 800 rpm for 2 min 30 s. The supernatant was added to the initial 25 ml containing the finest clay-size sediment. The residual detrital fractions left in the first centrifuge tube corresponded to the silt fraction (between 4-63  $\mu\text{m}$ ). The clay size fraction was subsequently centrifuged for 15 min at 3800 rpm and then placed in an oven at 70 °C overnight.

### **Evolution of the uranium activity ratio through the leaching steps**

In order to validate the leaching protocol used in this study, the evolution of ( $^{234}\text{U}/^{238}\text{U}$ ) through the different steps of the sequential leaching procedure was investigated as recommended by Lee (2009). The ( $^{234}\text{U}/^{238}\text{U}$ ) ratio of the residual sediment should decrease along with the progressive removal of all carbonate, Fe-Mn oxyhydroxide and organic phases, which are all presumably characterized by ( $^{234}\text{U}/^{238}\text{U}$ )  $>1$  (Fig. 2.5). In theory, the sequential leaching is completed when the outer-core of the mineral grains have been cleaned off any biogenic, authigenic and organic coatings, hence displaying a minimum ( $^{234}\text{U}/^{238}\text{U}$ ). If the residual ( $^{234}\text{U}/^{238}\text{U}$ ) ratio rises during the course of the sequential leaching method, then this indicates that the detrital grain at secular equilibrium (i.e. ( $^{234}\text{U}/^{238}\text{U}$ ) =1) is being dissolved, and hence that the leaching is too aggressive: the remaining grain is at secular equilibrium.

In order to validate the Ifremer leaching protocol for U-isotope analyses, the progressive evolution of ( $^{234}\text{U}/^{238}\text{U}$ ) during the leaching method has monitored using two river sediment samples (Loire and Clarence rivers). To this purpose, after each step of the leaching protocol, an aliquot of the residual sediment fraction was analyzed for U isotopes in both grain-size fractions. Note that a final leaching step was added during these leaching experiments, to ensure complete carbonate dissolution and assess whether the ( $^{234}\text{U}/^{238}\text{U}$ ) minimum value had been previously reached.

The measurements of ( $^{234}\text{U}/^{238}\text{U}$ ) in the Clarence and Loire samples showed that the residual detrital ( $^{234}\text{U}/^{238}\text{U}$ ) compositions decreased progressively during the course of the sequential leaching procedure (from 1.060 to 0.850 ; Fig. 2.6 ), especially for the case of Clarence River sample, indicating that the non-detrital  $^{234}\text{U}$ -enriched phases have been efficiently removed during our leaching procedure. Importantly, the final leaching steps were not accompanied by any ( $^{234}\text{U}/^{238}\text{U}$ ) increase in the residual detrital fractions, suggesting negligible dissolution of pristine detrital minerals at secular equilibrium.

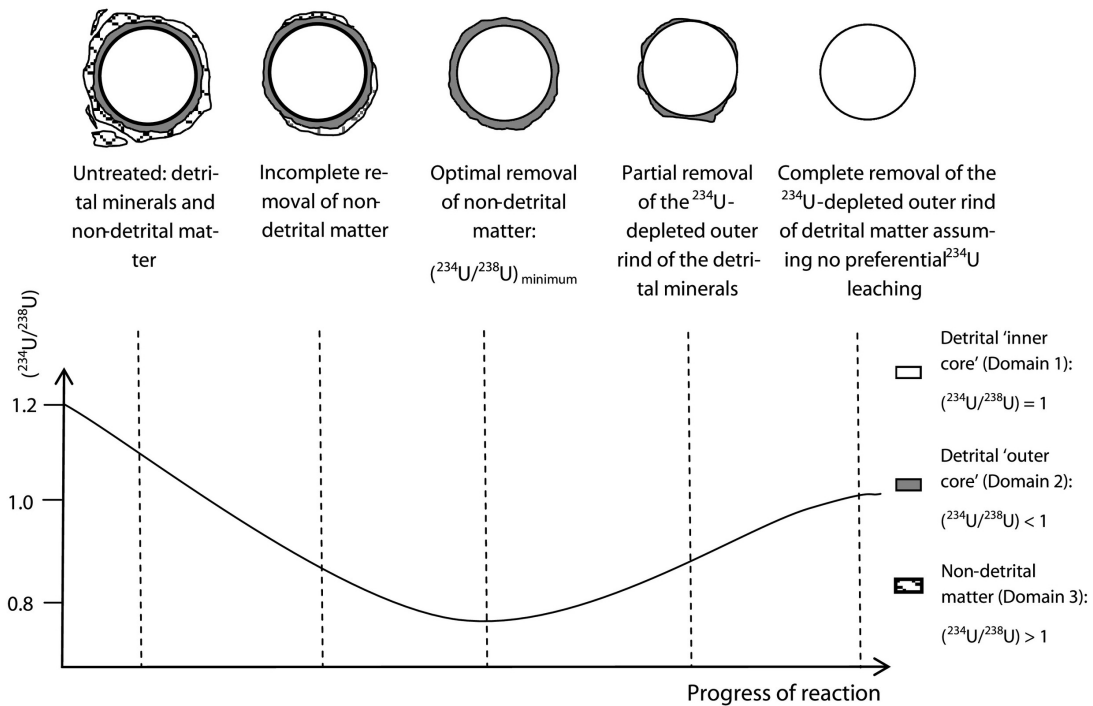


Figure 2.5 – Representation of the modeled evolution of  $(^{234}\text{U}/^{238}\text{U})$  after the removal of the authigenic and organic matters (Domain 3) from sediments. The optimal leaching end when the non detrital matters is completely removed without damaging the outer detrital phase (Domain 2) which correspond to the minimum value for  $(^{234}\text{U}/^{238}\text{U})$  (From Francke et al., 2018; after Lee, 2009 and Martin et al., 2015).

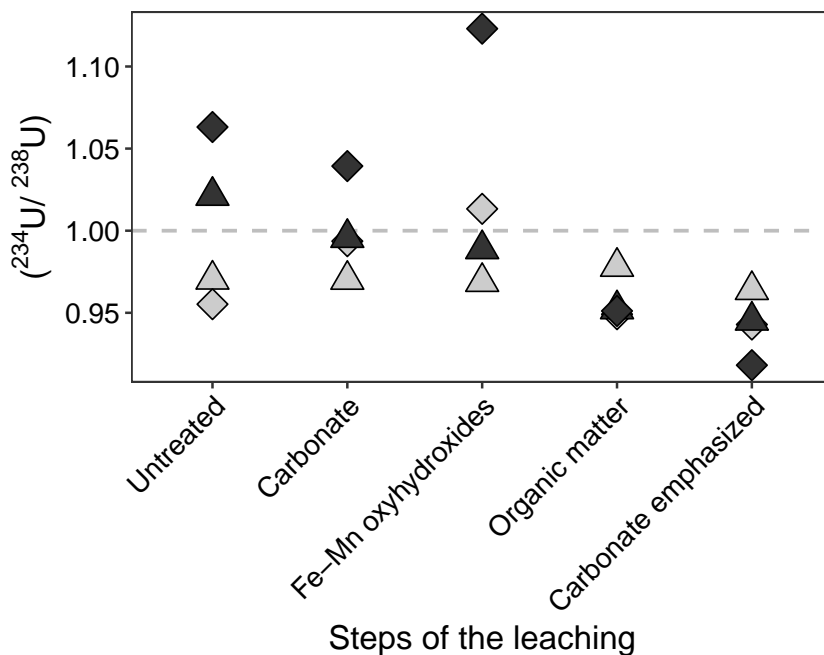


Figure 2.6 – Depletion of  $(^{234}\text{U}/^{238}\text{U})$  following the successive leaching steps for Clarence (dark grey) and Loire (light grey) sediments for silt (triangles) and clay (diamonds) size fractions. 2S.E. errors are smaller than the symbol size. The dashed line represents the secular equilibrium  $(^{234}\text{U}/^{238}\text{U}) = 1$ .

Note that a second test was also conducted to assess whether a possible fractionation could occur between  $^{234}\text{U}$  and  $^{238}\text{U}$  during the leaching method. To this purpose, two geological reference materials (BCR-2 and BHVO-2), with known ( $^{234}\text{U}/^{238}\text{U}$ ) ratios, were leached and analyzed. The obtained ( $^{234}\text{U}/^{234}\text{U}$ ) are within the error range of the accepted values (BCR-2:  $1.006 \pm 0.004$  and BHVO-2:  $1.006 \pm 0.002$ ), hence showing that our leaching method does not involve any particular ( $^{234}\text{U}/^{234}\text{U}$ ) fractionation.

### **Sonication leaching – UOW method**

The method used during the process of the Var sediment samples was developed by Francke et al. (2018) in the Wollongong Isotopes Geochronology Laboratory (WIGL) of Wollongong University. This method is rapid, hence allows to process large datasets of samples.

The sequential leaching procedure involves five distinct steps.

- 1.** The first step was used to remove the water-soluble fraction. Approximately 1 g of dry sediment were placed into 50 mL PP centrifuge tubes with 35 mL of water. The centrifuges tubes were shaken manually and then placed on a mixing wheel for minimum 1 hour. In order to remove the water, they were centrifuged at 4000 rpm for 10 minutes and the supernatant was then discarded.
- 2.** The second stage corresponds to the removal of the exchangeable fraction. For this purpose, 16 mL of 0.5M magnesium nitrate ( $\text{Mg}(\text{NO}_3)_2$ ) was added to each centrifuge tubes inside a fume hood. The centrifuge tubes were manually shaken and then sonicated 3 min at 20°C. The sediments were centrifuged at 4000 rpm for 10 min and the supernatant was discarded.
- 3.** The third step corresponds to the removal of the carbonate fraction. In each centrifuge tubes, 20 mL of 1M sodium acetate (NaOAc) solution was added. Each tube was manually shaken and then sonicated for 15 min at 20°C, taking great care to release any overpressure every 5 minutes by opening the tubes. They were centrifuged at 4000 rpm for 10 minutes to remove the supernatant. The centrifuges tubes were filled with water, shaken and centrifuged again at 4000 rpm for 10 min in order to rinse the residual fraction. The sediments were transferred in PFA centrifuges tubes for the rest of the procedure by adding approximately 15 mL of water. Once transferred, the solution was removed after centrifugation at 4000 rpm for 15 min.
- 4.** The fourth step was conducted to extract Fe and Mn oxide phases. About 20 mL of the 0.1M Hydroxylamine hydrochloride ( $\text{NH}_2\text{OH}\cdot\text{HCl}$ ) solution was added in the PFA centrifuge tubes. They were shaken until all sediments were in suspension and sonicated

for 18 min at 80°C with releasing the pressure every 6 minutes and shaken then manually. The samples were then cooled off by putting the tubes in cold water for few minutes. The sediments were centrifuged at 4000 rpm for 10 minutes and the solution is removed and rinsed with 40 mL of water which was then removed by centrifugation at 4000 rpm for 15 min.

5. The final step aimed at removing organic matter and sulphides. A quantity of 26 mL of 15% hydrogen peroxide (H<sub>2</sub>O<sub>2</sub>) and 0.02 M nitric acid (HNO<sub>3</sub>) solution was added to each PFA centrifuge tube. They were then transferred into an ultrasonic bath for a total of 6 times of 3 min each. Between each sonification period, the pressure was released. Whenever the reaction was too strong, the tubes were placed under cold water. Following the final ultrasonication step, the solution was removed after 10 minutes of centrifugation at 4000 rpm. In all samples, 5 mL of 3.2M ammonium acetate (CH<sub>3</sub>COONH<sub>4</sub>) in 20% v/v HNO<sub>3</sub> solution was added to completely recover the uranium leach from the previous solution. The tubes were manually shaken for 1 min and the solution was decant after 10 min of centrifugation at 4000 rpm. The sediments were transferred into PP tubes back, and rinsed three times with 18.2 MΩ-H<sub>2</sub>O, followed by centrifugation. The residual sediments were then air dried inside a fume hood.

### Comparison of the two-leaching protocol

In order to compare the two leaching protocols used during the course of this PhD, the same sediment samples used by Francke et al. (2018) to develop the UoW sequential leaching protocol were analyzed using the Ifremer's method. After each steps of the sequential leaching procedure, a fraction of the residue was removed to analyze the evolution of (<sup>234</sup>U/<sup>238</sup>U) during the procedure. The (<sup>234</sup>U/<sup>238</sup>U) values obtained for these two test samples using the Ifremer protocol agree well (<5 % of difference) with the data obtained using the procedure of Francke et al. (2018).

## 2.2.4 Sediments dissolution

### Alkaline digestion in furnace

The dry powders of detrital fractions were dried in an oven at 70°C for 24 hours to remove all humidity. About 0.100 g of a mixed <sup>229</sup>Th-<sup>236</sup>U tracer-solution (composition in Table 2.2) was added into a cleaned glassy carbon crucible and evaporated on hotplate. Then about 0,050 g of detrital sediment was added in the crucible together with ~0.300-0.500 g of sodium hydroxide pellets (NaOH) and ~0.800 g of sodium peroxide powder (Na<sub>2</sub>O<sub>2</sub>). The crucibles were placed into an furnace at 650°C for 12 minutes. After alkaline fusion, 10 mL of water 18.2 MΩ-H<sub>2</sub>O was added into the cooling crucible. The mixture was transferred into a polypropylene 50 ml centrifuged tubes, and each crucible was cleaned

with 18.2 MΩ-H<sub>2</sub>O, added to the centrifuge tube to reach about 30 mL, which resulted in the co-precipitation of Fe-oxyhydroxides, scavenging both Th and U (Bayon et al. 2009). The obtained mixture was centrifuged first for 2 min 30 at 2500 rpm then the supernatant was removed. The mixture was rinsed with 30 mL of 18.2 MΩ-H<sub>2</sub>O, stirred, and then centrifuged again for 3 min at 3000 rpm. The supernatant was discarded, and the residues were then taken 2 ml of 7.5M HNO<sub>3</sub> prior to being transferred in acid cleaned 15 mL Savillex vials.

Table 2.2 – Composition of the tracer-solution used at Ifremer and WIGL

	<sup>229</sup> Th (g/g)	<sup>236</sup> U (g/g)
Spike UOW	1.09 x10 <sup>-09</sup>	4.41 x10 <sup>-10</sup>
Spike Ifremer	3.92 x10 <sup>-10</sup>	3.34 x10 <sup>-08</sup>

### Hydrofluoric acid digestion

In each 30 mL PFA vials, about 30 mg of mixed <sup>236</sup>U-<sup>229</sup>Th tracer-solution (composition in Table 2.2) was added with 30 mg of sediments. Note that a diluted tracer-solution was used for the blank. For sample digestion, 1 mL of 48% Hydrofluoric acid (HF) was added. The vials were closed and left at room temperature for about 30 min. Then, 0.5 mL of 65% HNO<sub>3</sub> was dispensed. The closed vials were placed on a 100°C hotplate for overnight. Next, they were sonicated for 10 minutes and put on a hotplate for evaporation at 100°C until incipient dryness. Then, 0.5 mL of 65% HNO<sub>3</sub> and 1.5 mL of 30% HCl were added. The vials were closed and placed on a hotplate at 120°C and left for three days. The samples were dried down at 100°C. If undissolved residues were observed before evaporation a final step was added. It consisted of an addition of 0.5 mL of 31% of H<sub>2</sub>O<sub>2</sub> and left on a hotplate at 80°C for overnight. The samples were then dried down at 80°C. After that, 0.5 mL of 65% HNO<sub>3</sub> was added and then dried at 80°C. This step was repeated twice. Then, 2 mL of 7M HNO<sub>3</sub> was added in each vial and left on a 100°C hotplate for one hour. After 5 min of sonification, the solution was transferred into 15 mL polypropylene centrifuges tubes. They were centrifuged at 4000 rpm for 5 minutes before the uranium elution step.

## 2.3 Ion exchange chromatography

The isolation and purification of the U and Th fractions from the matrix was achieved by ion-exchange chromatography. The methods used at Ifremer and UOW are described below.

### 2.3.1 Ifremer method

The chromatographic protocol to separate uranium and thorium fractions is derived from Edwards et al. (1986) and Bayon et al. (2009). The elution was performed by ion exchange chromatography using an AG1-X8 resin (Biorad 200-400 mesh) in 10 mL columns. Following the protocol (Table 2.3), the resin was first cleaned with both MQ water and 6M HCl, before conditioning the resin with 7.5M HNO<sub>3</sub>. The samples could then be load on the column in 2 ml 7.5M HNO<sub>3</sub>. The matrix was subsequently washed in 7.5M HNO<sub>3</sub>. After that the Th fraction was recovered in 6M HCl, followed by the elution of U with 18.2MΩ-H<sub>2</sub>O.

Table 2.3 – U and Th separation protocol (adapted from Edwards et al., 1986)

Steps	Volume	Reagent
Clean	10	mL 18.2MΩ-H <sub>2</sub> O
	10	mL 6M - HCL
	10	mL 18.2MΩ-H <sub>2</sub> O
Conditioning	2	mL 7.5M - HNO <sub>3</sub>
	2	mL 7.5M - HNO <sub>3</sub>
Loading sample	2	mL 7.5M - HNO <sub>3</sub>
Clean	2	mL 7.5M - HNO <sub>3</sub>
	2	mL 7.5M - HNO <sub>3</sub>
Elution Th	1	mL 6M - HCL
	1	mL 6M - HCL
	1.5	mL 6M - HCL
	1.5	mL 6M - HCL
Elution U	2	mL 18.2MΩ-H <sub>2</sub> O
	2	mL 18.2MΩ-H <sub>2</sub> O
	2	mL 18.2MΩ-H <sub>2</sub> O
	2	mL 18.2MΩ-H <sub>2</sub> O

In order to assess the reliability of this protocol for analyzing river sediment samples (i.e. silicate matrix), three samples: two river sediments (Loire and Fly) and one carbonate were processed for column calibration. Each of these three test samples were first prepared

as explained in section 2.2 , using  $\sim 80$  mg of powder. To verify the reuse of the resin the Loire sediments were split into two parts: one being eluted through a resin already used several times, and the other one through a new resin. All the eluted fractions after the load of the samples were recovered. The Fly sediment was also split into two parts. The first one was eluted through an old resin and each fraction have been recovered. The second part has been used for a regular separation such as the carbonate sample, and only the fraction with the uranium elution was recovered. For the column calibration, 1 ml aliquots of eluted solution were collected during the entire U-Th separation chemistry, and subsequently analyzed by Q-ICPMS at the Pole Spectrometrie Océan (Brest, France), following the protocol detailed in section 2.4.2.

The resulting elution profile (Fig. 2.7) indicated that a fraction of Th was still being eluted during the recovery of the U fraction, together with substantial amounts of major cations such as Fe and Ca (Fe: 18 ppb; Ca: 50 ppb), even if these amounts were very small compared to the composition of the initial matrix.

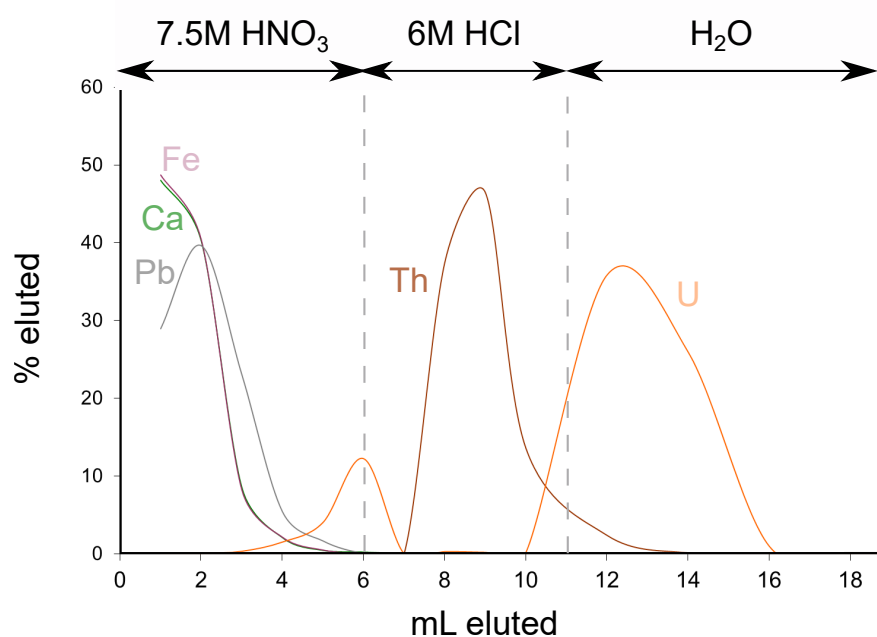


Figure 2.7 – Elution profile of the U and Th, with some major elements (Fe; Ca; Pb) using the AG1-X8 resin.

As a consequence, the protocol was modified accordingly to further purify the U fraction. To this end, the U fraction recovered during the last elution step was subsequently evaporated, taken again in 2 mL of HNO<sub>3</sub>, and re-loaded onto the same column. After further washing in 7.5M HNO<sub>3</sub>, the U fraction was then eluted in 18.2 MΩ-H<sub>2</sub>O. (Table 2.4).

Table 2.4 – Purification protocol of the U-fraction

Step	Volume	Reagent
Conditioning	3	mL 7.5M - HNO <sub>3</sub>
	3	mL 7.5M - HNO <sub>3</sub>
Loading sample	2	mL 7.5M - HNO <sub>3</sub>
Clean	2	mL 7.5M - HNO <sub>3</sub>
	2	mL 7.5M - HNO <sub>3</sub>
Elution U	2	mL 18.2 MΩ-H <sub>2</sub> O
	2	mL 18.2 MΩ-H <sub>2</sub> O
	2	mL 18.2 MΩ-H <sub>2</sub> O
	2	mL 18.2 MΩ-H <sub>2</sub> O

The evaluation of this modified protocol indicated efficient recovery of a pure uranium fraction (Fig. 2.8 ) with a final yield of 80%, which is similar using both new and old resin.

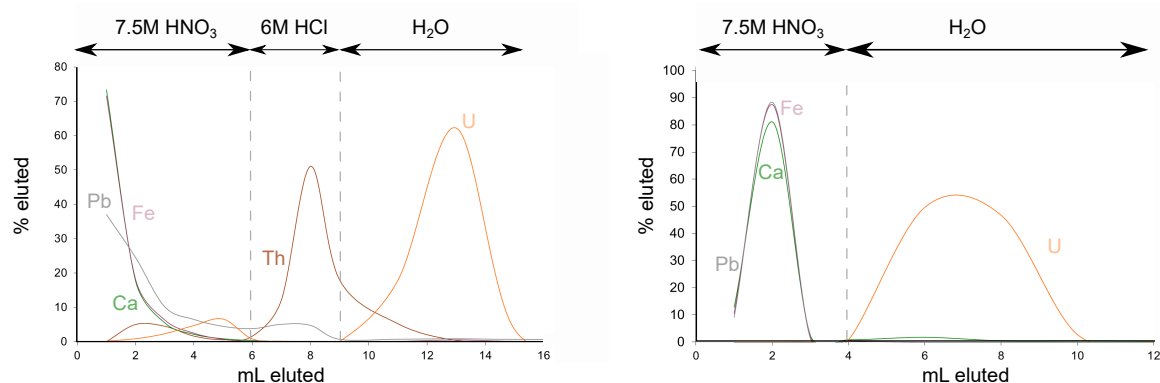


Figure 2.8 – Elution profiles of the U and Th, with some major elements (Fe;Ca;Pb) using the AG1-X8 resin for A. the separation of U and B. the purification of the U fraction.

Once the separation of U and Th is completed, the recovered fractions are evaporated and 2 mL of 0.3M HNO<sub>3</sub> (with 0.005M HF for the Th fraction) is added for the measurement.

### 2.3.2 UOW method

The separation and purification of uranium from the Var river sediments have been realized on the automated purification of U is performed using the prepFAST-MC™ system (ESI, Omaha, NE, USA). It is a fully-automated, low pressure (<100 psi), PFA chromatography system, which enables all the basic steps (e.g. sample loading, cleaning and conditioning of the column, removal of the matrix and elution of the target fraction)

that are required to isolate the elements of interest.

Uranium and Thorium are eluted using a pre-filled with AG1-X8 resin column "ThU - 0500" from ESI. Prior to sample loading (2 mL of 7M HNO<sub>3</sub>), the resin was washed with 3 mL of 6M HCl followed by 3 mL of 18.2 MΩ-H<sub>2</sub>O and then conditioned with 1 mL of 7M HNO<sub>3</sub>. Following sample loading, matrix was eluted in 1.5 mL of 6M HCl. Thorium was then eluted in 1 mL HCl followed by 1.5mL of 0.12M HCl to elute uranium fraction. Uranium fractions were dried down and re-dissolved in 4 mL of 0.3M HNO<sub>3</sub> for isotopic analysis. The obtained yield for U elution is around 70%. The yield is not very high, but the samples are combined with a tracer-solution with a known solution and the standard used are well recovered for each isotopes, therefore it is not an issue in this study.

Table 2.5 – Purification protocol of the U-fraction at WIGL

Step	Volume	Reagent
Clean	3 x 1 mL	7M - HNO <sub>3</sub>
	3 x 1 mL	0.1M - HCL
	3 x 1 mL	6M - HCL
	3 x 1 mL	18.2 MΩ-H <sub>2</sub> O
Conditioning	1 mL	7M - HNO <sub>3</sub>
Loading sample	0.5 mL	7M - HNO <sub>3</sub>
Wash matrix	1 mL	7M - HNO <sub>3</sub>
Elution Th	6 x 0.25 mL	6M - HCL
Elution U	6 x 0.25 mL	0.12M - HCL

## 2.4 Uranium analyses

Isotopic measurements were performed on a ThermoFisher Neptune Multi-Collector Inductively Coupled Plasma Mass Spectrometry (MC-ICP-MS, Thermo Scientific) at the Pole Spectrometrie Océan (Brest, France) and on a ThermoFisher Neptune Plus MC-ICP-MS at the Wollongong Isotope Geochronology Laboratory (WIGL, Australia). Uranium concentration of the studied samples were calculated either by isotope dilution, based on the measured isotopic composition of spiked samples by MC-ICPMS, or using Quadrupole Inductively Coupled Plasma Mass Spectrometry (Q-ICP-MS).

### 2.4.1 Isotopic measurement of Uranium isotopes

Uranium and thorium isotopes were measured on MC-ICP-MS. At the Pole Spectrometrie Océan (Brest, France) the instrument was equipped with APEX HF desolvating system and nebulizer PFA ST-2280 (100 $\mu$ L/min) as sample introduction system. Standard sample and X skimmer cones were used. The sensitivity on  $^{238}\text{U}$  was generally 5 V for 10 ppb at low resolution.

At the WIGL, the sample introduction system was composed of an APEX HF desolvating system and nebulizer PFA ST-2280 (100 $\mu$ L/min). Jet sample and X skimmer cones were used. The sensitivity on  $^{238}\text{U}$  was generally 6 V for 10 ppb at low resolution.

The measurement of U isotopes required to use a Secondary Electron Multiplier (SEM) to increase abundance sensitivity of the instrument. The mass 238 and 235 were analysed in the Faraday cups. Mass 234, 236, 236.5 and 235.5 were measured in ion counting detectors. The purified fractions of U and Th were introduced in 2 mL of 0.3M  $\text{HNO}_3$  and 2 mL of 0.3M  $\text{HNO}_3$  + 0.005M Hf respectively. Between each sample, the system was rinsed with 0.3M  $\text{HNO}_3$ . Samples analyses were realized in bloc of 40 cycles of measurements with an integration time of 4s. Blank analyses were realized in bloc of 20 cycles of measurement with an integration time of 4s.

- **Mass correction:** In order to correct from the instrumental mass bias and the Faraday/SEM yield, measured ratios were normalized to solution known reference material, using a standard-sample bracketing (SSB) method, during which one reference standard solution was analyzed every two samples. This standard solution corresponded to a synthetic standard (IRMM-184 or CRM U010 for U, and IRMM-035 or Th"U" for Th).
- **Pic tailing:** The measured signal of the mass of interest can suffer from large interferences related to the large abundance of a nearby mass, which creates a so-called tail effect. For instance,  $^{238}\text{U}$  is largely more abundant than  $^{234}\text{U}$  in natural sediments (typically with order of magnitude of  $\sim 10^5$ ), hence the signal  $^{238}\text{U}$  produces a 'tail' that can contribute to the measured signal on  $^{236}\text{U}$  (spiked) isotopes. Therefore, to correct the tail influence of  $^{238}\text{U}$  on the 234 and 236 atomic mass

unit (i.e. amu), intensity between 236 amu are measured (235.5 and 236.5 amu) and subtracting to the intensity of 236 amu (it implies that  $^{235}\text{U}$  do not create any tail). The same process applies for the possible tail of  $^{232}\text{Th}$  on both  $^{230}\text{Th}$  and  $^{229}\text{Th}$  by measuring 231.5, 230.5, 229.5 and 228.5 amu.

## 2.4.2 Concentration

### Measurement by isotopic dilution

The concentration of elements can be precisely calculated by isotopic dilution. For this purpose, an isotopic tracer solution (i.e. spike) is added into the sample. It is composed specifically with one or multiple isotopes from the element of interest with known isotopic abundances (Table 2.2). Then, the measurement of the mixture sample-spike allows one to determine the concentration of the sample. As an example, the following equation was used to determine U concentration in studied samples:

$$[U]_{sample} = [^{236}\text{U}]_{spike} \times \frac{M_{238}}{M_{236}} \times \frac{m_{spike}}{m_{sample}} \times \left(1 + \frac{1}{137.88}\right) \times \left(\frac{^{238}\text{U}}{^{236}\text{U}}_{samples} - \frac{^{238}\text{U}}{^{236}\text{U}}_{spike}\right) \quad (2.1)$$

with:  $M_{238}$  is the relative atomic mass of  $^{238}\text{U}$ ,  $m_{sample}$  and  $m_{spike}$  are the mass of the sample and the spike, respectively. In this thesis, the concentration of uranium and thorium of the world river sediments and half of the Var sediments were determined using this technique. The second half of measured U concentration on the Var core sediment samples were measured by Q-ICP-MS.

### Measurement on Q-ICP-MS

The uranium and thorium concentrations of the sediment samples that were not determined by isotopic dilution were measured using an iCAP Q ICP-MS. The sample introduction system comprised a peristaltic pump, a PFA nebulizer and a spray chamber. Sample cone and skimmer cone were used. An internal standard (71D) was added to all samples to correct from the instrumental derive.

The standard (STD) mode was used to measure elements of interest (i.e.  $^{115}\text{In}$ ,  $^{238}\text{U}$ ). First, a calibration curve was done by analyzing a series of uranium and thorium standard solutions (71A, Inorganic Ventures<sup>TM</sup>) covering a concentration range from 0.05 ppb to 100 ppb, yielding a correlation coefficient  $R^2 > 0.995$ . Prior to the ICP-MS analysis, an aliquot of the studied samples was taken from the parent solution in 7M  $\text{HNO}_3$ . It was then evaporated and taken up in 0.3M of  $\text{HNO}_3$  for analyze. Between each sample analysis, the system was rinsed with 0.3M  $\text{HNO}_3$  and blanks intensity were measured and subtracted from each sample. In order to validate the data, a quality control was set up

by analyzing a standard solution every five samples, with a known concentration of each analyzed elements.

### 2.4.3 Accuracy and precision of the data

Along the sample preparation and analyses, isotopic fractionation can occurred and affect the accuracy of the data. Total procedural accuracy since dissolution was evaluated by analysing reference materials (e.g. BCR-2, BHVO-1, QLO-1). Table 2.6 shows the results obtained for BCR-2, that was processed in each batch of samples. Other standards measurements (BHVO-2, QLO-1, SBC-1) are in Appendix A2.6, and are in good agreement with the reference values. The good reproducibility of the process was determined by analysis different aliquot of samples.

Table 2.6 – Values of BCR-2 obtained during the thesis compared with the referenced value.

	U (ppm)	2SD	( <sup>234</sup> U/ <sup>238</sup> U)	2SD	Date of analyse
BCR-2	1.65	0.08	1.000	0.002	14/12/2017
BCR-2	1.61	0.02	0.999	0.002	14/12/2017
BCR-2	1.67	0.02	0.998	0.002	14/12/2017
BCR-2	1.70	0.05	1.001	0.001	07/03/2018
BCR-2	1.62	0.02	1.002	0.001	07/03/2018
BCR-2	1.66	0.02	0.998	0.002	28/05/2018
BCR-2	1.63	0.03	1.002	0.001	28/05/2018
BCR-2	1.61	0.02	1.003	0.001	24/07/2018
BCR-2	1.75	0.02	1.001	0.002	24/07/2018
BCR-2	1.64	0.04	1.002	0.001	06/08/2018
BCR-2	1.65	0.02	1.003	0.003	11/10/2019
BCR-2	1.64	0.03	1.005	0.005	11/10/2019
BCR-2	1.61	0.02	1.001	0.004	26/02/2020
BCR-2	1.60	0.03	1.003	0.004	27/02/2020
BCR-2	1.63	0.02	1.000	0.004	28/02/2020
BCR-2	1.69	0.02	1.000	0.005	7/03/2020
BCR-2	1.89	0.02	1.001	0.008	23/03/2020
BCR-2	1.67	0.02	1.000	0.003	24/03/2020
<b>Mean</b>	1.66	0.18	1.001	0.003	
<b>Standard value</b>	<b>1.69</b>	<b>0.19</b>	1.001	0.001	Sims et al. (2008)

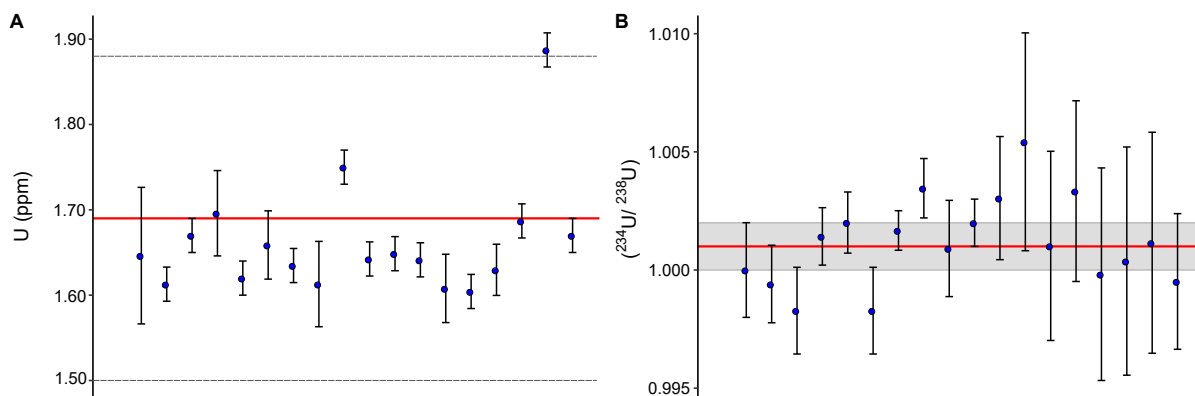


Figure 2.9 – Uranium concentration and ( $^{234}\text{U}/^{238}\text{U}$ ) for the standard BCR-2 compared with the reference value (from Sims et al. 2008).

The possible contamination of the sample during the preparation and analysis was assessed by blank control. For each batch (around twenty samples) a total procedure blanks were realized. Table 2.7 reports the mass of U measured in each blank. The average blank contribution is inside each batch  $<0.1\%$ .

Table 2.7 – Quantity of uranium obtained in the blank during the thesis.

U (pg)	Analysed date
94	23/11/2017
18	23/11/2017
64	14/12/2017
63	14/12/2017
84	07/03/2018
43	24/07/2018
81	06/08/2018
36	28/05/2018
67	21/08/2018
121	11/10/2019
24	12/10/2019
38	26/02/2020
153	27/02/2020
4	29/02/2019
91	7/03/2020
37	7/03/2020
8	23/03/2020
32	24/03/2020
59	mean

Precision of the analysis on the Neptune was determined by measuring synthetic standard NBL U005-A (Richter and Goldberg, 2003) and was consistently better than 1% for ( $^{234}\text{U}/^{238}\text{U}$ ).

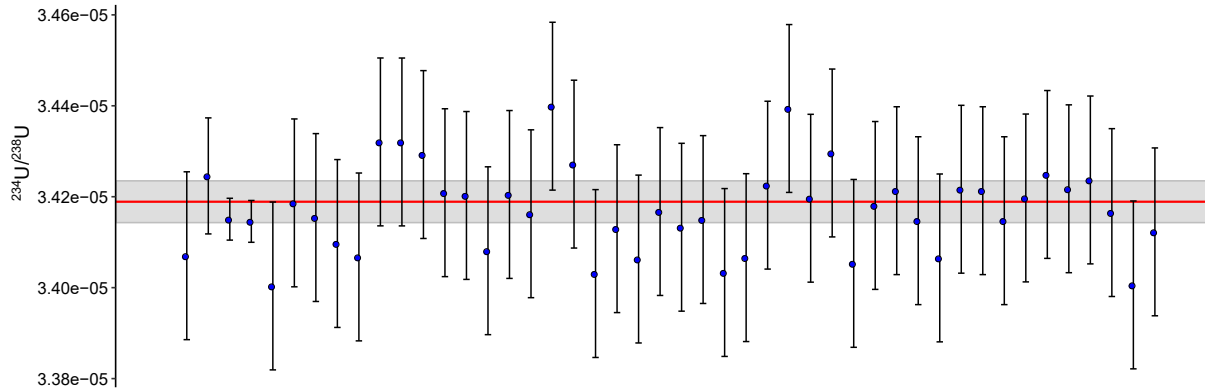


Figure 2.10 – Evolution of ( $^{234}\text{U}/^{238}\text{U}$ ) obtained for the standard U005A.

Precision of the analysis on the iCAP was determined by measuring the concentration of the standard 71A with a known concentration of 5 ppm.

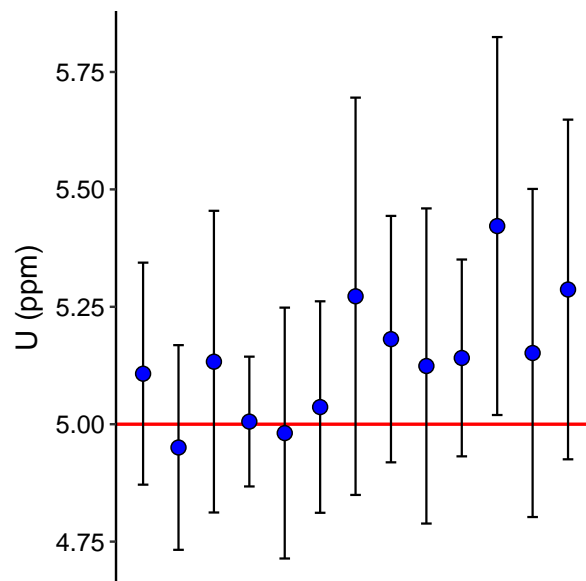


Figure 2.11 – Evolution of U (ppm) obtained for the standard 71A measured on the iCAP Q-ICP MS

## 2.5 Specific surface analyses

In this thesis, specific surface area ( $S_{BET}$ ) measurements were carried out on a Quantachrome Autosorb iQ by gas sorption at WIGL on leached sediments. About 1g of sediments were put in a 9 mm cell and degassed for approximately 7.5 h with a three-step temperature increase to 200 °C, prior to analysis using nitrogen as adsorbate gas.  $S_{BET}$  was estimated using the best fit of the multi-point BET equation on 5 - 7 adsorption points when  $P/P_0$  varies between 0.05 and 0.30. The correlation coefficient is  $R^2 > 0.999$  for all measurements.

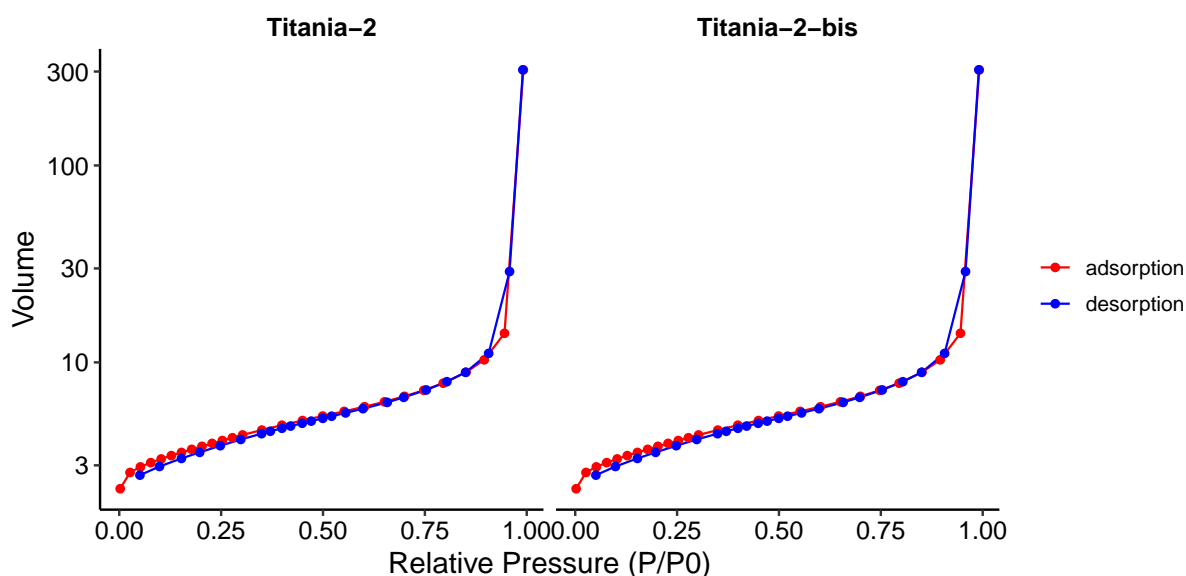


Figure 2.12 – Adsorption-desorption isotherms obtained for the standard Titania, which are representative of the isotherms obtained with the samples.

For this work, the surface roughness was taken into account with the estimation of the fractal dimension  $D$  and the Neimark–Kiselev method (Neimark, 1990) was used. Indeed the obtained adsorption-desorption isotherms were typical from microporous sediments (e.g. with pores  $< 2$  nm; Fig. 2.12) for all the analyzed sediments (Fig. 2.12 is representative of the isotherms obtained for the samples). The accuracy of the method was assessed with the measure of the specific surface area of the certified reference material BCR-173 (Titania) ( $S = 8.3 \text{ m}^2/\text{g}$ ;  $n=2$ , Table 2.8). The obtained values for BCR-173 are in the error range of the certified value. The precision was estimated by analysing two aliquots of the Var river sample EST-05.

Table 2.8 – Reference Material BCR-173 measured and certified values

	<b>Reference material</b>	<b><math>S_{BET}</math> (<math>m^2/g</math>)</b>	
Measured	Titania (a)	8.39	
	Titania (b)	8.38	
Certified Value	Titania	8.23	0.21

Table 2.9 – Precision of the specific surface area measurement access using two aliquot of the Var River sample EST-05

<b>Sample</b>	<b><math>S_{BET}</math> (<math>m^2/g</math>)</b>
EST-05 (a)	13.6
EST-05 (b)	14.1

## 2.6 Geographic Information System analyses

The spatial distribution of sedimentary ( $^{234}\text{U}/^{238}\text{U}$ ) ratios as the scale of a source to sink system has been studied with the case study of the Var catchment. To this purpose, and to look at the spatial variation of characteristic invariants to the Var basin (e.g. slope, curvature, elevation), we have made extensive use of the Geographic Information System (GIS) method. We used the software ArcGIS, with Hydrology toolboxes.

### 2.6.1 Basin and sub-basin delineation

The first step required to use correctly the Digital Elevation Model (DEM) is to fill the sinks in order to remove the imperfections from the DEM. A sink is a cell (or a group of cells spatially connected) where the flow direction cannot be estimated. It can be caused by the over-elevation of the neighbour cell compared to the considered one, or because two cells flow in each other. The sinks are filled with a value from 1 to the number of sink. After the fill of the sink, the "flow direction" tool can be applied on the obtained DEM. It results in a raster that indicates the direction of flow from each cell to its steepest downslope neighbor. From this raster, the tool "flow accumulation" is applied to calculate the accumulated flow to each cell, as determined by the accumulated weight of all cells that flow into each downslope cell. Then the pour point to cells of high accumulated flow need to be determined using the "snap pour points" tool, and the flow accumulation raster. In this case the pour point is the mouth of the Var River to obtain the border of the Var watershed. Once these steps realized, the "watershed" tool can be applied with the flow direction raster and the feature pour point data. The output is a raster with the delineation of the basin. The last step is to convert the raster into polygon while only the border of the considered basin is selected to have a polygon with the shape of the watershed. The principle of the sub-basin delineation is similar except that for the determination of the pour point, the localization of all the studied samples are imported. Then all the steps are repeated.

### 2.6.2 Extraction of the geomorphologic characteristics

The slope and curvature were calculated from the DEM raster using the slope and curvature tools from ArcGis. The minimum, maximum and mean values were then calculated and extracted for each sub-catchment. Spatial distribution of soil thickness was derived from the SoilGrids map with a 250 m resolution Hengl et al. (2017). The estimated sediment residence time derived from the geomorphology of the catchment was calculated by dividing the soil thickness with the denudation rates from Mariotti et al. (2019). The values of the estimation of the sediment residence time were then extracted for each sub-catchment.



# THE DISTRIBUTION OF ( $^{234}\text{U}/^{238}\text{U}$ ) ACTIVITY RATIOS IN RIVER SEDIMENTS

---

## Contents

---

<b>3.1</b>	<b>Introduction . . . . .</b>	<b>93</b>
<b>3.2</b>	<b>Methods . . . . .</b>	<b>95</b>
3.2.1	Samples . . . . .	95
3.2.2	Analytical procedures . . . . .	97
<b>3.3</b>	<b>Results . . . . .</b>	<b>98</b>
3.3.1	Leaching experiments . . . . .	98
3.3.2	Uranium in river sediments . . . . .	100
<b>3.4</b>	<b>Discussion . . . . .</b>	<b>102</b>
3.4.1	Influence of grain size on ( $^{234}\text{U}/^{238}\text{U}$ ) ratios of detrital sediments . .	102
3.4.2	The effect of weathering, climate and erosion on $^{234}\text{U}$ - $^{238}\text{U}$ fraction- ation . . . . .	102
3.4.3	The role of lithology . . . . .	109
3.4.4	The role of catchment size and sediment residence time on ( $^{234}\text{U}/^{238}\text{U}$ ) sedimentary ratio . . . . .	111
3.4.5	Complex interactions of environmental controls on sediment resi- dence time . . . . .	114
<b>3.5</b>	<b>Conclusion . . . . .</b>	<b>115</b>
<b>3.6</b>	<b>Acknowledgments . . . . .</b>	<b>116</b>

---

# The distribution of ( $^{234}\text{U}/^{238}\text{U}$ ) activity ratios in river sediments

Maude Thollon<sup>1,2,3</sup>, Germain Bayon<sup>1</sup>, Samuel Toucanne<sup>1</sup>, Anne Trinquier<sup>1</sup>,  
Yoan Germain<sup>1</sup>, Anthony Dosseto<sup>3</sup>

<sup>1</sup>IFREMER, Marine Geosciences Research Unit, 29280 Plouzané, France.

<sup>2</sup>Wollongong Isotope Geochronology Laboratory, School of Earth and Environmental Sciences, University of Wollongong, Wollongong, NSW 2522, Australia

<sup>3</sup>Université de Bretagne Occidentale, 29200 Brest, France.

Corresponding author: Maude Thollon; malt273@uowmail.edu.au

This article is an adapted version for the thesis manuscript of the article published in *Geochimica et Cosmochimica Acta* in September 2020.

## Abstract

Uranium (U) isotopes can be used to estimate the comminution age of sediments, i.e. the time elapsed from sediment production on continents, via weathering and physical erosion, to deposition in the sedimentary record. The calculation of this comminution age is based on measured ( $^{234}\text{U}/^{238}\text{U}$ ) activity ratios in river sediments, and inferred time-dependent recoil effect, which leads to the preferential release of  $^{234}\text{U}$  from mineral lattices during erosion processes. In this study, we report on a large-scale ( $^{234}\text{U}/^{238}\text{U}$ ) investigation of modern river sediments worldwide, with the aim to determine the extent to which parameters such as grain size, lithology, weathering, climate and geomorphology may influence the distribution of U isotopes in fine-grained sediments. Our extensive dataset (N=64) includes U isotopic measurements for many of the world's largest rivers, but also rivers draining particular climatic and geological settings. Our results indicate that sediments collected from river basins draining mostly igneous, metamorphic or volcanic rocks often display ( $^{234}\text{U}/^{238}\text{U}$ ) ratios  $>1$ , with clay-size fractions ( $<4\ \mu\text{m}$ ) being less depleted in  $^{234}\text{U}$  (higher  $^{234}\text{U}/^{238}\text{U}$ ) than corresponding silt-size fractions ( $4\text{-}63\ \mu\text{m}$ ). In contrast, sediments derived from multi-lithological basins or draining sedimentary rocks are typically characterized by ( $^{234}\text{U}/^{238}\text{U}$ ) ratios  $<1$ , with clays generally exhibiting more depleted  $^{234}\text{U}$  signatures than silts. Taken together, these observations suggest that the formation of secondary clay minerals in soils from basins draining mostly igneous, metamorphic rocks, is accompanied by partial incorporation by recoil injection of  $^{234}\text{U}$  initially released during weathering processes, possibly from U-rich minerals, such as sphene or apatite. Instead, in multi-lithological catchments draining sedimentary rocks, we propose that the erosion of recycled sediments having experienced several cycles of weathering,

possibly over glacial-interglacial timescales, could explain the much lower ( $^{234}\text{U}/^{238}\text{U}$ ) ratios observed in clay-size fractions. While no direct relationships can be identified between sediment ( $^{234}\text{U}/^{238}\text{U}$ ) ratios and lithology, weathering intensity, climatic or geomorphic parameters in corresponding river basins, we show that the catchment size probably plays an important role in controlling the distribution of ( $^{234}\text{U}/^{238}\text{U}$ ) in river sediments, through its direct influence on the sediment residence time. Finally, a multiple regression analysis of our data, combining various environmental parameters for the lithology, climate and geomorphology of studied river basins, indicates predicted ( $^{234}\text{U}/^{238}\text{U}$ ) values that are very similar to measured values (with  $R^2 \sim 0.8$ ). This finding provides further support for the usefulness of ( $^{234}\text{U}/^{238}\text{U}$ ) ratios in the sedimentary record for reconstructing past landscape changes and their effect on sediment transport and residence time in river basins.

### 3.1 Introduction

The morphology of the Earth's surface results from complex interactions between climate, tectonic and weathering (e.g. Dixon et al. 2009, West et al. 2005). Understanding the factors affecting landscape evolution is essential to predict the consequences of future climate change on soil resource availability and sediment discharge to the oceans. Additionally, the study of sediment transport processes and their timescales can be useful to quantify soil production and denudation on continents. Over the past decades, the development and application of novel geochemical proxies to river materials has significantly improved our understanding of the sedimentary and weathering processes occurring in river catchments (Négre et al. 1993, Gaillardet et al. 1997, 1999, Vigier et al. 2001, Clift et al. 2002, Bindeman et al. 2019, Bayon et al. 2016, 2018, 2020). However, the quantification of the timescale of these processes, such as the sediment residence time, still remains challenging (DePaolo et al. 2006, Romans et al. 2016). On the continents, the fractionation of uranium (U) isotopes is initiated in the Critical Zone, associated with the preferential loss of  $^{234}\text{U}$  relative to  $^{238}\text{U}$ , whenever chemical weathering and rock fracturing start affecting the bedrock. In theory, the degree of U-series fractionation in sediments can provide direct temporal constraints on the timing of sediment formation in soils and subsequent storage within the catchment and the sedimentary system (Chabaux et al. 2003a, DePaolo et al. 2006), which can be used to determine the so-called *comminution ages*, corresponding to the time elapsed since the production of small mineral grains (typically  $< 63 \mu\text{m}$ ).

In detail, the preferential depletion of  $^{234}\text{U}$  relative to  $^{238}\text{U}$  in mineral grains occurs during the decay of  $^{238}\text{U}$  to  $^{234}\text{Th}$ , where the daughter is recoiled (and subsequently decayed into  $^{234}\text{U}$ ) within the outer  $\sim 10\text{-}30 \text{ nm}$  periphery of the grains (Hashimoto et al. 1985, Kigoshi 1971, Maher et al. 2006, DePaolo et al. 2006, Chabaux et al. 2008, Lee et al. 2010,

Dosseto & Schaller 2016). As a consequence, soil solutions and river water are typically enriched in  $^{234}\text{U}$ , exhibiting  $(^{234}\text{U}/^{238}\text{U}) > 1$  (parentheses denote activity ratio), whilst fine-grained residual sediments in soils and suspended particulate loads in rivers display values  $< 1$  (Carl 1987, DePaolo et al. 2006, Maher et al. 2004, 2006, Moreira-Nordemann 1980, Plater et al. 1988). The measurement of  $^{234}\text{U}$  depletion is only significant (i.e. measurable) in fine-grained ( $< 63 \mu\text{m}$ ) sediments (DePaolo et al. 2006, Dosseto et al. 2006b, 2008a) where the surface/volume ratio is large enough so that the thin outer layer through which preferential  $^{234}\text{U}$  loss occurs is significant compared to the rest of the grain (which experiences no net loss of  $^{234}\text{U}$ ) (DePaolo et al. 2006). In theory, the comminution age method is based on two main assumptions: 1) the time-integrated recoil effect represents the main factor controlling  $(^{234}\text{U}/^{238}\text{U})$  in fine-grained sediments (DePaolo et al. 2006); and 2) the pristine (unweathered) rocks on continents are at secular equilibrium with regard to U-series (i.e. with activity ratios = 1) (DePaolo et al. 2012). However, a few studies have reported evidence that weathering processes can locally influence the degree of U-series disequilibrium in fine-grained sediments (Li et al. 2016a), or that the bedrock may depart from the secular equilibrium (Handley et al. 2013a), hence casting doubt on the validity of the above-mentioned assumptions. In fact, despite recent increasing interest for the use of U isotopes for tracing Earth surface processes (DePaolo et al. 2006, 2012, Dosseto et al. 2008a, 2010, 2014, 2015, Handley et al. 2013b, Lee et al. 2010, Li et al. 2017), the controls on the  $(^{234}\text{U}/^{238}\text{U})$  of river sediments are yet to be fully understood. To date, all previous studies focusing on U-series as tracers of continental erosion were dedicated to the case study of specific river basins, often yielding contrasted comminution ages and inferred sediment transport times. For instance, investigations conducted at the scale of the Amazon Basin resulted in a large range of sediment residence time from the Andean tributaries (3-4 kyr; Dosseto et al. 2006a, 2008a) and the lowland tributaries (100-500 kyr; Dosseto et al. 2006a). The Ganges tributaries have also been investigated in detail (Chabaux et al. 2006, 2012, Granet et al. 2007, 2010), with inferred sediment residence times ranging between 30-350 kyr. Other case studies include the Mackenzie River (Vigier et al. 2001) and smaller river systems in East Asia (Zhuoshui River, Lanyang River; Li et al. 2016b), yielding sediment transfer times of  $\sim 25$  kyr and  $\sim 110$  kyr, respectively. More recently, Li et al. (2016b) also determined relatively long sediment transfer times (from 250 to 600 kyr) for the Changjiang (Yangtze) River basin. These latter sediment residence times are surprisingly long considering the observed variability of the provenance of the sediment exported from the Yangtze River over the past 400 kyr, which implicitly suggests a much shorter storage time within the watershed (Beny et al. 2018).

An important pre-requirement for quantifying the timescale of sediment transport in continental watersheds using U isotopes, is to assess whether the distribution of  $(^{234}\text{U}/^{238}\text{U})$  in river suspended loads and sediments can be affected by other parameters, such as grain-size, lithology, climate and tectonic settings. Early works pointed out at the importance

of removing non detrital sediment fractions prior to analysing sediment samples (e.g. Lee 2009, Martin et al. 2015, Francke et al. 2018 and demonstrated the influence of grain size on U activity ratios and calculated sediment transfer times (Dosseto et al. 2014, Granet et al. 2010). More recently, Bosia et al. (2018) also emphasize the importance of analysing separate mineral phases. While it can be difficult to separate different mineral fractions from fine-grained sediments, one alternative option is to focus instead on particular grain-size fractions. In this study, we report ( $^{234}\text{U}/^{238}\text{U}$ ) measurements for both clay ( $<4\ \mu\text{m}$ ) and silt ( $4\text{-}63\ \mu\text{m}$ ) size detrital fractions extracted from an extensive set of river sediment samples worldwide. This study builds upon previous investigations of the same suite of sediment samples, which have proven particularly useful for identifying the various external factors (e.g. climate, lithology, weathering regime) that control the distribution of geochemical proxies in sediments (Bayon et al. 2015, 2016, 2018, 2020, Bindeman et al. 2019). Such a proxy evaluation study is of utmost importance prior to applying U isotopes in ancient sedimentary records for reconstructing past sediment transfer dynamics through time.

## **3.2 Methods**

### **3.2.1 Samples**

A total of 64 sediment samples were analysed during this study, collected from river catchments, estuaries, or submarine deltas near the mouth of rivers (Fig. 3.1; Bayon et al. 2015, 2016, 2018, 2020). All studied samples correspond to modern or relatively recent sediments presumably deposited during the last few centuries. A few sediment samples ( $n=17$ ) come from igneous/metamorphic terranes from the Precambrian cratons of North America (Canadian Shield), northern South America (Guiana Shield), Africa (West African and Congo Shields), Fennoscandia, northwest Ireland and a small river from the Hercynian Armorican Massif in France (Elorn River). Seven samples are derived from rivers draining both modern (Indonesia) and ancient (British Tertiary, Northern Ireland) volcanic provinces. The rest of studied samples ( $n=40$ ) correspond to rivers draining ‘mixed/sedimentary’ formations including some of the world’s major rivers (e.g. Amazon, Congo, Mississippi, Nile, Niger, Yangtze, Mackenzie, Volga, Murray, Orinoco), plus rivers draining sedimentary basins (e.g. Adour, Shannon).

The studied river catchments can also be classified according to their climate setting (Bayon et al. 2016, 2018), depending on their mean annual temperature (MAT), and mean annual precipitation (MAP). A total of 10 samples are representative of cold and dry regions with  $\text{MAT} < 8^\circ\text{C}$  and  $\text{MAP} < 800\text{mm}$  (e.g. Don, Fraser, Lule). Other sediments correspond to temperate and warm dry environments (e.g. Murray-Darling, Yellow River;  $n=18$ ), with  $\text{MAT} > 10^\circ\text{C}$  and  $\text{MAP} < 800\text{mm}$ , or from temperate and humid regions

(n=18), with  $8\text{ }^{\circ}\text{C} < \text{MAT} < 16\text{ }^{\circ}\text{C}$  and  $\text{MAP} > 1000\text{ mm}$  (e.g. Yangtze, Rhine). Finally, the rest of the studied samples come from sub-tropical humid regions, with  $\text{MAT} > 20\text{ }^{\circ}\text{C}$  and  $\text{MAP} < 1500\text{ mm}$  (e.g. Niger, Mekong, n=6) or from tropical regions with  $\text{MAT} > 20\text{ }^{\circ}\text{C}$  and  $\text{MAP} > 1500\text{ mm}$  (e.g. Amazon, Congo, Red River; n=12). The studied sediments can also be grouped using physical basin characteristics, such as lowlands, characterized by a maximum elevation of 500 m (e.g. Clarence, Swilly; n=21), uplands, with a maximum of elevation between 500 and 800 m (e.g. Severn, Shannon; n=6), mountainous regions (n=19 ; e.g. Loire, Fortescue), with maximum elevation between 800 and 3000 m, and high mountains (n=18), with maximum elevation  $> 3000\text{ m}$  (e.g. Ganges, Danube).

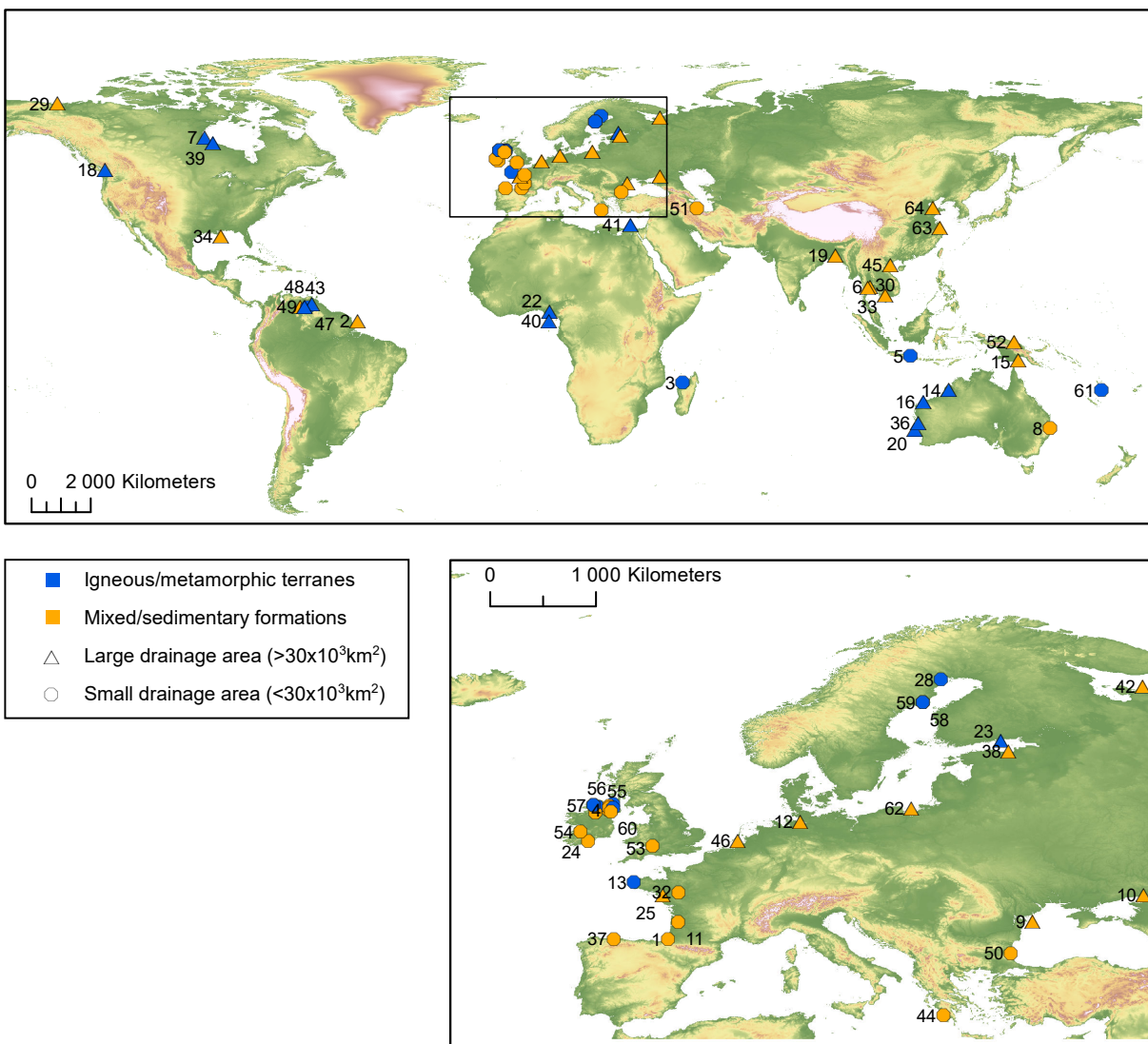


Figure 3.1 – World map with the location of studied sediment samples, the sediments derived from igneous & metamorphic rocks are in blue whereas those from sedimentary and mixed lithologies are in orange. The sediments from large catchments ( $> 30 \times 10^3\text{km}^2$ ) are symbolised by a triangle and those from small basins ( $< 30 \times 10^3\text{km}^2$ ) by a circle. The digital elevation model is derived from the ETOPO1 Global relief Model (<https://www.ngdc.noaa.gov/mgg/global/global.html>).

### 3.2.2 Analytical procedures

Three distinct U pools can be distinguished in any sediment sample (Martin et al. 2015): 1) a non-detrital pool hosted by various carbonate minerals, Fe-Mn oxyhydroxide phases, and organic compounds, associated typically with enriched ( $(^{234}\text{U}/^{238}\text{U}) > 1$ ) signatures (Plater et al. 1988, Andersson et al. 1998, 2001, Maher et al. 2006); 2) a depleted ( $(^{234}\text{U}/^{238}\text{U}) < 1$ ) detrital pool corresponding to the outer part of detrital minerals that have experienced partial dissolution and preferential loss of  $^{234}\text{U}$  due to recoil effect; and 3) a pristine detrital pool at secular equilibrium ( $(^{234}\text{U}/^{238}\text{U}) = 1$ ), which corresponds to the inner part of detrital grains that has not experienced  $^{234}\text{U}$  loss.

In this study, sequential leaching was conducted on all samples in order to remove any biogenic, authigenic and organic components prior to preparation for U isotopic measurements. First, the  $< 63 \mu\text{m}$  fraction of the bulk sediment was recovered by wet sieving. About  $\sim 3$  g of dry bulk sediment were treated successively with diluted acetic acid (AA), a mixed solution of 15% (v/v) AA and 0.1 M hydroxylamine hydrochloride (HH), and diluted hydrogen peroxide, in order to remove any carbonate, Fe-Mn oxyhydroxide and organic phases, respectively (Bayon et al. 2002). Finally, clay- ( $< 4 \mu\text{m}$ ) and silt- ( $4-63 \mu\text{m}$ ) size fractions of the residual detritus were separated by centrifugation using the two-step protocol reported in Bayon et al. (2015).

A series of experiments was conducted on different sediment samples in order to assess the reliability of our leaching protocol for efficiently removing the radiogenic non-detrital component of the sediment characterized by high ( $^{234}\text{U}/^{238}\text{U}$ ) ratios. To this purpose, following the approach previously developed by Lee (2009), the effect of each leaching step of our protocol was successively assessed by measuring U isotopic ratios in both leachates and corresponding residual phases from two sediment samples from the Loire and Clarence rivers (Fig. 3.2). To assess whether the leaching was completed, an additional final leaching step termed "carbonate emphasized" was performed at the end of this series of experiments. The validity of our sequential leaching protocol was also further assessed by analysing two sediment samples (1B-26H-cc and 1B-17H-cc) previously studied by Francke et al. (2018) using a different leaching method. Finally, two certified reference rock materials (BCR-2, BHVO-2) were processed using the same experimental protocol used in this study, to investigate whether sequential leaching could also lead to any particular U isotopic fractionation.

Both clay- and silt-size residual detrital fractions were digested by alkaline fusion (Bayon et al. 2009), to ensure complete dissolution and provide reassurance that the observed ( $^{234}\text{U}/^{238}\text{U}$ ) differences between silt and clay samples cannot be possibly caused by the partial dissolution of any accessory minerals. About 50 mg dry powdered sediment were placed into a glassy carbon crucible, after addition of  $^{238}\text{U}$  spike, and digested at  $650^\circ\text{C}$  (12 min) together with NaOH and  $\text{Na}_2\text{O}_2$ . Subsequent addition of ultrapure water to the

obtained melt results in the formation of iron oxide precipitates, leading to trace element scavenging (including U). Note that the good homogenization of the sediment powder and the spike during sample treatment is shown by the validity of measured U isotopic compositions in both rock standard and certified materials. After centrifugation, U-bearing Fe-oxyhydroxide phases were rinsed twice in ultrapure water and dissolved in 2 mL of 7.5 M  $\text{HNO}_3$ .

Uranium was isolated by ion exchange chromatography (AG1X-8 resin) using a protocol adapted from Bayon et al. (2009) and Edwards et al. (1986), which was repeated once to ensure complete U purification. The analyses were performed at the Pôle Spectrométrie Océan (Brest) on a Neptune Multi-Collector Inductively-Coupled Plasma Mass Spectrometer (MC-ICP-MS), using an APEX HF desolvating system. Instrumental mass correction was performed by standard bracketing of IRMM 184 standard solutions analysed every two samples.

Table 3.1 – U isotopic compositions of reference materials.

	Reference	$(^{234}\text{U}/^{238}\text{U})$	2s.e.	measured			measured after leaching		
				$(^{234}\text{U}/^{238}\text{U})$	2s.e.	n	$(^{234}\text{U}/^{238}\text{U})$	2s.e.	n
<b>BCR-2</b>	<i>Mathews et al., 2011</i>	1.001	0.001	1.003	0.006	12	1.009	0.002	1
<b>W-2</b>	<i>Sims et al., 2007</i>	1.000	-	0.997	0.009	5			
<b>BHVO-2</b>	<i>Mathews et al., 2011</i>	1.001	0.001	1.009	0.009	3	1.006	0.003	1
<b>SBC-1</b>				1.000	0.003	2			
<b>San Joaquin</b>				1.006	0.002	1			
<b>GSMS-2</b>				0.928	0.001	1			
<b>JSd-2</b>				1.008	0.002	1			

The external reproducibility and accuracy of measured uranium isotopic ratios were assessed through repeated analyses of various reference (NBL CRM U005-A) and rock (BCR-2, BHVO2, JSd-2) standard solutions, with results being in good agreement (within the error range) with references from the literature (Table 3.1). The uncertainty on measured ( $^{234}\text{U}/^{238}\text{U}$ ) due to sediment sampling and processing was further assessed by analysing three sediment samples collected at distinct locations in the Loire Estuary (Table 3.2), yielding a mean ( $^{234}\text{U}/^{238}\text{U}$ ) value  $0.959 \pm 0.001$  ( $2\sigma$  error) and  $0.953 \pm 0.001$  ( $2\sigma$  error) for silt- and clay-sized fractions, respectively. Total procedural blanks were systematically  $<65$  pg, hence negligible compared to the amount of analysed U for each studied sample ( $\sim 40$  ng).

## 3.3 Results

### 3.3.1 Leaching experiments

The measurements of ( $^{234}\text{U}/^{238}\text{U}$ ) in the Clarence and Loire samples show that the residual detrital ( $^{234}\text{U}/^{238}\text{U}$ ) compositions decreased progressively during the course of the sequential leaching procedure (from 1.0 to 0.8; Fig. 3.2), especially for the case of Clarence

Table 3.2 – U concentration and activity ratio for silt and clay of Loire River Sediments.

Sample sites	grain size fraction	U (ppm)	( $^{234}\text{U}/^{238}\text{U}$ )	2s.e.
Cordemais	silt	3.84	0.960	0.001
	clay	3.48	0.983	0.001
Donges	silt	3.82	0.958	0.002
	clay	2.83	0.938	0.001
Port Lavigne	silt	4.43	0.959	0.001
	clay	2.95	0.937	0.002

River sample, indicating that the non-detrital  $^{234}\text{U}$ -enriched phases have been efficiently removed during our leaching procedure. Importantly, the final leaching steps were not accompanied by any ( $^{234}\text{U}/^{238}\text{U}$ ) increase in the residual detrital fractions, suggesting negligible dissolution of pristine detrital minerals at secular equilibrium. Furthermore, the comparison of the ( $^{234}\text{U}/^{238}\text{U}$ ) values obtained for the two test samples using our protocol agree well (<5% of difference) with the data obtained using the procedure of Francke et al. (2018) (Table 3.1). Finally, the ( $^{234}\text{U}/^{238}\text{U}$ ) ratios determined on the geological reference materials following our leaching procedure also agree well with the recommended values (Table 3.1).

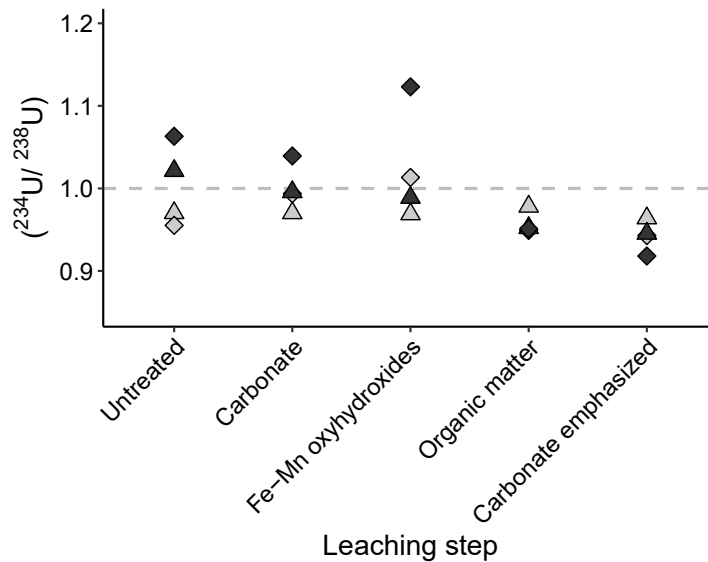


Figure 3.2 – Depletion of ( $^{234}\text{U}/^{238}\text{U}$ ) following the successive leaching steps for Clarence (dark grey) and Loire (light grey) sediments for silt (triangles) and clay (diamonds) size fractions.  $2\sigma$  errors are smaller than the symbol size. The dashed line represents the secular equilibrium ( $^{234}\text{U}/^{238}\text{U}$ ) = 1.

### 3.3.2 Uranium in river sediments

Measured U concentrations in studied clay- and silt-sized fractions range from 0.37 ppm (Glenariff) to 9.90 ppm (Lule), and from 0.22 ppm (Glenariff) to 10.11 ppm (Benue), respectively (Fig. 3.3, Table 3.3). In both silt and clay size fractions, the mean concentration values ( $\sim 3.0$  ppm and 3.3 ppm respectively) are higher than average estimate values for the upper crust continental – UCC (from 2.2 to 2.8 ppm, (Condie 1993, McLennan 2001)). The great majority of studied river sediment samples display slightly lower U concentrations in silts than in corresponding clay fractions. Note that no particular relationships were observed between U concentrations and the various parameters (e.g. climate, weathering, tectonic settings) that will be discussed in the sections below.

The ( $^{234}\text{U}/^{238}\text{U}$ ) ratios in clay and silt fractions range from 0.819 (Rhine) to 1.340 (Swilly) and from 0.897 (Mackenzie) to 1.152 (Murchinson), respectively (Fig. 3.3). Our data indicate a much larger ( $^{234}\text{U}/^{238}\text{U}$ ) variability amongst studied clay-sized fractions than in corresponding silts with a standard deviation of 0.14 and 0.05 respectively (Fig. 3.3, Table 3.3). The mean ( $^{234}\text{U}/^{238}\text{U}$ ) value is lower in silt than clay size fraction,  $0.987 \pm 0.002$  ( $2\sigma$  error) and  $1.001 \pm 0.003$  ( $2\sigma$  error) respectively. Interestingly, many sediment samples ( $n=21$  silts;  $n=27$  clays) display ( $^{234}\text{U}/^{238}\text{U}$ ) values above secular equilibrium ( $>1$ ).

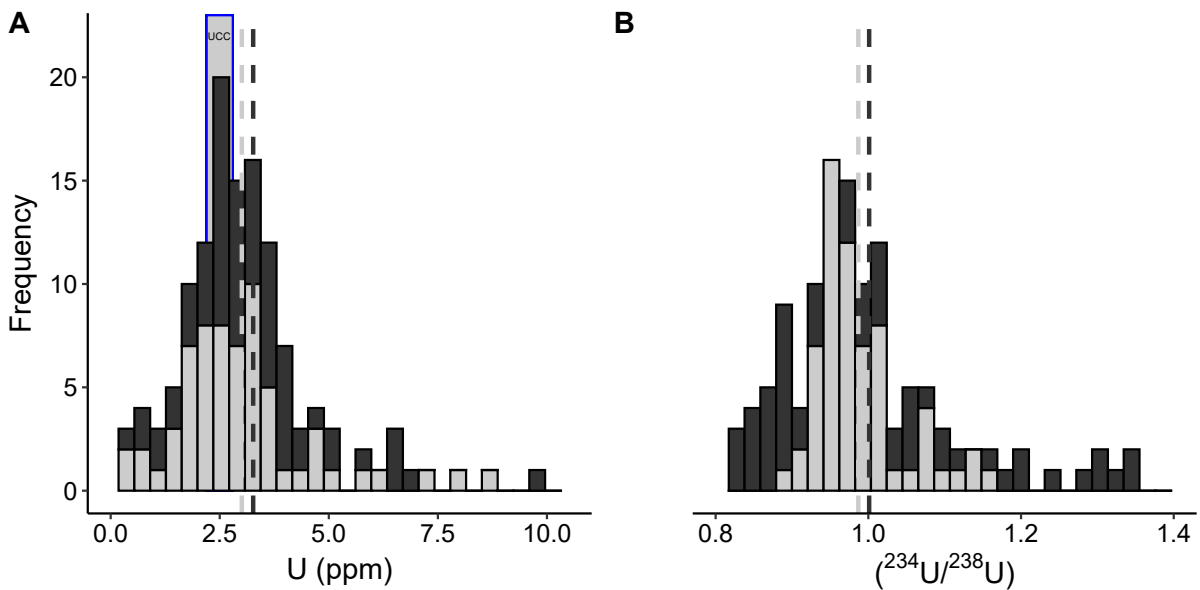


Figure 3.3 – Histogram of (A) uranium concentrations and (B) ( $^{234}\text{U}/^{238}\text{U}$ ) activity ratios in silt ( $n = 65$ , light grey) and clay ( $n = 65$ , dark grey) size fractions; the dashed lines represent the mean values for silt (light grey) and clay (dark grey), and the blue rectangle represents the values of the upper continental crust (UCC - (Condie 1993, McLennan 2001)).

Table 3.3 – Uranium concentration and activity ratio of silt and clay size fractions in river sediments and corresponding basin parameters

River (n= 64)	Main drained lithology	Country	Latitude	Longitude	clay U (ppm)	silt	clay ( <sup>234</sup> U/ <sup>238</sup> U)	2s.e.	silt ( <sup>234</sup> U/ <sup>238</sup> U)	2s.e.	bulk ( <sup>234</sup> U/ <sup>238</sup> U)	Clays $\epsilon_{Nd}$	Silts	% of silt	clay	
1	Adour	Mixed/sedimentary formations	France	43.49	-1.47	2.7	3.7	0.891	0.002	0.969	0.001	0.956	-11.0	-11.6	83	17
2	Amazon	Mixed/sedimentary formations	Brazil	3.10	-49.50	3.2	3.0	0.917	0.001	0.956	0.001		-10.5	-10.7		
3	Betsiboka	Igneous/metamorphic terranes	Madagascar	-15.52	45.72	1.6	2.0	1.049	0.002	1.122	0.002				51	49
4	Blackwater	Mixed/sedimentary formations	Ireland	54.51	-6.58	3.2	2.5	0.927	0.002	0.957	0.002	0.000	-11.6	-12.6		
5	Brantas	Volcanic Rocks	Indonesia	-7.44	112.46	0.6	0.6	0.980	0.003	0.988	0.003			4.1		
6	Chao Phraya	Mixed/sedimentary formations	Thailand	13.57	100.58	3.2	3.2	0.972	0.004	0.991	0.002	0.985	-8.4	-9.8	67	33
7	Churchill	Igneous/metamorphic terranes	Canada	58.97	-94.10	3.3	1.5	0.866	0.002	0.933	0.002			-28.7		
8	Clarence	Mixed/sedimentary formations	Australia	-29.43	153.25	3.2	5.1	0.961	0.002	0.946	0.002					
9	Danube	Mixed/sedimentary formations	Romania	45.06	29.62	2.4	2.8	0.872	0.002	0.954	0.001				84	16
10	Don	Mixed/sedimentary formations	Russia	47.29	39.10	1.8	1.8	0.993	0.009	0.985	0.006	0.985	-9.3	-11.0	92	8
11	Dordogne	Mixed/sedimentary formations	France	45.03	-0.59	2.7	3.3	0.888	0.002	0.952	0.001					
12	Elbe	Mixed/sedimentary formations	Germany	53.54	9.81	2.4	2.8	0.897	0.003	0.965	0.003			-10.8		
13	Elorn	Igneous/metamorphic terranes	France	48.40	-4.38	3.0	3.5	0.941	0.002	0.961	0.002	0.959	-10.9	-11.2	87	13
14	Fitzroy river	Igneous/metamorphic terranes	Australia	-17.73	123.64	3.0	2.9	1.098	0.002	0.973	0.002			-18.6		
15	Fly	Mixed/sedimentary formations	PNG	-8.67	144.00	2.6	2.3	0.894	0.001	0.948	0.001	0.933	-3.8	-4.9	71	29
16	Fortescue river	Igneous/metamorphic terranes	Australia	-21.29	116.14	2.6	2.1	1.072	0.004	1.029	0.002			-22.1		
17	Foyle	Igneous/metamorphic terranes	Ireland	54.76	-7.45	3.5	2.1	1.208	0.003	0.989	0.002	0.000	-15.2	-16.0		
18	Fraser	Volcanic Rocks	Canada	49.16	-123.37	1.7		0.948	0.004				-4.2	-8.5	86	14
19	Ganges	Mixed/sedimentary formations	Bangladesh	23.17	90.47	4.8	2.8			1.022	0.002			-15.4		
20	Gascogne	Igneous/metamorphic terranes	Australia	-29.83	113.77	3.3	2.2	1.197	0.001	1.082	0.002					
21	Glenariff	Volcanic Rocks	Ireland	55.02	-6.11	0.4	0.2	1.119	0.007	1.070	0.006	1.071	3.7	3.7	98	2
22	Jamata	Igneous/metamorphic terranes	Nigeria	6.13	6.76	4.1	8.1	1.052	0.002	0.932	0.001					
23	Kymijoki	Igneous/metamorphic terranes	Finland	60.46	26.91	3.7	3.6	0.961	0.003	0.972	0.002	0.970	-19.8	-19.2	76	24
24	Lee	Mixed/sedimentary formations	Ireland	51.88	-8.27	2.9	4.6	0.871	0.002	0.939	0.002					
25	Loire	Mixed/sedimentary formations	France	47.28	-1.90	3.0	4.4	0.937	0.002	0.959	0.001	0.955	-7.9	-8.3	80	20
26	Lough Erne	Mixed/sedimentary formations	Ireland	54.30	-7.64	4.0	3.8	0.908	0.002	0.976	0.003			-14.8		
27	Lower Bann	Mixed/sedimentary formations	Ireland	54.86	-6.48	1.6	1.5	0.935	0.003	0.966	0.002	0.965	-8.9	-8.9	98	2
28	Lule	Igneous/metamorphic terranes	Norway	65.68	21.82	9.9	3.1	1.317	0.002	1.076	0.002	1.093	-20.4	-18.0	93	7
29	MacKenzie	Mixed/sedimentary formations	Canada	69.26	-137.29	3.9	3.2	0.848	0.002	0.897	0.002	0.885	-12.2	-13.0	75	25
30	Mae Klong	Mixed/sedimentary formations	Thailand	13.43	99.95	4.1	3.6	1.004	0.001	1.008	0.001	1.007	-13.7	-14.3	71	29
31	Maine	Volcanic Rocks	Ireland	54.75	-6.32	0.6	0.3	1.298	0.002	1.138	0.006	1.150	0.6	0.1	93	7
32	Mayenne	Mixed/sedimentary formations	France	47.50	-0.55	3.5	2.6	1.003	0.001	0.945	0.002	0.957	-9.5	-9.6	80	20
33	Mekong	Mixed/sedimentary formations	Cambodia	10.96	105.06	3.9	3.3	1.008	0.002	1.051	0.002	1.034	-8.6	-10.5	61	39
34	Mississippi	Mixed/sedimentary formations	USA	28.93	-89.49	2.8	2.8	0.858	0.001	0.918	0.001	0.898	-10.8	-12.3	67	33
35	Moyola	Mixed/sedimentary formations	Ireland	54.75	-6.52	2.3	1.9	1.104	0.002	0.989	0.001	0.992	-16.1	-16.2	97	3
36	Murchison	Igneous/metamorphic terranes	Australia	-27.83	114.69	5.9	2.5	1.239	0.002	1.152	0.002			-23.6		
37	Nalon	Mixed/sedimentary formations	Spain	43.56	-6.07	3.6	4.8	0.892	0.002	0.947	0.001					
38	Narva	Mixed/sedimentary formations	Estonia	59.54	27.58	4.9	3.1	0.887	0.001	0.920	0.001	0.917	-16.7	-16.0	92	8
39	Nelson river	Igneous/metamorphic terranes	Canada	57.39	-91.80	2.8	1.4	0.823	0.002	0.932	0.002			-25.6		
40	Niger	Mixed/sedimentary formations	Nigeria	3.20	6.68	4.0	8.7	1.048	0.001	0.976	0.001	0.985	-11.9	-11.9	87	13
41	Nile	Volcanic Rocks	Egypt	32.51	30.38	2.2	3.0	0.947	0.001	0.978	0.001	0.968	-7.1	-9.6	69	31
42	Northern Dvina	Mixed/sedimentary formations	Russia	65.09	39.00	2.5	2.4	0.944	0.004	0.963	0.001	0.959	-17.7	-17.1	77	23
43	Orinoco	Mixed/sedimentary formations	Venezuela	7.65	-66.18	4.3	5.8	1.036	0.016	0.972	0.001	0.974	-13.8	-13.2	96	4
44	Pamisos	Mixed/sedimentary formations	Greece	37.02	22.02	2.8	2.1	0.849	0.001	0.942	0.004					
45	Red River	Mixed/sedimentary formations	Vietnam	20.26	106.52	4.4	3.2	0.888	0.001	0.942	0.001	0.928	-12.2	-12.8	74	26
46	Rhine	Mixed/sedimentary formations	Netherlands	51.91	4.48	3.7	3.2	0.819	0.003	0.943	0.001	0.926	-9.3	-9.1	86	14
47	Rio Aro	Igneous/metamorphic terranes	Venezuela	7.39	-64.01	3.6	4.7	1.162	0.005	1.014	0.001	1.042	-25.2	-28.5	81	19
48	Rio Caroni	Igneous/metamorphic terranes	Venezuela	8.33	-62.71	6.5	7.3	1.061	0.003	1.006	0.001	1.012	-20.9	-21.1	88	12
49	Rio Caura	Igneous/metamorphic terranes	Venezuela	7.58	-64.94	6.4	6.3	1.045	0.002	1.018	0.001	1.024	-21.1	-21.0	79	21
50	Ropotamo	Mixed/sedimentary formations	Bulgaria	42.32	27.75	2.1	2.0	1.007	0.004	0.967	0.006					
51	Sefid Rud	Mixed/sedimentary formations	Iran	37.47	49.94	2.6	2.2	0.946	0.002	0.943	0.002	0.943	-4.6	-4.5	90	10
52	Sepik river	Mixed/sedimentary formations	PNG	-3.13	142.78	1.8	1.1	0.957	0.002	0.984	0.003			0.4		
53	Severn	Mixed/sedimentary formations	UK	51.49	-2.78	2.6	2.6	0.849	0.001	0.947	0.002					
54	Shannon	Mixed/sedimentary formations	Eire	52.69	-8.91	3.6	3.3	0.873	0.001	0.935	0.001	0.925	-11.2	-11.5	83	17
55	Six Mile	Volcanic Rocks	Ireland	54.70	-6.15	1.2	0.8	1.278	0.004	1.128	0.002	1.146	-3.2	-2.8	88	12
56	Spercheios	Mixed/sedimentary formations	Ireland	54.93	-7.81	1.0	1.7	0.866	0.011	0.954	0.004					
57	Swilly	Igneous/metamorphic terranes	Ireland	54.93	-7.81	6.5	2.7	1.340	0.002	1.013	0.002	1.015	-13.9	-13.3	99	1
58	Thames	Mixed/sedimentary formations	Sweden	63.72	20.27	2.1	2.7	0.820	0.002	0.922	0.002			-12.4		
59	Ume	Igneous/metamorphic terranes	Sweden	63.72	20.27	5.0	3.2	1.180	0.002	1.011	0.002	1.021	-18.7	-17.6	94	6
60	Upper River Bann	Mixed/sedimentary formations	Ireland	54.38	-6.33	7.0	4.1	1.337	0.004	1.073	0.002					
61	Vanuatu	Volcanic Rocks	Vanuatu	-17.76	168.38	2.5	1.9	1.020	0.003	1.007	0.002					
62	Vistula	Mixed/sedimentary formations	Poland	54.65	19.28	2.7	1.8	1.300	0.021	1.101	0.008	1.135	-14.5	-14.5	83	17
63	Yangtze	Mixed/sedimentary formations	China	31.62	121.01	3.0	2.6	0.896	0.001	0.941	0.001	0.924	-10.5	-11.4	61	39
64	Yellow River	Mixed/sedimentary formations	China	37.80	118.91	2.5	2.2	0.972	0.003	1.001	0.002	0.999	-11.9	-10.9	93	7
	Mean values					3.3	3.0	1.001	0.003	0.987	0.002	0.936	-11.5	-12.7		

## 3.4 Discussion

### 3.4.1 Influence of grain size on ( $^{234}\text{U}/^{238}\text{U}$ ) ratios of detrital sediments

As modelled by DePaolo et al. (2006), the recoil loss factor is directly proportional to grain size, leading to separate time-dependent evolution of ( $^{234}\text{U}/^{238}\text{U}$ ) ratios in separate size fractions of the sediment. The influence of grain size on ( $^{234}\text{U}/^{238}\text{U}$ ) was also assessed by Dosseto et al. (2014), who analysed various size fractions of river suspended particulates from the Murray-Darling Basin in south-eastern Australia, ranging from the dissolved load (<10 kilo-daltons - kDa) to coarse silts (>25  $\mu\text{m}$ ). The above-mentioned studies showed that sedimentary ( $^{234}\text{U}/^{238}\text{U}$ ) ratios typically decrease with increasing grain size. To some extent, this ‘grain-size’ effect could explain the observed large range of sediment residence time determined in different river systems Granet et al. (2010).

In the studied sediment samples, the silt fraction generally represents between 60 and 95% of the bulk (<63  $\mu\text{m}$ ) detrital fraction (mean  $\sim 82 \pm 23\%$  2SE; (Bindeman et al. 2019)), meaning that the ( $^{234}\text{U}/^{238}\text{U}$ ) values of the silt-size fractions can be taken, to a first approximation, as representative of the bulk ( $^{234}\text{U}/^{238}\text{U}$ ) composition of the fine-grained detrital sediments investigated in this study.

A striking feature of our results is the fact that many clay-sized fractions are characterized by activity ratios higher than >1, often exhibiting higher values than in corresponding silts. As mentioned above, this observation is opposite to the grain-size effect predicted theoretically by DePaolo et al. (2006). In previous studies, samples exhibiting activity ratios >1 were generally discarded, because they were thought to be affected by the presence of radiogenic authigenic components (Dosseto et al. 2006a, Vigier et al. 2001, 2006, Granet et al. 2010, Martin et al. 2019). However, we are confident here that our clay-sized fractions solely correspond to detrital material, previously leached from any possible carbonate, oxide and/organic components. On this basis, we propose that measured activity ratios above 1 could reflect partial incorporation of  $^{234}\text{U}$  previously released from incongruent silicate weathering into neoformed clays (Plater et al. 1992, Dequincey et al. 2002).

### 3.4.2 The effect of weathering, climate and erosion on $^{234}\text{U}$ - $^{238}\text{U}$ fractionation

The disequilibrium between  $^{234}\text{U}$  and  $^{238}\text{U}$  in soils mainly reflects the recoil effect during water/rock interactions (Osmond & Ivanovich 1992, Riotte et al. 2003) and the preferential leaching of  $^{234}\text{U}$  relative to  $^{238}\text{U}$  embedded in recoil tracks (Fleischer 1980, 1982). It is important to investigate to which extent weathering could influence the distribution of ( $^{234}\text{U}/^{238}\text{U}$ ) ratios in river sediments and eventually lead to an over- or underestima-

tion of the sediment residence time in watersheds. In theory, bulk mineral dissolution should not lead to any significant fractionation between  $^{234}\text{U}$  and  $^{238}\text{U}$  (Chabaux et al. 2003a), so that chemical weathering intensity is not expected to have direct influence on sediment ( $^{234}\text{U}/^{238}\text{U}$ ). However, Li et al. (2016b) reported various correlations between ( $^{234}\text{U}/^{238}\text{U}$ ) and chemical weathering indices in leached river sediments ( $<50\ \mu\text{m}$ ), suggesting a link between U-isotope fractionation patterns and the type of weathering regime. Lower ( $^{234}\text{U}/^{238}\text{U}$ ) values ( $<0.90$ ), indicative of presumably longer sediment residence times, were determined in sediments having experienced intense chemical weathering in transport-limited regimes. In contrast, in weathering- (or kinetically) limited weathering regimes associated with high denudation rates and fast sediment transfer, Li et al. (2016b) proposed that high mineral dissolution rates could result in sedimentary ( $^{234}\text{U}/^{238}\text{U}$ ) ratios being close to 1. To some extent, this latter observation is counter-intuitive, because enhanced physical erosion in high mountain environments and other kinetically-limited weathering regimes could be alternatively associated with sediments having lower ( $^{234}\text{U}/^{238}\text{U}$ ) ratios, as a result of enhanced production of small grain-size sediments and associated  $^{234}\text{U}$  recoil loss. For these reasons, and because the chemical weathering signature of the sediments can be partly inherited from previous weathering cycles and sediment recycling (Dou et al. 2016), but also because the ( $^{234}\text{U}/^{238}\text{U}$ ) ratio only records the last million years of chemical weathering, Li et al. (2016b) remained cautious with the interpretation of the relationships between weathering indices and ( $^{234}\text{U}/^{238}\text{U}$ ). In our study, the ( $^{234}\text{U}/^{238}\text{U}$ ) composition of both silt-and clay size fractions does not display any relationships weathering indices, such as the Chemical Index of Alteration (CIA; Nesbitt & Young (1982); Fig. 3.4A) or the Chemical Index of Weathering (CIW; Harnois (1988); Fig. 3.4B). Considering only small catchments ( $<30 \times 10^3\ \text{km}^2$ ), in order to exclude any effect related to alluvial storage (which could further modify  $^{234}\text{U}/^{238}\text{U}$  activity ratios), no relationship was observed between ( $^{234}\text{U}/^{238}\text{U}$ ) and the CIA in river sediments (Appendix A3.1), while a weak correlation was identified with CIW in silt size fractions ( $R^2 = 0.56$  ; Appendix A3.2), with lower ( $^{234}\text{U}/^{238}\text{U}$ ) values being associated with higher CIW. Overall, our data indicate that chemical weathering intensity does not exert a first-order control on ( $^{234}\text{U}/^{238}\text{U}$ ) in river sediments, although enhanced weathering most likely results in preferential leaching of  $^{234}\text{U}$ , in agreement with the findings of Li et al. (2016b).

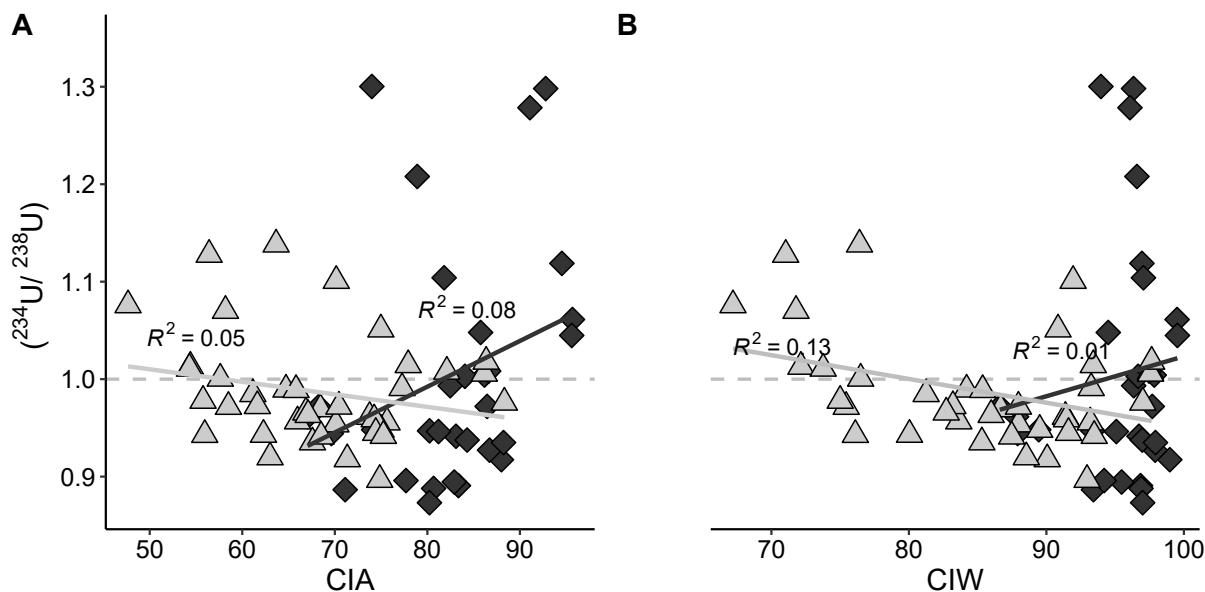


Figure 3.4 –  $(^{234}\text{U}/^{238}\text{U})$  activity ratio as function of (A) the Chemical Index of Alteration (CIA) in silt ( $n = 40$ , light grey) and clay ( $n = 34$ , dark grey) size fraction fractions; (B) the Chemical Index of Weathering (CIW) in silt ( $n = 40$ , light grey) and clay ( $n = 34$ , dark grey) size fraction fractions.  $2\sigma$  errors are smaller than the symbol size. No clear relation emerged between  $(^{234}\text{U}/^{238}\text{U})$  and weathering indices.

In addition to weathering, climate could also directly influence the observed degree of  $^{234}\text{U}$ - $^{238}\text{U}$  fractionation in river sediments. For instance, one would expect to observe an higher degree of  $^{234}\text{U}$ - $^{238}\text{U}$  fractionation in dry regions due to slow sediment transport (Kronfeld et al. 2004). Additionally, in cold arid regions, freeze-thaw physical weathering of rocks, which typically results in the formation of very fine sediments (Anderson 2005), could be accompanied by enhanced recoil effect and, in turn, low  $(^{234}\text{U}/^{238}\text{U})$  values in the residual fine-grained sediment (DePaolo et al. 2006). While glacial weathering in subarctic environments also drives intense rock physical weathering through glacial abrasion (Pedersen & Egholm 2013), resulting possibly in enhanced recoil effect and low  $(^{234}\text{U}/^{238}\text{U})$  ratios in corresponding sediments, Vigier et al. (2001) reported  $(^{234}\text{U}/^{238}\text{U})$  close to secular equilibrium in the suspended particulate loads of the Mackenzie River. In tropical regions with high rainfall, the degree of preferential  $^{234}\text{U}$  loss from detrital grains will be mostly dependent on the time elapsed in soils and associated recoil effect, which should lead to sediment  $(^{234}\text{U}/^{238}\text{U})$  close to secular equilibrium (Kronfeld et al. 2004, Robinson et al. 2004), as the sediment should be exported faster from regions experiencing heavy rainfall than from dryer catchments. However, high levels of precipitation could also drive high rates of physical erosion, which would increase mineral breakdown processes and hence result in lower  $(^{234}\text{U}/^{238}\text{U})$  (Dosseto et al. 2008b).

In this study, we investigated the potential relationship between climate and  $(^{234}\text{U}/^{238}\text{U})$

using the classification used by Bayon et al. (2016), which categorized studied river basins into distinct climate zones (see section 3.2.1; Fig. 3.5). A t-test comparison for each climatic zone indicates that there is statistically no significant ( $^{234}\text{U}/^{238}\text{U}$ ) variations (with all  $p$ -values  $>0.05$ ) between each climatic zones for both silt and clay fractions (Fig. 3.5), hence suggesting that climate does not play a major role in controlling the distribution of ( $^{234}\text{U}/^{238}\text{U}$ ) of river sediments. In order to separate any possible effect related to the size and lithology of studied river basins, we also investigated the influence of climate on ( $^{234}\text{U}/^{238}\text{U}$ ) in small catchments (Appendix A3.3) and igneous/metamorphic or sedimentary basins (Fig. 3.5), without identifying any clear relationships too. Additionally, no particular correlations were observed between ( $^{234}\text{U}/^{238}\text{U}$ ) in both silt and clay size fractions and MAT and MAP, regardless of the size and/or lithology of studied river basins (Fig. 3.5D; Appendix A3.4), hence supporting the view that ( $^{234}\text{U}/^{238}\text{U}$ ) in river sediments is not controlled by climate.

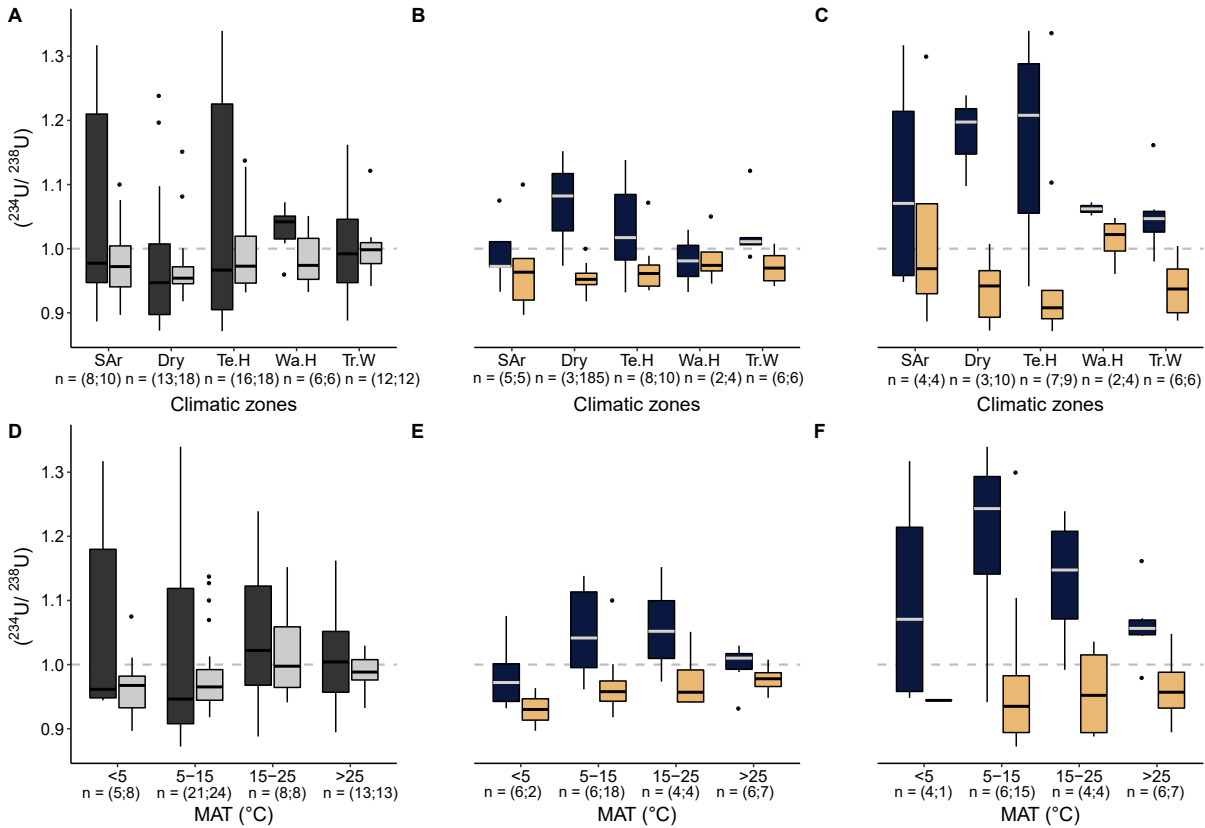


Figure 3.5 –  $(^{234}\text{U}/^{238}\text{U})$  activity ratios as a function of climatic zones as defined in Bayon et al. (2016): catchments are classified into five different climatic zones, defined according to the following arbitrary criteria: (1) ‘SAr’: cold and dry regions, with MAT  $<8\text{ }^{\circ}\text{C}$  and MAP  $<800\text{ mm}$ ; (2) ‘Dry’: Temperate and warm dry environments, with MAT  $>10\text{ }^{\circ}\text{C}$  and MAP  $<800\text{ mm}$ ; (3) ‘Te.H’: Temperate and humid regions, with  $8\text{ }^{\circ}\text{C} < \text{MAT} < 16\text{ }^{\circ}\text{C}$  and MAP  $>1000\text{ mm}$ ; (4) ‘Wa.H’: Tropical regions with humid conditions, with MAT  $>20\text{ }^{\circ}\text{C}$  and MAP  $<1500\text{ mm}$ ; and (5) ‘Tr.W’: Tropical wet regions, with MAT  $>20\text{ }^{\circ}\text{C}$  and MAP  $>1500\text{ mm}$ , depending on (A) grain size fractions (silt:light grey and clay: dark grey) or lithology (blue for igneous & metamorphic rocks and beige for sedimentary and mixed lithologies) in silt (B) and in clay (C) size fractions;  $(^{234}\text{U}/^{238}\text{U})$  activity ratios as a function of Mean Annual Temperature (MAT) of the catchment depending on (D) grain size fractions (silt:light grey and clay: dark grey) or lithology (blue for igneous & metamorphic rocks and beige for sedimentary and mixed lithologies) in silt (E) and in clay (F) size fraction. There is no apparent climate control on the  $(^{234}\text{U}/^{238}\text{U})$  activity ratios.

Physical erosion could also potentially play a role in controlling the U isotopic composition of detrital sediments. High mountain regions are typically subject to substantial denudation rates and rapid sediment export, while erosion is much reduced in floodplains and coastal areas (Burbank et al. 1996, von Blanckenburg 2006, Larsen & Montgomery 2012, Summerfield & Hulton 1994). High-elevation watersheds are generally characterized by “weathering-limited” regimes, where the rate of supply of detrital sediments is more rapid than the rate of silicate mineral dissolution. Sediment  $(^{234}\text{U}/^{238}\text{U})$  in such environments could remain close to 1, since there is limited time for substantial  $^{234}\text{U}$  loss from detrital grains. However, enhanced physical weathering in high mountain environments can also produce abundant fine-grained material with a high surface/volume ratio,

thus being more prone to  $^{234}\text{U}$  loss due to recoil effect. Li et al. (2016b) observed that ( $^{234}\text{U}/^{238}\text{U}$ ) ratios in Changjiang (Yangtze) and Zhuoshui rivers sediments increase with elevation in weathering-limited highlands, illustrating the relationship between U isotopes and erosion since higher elevations are also characterized by higher erosion rates. Under reduced physical erosion rates, such as in floodplains and lowlands, the residence time of sediments is relatively long, and this typically leads to more intense mineral dissolution. In such “transport-limited” weathering systems (Carson & Kirkby 1972, Stallard & Edmond 1983), the supply of fresh minerals is generally limited by the degree of soil removal in upper soil sequences (Riebe et al. 2004, West et al. 2005). As a result, the long duration of weathering is expected to result in low ( $^{234}\text{U}/^{238}\text{U}$ ) in fine-grained material. Li et al. (2017) identified a direct relationship between erosion rates and ( $^{234}\text{U}/^{238}\text{U}$ ) in sediments, showing that sedimentary ( $^{234}\text{U}/^{238}\text{U}$ ) ratio are generally lower in river basins characterized by low denudation rates, reflecting a long residence time of the sediment in soils. Here, there is no clear relationship between ( $^{234}\text{U}/^{238}\text{U}$ ) in silt and clay size fractions and the maximum elevation of the river basins (Fig. 3.6). Focusing on small catchments (Appendix A3.5) or grouping catchments according to their lithology yield similar observations for silt size fraction (Fig. 3.6B). In crystalline catchments (Fig. 3.6C), the ( $^{234}\text{U}/^{238}\text{U}$ ) of clay size fractions slightly decrease with increasing maximum elevation ( $R^2 = 0.46$ ). This suggests that the effect of physical weathering on producing fine grained sediments and thus promoting  $^{234}\text{U}$  loss, dominates over the role of physical erosion on reducing sediment residence time (and thus limiting  $^{234}\text{U}$  loss).

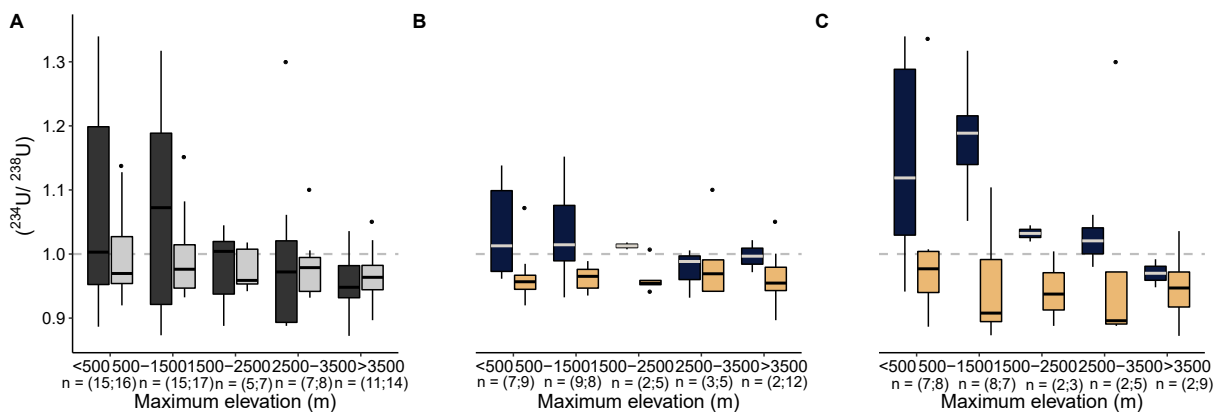


Figure 3.6 – ( $^{234}\text{U}/^{238}\text{U}$ ) activity ratios as function of maximum elevation of the catchment depending on (A) grain size fractions (silt: light grey and clay: dark grey); lithology (blue for igneous & metamorphic rocks and beige for sedimentary and mixed lithologies) in (B) silt and in (C) clay size fraction. There is no clear relationships between maximum elevation and ( $^{234}\text{U}/^{238}\text{U}$ ), except in crystalline catchments where ( $^{234}\text{U}/^{238}\text{U}$ ) of clay size fractions slightly decrease with increasing maximum elevation.

Table 3.4 – Characteristics of the studied samples and their sedimentary system

River (n= 64)	Type of rocks inside the basin (%)		Clays	Silts	bulk	Clays	Silts	bulk	Climatic zone	MAT (°C)	MAP (mm)	Maximum elevation (m)	DTB (cm)	Area (10 <sup>3</sup> km <sup>2</sup> )	
	Sedimentary	Igneous													Volcanics
1 Adour	45.3	15.8	0.3	83.4	68.5	71.0	96.8	86.7	88.4	Te.H	13	1260	2800	1717	16
2 Amazon	43.8	22.9	4.2	88.0	75.6		99.0	93.2		Tr.W	27	2030	5500	2342	6300
3 Betsiboka										Tr.W					
4 Blackwater	88.6	0.0	3.3	86.7	66.0	0.0	97.9	83.6	0.0	Te.H	9	1000	360	976	1.1
5 Brantas	9.0	0.0	65.7							Tr.W	25	2982	3480	3235	11
6 Chao Phraya	38.2	18.4	5.1	86.5	77.3	80.3	97.7	93.3	94.7	Tr.W	28	1500	2500	6378	160
7 Churchill	10.5	57.9	1.4							SAr	-3		800	1138	290
8 Clarence										Wa.H		1500	250		0.132
9 Danube	66.9	12.6	3.0		70.1			88.0		Dry	10	760	4100	2106	820
10 Don				82.5	61.1	62.9	96.3	81.3	82.5	SAr	7	580	180		420
11 Dordogne										Dry		800	1700		24
12 Elbe										Dry	7		800		148.3
13 Elorn	50.3	49.7	0.0	83.1	73.8	75.0	96.7	91.4	92.1	Te.H	11	1120	340	1289	0.3
14 Fitzroy river										Dry	19	760	490		1305
15 Fly	32.3	0.3	3.9	82.9	75.0	77.3	95.5	89.5	91.2	Tr.W	26	2850	4000	2456	76
16 Fortescue river	10.9	19.4	8.1							Wa.H	25		1150		727
17 Foyle	2.5	52.7	6.2	78.9	64.7	0.0	96.6	84.2	0.0	Te.H	9	1110	640	1063	2.9
18 Fraser	33.1	26.9	39.5	74.2	58.5	60.7	89.4	75.4	77.4	SAr	4	760	4000	2162	230
19 Ganges	29.6	27.1	6.4							Te.H	18		7000	3061	1080
20 Gasconne										Dry	22	235	500		79
21 Glenariff	12.4	0.0	64.4	94.5	58.2	59.1	96.9	71.8	72.4	Te.H	9	1000	410	1129	0.1
22 Jamata										Wa.H	29		820		
23 Kymijoki				67.1	61.6	62.9	87.8	83.2	84.3	SAr	3	600	100		37
24 Lee										Te.H					1.2
25 Loire	56.2	28.1	4.4	84.3	74.3	76.3	97.0	91.5	92.6	Dry	11	750	1900	1650	120
26 Lough Erne										Te.H	9		650		948
27 Lower Bann				88.2	66.9	67.4	97.9	82.7	83.1	Te.H	9	1000	640	943	5.8
28 Lule				47.7				67.2		SAr	-3	700	1000		25
29 MacKenzie	77.2	19.9	1.6	79.2	74.9	75.9	96.5	93.0	93.8	SAr	-4	380	3600	1099	1800
30 Mae Klong	62.0	15.2	3.7	86.2	82.1	83.3	93.4	97.6	97.6	Tr.W	28	1200	2200	6785	31
31 Maine	0.0	0.0	98.0	92.8	63.7	65.8	96.3	76.4	77.9	Te.H	9	1000	460	1032	0.29
32 Mayenne				84.1	74.4	76.4	96.7	91.6	92.6	Dry	12	630	420	1587	4.4
33 Mekong				86.6	75.0	79.5	97.5	90.8	93.4	Wa.H	21	1270	5100	5292	800
34 Mississippi	68.5	4.5	1.8	84.3	71.3	75.6	97.2	90.1	92.4	Dry	13	760	3700	3262	3300
35 Moyola	47.6	19.2	32.4	81.8	65.8	66.2	97.1	85.4	85.7	Te.H	9	1110	540	1087	0.3
36 Murchison	2.0	18.1	1.5							Dry	22		520	1442	82
37 Nalon										Dry			1400		3.7
38 Narva				71.1	63.0	63.7	93.4	88.5	88.9	SAr	6	640	320	1941	56
39 Nelson river	66.5	24.0	3.1							Te.H	-3		3400	2829	1100
40 Niger	5.6	40.3	1.2	85.8	88.3	88.0	94.5	97.0	96.7	Wa.H	29	1140	820	12474	2200
41 Nile	17.8	34.5	7.3	80.2	55.8	63.3	93.4	75.0	80.7	Dry	27	610	3800	11262	2900
42 Northern Dvina	56.4	0.0	0.0	69.6	67.1	67.7	87.9	86.0	86.4	SAr	1	740	200	2906	357
43 Orinoco	9.8	20.7	2.8	70.4				88.0		Wa.H	24	1400	6000	4587	1100
44 Pamisos										Dry			2300		0.5
45 Red River	80.4	14.6	1.7	80.7	75.2	76.7	96.9	93.5	94.4	Tr.W	24	1750	3100	1126	160
46 Rhine	63.0	12.1	3.2	75.5	55.9	58.7	93.0	76.1	78.5	Te.H	8	1210	3500	1639	220
47 Rio Aro	0.0	54.6	25.6	77.9				93.4		Tr.W	25	3700	810	2738	30
48 Rio Caroni	1.8	18.0	29.3	95.7	86.2	87.3	99.5	97.6	97.8	Tr.W	25	2800	2660	2082	95
49 Rio Cauca	1.8	60.6	23.9	95.6	86.3	88.3	99.5	97.7	98.0	Tr.W	25	3700	2350	2086	48
50 Ropotamo										Dry			400		0.2
51 Sefid Rud	45.4	7.2	29.1	81.2	62.3	64.2	95.1	80.0	81.5	Dry	14	520	4230	1002	13
52 Sepik river	36.3	12.8	1.9							Tr.W	25		4000	1684	78
53 Severn										Dry			610		11.4
54 Shannon	96.0	0.0	0.7	80.2	67.6	69.7	97.0	85.3	87.3	Te.H	9	1200	570	923	23
55 Six Mile	0.1	0.0	96.6	91.1	56.4	60.6	96.1	71.0	74.0	Te.H	9	1000	420	813	0.3
56 Spercheios										Dry			2300		1.8
57 Swilly					54.4	54.0		72.1	71.6	Te.H	9	1110	15	905	0.1
58 Thames										Dry	10		330		12.9
59 Ume					54.3	51.0		73.8	69.3	SAr	1	520	1000		26
60 Upper River Bann										Te.H			110		2
61 Vanuatu										Tr.W			1900		
62 Vistula	23.5	0.1	0.0	74.0	70.2	70.8	94.0	91.9	92.3	SAr	8	750	2500	2235	200
63 Yangtze	69.5	10.6	3.8	77.7	68.5	72.1	94.2	87.5	90.1	Te.H	16	1270	3200	1614	1800
64 Yellow River	40.3	9.2	2.0	68.3	57.6	58.4	86.6	76.5	77.2	Dry	13	760	5100	2469	750

Percentage of type of rocks inside the basin are from Bayon et al. (2020).

CIA values (refers to Chemical Index of Alteration) are from Bayon et al. (2015).

CIW calculated based on data from Bayon et al. (2015).

Climatic categories are from Bayon et al. (2018) with (1) 'SAr': cold and dry regions, with MAT < 8 °C and MAP < 800 mm; (2) 'Dry': Temperate and warm dry environments, with MAT > 10 °C and MAP < 800 mm; (3) 'Te.H': Temperate and humid regions, with 8 °C < MAT < 16 °C and MAP > 1000 mm; (4) 'Wa.H': Tropical regions with humid conditions, with MAT > 20 °C and MAP < 1500 mm; and (5) 'Tr.W': Tropical wet regions, with MAT > 20 °C and MAP > 1500 mm.

Mean annual temperature (MAT) and mean annual precipitation (MAP) data are from Bayon et al. (2016, 2018).

Maximum elevation and area of river basins was either derived from Milliman & Farnsworth (2013), or determined in the geographical information system (GIS) software ArcGis (ESRI 2001, ArcGis Desktop 10.3.1) using the hydrological data and maps based on shuttle elevation derivatives HydroBASINS (Lehner and Grill, 2013)

Depth to bedrock (mean absolute depth to bedrock) were extracted from the SoilGrids system (<https://www.soilgrids.org>).

### 3.4.3 The role of lithology

The degree of rock weathering and erosion on continents is strongly dependent on lithology (Meybeck 1987, Bluth & Kump 1994). For instance, the evidence that sedimentary rocks weather much faster than crystalline igneous or metamorphic rocks could possibly impact the distribution of ( $^{234}\text{U}/^{238}\text{U}$ ) in sediments.

In basins underlain by carbonaceous sedimentary rocks, the combination of both high weathering and high physical denudation rates (Bluth & Kump 1994, Suchet et al. 2003, Palumbo et al. 2010) could result in short sediment residence time and as a consequence to reduced degrees of  $^{234}\text{U}$ - $^{238}\text{U}$  fractionation in corresponding sediments. In such sedimentary basins, ( $^{234}\text{U}/^{238}\text{U}$ ) in detrital grains could be expected to be close to secular equilibrium, as long as the source sedimentary rocks are initially in secular equilibrium (e.g. Sarin et al. 1990). In contrast, weathering is slower in river basins dominated by igneous or metamorphic rocks, and this could result in lower sediment ( $^{234}\text{U}/^{238}\text{U}$ ) ratios. With regard to U isotopes, multi-lithological catchments could behave similarly to sedimentary basins, as marls and other carbonaceous sedimentary rocks typically weather more rapidly than igneous and metamorphic rocks, hence possibly resulting in ( $^{234}\text{U}/^{238}\text{U}$ ) near secular equilibrium in erosional products.

To determine the role of lithology on ( $^{234}\text{U}/^{238}\text{U}$ ) ratios in river sediments, we compared ( $^{234}\text{U}/^{238}\text{U}$ ) of both silt and clay fractions with the percentage of sedimentary, igneous, and volcanic rocks for corresponding river catchments (Bayon et al. 2020; Table 3.3). Interestingly, while there is no correlation with the percentage of igneous or volcanic rocks, we observe a broad relationship between ( $^{234}\text{U}/^{238}\text{U}$ ) and the percentage of carbonate rocks (silt:  $R^2 = 0.42$  ; clay:  $R^2 = 0.50$  ; Fig. 3.7B). Additionally, the possible effect of the lithology can be also assessed by comparing measured ( $^{234}\text{U}/^{238}\text{U}$ ) ratios to corresponding neodymium (Nd) isotopic compositions for the same sediment fractions (Bayon et al. 2015, 2020) (expressed here as  $\varepsilon_{Nd}$  values; Fig. 3.7A). In contrast with U isotopes, sedimentary neodymium isotopic signatures from the initial rocks are preserved during all weathering, transport and depositional processes (e.g. Goldstein et al. (1984), and hence can be used as sediment provenance tracers (e.g. Goldstein & Hemming (2003)). To a large extent, the distribution of  $\varepsilon_{Nd}$  values in river-borne sediments reflects the mean age of average source rocks in corresponding drainage basins (Goldstein & Jacobsen 1987), and hence can be used, to a first approximation, as a lithological tracer for discriminating between sediments derived from ‘old’ igneous/metamorphic provinces (characterized by low  $\varepsilon_{Nd}$  values typically below -14; Bayon et al. (2015)), and ‘young’ volcanic basins (with  $\varepsilon_{Nd}$  values typically  $>-5$ ). Large river systems draining a large diversity of continental rocks generally display intermediate  $\varepsilon_{Nd}$  values Goldstein et al. (1984), Bayon et al. (2015), which make Nd isotopes less suitable as lithological tracers. In this study, there is no direct relationship between  $\varepsilon_{Nd}$  and ( $^{234}\text{U}/^{238}\text{U}$ ) in both size fractions (Fig. 3.7A).

A t-test indicates a statistically significant difference between sediments originating from crystalline basins ( $-15 < \varepsilon_{Nd}$  or  $\varepsilon_{Nd} > -5$ ), which have ( $^{234}\text{U}/^{238}\text{U}$ ) mostly  $> 1$  and sediments that are from sedimentary basins ( $-15 > \varepsilon_{Nd} > -5$ ), which generally have ( $^{234}\text{U}/^{238}\text{U}$ ) below 1, with a  $p$ -value between these two groups of 0.0015 ( $< 0.05$ ).

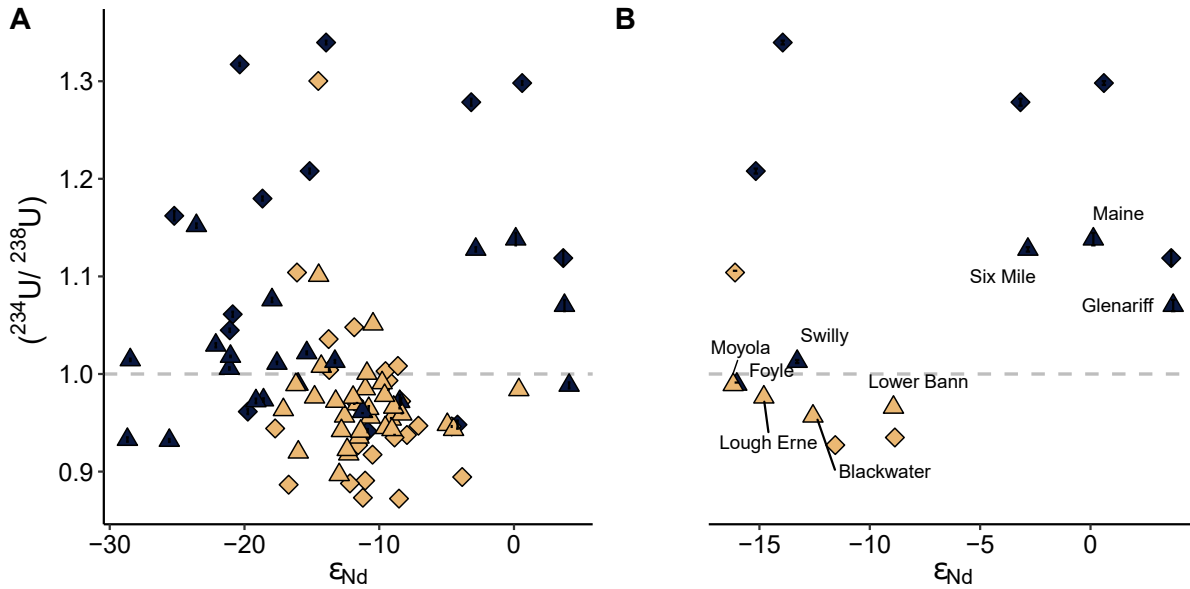


Figure 3.7 – ( $^{234}\text{U}/^{238}\text{U}$ ) activity ratios as a function of (A)  $\varepsilon_{Nd}$  values (from Bayon et al., 2015; 2020) in sediments (diamonds: clay, triangles: silt (blue for igneous & metamorphic rocks and beige for sedimentary and mixed lithologies) for all studied rivers (silt,  $n = 51$ ; clay,  $n = 40$ ), (B)  $\varepsilon_{Nd}$  values for Northern Ireland rivers (silt,  $n = 9$ ; clay,  $n = 8$ ). There is no direct control of the global lithology on the variation of ( $^{234}\text{U}/^{238}\text{U}$ ), however the percentage of sedimentary rocks inside the basin influence ( $^{234}\text{U}/^{238}\text{U}$ ).

The role of lithology on ( $^{234}\text{U}/^{238}\text{U}$ ) can be further explored considering the case study of rivers from Northern Ireland. As discussed in Bayon et al. (2018), rivers from Northern Ireland drain watersheds characterized by distinct geological formations, including Cenozoic basaltic rocks (River Bush, River Maine, Six-Mile Water), old Proterozoic metamorphic terranes (River Foyle, River Swilly, Moyola), and Paleozoic/Mesozoic sedimentary rocks (Blackwater, Lough Erne, Lower River Bann). Northern Ireland was completely covered by the British-Irish ice sheet during the last glacial period (Clark et al. 2012b). As a consequence, the fine-grained particulate loads transported by Northern Irish rivers are most likely derived from the erosion of late glacial deposits and/or post-glacial soil sequences that developed in the region after the retreat of the ice-sheet (i.e. paraglacial processes; Church & Ryder 1972), hence from soils having similar ages of formation (Dempster et al. 2013). In addition, all studied river systems are characterised by very similar climatic conditions. Therefore, any observed ( $^{234}\text{U}/^{238}\text{U}$ ) variation amongst studied sediment samples is likely to reflect lithological effects, rather than differences in sediment

transfer, soil age or climate. Rivers draining the British Tertiary volcanic province carry clay- and silt-sized detrital fractions both characterized by  $(^{234}\text{U}/^{238}\text{U}) > 1$  (Fig. 3.7B). The three rivers draining Proterozoic metamorphic rocks display clays with  $(^{234}\text{U}/^{238}\text{U}) > 1$  and coarser silt fractions with activity ratios close to 1 (Fig. 3.7C). The sediments from the Paleozoic/Mesozoic sedimentary rocks have  $(^{234}\text{U}/^{238}\text{U}) < 1$  in both silt and clay size fraction. Thus, in the case of Northern Ireland, river sediments derived from sedimentary basins also appear to exhibit  $(^{234}\text{U}/^{238}\text{U})$  ratios lower than those from crystalline basins. For such sedimentary basins, the presence of relatively low  $(^{234}\text{U}/^{238}\text{U})$  signatures in river sediments could reflect a residual  $(^{234}\text{U}/^{238}\text{U})$  composition  $< 1$  in corresponding source rocks, although it remains unclear how any significant  $^{234}\text{U}$ - $^{238}\text{U}$  disequilibrium could possibly occur in rocks older than 1 Ma. A more plausible explanation is that the lower  $(^{234}\text{U}/^{238}\text{U})$  values determined in sediments from sedimentary basins reflect the fact that sedimentary rock weathering most likely results in finer particle sizes compared to the alteration and erosion of crystalline silicate rocks. However, the t-test comparison between grain sizes from each lithological group indicates that there is no statistically significant variation of  $(^{234}\text{U}/^{238}\text{U})$  with  $p$ -values  $> 0.05$  (0.94) for sediments from sedimentary and mixed lithologies, and close to 0.05 (0.06) for sediments from igneous & metamorphic rocks. The observed  $(^{234}\text{U}/^{238}\text{U}) > 1$  in sediments derived from crystalline basements could reflect the fact that neo-formed clays produced from crystalline silicate rocks are more prone to subsequent re-adsorption of  $^{234}\text{U}$  on secondary clays, although further investigation will be required to test this hypothesis. To summarize, while the lack of any strong relationship between U and Nd isotopes suggests that the lithology does not represent a major control on the distribution of  $(^{234}\text{U}/^{238}\text{U})$  ratios of river sediments, the apparent correlation observed between  $(^{234}\text{U}/^{238}\text{U})$  and the percentage of carbonate rocks in river catchments implicitly suggests that the degree of U isotope fractionation in fine-grained sediments is partially dependent on the lithology of source rocks, probably reflecting the fact that they are being eroded more rapidly (and presumably into finer particle sizes) than crystalline silicate rocks.

#### **3.4.4 The role of catchment size and sediment residence time on $(^{234}\text{U}/^{238}\text{U})$ sedimentary ratio**

As mentioned in the Introduction, the sediment transfer time within any given watershed is expected to exert a major control on sedimentary U isotopic ratios. The residence time of sediments in river basins is mainly influenced by the possibility of storage along its pathway from the hillslopes to the alluvial plain or the nearby ocean margin. Sediment transport along river systems is generally complex and mostly related to geomorphic parameters (Harvey 2002). Several studies highlighted the relationships between sedimentary fluxes and both external (climate, sea-level) and internal factors (drainage

area, relief, lithology) (Milliman & Syvitski 1992, Syvitski et al. 2003). In particular, the drainage area and relief are the main parameters that govern the quantity of sediments delivered downstream of alluvial plains (Hovius 1998, Milliman & Syvitski 1992, Syvitski et al. 2003, Walling & Webb 1996).

In general, the capacity of sediment storage in river basins is controlled by their geomorphological characteristics. On hillslopes, storage is dependent on soil thickness and the mean slope of the watershed, with thick soil sequences being typically associated with reduced erosion and vice versa. In this study, no global correlations were identified between ( $^{234}\text{U}/^{238}\text{U}$ ) and mean soil thickness (Fig. 3.8A), even when considering small catchments only (Appendix A3.6). However, when investigating separately the relationship between ( $^{234}\text{U}/^{238}\text{U}$ ) and soil thickness in igneous/metamorphic and sedimentary basins (Fig 3.8B & C), we can notice a slight decrease of the ( $^{234}\text{U}/^{238}\text{U}$ ) ratios as the average depth to bedrock decreases in sedimentary watersheds. In contrast, clays separated from crystalline basins display a trend exhibiting decreasing ( $^{234}\text{U}/^{238}\text{U}$ ) ratios when the depth to bedrock increases (Fig. 3.8C), in agreement with the fact that sediments will spend more time in thicker soil sequences (thus  $^{234}\text{U}/^{238}\text{U}$  activity ratios will decrease accordingly). Ideally, sediment samples collected at the bottom of hillslopes would be best suited to investigate the role of hillslope storage on the ( $^{234}\text{U}/^{238}\text{U}$ ) of sediments, rather than at the river mouth, where the effect of alluvial storage adds complexity to the interpretation. This may explain the apparent lack of clear control of hillslope storage on the ( $^{234}\text{U}/^{238}\text{U}$ ) of sediments.

In river basins where alluvial storage is significant, the sediment residence time could be a function of the size of the alluvial plain and its storage efficiency. Previous studies have shown that specific sedimentary fluxes decrease with the size of the drainage area (Milliman & Syvitski 1992, Syvitski & Milliman 2007), whenever storage efficiency is increasing. No strong relationship is apparent when looking at the variation of clay- and silt-size ( $^{234}\text{U}/^{238}\text{U}$ ) depending on the size of the catchment (Fig. 3.8D, Table 4), except when considering the rivers draining igneous & metamorphic rocks, in which activity ratios decrease as the size of the catchment increases (Fig. 3.8E & 3.8F). These observations clearly suggest that the size of the catchment and inferred sediment residence time exerts a major role in controlling the degree of  $^{234}\text{U}$ - $^{238}\text{U}$  fractionation in river sediments. The observed slight increase of ( $^{234}\text{U}/^{238}\text{U}$ ) in river sediments from the largest catchments could indicate that incorporation of  $^{234}\text{U}$  into neo-formed clays occurs during the storage of the sediments along the alluvial plain. It is interesting to note that no trend is visible for sediments derived from basins draining sedimentary rocks and mixed lithologies. One hypothesis to explain this absence of relationship could be that the weathering in sedimentary rocks create grains with inherited shapes, by breaking the cement linking them, whereas in crystalline basins silicate weathering generates new grains with fresh mineral surfaces prone to dissolution. The fractionation of  $^{234}\text{U}$  over  $^{238}\text{U}$  being influenced by the

shape of the grain, this could explain the observed difference ( $^{234}\text{U}/^{238}\text{U}$ ) and the drainage area in sedimentary and crystalline basins.

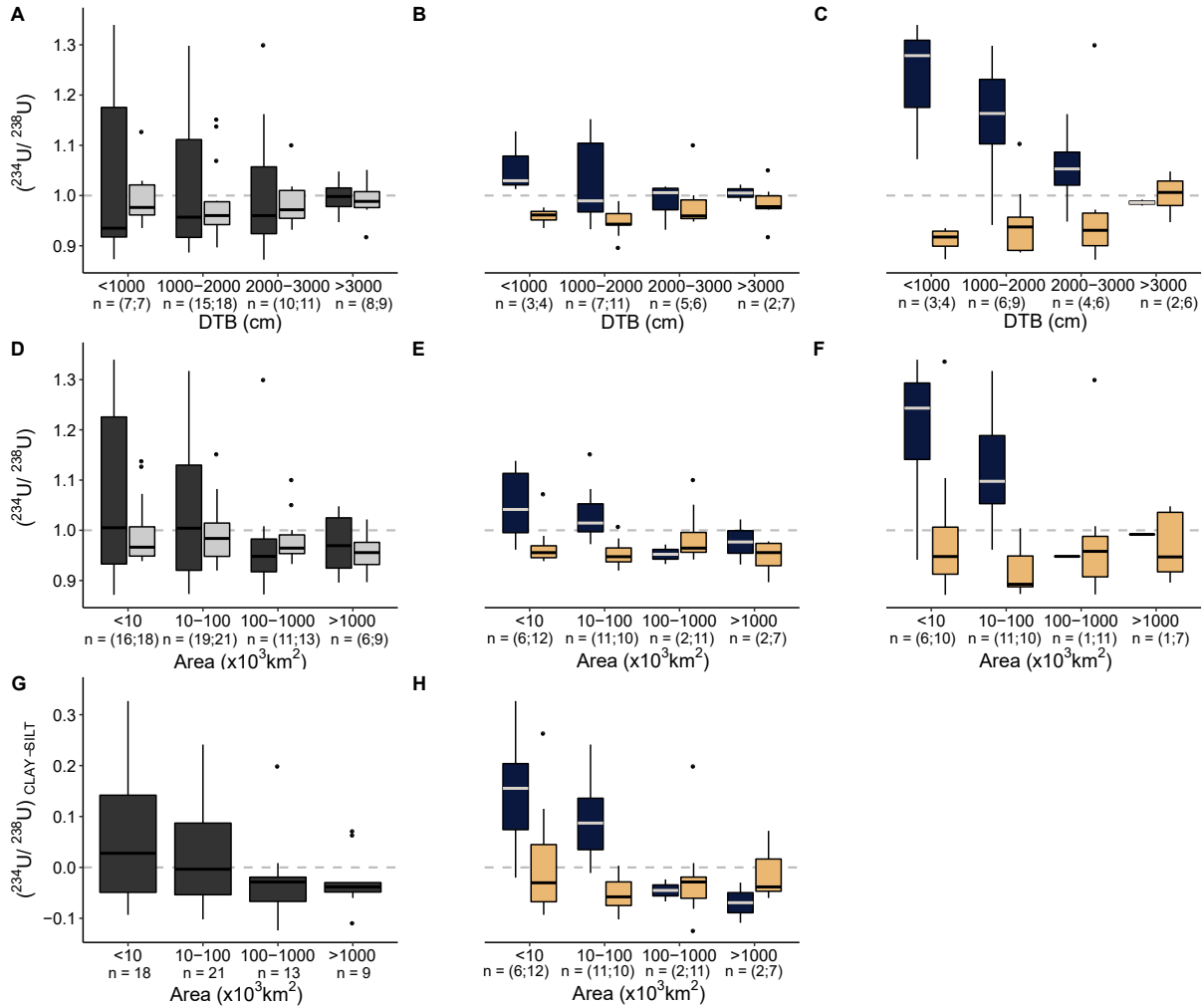


Figure 3.8 – ( $^{234}\text{U}/^{238}\text{U}$ ) activity ratios as a function of Depth To Bedrock (DTB; in cm) (A) depending on grain size fractions (silt: light grey and clay: dark grey) (B) lithology (blue for igneous & metamorphic rocks and beige for sedimentary and mixed lithologies) in silt and (C) in clay size fraction; ( $^{234}\text{U}/^{238}\text{U}$ ) activity ratios as a function of drainage area (in  $\text{km}^2$ ) (D) depending on grain size fractions (silt:light grey and clay: dark grey) (E) lithology (blue for igneous & metamorphic rocks and beige for sedimentary and mixed lithologies) in silt and (F) in clay size fraction; (G) difference of ( $^{234}\text{U}/^{238}\text{U}$ ) between clay and silt size fractions, as a function of the basin drainage area, (H) grouped in two lithological categories (blue for igneous & metamorphic rocks and beige for sedimentary and mixed lithologies). The ( $^{234}\text{U}/^{238}\text{U}$ ) activity ratio is mainly dependent of the size of the drainage area.

Coarse-grained sediments are generally stored more efficiently in watersheds, hence being associated with greater transfer time, while in contrast, fine-grained particles such as clays are more rapidly exported from river systems (Russell 1955). This time-integrated differential behaviour between coarse and fine particles possibly accounts for the observed relationship in Fig. 3.8G, showing that in small sedimentary basins (area  $<30 \times 10^3 \text{ km}^2$ ),

the ( $^{234}\text{U}/^{238}\text{U}$ ) activity ratio is lower in silt-size fractions compared to clays (Fig. 3.8H). As silt-size particles reside for a presumably longer time than clays in river systems, they are likely to be comparatively depleted in  $^{234}\text{U}$ , leading to lower ( $^{234}\text{U}/^{238}\text{U}$ ) signatures than in corresponding clays (Fig. 3.9). Conversely, in larger sedimentary systems, the difference in ( $^{234}\text{U}/^{238}\text{U}$ ) between clay and silt fractions is null or slightly negative (Fig. 3.8H), which could suggest that extensive storage in the alluvial system can buffer differences in transport rate between the two size fractions (Fig. 3.9).

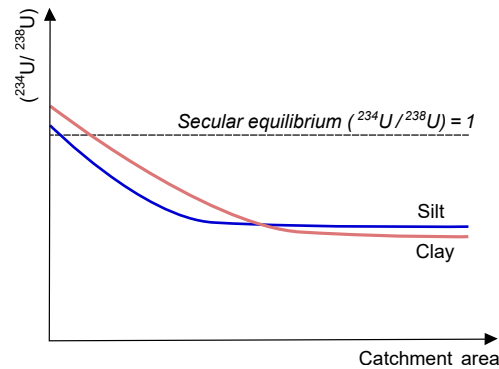


Figure 3.9 – Schematic evolution of ( $^{234}\text{U}/^{238}\text{U}$ ) in silt and clay fractions as a function of the catchment size. In small catchments, the clay fraction may be exported too rapidly to develop significant  $^{234}\text{U}$  depletion, with ( $^{234}\text{U}/^{238}\text{U}$ ) remaining close to the secular equilibrium, while a slower transport for silts results in more pronounced  $^{234}\text{U}$  depletion and ( $^{234}\text{U}/^{238}\text{U}$ ) ratios  $<1$ . In large river systems, alluvial storage buffers the difference in the transport rates of clays and silts, implying that both fractions show significant  $^{234}\text{U}$  depletion.

### 3.4.5 Complex interactions of environmental controls on sediment residence time

In a sedimentary system, many external and internal parameters interact together to result in a variety of different landscape morphologies. Thus, after having shown in the above discussion that the distribution of ( $^{234}\text{U}/^{238}\text{U}$ ) in river sediments is not controlled by any single parameter, it is interesting to investigate the combined influences of several parameters on measured ( $^{234}\text{U}/^{238}\text{U}$ ) ratios. For this purpose, we used a multiple regression analysis between ( $^{234}\text{U}/^{238}\text{U}$ ) in both silt and clay fractions and all the environmental parameters that were discussed above: MAP and MAT for the climatic parameters; CIA for the degree of chemical weathering; the percentage of sedimentary rocks outcropping in river catchments and  $\varepsilon_{Nd}$  for the lithology; the depth to bedrock, the catchment size and maximum elevation for the physical basin characteristics. The obtained predicted ( $^{234}\text{U}/^{238}\text{U}$ ) agree well with measured ( $^{234}\text{U}/^{238}\text{U}$ ) values, with  $R^2 = 0.68$  ( $n = 30$ ; Figure 3.10) for silt-size fractions. As a consequence, this implies that about 70% of the variability of U activity ratios in river sediments can be explained by the sum of these different environmental parameters. Note however that the obtained  $p$ -value for each in-

dividual variable is only significant for the percentage of sedimentary rocks within the basin, suggesting that all the resulting relationship need to be considered with caution. For the clay-size fractions, the same parameters can predict 80% of ( $^{234}\text{U}/^{238}\text{U}$ ) (n=28;  $R^2 = 0.80$ ), with  $p$ -values being only statistically significant for MAP ( $p$ -value = 0.01 <0.05), the maximum elevation of the basin ( $p$ -value = 0.02 <0.05) and the depth to bedrock ( $p$ -value = 0.01 <0.05). Despite inherent uncertainties, this multiple regression analysis indicates that many environmental factors govern the distribution of ( $^{234}\text{U}/^{238}\text{U}$ ) and the sediment residence time in river catchments.

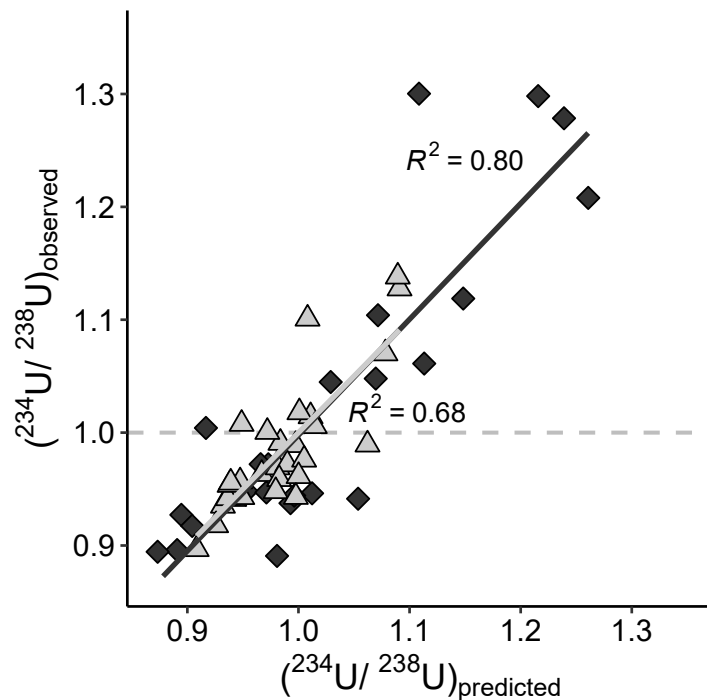


Figure 3.10 – ( $^{234}\text{U}/^{238}\text{U}$ ) activity ratio observed in river sediments compared with ( $^{234}\text{U}/^{238}\text{U}$ ) activity ratio predicted with a multiregression analysis while considering: MAP, MAT, CIA, the percentage of carbonate rocks,  $\epsilon_{Nd}$ , the depth to bedrock, the Area and the maximum of elevation of the catchment, (silt: light grey and clay: dark grey).  $2\sigma$  errors are smaller than the symbol size. The fractionation of uranium isotopes is dependant of multiple factors that control sedimentary processes, which reflect the complexity of sedimentary system.

### 3.5 Conclusion

Our large-scale investigation of river sediments worldwide demonstrates a strong grain size decoupling of U isotopes. A significant proportion of fine-grained (clay-size) sediments in river basins are characterized by ( $^{234}\text{U}/^{238}\text{U}$ ) values above secular equilibrium ( $>1$ ), especially in crystalline basins regions dominated by volcanic and igneous/metamorphic rocks, possibly reflecting the preferential incorporation of dissolved  $^{234}\text{U}$  into secondary clays upon weathering. Neither weathering intensity, climate, erosion nor lithology appear to directly govern the distribution of ( $^{234}\text{U}/^{238}\text{U}$ ) values in river sediments, although

the erosion of sedimentary rocks most likely results in a higher degree of  $^{234}\text{U}$ - $^{238}\text{U}$  fractionation compared to crystalline silicate rocks, possibly reflecting the fact that it can generate finer sediments that are more prone to  $^{234}\text{U}$  loss through recoil effect. Overall, the size of the catchments is identified as being one of the main parameters explaining the observed distribution of ( $^{234}\text{U}/^{238}\text{U}$ ) in river sediments, via its impact on the sediment residence time. In catchments draining crystalline basement rocks, the difference between ( $^{234}\text{U}/^{238}\text{U}$ ) in silt- and clay-size fractions is best explained by the fact that clays are exported more rapidly than silts, resulting in different size-dependent ( $^{234}\text{U}/^{238}\text{U}$ ) signatures. In large river basins, sediment storage in alluvial plains also impact the distribution of ( $^{234}\text{U}/^{238}\text{U}$ ) in river sediments, causing significant  $^{234}\text{U}$  loss regardless of grain size. Taken together, our findings confirm that U isotopes are sensitive tracers of the sediment residence time in river basins, providing further evidence for their utility in the sedimentary record to reconstruct past variations in sediment residence time and their links to landscape evolution.

### 3.6 Acknowledgments

We gratefully acknowledge all who very kindly provided us with the studied samples: O. Adeaga, J. Allard, C. Bigler, F. Busschers, G. Calvès, K. Cohen, P. Debrock, B. Dennielou, F.X. Gingele, D. Haynes, P.R. Hill, B. Hoogendoorn, S. Jorry, G. Kowaleska, T. Leipe, S. Leroy, L. Lopez, J. P. Lunkla, I. Mendes, D. Meunier, C. Nittrouer, A. Pasquini, V. Ponomareva, Y. Saito, E. Schefuss, V. Shevchenko, L. Tiron, D. Toucanne, S. VanLaningham, A. Wheeler. We are also thankful to A. Francke for providing samples to test the leaching protocol. We thank Pr. F. Chabaux and two anonymous reviewers for their helpful comments that greatly improved this manuscript. The project was funded through a joint IFREMER - University of Wollongong postgraduate scholarship.

# THE VAR SEDIMENT ROUTING SYSTEM: SPATIAL RESIDENCE TIME VARIATION

---

## Contents

---

<b>4.1</b>	<b>Study site: the Var basin . . . . .</b>	<b>118</b>
4.1.1	Environmental setting . . . . .	118
4.1.2	A source to sink system . . . . .	120
<b>4.2</b>	<b>Controls on the regolith residence time in an Alpine river catchment . . . . .</b>	<b>124</b>
<b>4.3</b>	<b>Introduction . . . . .</b>	<b>125</b>
<b>4.4</b>	<b>Study site . . . . .</b>	<b>126</b>
<b>4.5</b>	<b>Materials and Methods . . . . .</b>	<b>127</b>
<b>4.6</b>	<b>Results . . . . .</b>	<b>129</b>
<b>4.7</b>	<b>Discussion . . . . .</b>	<b>131</b>
4.7.1	Assessing the role of lithology and weathering regimes on the U isotope ratio . . . . .	131
4.7.2	Geomorphologic control on ( $^{234}\text{U}/^{238}\text{U}$ ) ratios . . . . .	133
4.7.3	Quantification of regolith residence times in the Var River catchment	135
4.7.4	Geomorphic controls on regolith residence time . . . . .	139
<b>4.8</b>	<b>Conclusion and perspectives . . . . .</b>	<b>140</b>

---

## 4.1 Study site: the Var basin

### 4.1.1 Environmental setting

#### Morphology

The Var River has three main tributaries: Tinee, Vesubies, Esteron. The Tinee and Vesubie rivers drain the highest and northern parts of the basin, while Esteron and Var drain the western and south-western part of the watershed (Fig. 4.1). The maximum elevation reaches 3200 m in the northern part of the basin (in the Tinee and Vesubie basins) with a mean elevation of 1200 m for all system. The average slope of the basin is 23°, with steeper slope in the north with slope reaching up to around 30° and 31° for the Tinee and Vesubie sub-catchment, respectively. The morphology of this mountainous catchment is characterized by hillslope erosional processes of formerly glaciated basin (Julian 1977) with a very limited alluvial plain (<25 km).

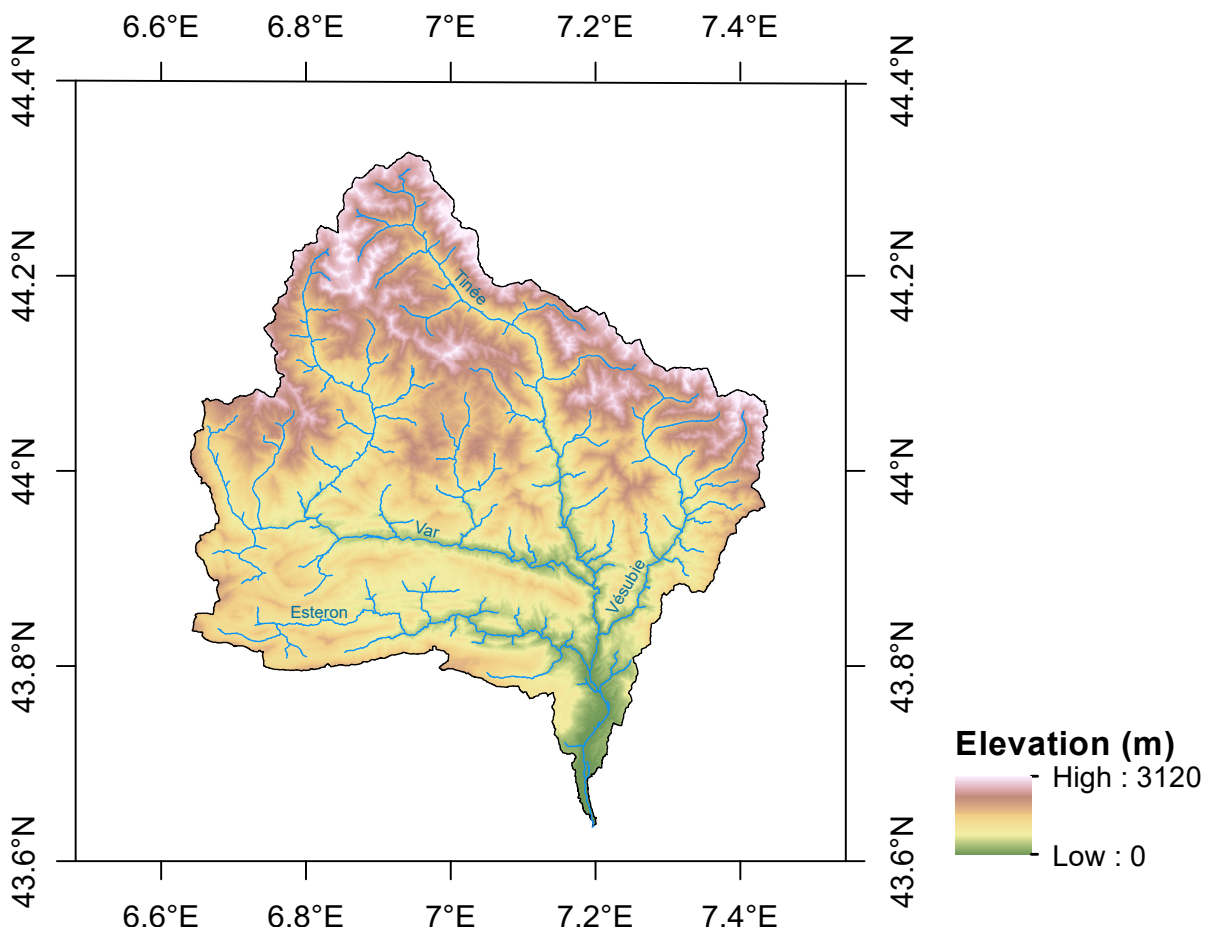


Figure 4.1 – Digital elevation model of the Var basin (S-E France) derived from the French Institute National de l'Information Geographique et Forestière (<http://professionnels.ign.fr/donnees>).

## Geology

The northern part of the catchment, which is drained by the Tinee and Vesubie tributaries is formed by the Mercantour Massif which is a Paleozoic External Crystalline Massifs. It is composed of three distinct geological units: the Malinvern Argentera and the Tinee complex, which are mainly composed of gneiss and migmatites, and the Argentera granitic unit. Locally, Permian shales and sandstone pelites are also encountered at both the periphery of the Mercantour massif and in the central part of the Var river basin. The southern and the central part, which is drained by the Var River and the Esteron tributary, is mainly composed of Mesozoic carbonaceous rocks. It can locally be associated with various sandstones, marls and limestones of Cenozoic age (Kerckhove & Montjuvent 1979, Rouire et al. 1980). The delta has been an important depocentres throughout during Holocene (Anthony 1995) with variation of deposits from gravels (late Pleistocene), fine-grained sediment (early to middle Holocene), fine-grained and gravel-dominated deposits (upper post middle to late Holocene; Anthony & Julian 1999). These variation in the delta sedimentation have been attributed to climatic change inducing sea-level variation (Dubar & Anthony 1995).

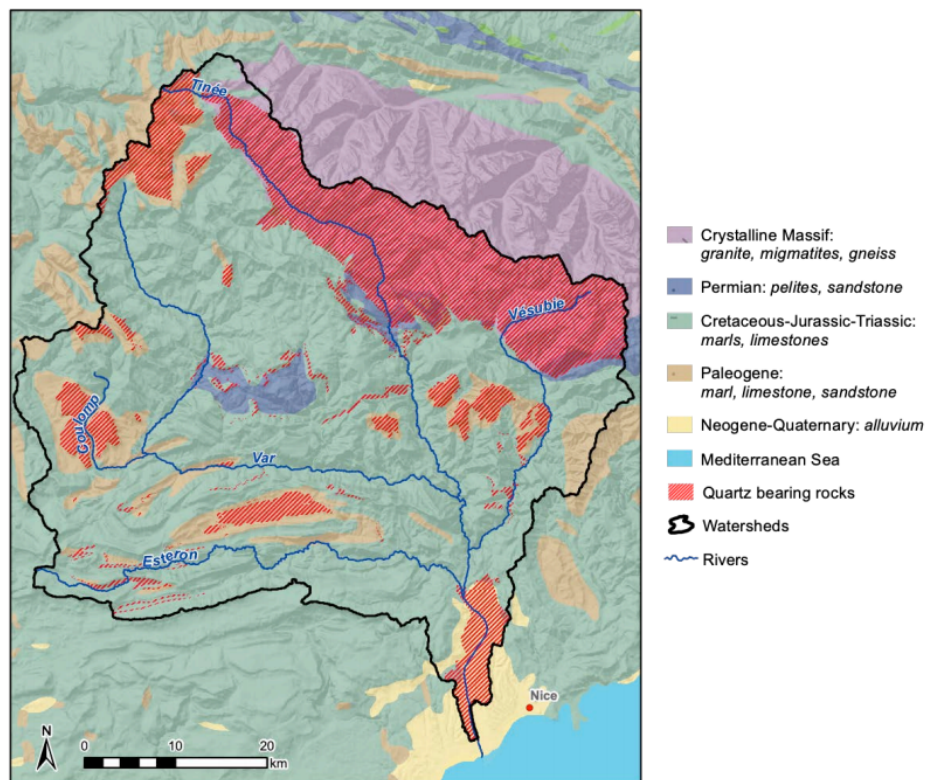


Figure 4.2 – Geological map of the Var basin including the presence of the dams (from Mariotti 2020).

## Climate

The catchment has the characteristic of a Mediterranean climate with hot and dry summers alternating with cool and wet winter. At the river mouth, in Nice (2 meters above sea level), the mean annual temperature recorded between 1942 and 2020 is 16 °C, with a mean temperature around 24 °C during summer and 10 °C in winter. The mean annual precipitation recorded between 1942 and 2020 is 733 mm on 61 days with precipitation >1 mm (climatic data from Meteo France database; <https://donneespubliques.meteofrance.fr>). On the northern part of the catchment, the elevation influences the weather with a mountainous climate. The records at Saint Martin de Vesubie (1064 meters above sea level) indicate a mean annual temperature of 11.9 °C between 1981 and 2010 with a mean temperature around 20°C in summer and 5°C in winter. Between 1989 and 2010, the mean annual precipitation is 1138 mm divided in 89 days with precipitation >1 mm. Events with extrem rainfall occurs in the Var basin, and are referred as "Mediterranean episodes". These Mediterranean episodes are linked to hot, humid and unstable upwelling air from the Mediterranean, which can generate violent thunderstorms that are sometimes stationary. They occur particularly in autumn, when the sea is at its warmest, which favours strong evaporation. The precipitation can reach 200 mm in about 24h. The last episode occurred in October 2020, with 200 to 300 mm and up to 450-500 mm in the interland (MeteoFrance).

## Land cover

The present day vegetation in southern France depends of the Mediterranean climate. In high elevation area (> 2000 m), the vegetation cover is mainly composed of grassland. At lower elevation the vegetation is dominated by forest: with from sea-level to the highest elevation a transition between drought resistant oak to conifers forest above 1000 m (Beaudouin et al. 2007; corine land cover from 2012 from the geoportail database, <https://www.geoportail.gouv.fr/donnees/corine-land-cover-2012>). Downstream, the catchment is largely urbanized with the Nice city with an urban area composed of more >1,000,000 habitants (INSEE, 2016).

### 4.1.2 A source to sink system

#### Denudation

The denudation rate of the whole Var basin calculated from  $^{10}\text{Be}$  (Mariotti et al. 2019) and determined from sediment flux (Bonneau et al. 2017) is around  $0.24 \pm 0.04 \text{ mm.yr}^{-1}$  and  $0.22 \text{ mm.yr}^{-1}$  respectively. Within the basin variations between  $0.10 \pm 0.01$  to  $0.057 \pm 0.09 \text{ m.yr}^{-1}$  are observed and is representative of the denudation variability across the Alps (Mariotti et al. 2019).

The denudation processes are mostly slope dominated (Mariotti et al. 2019). In consequence, slope instability processes produced local intense erosion, which constitute the main sediment source (Julian & Anthony 1996). Some important stochastic erosional processes such as landslides took place in the Var basin. Screes happens in the steepest part of the basin (Julian 1977). The most famous and studied is named La Clapière landslide in the Tinee valley. Successive destabilization events occurred since 10 ka (Bigot-Cormier et al. 2005) and one of the major voluminous events occurred in 1979 (Anthony & Julian 1999, Casson et al. 2003, El Bedoui et al. 2009).

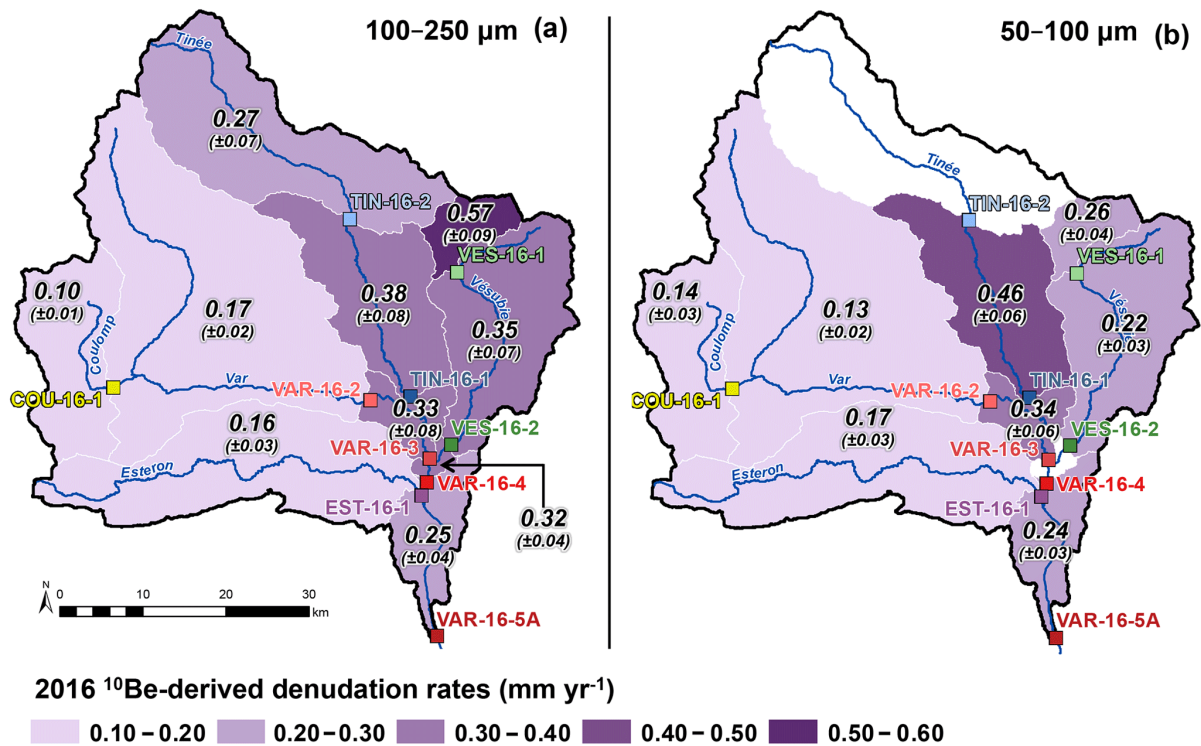


Figure 4.3 – Spatial variation of the <sup>10</sup>Be derived denudation rates inside the Var basin derived from two different grain sizes sediments: a) 100-250 μm and b) 50-100 μm (from Mariotti et al. 2019).

## Fluvial transport

The Var River has an annual sediment discharge estimated at 1.63 million tons/yr and a specific flux of 580 tons/km<sup>2</sup>/yr (Mulder et al. 1997, 1998). The discharge is variable over the year with moderate to high flood in spring, autumn and winter. In autumn it is caused by heavy rainfall and by the Alpine snow melts during spring (Sage 1976, Anthony & Julian 1999). It can lead to episodic floods with magnitude that can reach in only a few hours 100 m<sup>3</sup>/s while the mean annual discharge is around 70 m<sup>3</sup>/s (Dubar & Anthony 1995). Such disturbances sometimes give rise to infrequent but extreme rainfall episodes that generate high-magnitude floods (Anthony & Julian 1999). The last one occurred this autumn (2020) with the extrem rainfall (up to 450-500 mm in the interland;

e.g. Saint-Martin de Vesubie; Meteo-France, 2020; Fig. 4.4). These led to massive floods associated with mudslides. Nowadays, the urbanisation of the basin is also characterised by the presence four hydropower dams in the upper part of the basin, with only one with a significant water storage capacity (Lac Long dam;  $4.7 \times 10^6 \text{ m}^3$ ). In the lowest part of the sediment routing system, nine dams were built in the 1970s to increase sediment deposition and protect the city of Nice (Anthony & Julian 1999).

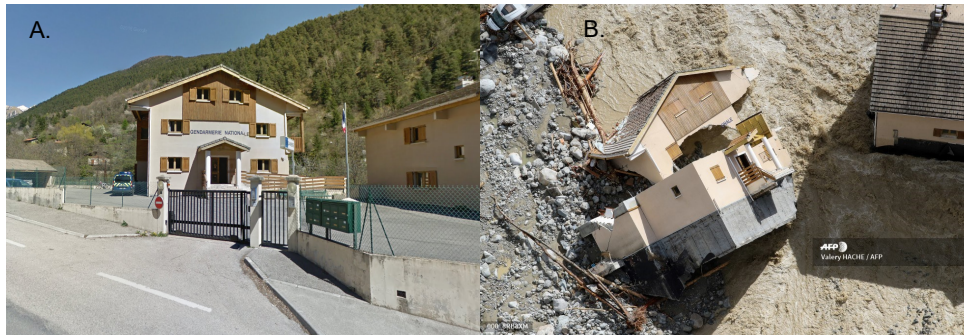


Figure 4.4 – Pictures of the Vesubie before and after the tempete Alex (October 2020) (From AFP). It demonstrates the extreme climatic events occurring into the Mediterranean basin.

### Submarine transport and deposition

Two sub-marine canyons, the Var Canyon and the Paillon Canyon, incise the narrow continental shelf near Nice. These incisions provide a submarine conduit for the transport of fluvial sediment from the Var and Loup rivers and the Paillon River, respectively. The two canyons merge rapidly into one channel at the base of the continental slope to the middle valley. On the right-hand bank of the valley a prominent levee, the Var Sedimentary Ridge, is formed by accumulation of sediments. At the end of the lower valley there is a distal lobe.



Figure 4.5 – Picture of the Var delta showing the sedimentary delivery to the turbiditic deposition zone after the tempete Alex.

Up to 63% of sediments exported at the Var River mouth were delivered to the Var Canyon through hyperpycnal currents, making them the main sediment transfer processes in the Var Turbiditic System (Mulder et al. 1997). Hyperpycnal currents must be of a sufficient magnitude to be recorded as a turbidite layer on the Var Sedimentary Ridge (VSR) (Jorry et al. 2011). Only a few of these events are recorded on the VSR because of the inability of most flows to overtop the ridge wall (Mulder et al. 1998). In the middle valley, the VSR crest height reaches 300m above the main channel floor in its western part but decreases eastward down to a few tens of meters. A secondary sedimentary deposition process, which is significant enough to be recorded in the Var Turbiditic System, involves turbidity currents induced by the mass wasting of large portions of the continental slope (Piper & Savoye 1993, Mulder et al. 1997, 1998, 2001, Migeon et al. 2012 ; Fig. 4.5). An example of this process occurred in 1979, and was triggered by landfilling operations in the Nice airport area (Dan et al. 2007).

## 4.2 Controls on the regolith residence time in an Alpine river catchment

### Abstract

Understanding the natural mechanisms affecting the evolution and morphology of river systems through time is important in the context of on-going climate change. To this end, one major challenge is to quantify the timescale of sedimentary processes, such as erosion, transport and deposition, in catchments, and their relationships with geomorphologic parameters (e.g. elevation, curvature, slope).

In this study, we report uranium activity ratios ( $^{234}\text{U}/^{238}\text{U}$ ), specific surface area measurements and derived comminution ages for a series of fine-grained ( $<63\ \mu\text{m}$ ) fluvial sediments from the Var River basin (France). The Var River is a small mountainous catchment characterized by efficient sediment transport and the absence of alluvial plain, and thus significant alluvial storage. It implies that measured U comminution ages mainly reflect storage on hillslopes. Our geochemical investigation was combined to a detailed spatial analysis of the catchment to investigate how the sediment residence time varies with geomorphic parameters (e.g. slope, curvature, elevation). Moreover, spatial data on soil thickness and  $^{10}\text{Be}$  derived denudations rates were used to infer regolith residence time. Our results indicates an absence of lithologic control on the fractionation of  $^{234}\text{U}$ - $^{238}\text{U}$ , but ( $^{234}\text{U}/^{238}\text{U}$ ) rather reflects the weathering regime. In transport-limited regime, the longer residence time in well-developed soil results in greater  $^{234}\text{U}$  loss. Furthermore, the topography controls the ( $^{234}\text{U}/^{238}\text{U}$ ) ratios with high-elevated catchments, with steeper slopes, characterized by a short regolith residence time and thus a limited  $^{234}\text{U}$  depletion. We show that the regolith residence time determined with U isotopes agree well with estimated regolith residence infer with prediction of soil thickness spatial distribution and  $^{10}\text{Be}$  denudation rate. This validates the use of U isotopes to determine sediment residence times and suggests that residence times in the Var basin mostly reflects hillslope storage, i.e. regolith residence time.

### 4.3 Introduction

Sedimentary processes occurring at the Earth surface (e.g. weathering, sediment transport and deposition) control the landscape morphology. To understand the landscape evolution, it is important to quantify the timescale of these processes and the response time of the landscape to adapt to environmental changes. For this purpose, the study of sediment residence time can provide information on the timescale of Earth surface processes (DePaolo et al. 2006). This residence time represents the time elapsed since parent material was converted into regolith and encompasses hillslope and alluvial storage and transport (DePaolo et al. 2006).

In basin where alluvial storage and soil creep are negligible, the sediment residence time is mainly controlled by the thickness of soil sequences and the overall denudation rate. The quantification of sediment residence times in river basins can provide unique information about both weathering and erosion processes within catchments, where the average soil thickness can be viewed as reflecting the balance between soil production and soil denudation (Carson & Kirkby 1972, Dietrich et al. 1995, Heimsath et al. 1997). Soil thickness is function of several geomorphic parameters including the slope and curvature (Heimsath et al. 1997), which have a direct influence on soil residence times.

In fine-grained detrital sediments (typical  $<63 \mu\text{m}$ ), uranium (U) isotopes fractionate as  $^{234}\text{U}$  is preferential lost from sediments over  $^{238}\text{U}$ , as a result of recoil (Kigoshi 1971) and preferential leaching (Fleischer 1980, 1982). This time-dependent fractionation has been used to determine the *comminution age* of sediments, that is the time elapsed since the production of sediments finer than  $<63 \mu\text{m}$  (DePaolo et al. 2006, Dosseto et al. 2006a, 2008a). In fluvial sediments, the comminution age is equivalent to the regolith residence time, as defined above. Thus, U isotopes in fluvial sediments can be used to determine the regolith residence time at the catchment scale.

The aim of this study is to investigate the controls on sediment residence time, and compare U isotopes to alternative approach for inferring this residence time. To this purpose, we have measured uranium isotopes of a series of sediments from the Var River basin (S.E. France). This mountainous catchment is well constrained by previous studies (sediments sources: Bonneau et al. 2017; denudation rate: Mariotti et al. 2019) and is considered as a reactive routing system (Julian 1977). Therefore, it should be characterized by short sediment residence time, as no temporary alluvial storage are expected. Uranium isotope compositions and inferred residence times are compared to a range of climatic, geologic and geomorphic parameters. Spatial data on soil thickness and  $^{10}\text{Be}$ -derived erosion rates are also used to infer regolith residence times, which are compared to those obtained from U isotopes.

## 4.4 Study site

The Var River catchment (drainage area: 2800 km<sup>2</sup>) is located in the Alpine mountainous region of south-eastern France. The Var River is 120 km long and has four major tributaries: Tinee, Vesubie, Esteron and Cian (Fig 4.6A). The Tinee and Vesubie drain northern and elevated part of the basin, while Esteron and Cian drain the south-western part of the catchment. The maximum elevation reaches 3200 m in the northern part of the basin and a mean elevation of 1200m for the all system. The average slope of the basin is 23°, with steeper slope in the north (~30° and 31° for the Tinee an Vesubie sub-catchment respectively). Another major characteristic of the Var River basin is that the near absence of a floodplain (<25 km long) in the downstream portion of the river.

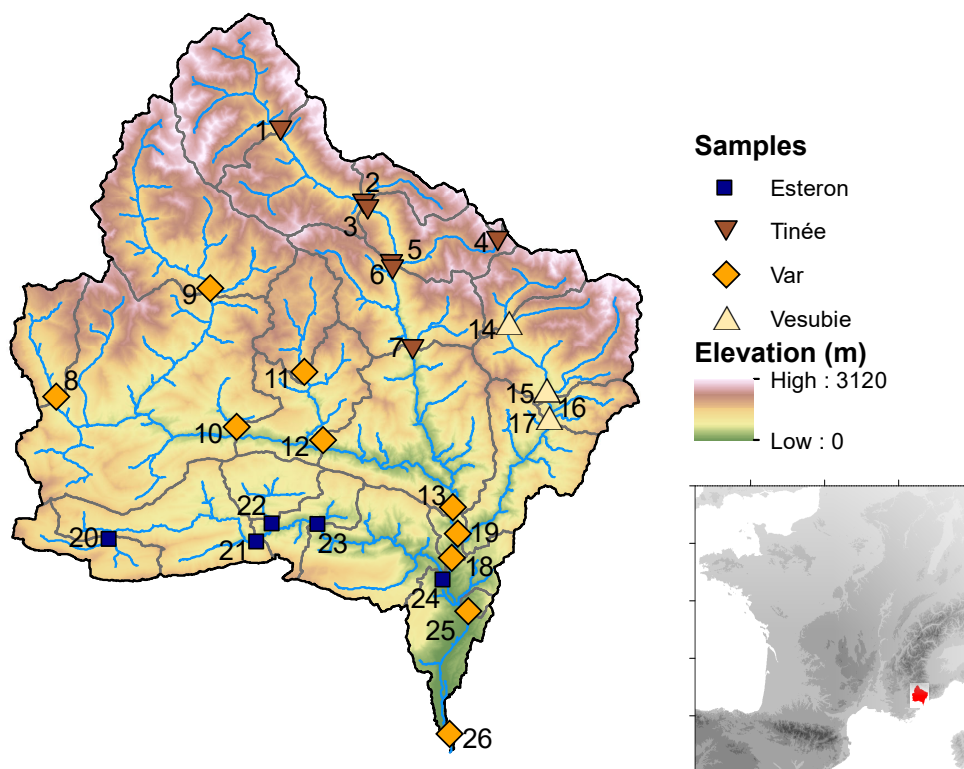


Figure 4.6 – Digital elevation model from the Var basin derived from the French Institute National de l'Information Geographique et Forestiere (<http://professionnels.ign.fr/donnees>). The symbols represent the location of the studied samples with blue square for the Esteron River sediments, brown triangle for the Tinee River sediments, yellow diamond for the Var River sediments, beige triangle for the Vesubie River sediments. The grey lines symbolise the sub-catchments.

The northern part of the catchment is formed by the Mercantour Massif which is a Paleozoic External Cristalline Massif. It is composed of three distinct geological units: the Malinvern Argentera and the Tinee complex, which are mainly composed of gneiss

and migmatites, and the Argentera granitic unit. Locally, Permian shales and sandstone pelites are also encountered at both the periphery of the Mercantour massif and in the central part of the Var river basin. The southern and the central part of the river catchment is mainly composed of Mesozoic carbonaceous rocks, being locally associated with various sandstones, marls and limestones of Cenozoic age (Kerckhove & Montjuvent 1979, Rouire et al. 1980).

The Var River has an annual sediment discharge estimated at 1.63 million tons/yr and a specific flux of 580 tons/km<sup>2</sup>/yr (Mulder et al. 1997, 1998). The discharge is variable over the year with moderate to high flood in spring, because of Alpine snow melts, in autumn due to heavy rainfall, and in winter (Sage 1976, Anthony & Julian 1999). It can lead to stochastic erosional process with magnitude that can reach in only a few hours 100 m<sup>3</sup>/s while the mean annual discharge is around 70 m<sup>3</sup>/s (Dubar & Anthony 1995). The climate is variable inside the catchment with Mediterranean climate in the south (hot and dry summers with cool and wet winter) and the northern part is dominated by a mountainous climate.

The present day vegetation in southern France depends of the Mediterranean climate. In high elevation area (> 2000 m), the vegetation cover is mainly composed of grassland. At lower elevation the vegetation is predominate by forest: with from sea-level to the highest elevation a transition between drought resistant oak to conifers forest above 1000 m (Beaudouin et al. 2007; corine land cover from 2012 from the geoportail database, <https://www.geoportail.gouv.fr/donnees/corine-land-cover-2012>). Downstream, the catchment is largely urbanized with the Nice city with an urban area composed of more >1,000,000 habitants (INSEE, 2016).

## 4.5 Materials and Methods

Twenty six sediments used were collected in 2011 and 2012 along the Var River and its main tributaries. They were sieved on site at 135  $\mu$ m. This suite covers the lithological diversity across the entire catchment. Eleven samples were collected from the Tinee and Vesubie catchments, which mainly drain metamorphic rocks, and 15 samples from the Var, Esteron and Cian catchments, which drain sedimentary rocks.

Geomorphic parameters (elevation, slope and curvature) for each sub-catchment were assessed using a 5 m resolution digital elevation model (DEM) from the French Institute National de l'Information Géographique et Forestière (<http://professionnels.ign.fr/donnees>). Spatial distribution of soil thickness was derived from the SoilGrids map with a 250 m resolution (Shangguan et al. 2017, Hengl et al. 2017). This estimation is based on a compilation of soil profiles (132,193 points) and borehole drilling logs (1,574,776 points) with

the addition of pseudo-observations of depth to bedrock.

Samples were prepared for U isotopic analysis at the Wollongong Isotope Geochronology Laboratory (WIGL), University of Wollongong. Determination of comminution age is based on the preferential loss of  $^{234}\text{U}$  over  $^{238}\text{U}$  in detrital sediment (DePaolo et al. 2006). This depletion of  $^{234}\text{U}$  is only significant in fine-grained ( $<63\ \mu\text{m}$ ) sediments, where the surface/volume is large enough to induce a substantial loss of  $^{234}\text{U}$  Kigoshi (1971), DePaolo et al. (2006). Therefore, sediments were first wet sieved to recover the  $<63\ \mu\text{m}$  fraction. Sediments are generally an assembly of detrital minerals and authigenic phases (i.e. carbonates, Fe-Mn oxyhydroxides) and organic matter. These non-detrital components are generally enriched in U from solutions, which are characterized by  $(^{234}\text{U}/^{238}\text{U}) > 1$ , and thus inherit their U isotopic composition (Plater et al. 1988, 1992, Andersson et al. 1998, 2001, Maher et al. 2006). Consequently, the authigenic phases and organic matter need to be removed as it can mask the  $^{234}\text{U}$  loss. It needs to be realized without altering the surface of the detrital grains as the  $^{234}\text{U}$  loss occurs within the first 30 nm of the grains' surface (Kigoshi 1971). To achieve this, about 1 g of  $<63\ \mu\text{m}$  sediments was treated following the sequential leaching protocol developed by Francke et al. (2018), which allows removal of any non-detrital components without affecting detrital grains. Following leaching, a  $^{229}\text{Th} - ^{236}\text{U}$  tracer solution was added to 30 mg of the residual detrital sediment. The mixture was dissolved in  $\text{HNO}_3$ - HF solution, followed by aqua-regia and finally re-dissolved in 2 mL of 7 M  $\text{HNO}_3$  prior to chromatography.

Ion exchange chromatography was performed on the dissolved samples to isolate uranium prior to isotopic analysis. This was undertaken on an ESI prepFAST automated chromatography system with a "THU-0500" column prefilled with AG1-X8 resin. Prior to sample loading (2 mL of 7 M  $\text{HNO}_3$ ), the resin was washed with 7M  $\text{HNO}_3$ , 0.1M HCl, 6M HCl and water and then conditioned with 7M- $\text{HNO}_3$ . Following sample loading, matrix was eluted in 7M- $\text{HNO}_3$  and uranium in 0.12M HCl. Uranium elutions were dried down and re-dissolved in 0.3M of  $\text{HNO}_3$  for isotopic analysis. Uranium isotope analyses were performed at WIGL on a ThermoFisher Neptune Plus Multi-Collector Inductively-Coupled Plasma Mass Spectrometer (MC-ICP-MS), using an APEX HF desolvating system and nebulizer PFA ST-2280 as sample introduction system. Jet sample and X skimmer cones were used. Standard bracketing was used to correct for SEM-Faraday cup yield and mass bias, using NBL U010 as primary standard (Richter & Goldberg 2003). Analysis accuracy was determined by measuring synthetic standard NBL U005-A (Richter & Goldberg 2003) and was consistently better than 0.5% for  $(^{234}\text{U}/^{238}\text{U})$ . Total procedural blanks were measured, and the contribution is less than 0.1% to the sample  $(^{234}\text{U}/^{238}\text{U})$ . Total procedural accuracy was evaluated by analysing the reference material BCR-2 (Sims et al., 2008), with results in good agreement with reference values (Table 5.1).

Table 4.1 – BCR-2 standard values measured during the Var River sediments study.

<b>Standard</b>	<b>U (ppm)</b>	<b>2SD</b>	<b>(<sup>234</sup>U/<sup>238</sup>U)</b>	<b>2SD</b>
BCR-2	1.65	0.02	1.003	0.003
BCR-2	1.64	0.02	1.005	0.005
BCR-2	1.61	0.04	1.001	0.004
BCR-2	1.60	0.02	1.003	0.004
<b>Mean</b>	<b>1.63</b>	<b>0.02</b>	<b>1.001</b>	<b>0.004</b>
<b>Reference value</b>	<b>1.69</b>	<b>0.19</b>	<b>1.001</b>	<b>0.001</b>

Specific surface area measurements were carried out on 11 leached sediments by gas sorption analysis using a Quantachrome Autosorb iQ at WIGL. About ~1g of sediments were first degassed for approximately 7.5 h with a three-steps temperature increase to 200°C (5 °C/min to 80 °C, soak time 30 min, followed by 1 °C/min to 100 °C, soak time 60 min, followed by 5 °C/min to 200 °C, soak time 300 min). Nitrogen was used as the adsorbate gas. The specific surface area was estimated using the best fit of the multi-point BET equation (with a correlation coefficient  $R^2 > 0.999$  for all measurement).

## 4.6 Results

Spatial analysis of the DEM shows that the Var and Esteron sub-catchments have the shallowest mean slopes (27° and 23° respectively) and lower mean elevation (1334 and 904 meters respectively - values are for the lowermost sampling location of each sub-catchment), compared to Tinee and Vesubie (mean slope of 30° and 31° respectively and mean elevation 1946 and 1541 meters respectively). Spatial distribution of estimated soil thickness indicates that soils are the thickest in the Var sub-catchment (mean thickness >46 m) and the thinnest in the Tinee (mean thickness ~2 m). The values are obtained from the lowest sampling locations for each sub-basin, thus taking into account the entire upstream drainage area.

Measured U concentrations range from  $1.11 \pm 0.01$  (2SD) to  $4.29 \pm 0.01$  (2SD) ppm (Table 4.2). The mean values of all samples from a given catchment are  $2.2 \pm 0.3$  (2SD; n=9),  $1.9 \pm 0.3$  (2SD; n=6),  $3.1 \pm 0.6$  (2SD; n=6),  $2.9 \pm 0.5$  (2SD; n=5) ppm for the Var, Esteron, Tinee and Vesubie catchments, respectively. The mean value for all studied <63 µm sediments ( $2.5 \pm 0.3$  ppm) is similar to the average U concentration for the upper continental crust (from 2.2 to 2.8 ppm; Condie 1993, McLennan 2001). The (<sup>234</sup>U/<sup>238</sup>U) activity ratios range between  $0.869 \pm 0.004$  (2SD) and  $1.073 \pm 0.004$  (2SD) (Table 4.2), with a mean value of  $0.94 \pm 0.02$  (2SD ; n=9) ,  $0.93 \pm 0.03$  (2SD ; n=6),  $1.02 \pm 0.02$  (2SD; n=6) and  $1.02 \pm 0.02$  (2SD ; n=5) for the Var, Esteron, Tinee and Vesubie catchments respectively.

Table 4.2 – Table of U concentration, ( $^{234}\text{U}/^{238}\text{U}$ ) and  $S_{BET}$  measured in Var River sediments.

Riviere	n	Echantillon	U (ppm)	2SD	( $^{234}\text{U}/^{238}\text{U}$ )	2SD	$S_{BET}$ ( $\text{m}^2/\text{g}$ )	2SD
Esteron	20	BV-EST-05	2.13	0.01	0.938	0.004	13.7	0.4
Esteron	21	BV-EST-04	1.63	0.01	0.964	0.004		
Esteron	22	BV-RIO-01	2.10	0.01	0.949	0.004		
Esteron	23	BV-EST-03	1.62	0.01	0.949	0.004	11.1	0.4
Esteron	24	BV-EST-01	2.43	0.01	0.874	0.004		
Tinee	1	BV-TIN-05	1.83	0.01	1.043	0.004	5.8	0.4
Tinee	2	BV-TIN-03	3.07	0.01	0.985	0.004		
Tinee	3	BV-TIN-04	2.74	0.01	1.020	0.004		
Tinee	4	BV-NEG-01	4.28	0.01	1.049	0.004		
Tinee	5	BV-MOL-01	4.05	0.01	1.073	0.004	3.0	0.4
Tinee	6	BV-TIN-02b	3.08	0.01	0.999	0.004	7.0	0.4
Tinee	7	BV-TIN-07	2.62	0.01	0.983	0.004	6.4	0.4
Var	8	BV-COU-02	2.27	0.01	0.869	0.003		
Var	9	BV-VAR-08	2.43	0.01	0.947	0.004	9.9	0.4
Var	10	BV-VAR-03	2.05	0.01	0.954	0.004		
Var	11	BV-CIA-03	2.13	0.01	0.962	0.004		
Var	12	BV-VAR-04	1.57	0.01	0.961	0.004	7.9	0.4
Var	13	BV-VAR-11	1.10	0.01	0.957	0.004	4.8	0.4
Var	19	BV-VAR-01	2.64	0.01	0.942	0.003		
Var	25	BV-VAR-15	2.81	0.01	0.934	0.003		
Var	26	BV-VAR-06	2.70	0.01	0.953	0.003	9.3	0.4
Vesubie	14	BV-VES-03	2.69	0.01	1.055	0.003		
Vesubie	15	BV-VES-02	3.47	0.01	1.026	0.003		
Vesubie	16	BV-GUA-01	3.70	0.01	0.990	0.003		
Vesubie	17	BV-VES-04	2.27	0.01	1.020	0.003	5.1	0.4
Vesubie	18	BV-VES-01	2.69	0.01	1.007	0.004		

Specific surface area varies between  $3.0\pm 0.4$  and  $13.7\pm 0.4$   $\text{m}^2/\text{g}$  (Table 4.2) with a mean value of  $7\pm 2$   $\text{m}^2/\text{g}$  (2.S.D; n=11). The observed range is lower than that reported in previous studies: for instance, 12.8 - 33.6  $\text{m}^2/\text{g}$  for 2-53  $\mu\text{m}$  leached sediments from Pleistocene alluvial deposits in the Flinders Ranges (South Australia; Handley et al. 2013a); 17.2 - 18.3  $\text{m}^2/\text{g}$  for  $<63$   $\mu\text{m}$  leached sediment from cores of the Var basin (Francke et al. 2018) and between 33.1 to 47.2  $\text{m}^2/\text{g}$  for  $<63$   $\mu\text{m}$  leached sediments from Lake Ohrid (Greece; Francke et al. 2019). Note sediments in Handley et al. (2013a) were leached using a protocol different to that from Francke et al. (2018, 2019) (which is the one we have used here).

## 4.7 Discussion

### 4.7.1 Assessing the role of lithology and weathering regimes on the U isotope ratio

The Var river and its tributaries drain two distinct lithological units: a metamorphic complex, located in the northern part of the watershed and drained by both the Tinee and the Vesubie rivers; and extensive Mesozoic/Cenozoic sedimentary deposits in the southern part of the basin that are drained by the Var and the Esteron rivers. Bonneau et al. (2017) measured neodymium isotopes composition (noted  $\varepsilon_{Nd}$ ) on the  $<63 \mu\text{m}$  fraction of some of the sediments used in this study. Results show two groups: Vesubie sediments have  $\varepsilon_{Nd}$  values between -8 and -9 while all other sediments show  $\varepsilon_{Nd}$  values between -10.5 and -11.5 (Fig. 4.7A). The Nd isotopic composition of river sediments directly reflects that of the source rocks they are derived from, and hence can be used as a tool to assess whether measured ( $^{234}\text{U}/^{238}\text{U}$ ) ratios may be explained by a source effect. Uranium activity ratios determined in samples from both the Tinee and Vesubie tributaries are  $>1$  (Fig. 4.7A), while those from the Var and the Esteron display ( $^{234}\text{U}/^{238}\text{U}$ ) ratios below secular equilibrium ( $<1$ ). This observation suggests that lithology is not a major control on observed variability in ( $^{234}\text{U}/^{238}\text{U}$ ) across the Var watershed, as it has been shown in other studies (e.g. Dosseto et al. 2014, Thollon et al. 2020).

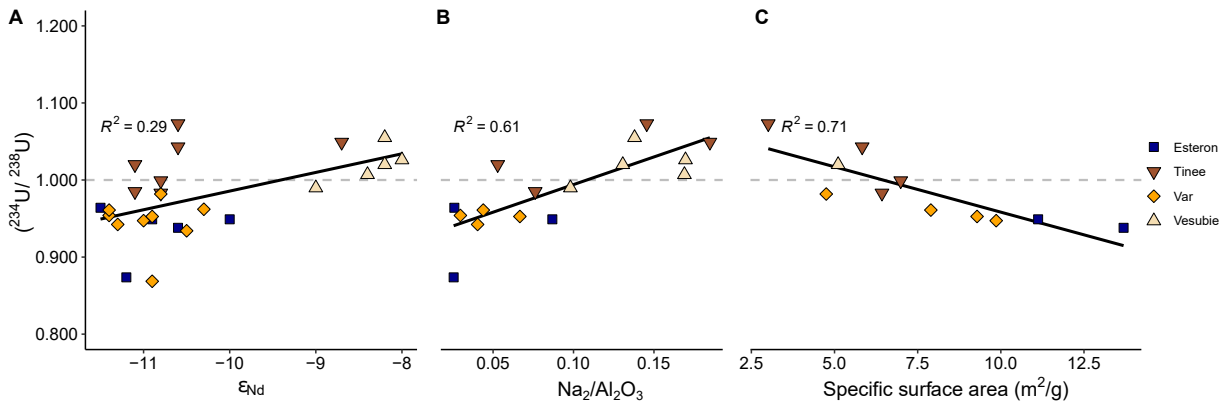


Figure 4.7 – Variation of ( $^{234}\text{U}/^{238}\text{U}$ ) as a function of (A)  $\varepsilon_{Nd}$  compositions (Bonneau et al. 2017), (B) specific surface area and (C)  $\text{Na}_2\text{O}/\text{Al}_2\text{O}_3$  ratios (Bonneau et al. 2017) (blue square for the Esteron, brown triangle for the Tinee, yellow diamond for the Var and beige triangle for the Vesubie subcatchments).  $2\sigma$  errors are smaller than the symbol size. The dashed line represents secular equilibrium for  $^{234}\text{U}$ - $^{238}\text{U}$ .

Type of weathering regime in different locations of the watershed could also have an impact the degree of fractionation between  $^{234}\text{U}$  and  $^{238}\text{U}$  in river sediments (Li et al. 2016a). Under kinetically-limited weathering conditions, such as in high-topography regions, the sediment is exported rapidly at a rate faster than the dissolution rate of silicate minerals (Stallard 1985, West et al. 2005). In such condition, ( $^{234}\text{U}/^{238}\text{U}$ ) is expected to have

undergone little fractionation and therefore be close to secular equilibrium. In contrast, in floodplains and other areas characterized by transport-limited weathering regimes, the increase of sediment residence times in soils is typically accompanied by more intense weathering reactions (West et al. 2005, Lupker et al. 2012), which results in the formation of thicker soil sequences. Hence the sediment is expected to spend a long time in the soil profile, increasing the  $^{234}\text{U}$  loss possibility, which result in low ( $^{234}\text{U}/^{238}\text{U}$ ). In the Var catchment, the Tinee and Vesubie sub-catchments show characteristics of a kinetic-limited weathering regime, with high denudation rates ( $>0.25$  mm/yr; Mariotti et al. 2019), steep slopes (mean slope of  $29^\circ$  and  $31^\circ$  for the Tinee and Vesubie) and thin soils (generally less than 10 meters). Conversely, the Var and Esteron sub-catchments show characteristics of a transport-limited weathering regime, with slow denudation rates ( $<0.20$  mm/yr; Mariotti et al. 2019), shallow slopes (mean slope of  $26^\circ$  and  $22^\circ$  for the Var and Esteron) and thick soils (generally above 10 meters; with a great variability for the Var sub-catchment). Sediments from the Tinee and Vesubie show ( $^{234}\text{U}/^{238}\text{U}$ ) values  $>1$  ( $1.022 \pm 0.069$  and  $1.020 \pm 0.048$ , respectively) while those from the Var and Esteron have ( $^{234}\text{U}/^{238}\text{U}$ ) values overall  $<1$  ( $0.945 \pm 0.063$  and  $0.935 \pm 0.070$ , respectively). This observation suggests that the ( $^{234}\text{U}/^{238}\text{U}$ ) of sediments is influenced by the weathering regime: in kinetic-limited regimes, because soils are rapidly eroded, there is not enough time to lose  $^{234}\text{U}$  significantly. This results in ( $^{234}\text{U}/^{238}\text{U}$ ) ratios  $>1$ , as imparted by authigenic phases (possibly incompletely removed during leaching). In transport-limited regimes, long storage times in thick soils results in measurable  $^{234}\text{U}$  depletion and ( $^{234}\text{U}/^{238}\text{U}$ ) ratios  $<1$ . The influence of chemical weathering can also be investigated using mobile over immobile elemental ratios, such as  $\text{Na}_2\text{O}/\text{Al}_2\text{O}_3$  (Fig. 4.7B). The  $\text{Na}_2\text{O}/\text{Al}_2\text{O}_3$  ratio decreases with ( $^{234}\text{U}/^{238}\text{U}$ ) (Fig. 4.7B;  $R^2 = 0.61$ ). Sodium is a highly mobile element that is efficiently removed from soils during chemical weathering of primary minerals, whereas Al is immobile and remains incorporated into secondary clays. The positive relationship between ( $^{234}\text{U}/^{238}\text{U}$ ) and  $\text{Na}_2\text{O}/\text{Al}_2\text{O}_3$  (Fig. 4.7B) suggests that under transport-limited weathering conditions (low  $\text{Na}_2\text{O}/\text{Al}_2\text{O}_3$ ), the longer regolith residence times lead to more extensive  $^{234}\text{U}$  loss in mineral grains stored in soils (low ( $^{234}\text{U}/^{238}\text{U}$ )), while sediments derived from the high-topography areas with low chemical weathering intensities (high  $\text{Na}_2\text{O}/\text{Al}_2\text{O}_3$ ) display reduced or no  $^{234}\text{U}$  loss (( $^{234}\text{U}/^{238}\text{U}$ ) close to secular equilibrium). These results do not necessarily indicate a control of weathering intensity on the fractionation of  $^{234}\text{U}$ - $^{238}\text{U}$  but rather a co-variation between them as a result of their dependence of residence time. Uranium isotope ratios show a negative correlation with the specific surface area (Fig. 4.7C), indicative of the role of physical weathering on the ( $^{234}\text{U}/^{238}\text{U}$ ) ratio. This observation suggests that  $^{234}\text{U}$  loss is driven by the physical fragmentation of sediments, more prominent in steep, fast-eroding catchments of the Tinee and Vesubie Rivers.

## 4.7.2 Geomorphologic control on ( $^{234}\text{U}/^{238}\text{U}$ ) ratios

The degree of the fractionation of  $^{234}\text{U}$  relative to  $^{238}\text{U}$  due to recoil effect is time dependent, hence the ( $^{234}\text{U}/^{238}\text{U}$ ) distribution in river sediments is strongly influenced by river-basin geomorphology, and likely to display correlations with parameters such as the slope, curvature, or elevation. Davis (1892) and Gilbert (1909) were amongst the first to establish a direct link between the transport of sediment and the slope. Culling (1960) also proposed that a proportional relationship existed between sediment fluxes and hillslope gradients; an observation further supported later on by various field studies (McKean et al. 1993, Small et al. 1999). This linearity between topographic slope and sediment fluxes has been used in landscape evolution models (e.g Ahnert 1970, Dietrich et al. 1995, Howard 1997, Willgoose et al. 2008). Additionally, many works have also emphasized the importance of gravity processes, such as landslides, overland flows, and creeping, in dominating the export of sedimentary material from river basins (Carson & Kirkby 1972, Hovius et al. 1997, Montgomery & Dietrich 1995, Selby 1993). Montgomery & Brandon (2002) highlighted the different geomorphological control on erosion rates between low- and high-topography reliefs. In low-relief landscapes, the mean slopes or the local relief can be linearly correlated with the erosion rate. In contrast, in high-relief landscapes, this relationship is nonlinear (Roering et al. 2001, Montgomery & Brandon 2002, Binnie et al. 2007, Dixon et al. 2016). This nonlinear relationship is the result of the transition between diffusive to non-diffusive transport dynamics above a threshold slope angle (Roering et al. 2001, Montgomery & Brandon 2002, Binnie et al. 2007). This specific slope angle is about  $30^\circ$  in the Var basin (Mariotti et al. 2019). In the case of our study, the average slope of studied sub-catchments could indirectly influence measured ( $^{234}\text{U}/^{238}\text{U}$ ) ratios, as a parameter reflecting both denudation rates and sediment transport fluxes.

In the sediments from the Var basin, ( $^{234}\text{U}/^{238}\text{U}$ ) show a weak positive relationship with slope and negative relationship with curvature (Fig. 4.8A&B). Furthermore, the sediment surface area shows a strong negative relationship with slope and a negative relationship with curvature (Fig. 4.8CD), reflecting that in steep catchments physical weathering is more active.

The relationship between ( $^{234}\text{U}/^{238}\text{U}$ ) and catchment mean elevation also illustrates the role of topography on the U isotope composition of fluvial sediments (Fig. 4.8E). In high-elevation areas, soil production and sediment storage capacity are both limited, due to efficient sediment export. This results in a short regolith residence time, and limited to no  $^{234}\text{U}$  loss. In contrast, in low-elevation regions, thicker soil sequences and enhanced sediment storage capacity result in longer regolith residence times and more extensive  $^{234}\text{U}$  depletion.

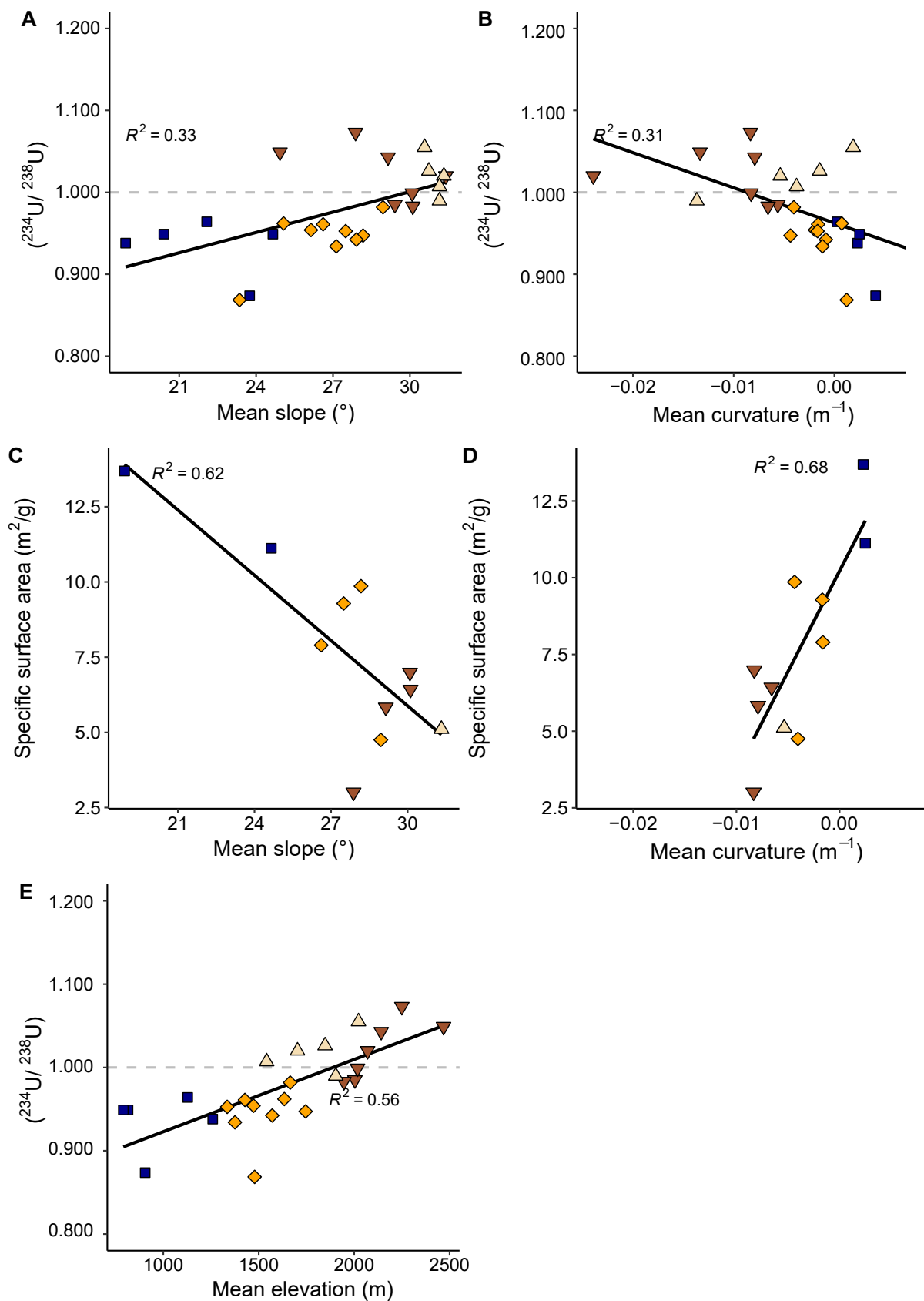


Figure 4.8 – Variation of  $(^{234}\text{U}/^{238}\text{U})$  as a function of (A) slope, (B) curvature; specific surface area depending on (C) slope (D) curvature, and  $(^{234}\text{U}/^{238}\text{U})$  depending on elevation (blue square for the Esteron, brown triangle for the Tinee, yellow diamond for the Var and beige triangle for the Vesubie subcatchments).  $2\sigma$  errors are smaller than the symbol size. The dashed line represents secular equilibrium for  $^{234}\text{U}$ - $^{238}\text{U}$ .

### 4.7.3 Quantification of regolith residence times in the Var River catchment

The sediment residence time can be derived from U isotopes using the comminution age model (DePaolo et al. 2006):

$$t_{com} = -\frac{1}{\lambda_{234}} \ln \left[ \frac{A_{meas} - (1 - f_{\alpha})}{A_0 - (1 - f_{\alpha})} \right] \quad (4.1)$$

where  $\lambda_{234}$  is the  $^{234}\text{U}$  decay constant (in  $\text{yr}^{-1}$ ),  $f_{\alpha}$  the recoil loss factor,  $A_{meas}$  is the measured ( $^{234}\text{U}/^{238}\text{U}$ ) in the sediment and  $A_0$  is the ( $^{234}\text{U}/^{238}\text{U}$ ) activity ratio at  $t=0$ . In theory,  $A_0$  represents the uranium activity ratio from the parent material that should be in secular equilibrium, i.e. ( $^{234}\text{U}/^{238}\text{U}$ ) = 1, and  $A_{meas}$  in detrital sediments should exhibit values  $<1$  resulting from the preferential loss of  $^{234}\text{U}$ . However, some river sediments in the Var catchment displayed ( $^{234}\text{U}/^{238}\text{U}$ ) values  $>1$ , implying an evolution of the ration from  $A_0 >1$ . Some ( $^{234}\text{U}/^{238}\text{U}$ ) higher than 1 have already been reported in river sediments (e.g. Vigier et al. 2001, 2005, Granet et al. 2007, Martin et al. 2015). Therefore, the maximum measured ( $^{234}\text{U}/^{238}\text{U}$ ) value was attributed to  $A_0$ . The recoil loss factor is calculated as follows (Kigoshi 1971, Luo et al. 2000):

$$f_{\alpha} = \frac{1}{4} L S \rho \quad (4.2)$$

where  $L$  is the  $^{234}\text{Th}$  recoil length (taken to be 30 nm; Dosseto & Schaller 2016),  $\rho$  is the density of the sediment (assumed to be  $2.65 \text{ g/cm}^3$ ) and  $S$  is the surface area ( $\text{m}^2/\text{g}$ ) measured by gas sorption analysis. Because micro- ( $<2 \text{ nm}$  in diameter) or mesopore (2-50 nm in diameter) increase the measured surface area during gas sorption analysis due to the the diameter of the adsorbent molecule of the same order, without contribution to  $^{234}\text{U}$  loss in detrital material. It led to an overestimation of the recoil loss factor (Maher et al. 2006). For micro- and mesoporous material a fractal correction need to be applied (Bourdon et al. 2009). The shape of the adsorption-desorption isotherms assessed during gas sorption analyses indicates the nature of the material (Sing 1985). In this study, the isotherms of the samples are type II isotherms, characteristic of non-porous or macroporous material (Sing 1985). Hence, no fractal correction is required (Francke et al. 2018) and the measured surface area was directly used to calculate the recoil loss factor. In the case where the surface area was not measured for a given sample, a random value was taken between the minimum and the maximum values measured. Sediment residence times were calculated using Monte Carlo simulation (10,000 simulations). For each sample,  $A_{meas}$  was taken randomly within the range of measured ( $^{234}\text{U}/^{238}\text{U}$ ) activity ratios and its error as provided in Table 1. As not every specific surface area were measured, for the samples without data, a random value was choose between the minimum and maximum values measured. As explained above, for fluvial sediments, the comminution

age is equivalent to the sediment residence time, which encompasses storage in weathering profiles on the hillslope and transport in the fluvial system. Calculated sediment residence times vary between 66 and 286 kyr for the Tinee, 78 and 229 kyr for the Vesubie, 219 and 636 kyr for the Var and 251 and 643 kyr for the Esteron. The highest value of 642 kyr being calculated for EST-01 located at the lower part of the Esteron sub-catchment (Fig. 4.9A). These residence times are much longer than what would be expected for a mountainous river catchment characterised by efficient sediment transport. However, most of the residence time can be explained by hillslope storage (Suresh et al. 2014): while a 4-m soil eroding at 9-24 mm/kyr would yield residence times of only 30 kyr, when considering soil creep at a rate of 0.8 mm/kyr down a 265 m long hillslope, this can increase the residence time to values as high as 220 kyr despite the thin soil thickness and fast erosion rates.

In order to validate the U-based sediment residence time, we also estimated the sediment residence combining spatial data for estimated soil thickness (SoilGrids;Shangguan et al. 2017, Hengl et al. 2017) and  $^{10}\text{Be}$ -derived denudation rates (Mariotti et al. 2019). For each location where sediments were sampled for in-situ  $^{10}\text{Be}$ , soil thickness and denudation rates are spatially averaged by the area drained at the sample location. Thus, the ratio of soil thickness to denudation rate yields a spatially averaged soil residence time. Because there is little accommodation space for fluvial storage, this soil residence time can be considered equivalent to the regolith residence time, and compared to the regolith residence time inferred from U isotopes at the same location.

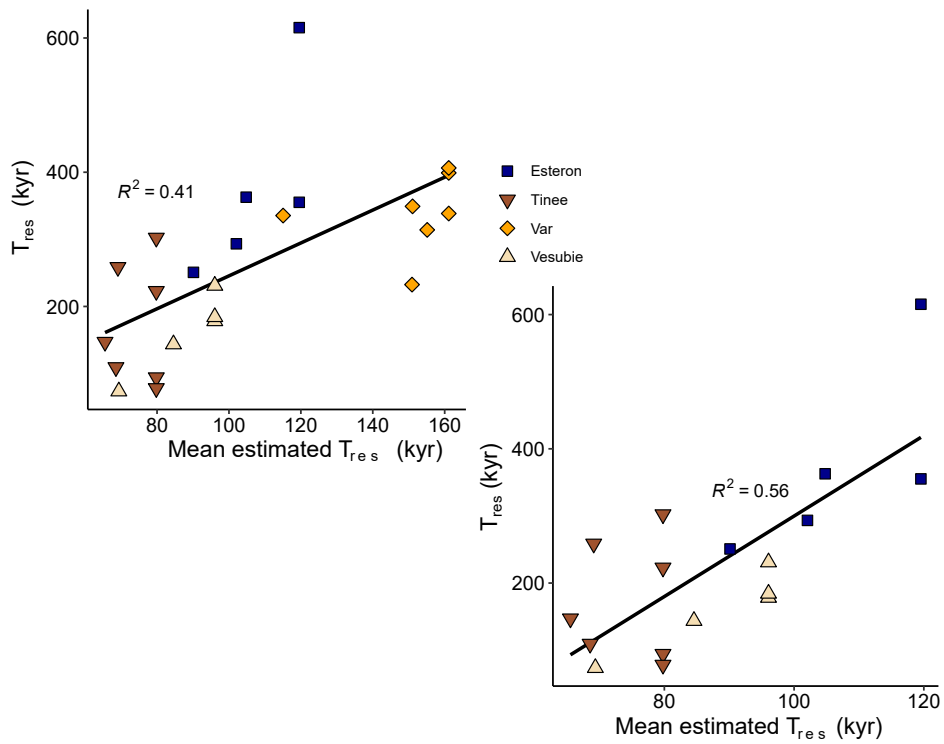


Figure 4.9 – Variation of sediment residence times calculated using U isotopes (y axis) as a function of the regolith residence times estimated based on the mean soil thickness (SoilGrids) and  $^{10}\text{Be}$ -derived denudation rate of each sub-catchment (data from Mariotti et al. 2019) (blue square for the Esteron, brown triangle for the Tinee, yellow diamond for the Var and beige triangle for the Vesubie subcatchments).

Table 4.3 – Sediment residence time derived from ( $^{234}\text{U}/^{238}\text{U}$ )

<b>Samples</b>	<b><math>T_{res}</math> (kyr)</b>	
BV-EST-05	251	$\pm 18$
BV-EST-04	312	$\pm 81$
BV-RIO-01	361	$\pm 105$
BV-EST-03	274	$\pm 19$
BV-EST-01	643	$\pm 130$
BV-TIN-05	118	$\pm 5$
BV-TIN-03	251	$\pm 52$
BV-TIN-04	155	$\pm 29$
BV-NEG-01	84	$\pm 12$
BV-MOL-01	66	$\pm 2$
BV-TIN-02b	219	$\pm 13$
BV-TIN-07	286	$\pm 16$
BV-COU-02	636	$\pm 116$
BV-VAR-08	322	$\pm 23$
BV-VAR-03	348	$\pm 91$
BV-CIA-03	300	$\pm 79$
BV-VAR-04	346	$\pm 22$
BV-VAR-11	393	$\pm 23$
BV-VAR-01	381	$\pm 109$
BV-VAR-15	411	$\pm 107$
BV-VAR-06	306	$\pm 19$
BV-VES-03	78	$\pm 12$
BV-VES-02	133	$\pm 23$
BV-GUA-01	229	$\pm 48$
BV-VES-04	189	$\pm 8$
BV-VES-01	175	$\pm 33$

The comparison of regolith residence times from U isotopes and from the combination of soil thickness and  $^{10}\text{Be}$ -derived denudation rates show a positive correlation ( $R^2=0.41$ ; Fig. 4.9a). The correlation coefficient increased ( $R^2=0.56$ ) when the Var samples are not considered, suggesting a possible overestimation of the soil thickness by SoilGrids due to the presence of alluvium deposits. A noteworthy feature in Figure 4.9 is the lower regolith residence times determined using soil thickness and  $^{10}\text{Be}$ -derived denudation rates than to those calculated using the comminution age method (Fig. 4.9a). One possible explanation for this discrepancy is that because the  $^{10}\text{Be}$ -derived denudation rates determined using the sand fraction, which could have a longer residence time than the silt fraction on which

U isotopes are measured. For instance, DePaolo et al. (2006) have shown that ( $^{234}\text{U}/^{238}\text{U}$ ) is lower in finest sediment grain and thus infer sediment residence time are longer. Alternatively, longer residence times determined using U isotopes could be an over-estimation as a result of sediment recycling (Carretier et al. 2020).

Despite of this discrepancy, the observed general correlation between independently calculated residence times provides additional support for the utility of the comminution age method for estimating sediment residence in watersheds.

#### 4.7.4 Geomorphic controls on regolith residence time

The regolith residence time is a function of storage in two distinct reservoirs: the hillslope and the alluvial plain. The latter is considered negligible for this catchment as the Var alluvial plain has a small extent compared to the rest of the catchment (Julian 1977). This is supported by the correlation between regolith residence time and soil thickness ( $R^2 = 0.35$ ; Fig. 4.10A), one of the major controls on the residence time at the hillslope scale. If alluvial storage was significant, it would likely blur this relationship. Regolith residence times calculated with U isotopes also show a relationship with mean slope (and to a lesser extent, mean curvature) showing that in steep catchments, the regolith residence time is shorter as a consequence of faster hillslope erosion. Residence times also show a negative relationship with mean elevation, illustrating that alpine sub-catchments are characterised by short hillslope storage times (Fig. 4.10D).

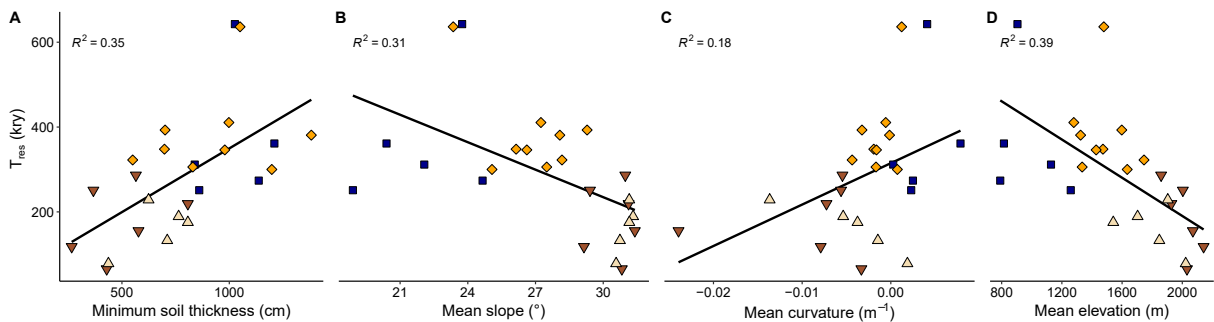


Figure 4.10 – Variation of the regolith residence time as a function of (A) the soil thickness, (B) slope, (C) curvature, (D) elevation. The value for each parameter represents its spatial average at the sampling location (blue square for the Esteron, brown triangle for the Tinee, yellow diamond for the Var and beige triangle for the Vesubie subcatchments).

In the sections above, we determined the influence of the geomorphologic parameters on both ( $^{234}\text{U}/^{238}\text{U}$ ) and on the specific surface area, as the sediment residence time groups both of these characteristics, we studied through a multiple regression analysis between sediment residence time and the geomorphologic parameters (e.g. the soil thickness, the slope, the curvature and the elevation). The predicted sediment residence time are in agreement with the calculated residence time, with  $R^2 = 0.66$ . These predicted

data increase in correlation when considering the lithologic source tracer ( $\varepsilon_{Nd}$ ;  $R^2 = 0.79$ ) suggesting that lithology can play a role in regolith residence time (Fig. 4.11). This implies that about 80% of the variability of regolith residence time can be explained by the sum of these different parameters. Note however that the obtained p-value for each individual variable is not statistically significant, suggesting that the resulting relationship needs to be considered with caution. Despite these uncertainties, the multi-variables approach highlights the fact that regolith residence time in the Var basin is mainly controlled by hillslope storage and the basin morphology.

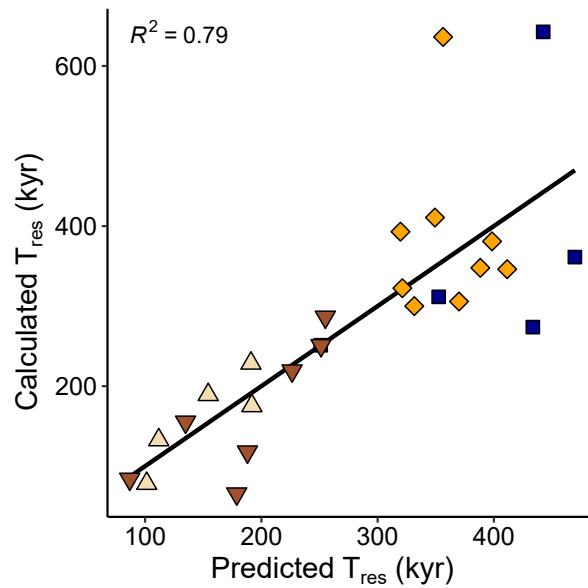


Figure 4.11 – Residence time calculated using U isotopes, compared with the residence time predicted with a multi-regression analysis while considering the slope, curvature, elevation, soil thickness and lithology factors.

## 4.8 Conclusion and perspectives

We investigated the sediment residence time variation in the Var basin by measuring ( $^{234}\text{U}/^{238}\text{U}$ ) ratios in sediments sampled along the Var River and its tributaries. We compared the ( $^{234}\text{U}/^{238}\text{U}$ ) variation with geomorphic parameters (e.g. slope, curvature, elevation) obtained by a detailed spatial analysis of the catchment. In addition we used a second approach based on spatial data on soil thickness and  $^{10}\text{Be}$ -derived denudation rates to estimate regolith residence time and compare with our residence time obtained with U isotopes.

We show that the lithology of the draining area has no direct influence on the preferential loss of  $^{234}\text{U}$ . Our results suggest that the fractionation of  $^{234}\text{U}$ - $^{238}\text{U}$  reflects the weathering regime of the basin. Indeed, in kinetically-limited weathering conditions (e.g. high elevation area), ( $^{234}\text{U}/^{238}\text{U}$ ) is close to 1 because of the fast removal of sediments limiting the

$^{234}\text{U}$  loss. Conversely, ( $^{234}\text{U}/^{238}\text{U}$ ) is low in transport-limited regime due to the facility with which the soil develops, increasing the sediment storage on hillslope. Furthermore, the morphology shows a control on the variability of ( $^{234}\text{U}/^{238}\text{U}$ ) in particular through the slope and curvature, which is coherent with the co-variation of weathering regime and the morphology of the basin. The regolith residence time we estimated using spatial data on soil thickness and  $^{10}\text{Be}$ -derived denudation rates have a good correlation with the residence time calculate with ( $^{234}\text{U}/^{238}\text{U}$ ). This correlation indicates that in a reactive system as the Var basin, the sediment residence time represents the regolith residence time and therefore the duration of the fluvial transport can be considered as negligible. The results of this study confirms the ability of ( $^{234}\text{U}/^{238}\text{U}$ ) to infer sediment residence time and point out there great ability to respond to morphologic variation. This control of the morphology on ( $^{234}\text{U}/^{238}\text{U}$ ) suggests that sediment residence time based on U isotopes could be used as approximation of weathering regime.



# THE VAR SEDIMENT ROUTING SYSTEM: PALEO-RESIDENCE TIME VARIATIONS

---

## Contents

---

<b>5.1</b>	<b>The climatic cyclicity during the Quaternary . . . . .</b>	<b>144</b>
5.1.1	Long terms climatic cycles . . . . .	144
5.1.2	Millennial-scale climate changes . . . . .	145
5.1.3	The climatic context in the Alps during the Quaternary . . . . .	147
<b>5.2</b>	<b>Temporal sediment residence time variations . . . . .</b>	<b>149</b>
5.2.1	Stratigraphy of the Var sedimentary ridge . . . . .	149
5.2.2	Methods . . . . .	151
5.2.3	Uranium variations over time - Results . . . . .	153
5.2.4	Interpretation . . . . .	157
5.2.5	Conclusion . . . . .	165

---

## 5.1 The climatic cyclicity during the Quaternary

### 5.1.1 Long terms climatic cycles

During the Quaternary (since 2.6 Myr), a cyclicity between glacial and interglacial periods exist. The cyclicity period increased from 40 000 yr between 2.6 and 0.9 Myr to every 100 000 yr for the last 0.9 Myr. The glacial-interglacial variability is controlled by insolation variations caused by terrestrial orbital parameters according to the astronomical theory of climate first formulated by M. Milankovitch in 1947 (see Berger 1988 for a review). These variations are reinforced by complex retroaction between the ocean, atmosphere and cryosphere.

The alternation of glacial and interglacial periods throughout the Quaternary is nicely depicted in the oxygen isotopic composition ( $^{18}\text{O}/^{16}\text{O}$  or  $\delta^{18}\text{O}$ ) of the sea water and the ice trapped at the pole. The cold, glacial periods are characterized by a decrease of light isotopes compared to the heavy ones in the sea-water as the light isotopes are trapped in the polar ice. Conversely, during warm, interglacial periods the light oxygen isotopes are released into the water, hence  $\delta^{18}\text{O}$  of sea water decreased. This led the community to use the notion of *Oxygen Isotopic Stage* - OIS or *Marine isotopic Stage* – MIS to describe the main climatic features of the Quaternary (Railsback et al. 2015).

### The Last Glacial Period

The last glacial period (71 - 11.7 kyr) is characterized by the growth of North Hemisphere ice sheets, the two major being the Laurentide Ice Sheet in North American and the Eurasian Ice sheet in northern Europe (Ehlers & Gibbard 2007). During the last glacial maximum (LGM, ca. 26.5 ka - 19 ka; Clark et al. 2009), that occurred during the MIS 2, the ice sheets extended to their maximum and covered about 25% of the continental surfaces. At that time, the difference with actual value of the mean temperature at the Earth's surfaces was about 4 to 5 °C lower than the actual values. This difference increased in high latitude (2-6 °C) and reached a maximum in the North Atlantic region (6 to 10 °C; CLIMAP, 1981; Community Climate System Model Version 3 - CCSM3, 2006). This climate and the development of the ice sheets led to a prominent fall in sea level of about 110 to 125 meters (Fairbanks 1989, Yokoyama et al. 2000, Siddall et al. 2003, Clark et al. 2009). The arid climatic conditions at every latitudes during the last glacial period have impacted the vegetation cover, which was poorly developed in comparison to today (Sarnthein 1978, Mahowald et al. 1999, Gasse 2000, Baker et al. 2001, Wu et al. 2007). The end of the last glacial period occurred from about 19-20 ka when the ice sheets started to retreat and promoted a concomittant rapid sea-level rise of 10-15 meters (Clark et al. 2009) that is considered as the onset of the last glacial-interglacial transition (or

Termination I). From that time to the Early Holocene ( $\sim 11$  ka), the decay of ice sheets caused global mean sea level to rise by approximately 80 m (Clark et al. 2012). Simultaneously, the carbon cycle has been affected, resulting in the emission of greenhouse gases to the atmosphere. The variation in the atmosphere and ocean circulation affected the global distribution and fluxes of water and heat (Clark et al. 2012).

## **Holocene**

The Holocene (last 11.7 kyr) is the actual interglacial period. The summer insolation at the beginning of the Holocene period, between 9 and 6 ka, was up to 5-8% higher than actual (Denton & Karlén 1973). This led to a maximum in both temperature and precipitation (Holocene thermal Maximum). Around 6 ka the Laurentide and Eurasian ice sheets has completely disappeared (Ruddiman 2001) and determined the end of the sea-level rise (Lambeck & Chappell 2001). From then begin the global aridification and the global cooling until the current conditions (i.e. rapid warming induced by increasing anthropogenic greenhouses gases) are reached (Wanner et al. 2008, Marcott et al. 2013). The physical mechanism responsible for this global cooling in the second part of the Holocene is still debated (Liu et al. 2014).

### **5.1.2 Millennial-scale climate changes**

During the Holocene, the climate was considered as stable in comparison with the great instability recorded during the glacial periods and the MIS3 of the last glacial period in particular (Fig. 5.1). This instability follows a cyclicity of the order of a thousand years, which is too low to be explained by the orbital variations alone and are named suborbital- or millennial variations (Dansgaard et al. 1993, Bond et al. 1993).

The climate at the Earth's surface is partly controlled by oceanic circulation. This one, on a global scale, is controlled by the density gradients maintained between water masses that are determined by temperature and salinity. Cold and deep water are produced in the North Atlantic area and are conducted to the south. This process is referenced as the Atlantic Meridional Overturning Cell (AMOC). Simultaneously, the warm and surface saltwater of the northern Pacific circulate through the Indian Ocean to the North Atlantic. During their path, they get cooled and in winter, become denser than the surrounding waters, and deep. The thermohaline circulation, principally caused by the AMOC, greatly influenced the heat distribution from low to high latitude (Stocker & Schmittner 1997, Cunningham et al. 2007, Moore et al. 2012).

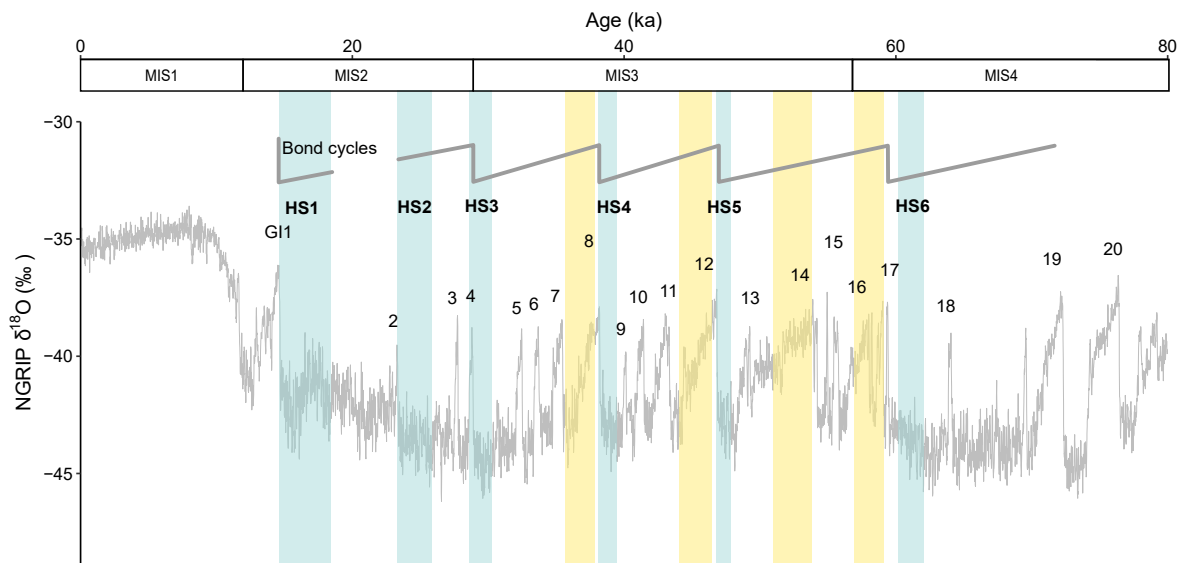


Figure 5.1 – Variation of  $\delta^{18}\text{O}$  record in the Greenland ice showing the climatic variations in the Northern Hemisphere, and the Bond cyclicity represented with the grey line (Rasmussen et al. 2006, Svensson et al. 2006).

The storage of the freshwater inside the ice sheets during the glacial period interacted with the surface hydrology and caused disturbance in the AMOC. Any variation in the AMOC intensity led to climatic variation: when the intensity of the AMOC decrease, the Atlantic North area cools while the low latitude and the Southern Hemisphere get warmer, whereas the AMOC intensity increase the southern water warms the high latitudes. This principle of balance between the two-hemisphere emitted by Crowley (1992) is referred as "bipolar seesaw" by Broecker (1998).

### Dansgaard-Oeschger and Bond cyclicity

The study of the  $\delta^{18}\text{O}$  variation inside the Greenland ice core highlighted a higher than glacial-interglacial frequency climatic cyclicity: about 2 000 yr (Johnsen et al. 1992, Dansgaard et al. 1993). It occurred principally during the MIS 3 and the last glacial period, with 25 cycles. This climatic variation, named Dansgaard-Oeschger (DO) is distinguished by an abrupt increase of the temperature in only few decades (interstadials) with an amplitude between 5 to 16 °C (Landais et al. 2004, 2006, Huber et al. 2006, Capron et al. 2010, Guillevic et al. 2013, Kindler et al. 2014) followed by a slower decrease over 1 000 to 2 000 yr that end with a cold phase over few centuries (stadials).

The DO events can be gathered (by 3 or 4) in 6 oscillations that are named Bond cycles. Each one follows a gradual cooling trend, passing through increasingly cold stages and interstadals, then ending with the destabilization of the Laurentide Ice Sheet and the massive iceberg discharge in the North Atlantic, the so-called Heinrich event (Heinrich 1988)

before the return to a new and brutal warming (Bond et al. 1993).

### 5.1.3 The climatic context in the Alps during the Quaternary

#### Climat and vegetation

During the LGM, the sea-surfaces temperature in the occidental Mediterranean are between 4 and 8°C less than the actual values (Hayes et al. 2005). Ortu et al. (2008) determined temperature 15 °C less than the actual values in high altitude south Alps lake in winter and precipitation that oscillated between 200 and 400 mm. The decrease of temperature and the low precipitation rate induced a vegetation dominated by the grass plants (Beaudouin et al. 2007, Ramstein et al. 2007, Combourieu-Nebout et al. 2010) while the coast areas are composed of temperate forest (Prentice et al. 1993, Allen et al. 1999, Combourieu-Nebout et al. 2010).

In the south of Europe and in the northern Mediterranean borderlands, cold and arid periods of the last glacial (stadials and Heinrich stadials) alternate with warm and humid periods (interstadials). Speleothems reveals that the European Alps were prone to these rapid climatic variations, as shown by the recognition of the Dansgaard-Oeschger variability recognized in numerous caves in Greenland (Spötl et al. 2007, Boch et al. 2011, Columbu et al. 2017). During the stadials the vegetation was dominated by herbaceous plants (Allen et al. 1999, Fletcher et al. 2010a), and the aridification induced semi-desertic taxa, particularly during Heinrich stadials (Combourieu-Nebout et al. 2002, Fletcher & Goñi 2008). On the opposite, during the interstadials the vegetation above in latitude above 40°N including the Mediterranean basin, was characterised by the increase of forest during the intersadials (with major increased during the D-O 14 and 12). A marked increase in the spatial extent of the Mediterranean forest (toward higher altitudes) occurred at the beginning of the Holocene (Tinner & Kaltenrieder 2005, Ortu et al. 2008, Combourieu-Nebout et al. 2010). This is caused by the increased of temperature (2°C higher than actual) and precipitation (100 mm than actual) (Magny 2004, Zanchetta et al. 2007).

#### Glacier evolution

The last glacial period is referred as the Wurm glaciation in the Alpine region. During this period, there has been two major advances in the glacier's positions. The first one occurred during the MIS 4, with no real proof of the advance of the eastern Alps (Reitner 2005), however the presence of glaciers at low elevation in the western Alps is confirmed (Frenzel n.d., Schluechter et al. 1987). At MIS3, glaciers have disappeared from the area (Schluechter et al. 1987, Preusser et al. 2003, Ivy-Ochs et al. 2008), and in particular from the Var basin (Mariotti et al., 2020). The second and more important glacier advance occurred during the MIS 2, with a major episode during the LGM, started around 30

kyr (Schluechter et al. 1987, Schoeneich 1998, Jorda et al. 2000, Preusser et al. 2003, Monegato et al. 2007). During the LGM, three glaciers respectively covered the valley of the Vesubie, the Tinee, and the upper part of the Var (Julian 1977, Buoncristiani & Campy 2004). Together they covered about 17% of the drainage air (Jorry et al. 2011). After the LGM, the glaciers have receded very quickly from 21-20 kyr, and they had entirely disappeared by 17 ka (Ivy-Ochs et al. 2004, Ivy-Ochs et al. 2008). Nowadays, Alpine glaciers are restricted to high elevation sites and there are no more glaciers in the Var region.

## 5.2 Temporal sediment residence time variations

### 5.2.1 Stratigraphy of the Var sedimentary ridge

The Var sediment routing system, which includes the Var Sedimentary Ridge (VSR) in the deep Ligurian Sea, is considered as a reactive system (*sensu* Allen 2008*b*) because of its small alluvial plain (<50 km) limiting temporal sedimentary storage (Anthony & Julian 1999) and the strong correlation observed between climate changes and sediment flux over the last glacial cycle (Bonneau et al. 2014). The VSR is a giant turbiditic levee formed by countless turbidity currents (and associated spillover deposits) which transfer episodically sediments from source to sink (Piper & Savoye 1993, Migeon et al. 2001, Jorry et al. 2011). These turbidity currents are produced by floods of the Var River (Mulder et al. 1998, 2001, Mas et al. 2010). ‘Flood turbidites’ on the VSR are well preserved and present a continuous stratigraphy (Jorry et al. 2011, Bonneau et al. 2014).

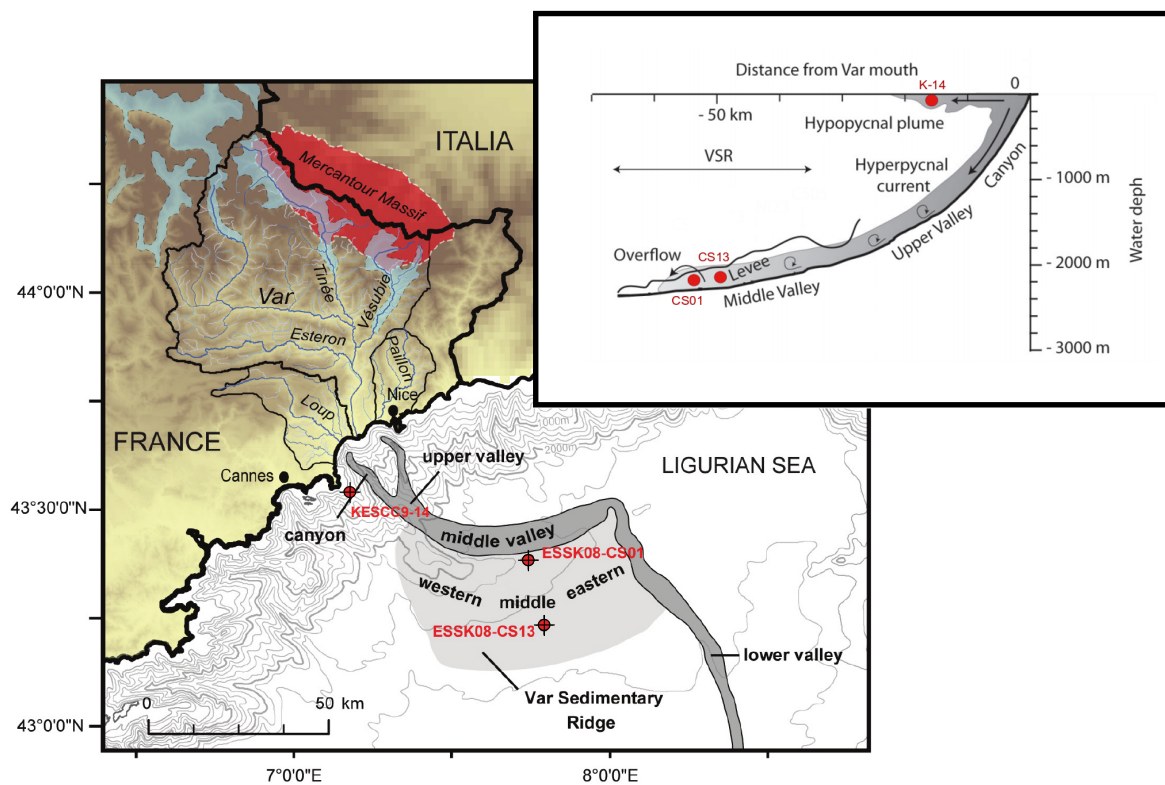


Figure 5.2 – Cores locations of the studied cores along the Var canyon and the Var Sedimentary Ridge with a schematic profile of the deposition area (adapted from Bonneau et al. 2014).

Bonneau et al. (2014) highlighted a significant correlation of planktonic  $\delta^{18}\text{O}$  stratigraphic records from different cores (including ESSK08-CS01 and ESSK08-CS13) localised along the VSR (Fig. 5.2). To do so, these authors sampled the hemipelagic deposits found

between the turbidites (as described in Bonneau et al. 2014), which contain the necessary material for oxygen isotopic measurements (and radiocarbon dating). This approach enabled a detailed reconstruction of the stratigraphy of the VSR by using the  $\delta^{18}\text{O}$  of planktic foraminifera since the obtained  $\delta^{18}\text{O}$  records perfectly match the one from the Greenland ice (e.g. Svensson et al. 2006; Fig. 5.3). As a prominent example, a high variability of the  $\delta^{18}\text{O}$  is observed during the last glacial period and the MIS 3  $\sim$ 30-50 ka with the recognition of the Dansgaard-Oeschger variability. This variability has previously been shown in the western Mediterranean Sea (e.g. Cacho et al. 1999). This reveals that erosion from turbidity currents has no significant impact on the preservation and continuity of the stratigraphic record on the VSR.

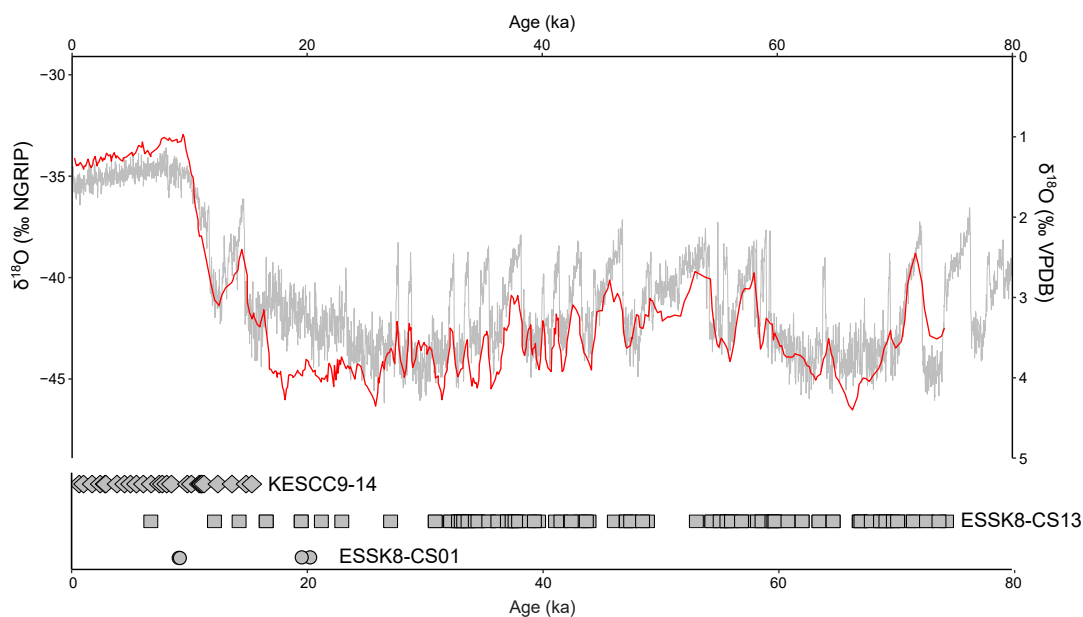


Figure 5.3 – Composite  $\delta^{18}\text{O}$  curve of *Globigerina bulloides* (VPDB = Vienna Peedee belemnite ; from Bonneau et al. 2014) with the  $\delta^{18}\text{O}$  record from the North Greenland Ice Core Project (NGRIP; Rasmussen et al. 2006, Svensson et al. 2006). The obtained correlation between the two curves has been validate by  $^{14}\text{C}$  datation (Bonneau et al. 2014). The studied sediments from the cores KESCC9-14, ESKK8-CS13 and ESKK8-CS01 are represented in grey to represent the period recovered by our data.

Based on the above, a precise age model for cores ESKK08-CS01 and ESKK08-CS13 was produced (Bonneau et al. 2014). It allows the reconstruction of a high-resolution record of the turbidite / flood activity over the last 75 ka. The obtained resolution, commonly found in continuous depositional zone (e.g. open ocean), is unprecedented in turbidite environments. Bonneau et al. (2017) revealed the possibility to explore land-sea dynamics and signal transmission from the erosion zone to the depositional area at high resolution over the last 75 ka using the core ESKK08-CS01 and ESKK08-CS13. Hence, we aim to get further by looking at erosive variation signal over this period. This approach is complementary of the one led by Mariotti et al. (2020) to study past denudation rate in the Var basin.

## 5.2.2 Methods

In this study, sediment from three cores were used. Two cores, ESSK08-CS01 (2146 m of water depth) and ESSK08- CS13 (2473 m of water depth), were recovered along the VSR during the ESSDIV cruise on the N/O Pourquoi pas? (2008). The third core, KESC9-14 (550 m of water depth), has been sampled in 2008 during the ESSCAR-9 cruise on the N/O Le Suroit. It is located on an interfluve, above surrounding canyons, directly off the Var river mouth. This core covers only the Holocene period (Ciobanu et al. 2012) Houedec et al., submitted). Sediments from the KESC9-14 are fine-grained deposits (considered in our study as the undifferentiated size fraction;  $n=27$ ) from hypopycnal plumes. Conversely, ESSK08-CS01 and ESSK08- CS13 are levees-channel deposits consisting of alternations of millimeter to decimeter-scale turbiditic sandy/silty sequences and hemipelagic (i.e. foram-rich) muds. Therefore for each interval of interest, two grain size were sampled: first the hemipelagic facies in between the turbidites (considered in our study as the clay size fraction;  $n= 64$ ) and, second, the uppermost and silty part of the turbidite facies (considered in our study as the silt size fraction;  $n=52$ ). Two grain size fractions were sampled to determine if the grain size sorting caused by turbiditic activity could influence the signal transmission.

Samples were prepared for U isotopic analysis at the Wollongong Isotope Geochronology Laboratory (WIGL), University of Wollongong. Sediments were first wet sieved to separate the  $<63 \mu\text{m}$  fraction, where the surface/volume is large enough to induce a substantial loss of  $^{234}\text{U}$  (DePaolo et al. 2006, Martin et al. 2015). To remove the authigenic phases and organic matter, which are generally enriched in  $^{234}\text{U}$  (Plater et al. 1988, 1992, Andersson et al. 1998, 2001, Maher et al. 2006), about 1 g of  $<63 \mu\text{m}$  sediments was treated following the sequential leaching protocol developed by Francke et al. (2018). About 30 mg of the residual detrital sediment were dissolved in  $\text{HNO}_3$  and HF, followed by aqua regia, and finally re-dissolved in 2 mL of 7 M  $\text{HNO}_3$  prior to chromatography. Ion exchange chromatography was performed on the dissolved samples to isolate uranium prior to isotopic analysis. This was undertaken on an ESI prepFAST automated chromatography system with a pre-filled “ThU – 0500” column with AG1-X8 resin from ESI. Prior to sample loading (2 mL of 7 M  $\text{HNO}_3$ ), the resin was washed with 7M  $\text{HNO}_3$ , 0.1M HCl, 6M HCl and water and then conditioned with 7M- $\text{HNO}_3$ . Following sample loading, matrix was eluted in 7M- $\text{HNO}_3$  and uranium in 0.12M HCl. Uranium elutions were dried down and re-dissolved in 0.3M of  $\text{HNO}_3$  for isotopic analysis.

Uranium concentrations were performed at WIGL on a iCAP Q Inductively-Coupled Plasma Mass Spectrometer (ICP-MS). The sample introduction system comprised a peristaltic pump, a PFA nebulizer and a spray chamber. Sample cone and skimmer cone were used. An internal standard (71D) was added to all samples to correct from the instru-

mental derive. Prior to the ICP-MS analysis, an aliquot of the studied samples was taken from the parent solution in 7M HNO<sub>3</sub>. It was then evaporated and taken up in 0.3M of HNO<sub>3</sub> for analyze. Between each sample analysis, the system was rinsed with 0.3M HNO<sub>3</sub> and blanks intensity were measured and subtracted from each sample. In order to validate the data, a quality control was set up by analyzing a standard solution (71A) every five samples, with a known concentration of each analyzed elements.

Uranium isotope analyses were performed at WIGL on a ThermoFisher Neptune Plus Multi-Collector Inductively-Coupled Plasma Mass Spectrometer (MC-ICP-MS), using an APEX HF desolvating system and (nebuliser) as sample introduction system. Jet sample and X skimmer cones were used. Standard bracketing was used to correct for SEM-Faraday cup yield and mass bias, using NBL U010 as primary standard (Richter & Goldberg 2003). Analysis accuracy was determined by measuring synthetic standard NBL U005-A (Richter & Goldberg 2003) and was consistently better than 0.7% for (<sup>234</sup>U/<sup>238</sup>U). Total procedural blanks were measured, and their contribution were less than 0.1% to the sample (<sup>234</sup>U/<sup>238</sup>U). Total procedural accuracy was evaluated by analysing BCR-2 reference material (Sims et al. 2008), with results in good agreement with reference value.

Table 5.1 – BCR-2 standard values measured during the Var cores sediments study.

<b>Standard</b>	<b>U (ppm)</b>	<b>2SD</b>	<b>(234/238)</b>	<b>2SD</b>
BCR-2	1.63	<i>0.03</i>	1.000	<i>0.004</i>
BCR-2	1.69	<i>0.02</i>	1.000	<i>0.005</i>
BCR-2	1.89	<i>0.02</i>	1.001	<i>0.005</i>
BCR-2	1.67	<i>0.02</i>	1.000	<i>0.003</i>
<b>Mean</b>	<b>1.72</b>	<b><i>0.12</i></b>	<b>1.001</b>	<b><i>0.001</i></b>
<b>Reference value</b>	<b>1.69</b>	<b><i>0.19</i></b>	<b>1.001</b>	<b><i>0.001</i></b>

Specific surface area measurements were carried out on 11 leached sediments by gas sorption analysis using a Quantachrome Autosorb iQ at WIGL. About ~1 g of sediments were first degassed for approximately 7.5 h with a three-steps temperature increase to 200°C (5 °C/min to 80 °C, soak time 30 min, followed by 1 °C/min to 100 °C, soak time 60 min, followed by 5 °C/min to 200 °C, soak time 300 min). Nitrogen was used as the adsorbate gas. The specific surface area was estimated using the best fit of the multi-point BET equation (with a correlation coefficient  $R^2 > 0.999$  for all measurement). The fractal dimension D were determined using the Neimark-Kiselev method (Neimark 1990).

The sediment residence time was calculated using the comminution age approach developed by DePaolo et al. (2006) which was modified by Francke et al. (2019) to consider

$^{234}\text{U}$  loss after deposit:

$$t_{res} = \frac{-1}{\lambda_{234}} \ln \left[ \frac{[A - (1 - f_{post})] e^{-\lambda_{234} t_{dep}} + (1 - f_{post}) - (1 - f_{pre})}{A_0 - (1 - f_{pre})} \right] \quad (5.1)$$

In the case where the surface area was not measured for a given sample, a random value was taken between the minimum and the maximum values measured. Sediment residence times were calculated using Monte Carlo simulation (10,000 simulations). For each sample,  $A_{meas}$  was taken randomly within the range of measured ( $^{234}\text{U}/^{238}\text{U}$ ) activity ratios and its error, and the maximum measured ( $^{234}\text{U}/^{238}\text{U}$ ) value was attributed to  $A_0$  as we obtained ( $^{234}\text{U}/^{238}\text{U}$ ) > 1 in sediments. As not every specific surface area were measured, for the samples without data, a random value was choose between the minimum and maximum values measured.

### 5.2.3 Uranium variations over time - Results

The KESC9-14 core cover mainly the Holocene period, while the ESSK08- CS01 and ESSK08- CS13 are principally composed of sediments from the Late Glacial Period. The similarity in the results obtained by these cores for the covered overlaps between 9-15 ka allows us to overcome the possible site effect.

#### Concentration

Uranium concentration in core KESC9-14 ranges from 2.33 to 5.58 ppm for the Holocene period (mean =  $3.7 \pm 0.5$  2SD; n = 27). In cores ESSK08- CS01 and ESSK08- CS13, U concentrations vary from  $0.05 \pm 0.03$  (2SD) to  $4.00 \pm 0.05$  ppm (2SD) in the clay fraction over the last 75 ka (mean =  $2.7 \pm 0.3$  ppm 2SD; n = 64). For the silt size fraction, U range from  $0.65 \pm 0.05$  (2SD) to  $4.99 \pm 0.05$  (2SD) ppm (mean =  $2.9 \pm 0.3$  2SD ppm; n=52, Fig. 5.4, Appendix A5.1).

During the Holocene (0-11.7 ka), U concentrations are higher (mean=3.83 ppm, n=26) than the value for the upper continental crust (UCC, between 2.5-2.8 ppm; grey rectangle in Fig. 5.4). Conversely, during the last glacial period (>11.7 ka), the concentration is relatively close to the UCC concentration with a mean of 2.90 ppm (n=116).

Over the Last Glacial Period there is some variation in U concentrations. During the MIS 4 (75-57 ka), U concentrations are relatively stable, just above the actual values of the UCC. At the beginning of the MIS 3, the uranium concentration decreased and is globally within the range of UCC values, with an extreme value close to 0 at 56.8 ka for the clay grain size fraction. In the middle of the MIS 3 (~39.2 ka), the uranium concentration increases slightly above the UCC to decrease abruptly to 0.6 ppm at 32-33ka. In the middle of the MIS 2 (20 ka), the U concentration for clay-size fractions is in the UCC range, whereas the indistinct grain size fraction is above and increase until the transition

with the MIS 1 where it reach a maximum of 5.58 ppm at 12.4 ka.

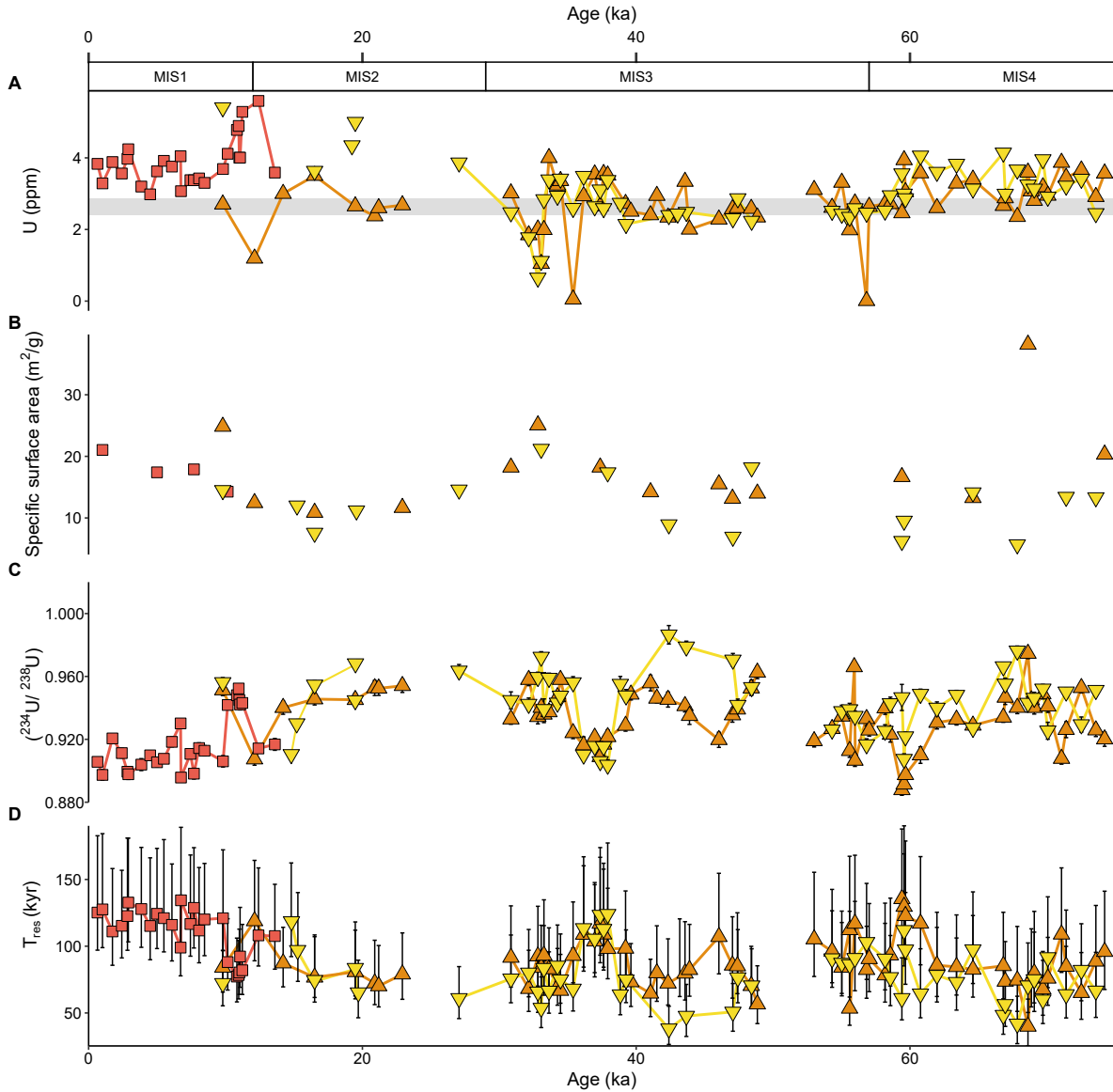


Figure 5.4 – Results for the core sediments: A. Uranium concentrations (ppm), B. specific surface area ( $m^2/g$ ), C.  $(^{234}U/^{238}U)$ , D. and the calculated sediment residence time  $T_{res}$  (kyr) in indistinct grain size (red square; i.e. KES9-14 samples), silt size fraction (yellow triangle) and clay size fraction (orange triangle),  $2\sigma$  errors are smaller than the plot size if no represented. The grey rectangle represents the value of the U concentration in the Upper Continental Crust (UCC).

### Uranium activity ratio

Over the last 75 ka, ( $^{234}\text{U}/^{238}\text{U}$ ) range from  $0.888\pm 0.003$  (2SD) to  $0.987\pm 0.004$  (2SD) (Fig. 5.4) with a mean value of 0.934 (n=143). In the KESC9-14 core, ( $^{234}\text{U}/^{238}\text{U}$ ) range between  $0.896\pm 0.004$  (2SD) to  $0.952\pm 0.003$  (2SD), with a mean of 0.917 (n=27). ( $^{234}\text{U}/^{238}\text{U}$ ) variate between  $0.888\pm 0.004$  (2SD) and  $0.975\pm 0.004$  (2SD) for the clay size fraction (mean = 0.934, n=64) from  $0.904\pm 0.004$  (2SD) to  $0.987\pm 0.004$  (2SD) for the silt fraction (mean = 0.943, n=52) in the cores ESK08-CS01 and ESK08-CS13. No correlation between ( $^{234}\text{U}/^{238}\text{U}$ ) and U concentration are observed (Fig. 5.5).

For the Holocene, values are stable around 0.945 (n=26) ranging from  $0.896\pm 0.004$  (2SD) to  $0.956\pm 0.004$  (2SD). For the Last Glacial Period, ( $^{234}\text{U}/^{238}\text{U}$ ) range from  $0.888\pm 0.003$  (2SD) to  $0.987\pm 0.004$  (2SD) with a mean value of 0.937 (n = 116).

Over the Last Glacial Period, the ( $^{234}\text{U}/^{238}\text{U}$ ) values oscillate between  $0.920\pm 0.005$  (2SD) and  $0.945\pm 0.005$  (2SD) for both silt and clay size fraction during the MIS 4 with an increase close to secular equilibrium around 68 ka to  $0.975\pm 0.003$  (2SD) for the clay and  $0.976\pm 0.005$  (2SD) for the silt size fraction. At the end of the MIS 4 (~59.5 ka), the values decrease to  $0.888\pm 0.003$  (2SD) and  $0.907\pm 0.003$  (2SD) for the clay and silt, respectively. From the beginning of the MIS 3 (50 ka), the values decrease from  $0.963 (\pm 0.004)$  (2SD) to  $0.920\pm 0.005$  (2SD) for the clay and slightly decrease for the silt to increase right after to  $0.987\pm 0.006$  (2SD) until 42 ka. The ( $^{234}\text{U}/^{238}\text{U}$ ) ratio decrease until 35 ka and increase back until the end of the MIS 2. The values are then stable around 0.945 until 12 ka, and then decrease slowly until the end of the Holocene to values generally lower than 0.910.

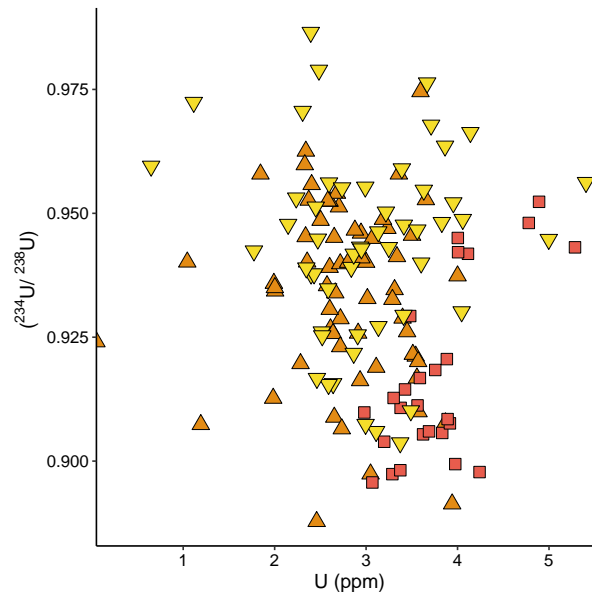


Figure 5.5 – ( $^{234}\text{U}/^{238}\text{U}$ ) in function of the concentration in indistinct grain size (red square; i.e. KESC9-14 samples), silt size fraction (yellow triangle) and clay size fraction (orange triangle),  $2\sigma$  errors are smaller than the plot size.

### **Specific surface area**

The specific surface area of sediments from cores KESC9-14, ESSK08-CS01 and ESSK08-CS13 vary from 5.7 to 21.2 m<sup>2</sup>/g for the silt size fraction (mean = 12.1 m<sup>2</sup>/g; n=14), from 10.9 to 38.1 m<sup>2</sup>/g for the clay fraction (mean = 17.6 m<sup>2</sup>/g, n = 15), and from 11.5 to 21.0 m<sup>2</sup>/g in the undifferentiated fraction (mean = 15.7 m<sup>2</sup>/g, n = 6).

The specific surface area increased over the Holocene (0-11.7 ka) from 17 to 21 m<sup>2</sup>/g (mean = 18.3 m<sup>2</sup>/g, n=6). Conversely for the Last Glacial Period, the specific surface area fluctuated between 5.7 and 38.1 m<sup>2</sup>/g (mean = 14.5 m<sup>2</sup>/g, n=29).

Over the Last Glacial Period, we observe variation of the measured specific surface area. During the MIS 4, measured specific surface areas are very spread out with values for the clay size fraction varying around 20 m<sup>2</sup>/g with one exceptional data reaching 40 m<sup>2</sup>/g. From the MIS 3 the values increased for both silt and clay size fractions and start decreasing at the end of the MIS 3 (~32 ka) until the middle of the MIS 2 (16 ka) where clay sized specific surface area is around 11 m<sup>2</sup>/g and for silt it is 7.55 m<sup>2</sup>/g. Then it increased until the end of the MIS 1 with values around 20 m<sup>2</sup>/g.

### **Sediment residence time**

The obtained sediment residence time variations show, as expected inverse variation from the (<sup>234</sup>U/<sup>238</sup>U) (Fig. 5.6). Low (<sup>234</sup>U/<sup>238</sup>U) indicate long sediment residence time. The sediment residence time inferred from both (<sup>234</sup>U/<sup>238</sup>U) and the specific surface area range from 40 to 135 kyr for the clay size fraction (mean = 87 kyr) from 38 to 123 kyr for the silt fraction (mean = 77) in the cores ESSK08-CS01 and ESSK08-CS13. The variation in the core KESC9-14 ranges from 77 to 134 kyr with a mean of 110 kyr.

Over the Holocene, the sediment residence time ranges between 72 kyr to 134 kyr with a mean value of 108 kyr (n=26). During the Last Glacial Period sediment residence time vary between 38 kyr and 135 kyr with a mean value of 83 kyr (n=116).

The largest fluctuations of the sediment residence time occurred during the Last Glacial Period with maximum sediment residence time at the end of the MIS 4 (117 kyr at 60 ka), the middle of the MIS 3 (123 kyr around 36-38 ka) and the end of the MIS 2. On the other hand, the minimum sediment residence time were found at ca. 41 ka, 48 ka and 58 ka, 68 and 72 ka.

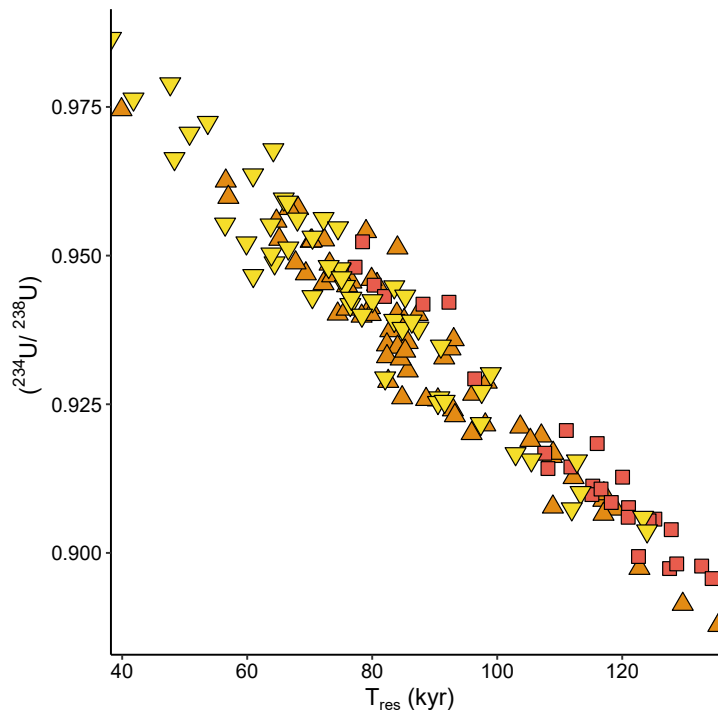


Figure 5.6 –  $(^{234}\text{U}/^{238}\text{U})$  depending on the calculated sediment residence time  $T_{res}$  in indistinct grain size (red square; i.e. KESC9-14 core samples), silt size fraction (yellow triangle) and clay size fraction (orange triangle).

## 5.2.4 Interpretation

### Exploring the relationship between climate and sediment residence time in the Var routing system

**Glacial-Interglacial variability** The mean  $(^{234}\text{U}/^{238}\text{U})$  over the glacial period is 0.937 ( $\pm 0.019$  1.S.D.) and the associated sediment residence time is around 137 kyr. During the Holocene,  $(^{234}\text{U}/^{238}\text{U})$  is lower, around 0.920 ( $\pm 0.021$  1.S.D.) and, as a consequence, the sediment residence time is higher (181 kyr). This result revealing reduced sediment residence time during the last glacial period is coherent with the fact that the Pleistocene cold period was associated with the presence of mountain glaciers. Indeed, glaciers are known to substantially increase erosional and weathering processes (Hallet et al. 1996, Anderson 2005) and therefore reduce the sediment residence time by limiting the time spent within the regolith. In the same way, DePaolo et al. (2006) interpreted past variations in sediment residence time obtained with  $(^{234}\text{U}/^{238}\text{U})$  measurements in cores from the North Atlantic region as the result of variations of ice sheet cover/volume over North America. Conversely, during interglacials, the vegetation growth limits the transport of sediment (by stabilizing soils) and enhances the sediment storage which, in turn, increase the sediment residence time.

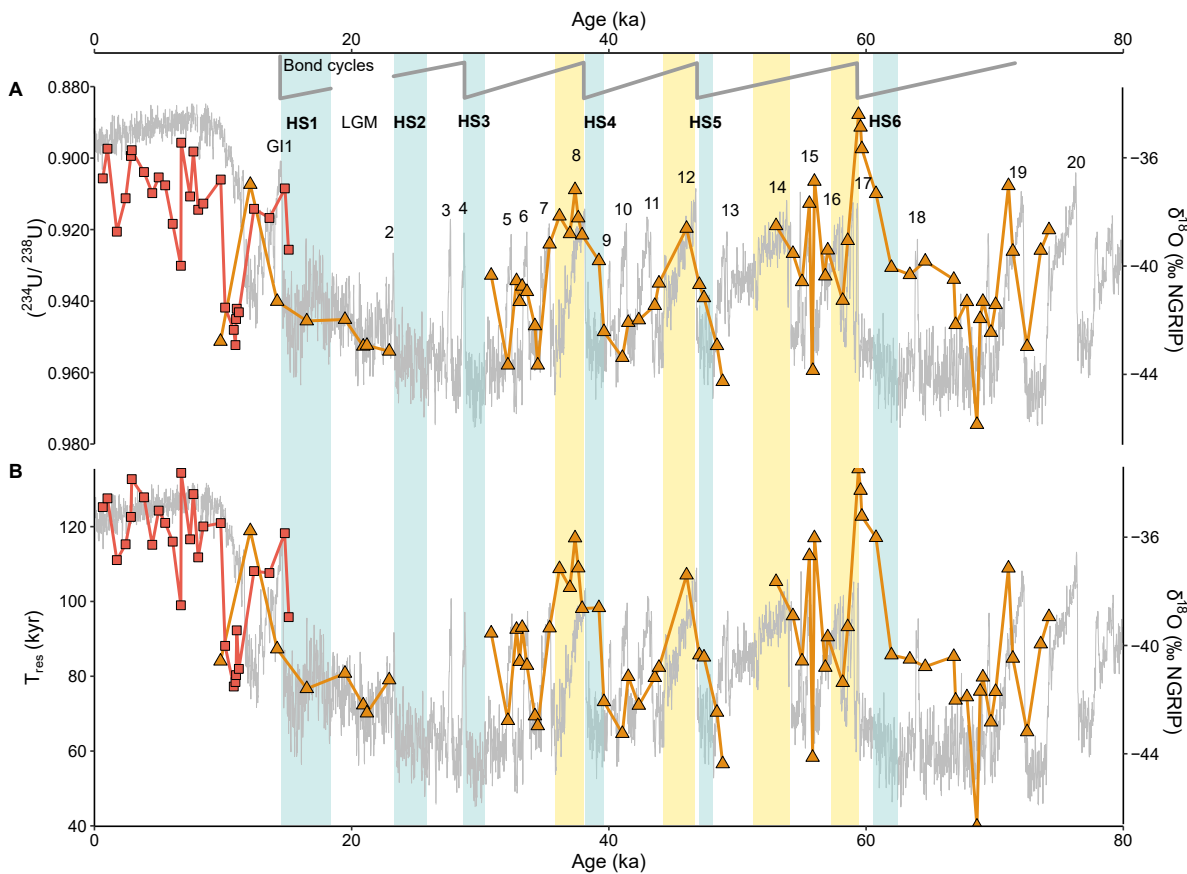


Figure 5.7 – Variation of A.  $(^{234}\text{U}/^{238}\text{U})$  and B. Sediment residence time over the last 75 ka with the variation in grey of the  $\delta^{18}\text{O}$  record from the North Greenland Ice Core Project (NGRIP; Rasmussen et al. 2006, Svensson et al. 2006). The blue rectangles represent the Heinrich stadials and the yellow rectangles are the major GI.

### Millennial-scale glacial variability

Over the last glacial period, the  $(^{234}\text{U}/^{238}\text{U})$  variability follows to a first order the climatic fluctuations. Indeed,  $(^{234}\text{U}/^{238}\text{U})$  is low during the warm and wet climatic phases of the studied period, i.e. the Greenland Interstadials (GI; Fig. 5.7). The  $(^{234}\text{U}/^{238}\text{U})$  ratio are particularly low ( $<0.920$ ) during the major (i.e. warmer, longer) interstadials, namely the GI-8, 12, 14, 15, 17 and 19. During the other ‘second-order’ GI (e.g. GI=5,6,7,11 etc.), the uranium activity ratios do not seem to decrease as much as during the major GI. Conversely during the cold and dry climatic phases, i.e. the LGM and the Heinrich stadials,  $(^{234}\text{U}/^{238}\text{U})$  are closer to the secular equilibrium with values around 0.980. Hence, the observed  $(^{234}\text{U}/^{238}\text{U})$  variability does not follow the Dansgaard-Oeschger variability but the Bond cycles (i.e. from major GIs to the subsequent Heinrich stadials). It suggests long sediment residence time (low  $(^{234}\text{U}/^{238}\text{U})$ ) during the warm interstadials and low sediment residence time ( $(^{234}\text{U}/^{238}\text{U})$  close to 1) during the cold stadials and the Heinrich stadials in particular.

## Interpreting ( $^{234}\text{U}/^{238}\text{U}$ ) ratios in the light of the sedimentary input

In order to interpret our data in the most accurate way, we compared our ( $^{234}\text{U}/^{238}\text{U}$ ) data with background information on sedimentary processes in the Var basin. This includes the turbidite accumulation data of Bonneau et al. (2014) as an indicator of sediment availability in the routing system and of flood activity of the Var river.

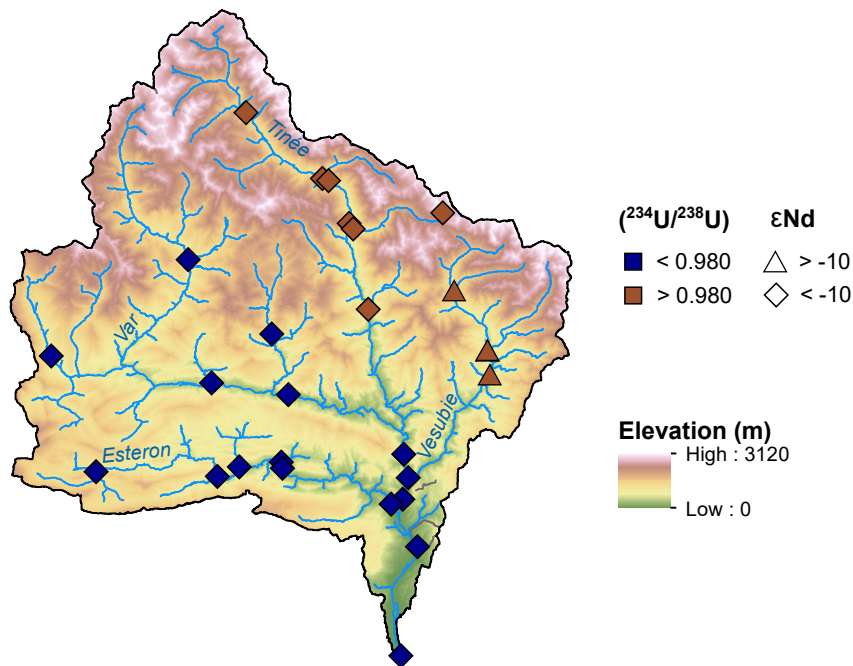


Figure 5.8 – Spatial variation of ( $^{234}\text{U}/^{238}\text{U}$ ) and  $\epsilon_{\text{Nd}}$  (data from Bonneau et al. 2017) in the Var basin.

During the major GI, the low ( $^{234}\text{U}/^{238}\text{U}$ ) are synchronous with practically absent turbiditic flows in the Var canyon (i.e. rare river floods, Fig 5.7; Bonneau et al. 2014). This correlation is in good agreement with ‘long’ sediment residence time ( $>100$  kyr). The low values are comparable with the actual ( $^{234}\text{U}/^{238}\text{U}$ ) values for the Var and Esteron sub-catchment (Fig. 5.8, Chapter 4), which are representative of a transport-limited regime, i.e. the soil production is more effective than the soil denudation and the soil thickness increased. Thus, during these major GI, the basin can be compared to a transport-limited regime. Conversely, during the cold and dry Heinrich stadials, ( $^{234}\text{U}/^{238}\text{U}$ ) is closer to 1 and the turbiditic flows in the Var canyon increased. During the LGM, despite the presence of important glacier coverage, the ( $^{234}\text{U}/^{238}\text{U}$ ) is close to 1 with shorter sediment residence time ( $<100$  kyr). These ( $^{234}\text{U}/^{238}\text{U}$ ) values can be compared with the values obtained in the modern sediments from the Tinee and Vesubie sub-catchments, which have

( $^{234}\text{U}/^{238}\text{U}$ ) close to secular equilibrium (Fig. 5.8, Chapter 4). These two sub-catchments are compared to weathering-limited regime, i.e. the denudation rates were higher than the soil production rate (soil thickness decreased therefore sediment spent less time in the weathering profile minimizing sediment residence time). Hence, it indicates that the Var basin, during cold periods can be considered as weathering-limited regime.

These results show for the first-time that glacial, millennial-scale climate changes strongly impact the sediment residence time in routing systems. This response of the sedimentary systems to short-term climatic variations sustain the idea that climate perturbations can be transferred to and be preserved in the deep-sea sediment record. This challenges the conclusion of Jerolmack & Paola (2010) and of Armitage et al. (2013), who suggested that climate driven environmental signal were temporally buffered. Conversely it supports the numerical approach provided by Simpson & Castelltort (2012), which indicates a high frequency signal transmission in sedimentary record.

We are now investigating the origin of this relationship between climate and sediment residence time. To do this, we will discuss the impact of glaciers on the one hand, and the impact of vegetation on the other, which can also be used as a proxy of precipitation rate variation. These are the two major forcing parameters likely to explain our data (the tectonics in the zone being stable on the time scale studied).

## **Investigation of the sediment residence control**

### **The potential glacial effect**

In the European Alps, during the last glacial period and the LGM, the presence of widespread glaciers is well documented, including in the Var catchment (e.g. Buoncristiani & Campy 2004). Glaciers are known to be efficient erosive agents (Hallet et al. 1996) and their presence likely explained our obtained ( $^{234}\text{U}/^{238}\text{U}$ ) variation at the glacial - interglacial scale (see Part 5.2.4.1 above). This assumption is also supported by source studies which show that glacial sediment delivered by the Var are mostly coming from the upper part of the basin (Tinee and Vesubie tributaries; Bonneau et al. 2017), where erosive processes are increased by the presence of glacier.

The relationship between erosion and glacier fluctuation can be questioned before the LGM, and especially during the MIS 3. For the MIS 3 period, which includes the highest glacial climate and ( $^{234}\text{U}/^{238}\text{U}$ ) variabilities, the upstream part of the Var basin was likely not covered by glaciers (Buoncristiani & Campy 2004). The minimal (if any) influence of the glacier during the MIS 3 is also supported new denudation rate data ( $^{10}\text{Be}$ ; Mariotti et al., 2020). The  $^{10}\text{Be}$ -derived denudation rate increased only during the LGM, when considering the last 75 ka and are stable during the MIS 3 (Mariotti et al., 2020). Finally,  $\varepsilon_{Nd}$  data (i.e. a proxy for sediment provenance) associated with rare earth element

abundances, major and minor elements data indicate that the main driving mechanism of sediment input to the VSR during MIS 3 was not restricted to the upper watershed (where glaciers are expected), but likely impacted the whole Var basin (Bonneau et al. 2014, 2017). Taken together, these lines of evidence indicate that glacier fluctuations cannot explain the ( $^{234}\text{U}/^{238}\text{U}$ ) ratio variability during MIS 3.

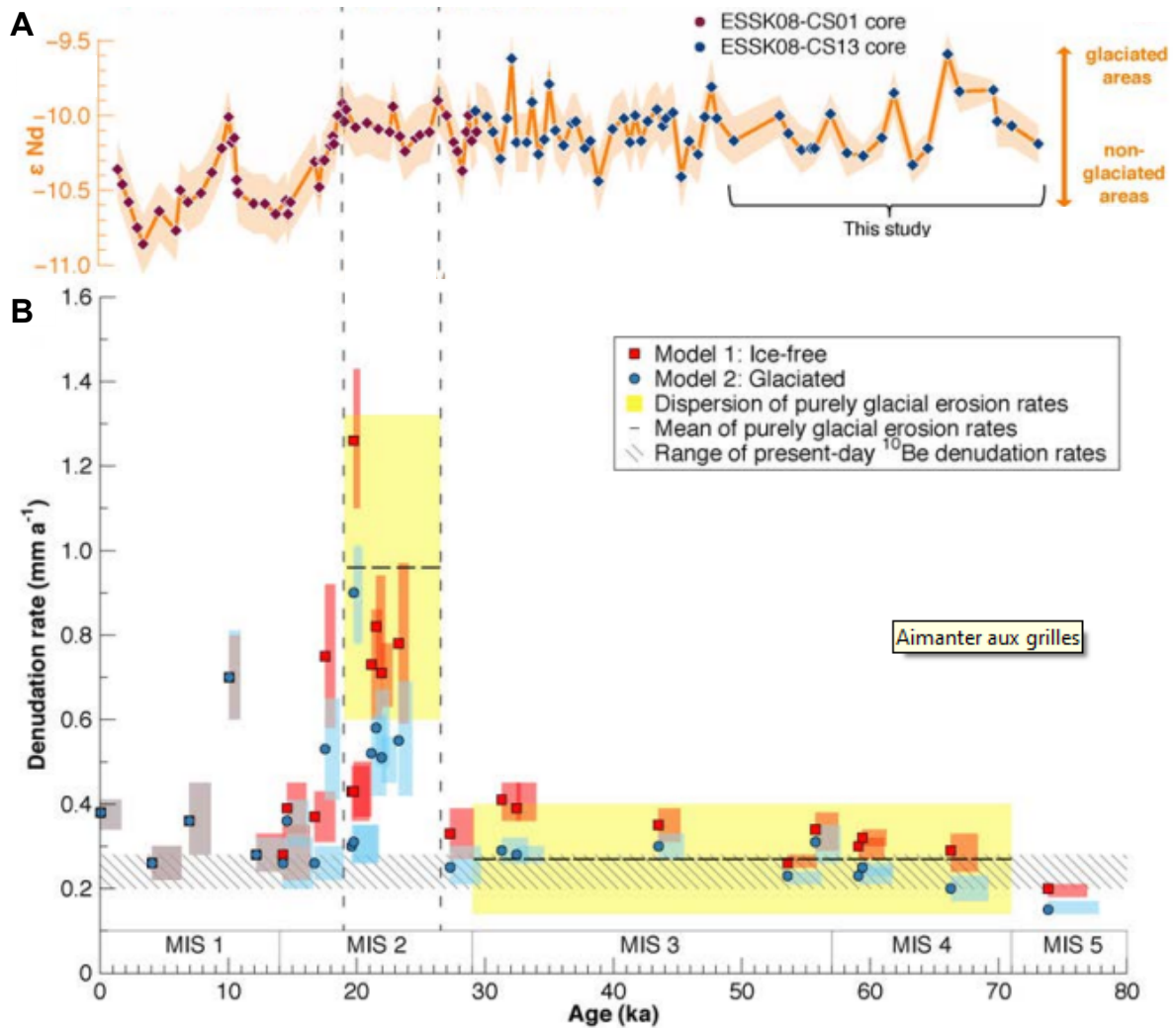


Figure 5.9 –  $\epsilon_{Nd}$  variation in the Var basin (from Bonneau 2014, Mariotti 2020); turbidites frequency and  $^{10}\text{Be}$  derived denudation rate (from Mariotti 2020).

### The vegetation impact on sediment residence time

If glaciers do not likely explain the obtained variation of sediment residence time during the MIS 3, the vegetation could influence it. Indeed, Dosseto et al. (2010) determined a vegetation control of sediment residence time over glacial-interglacial cycles. Later, Francke et al. (2019) corroborate this idea studying Late Glacial to Holocene sediment from the Balkans. Therefore, it is interesting to compare the paleo-variation of sediment residence time in the Var sediment routing system with palynological data available in

the surrounding regions. Fletcher et al. (2010a) produced a palynological synthesis of the available data for the last glacial cycle in the western Mediterranean area. A major result of this synthesis is the concordance of the temperate forest growth, marker for warm summers / rainy winters during the Greenland interstadials and in particular during the major GI (8, 12,14, and 16-17) that define the onset of each Bond cycle (Fig. 5.10). This regional pattern is well expressed in the western Mediterranean region (Sanchez Goni & Harrison 2010, Fletcher et al. 2010b). For this reason, we compare our ( $^{234}\text{U}/^{238}\text{U}$ ) ratio to the palynological data from Lagaccione, northern Italy (Figure 5.10). These data have their own chronology based on their stratigraphy.

The observed temporal variability of the temperate forest extension at Lagaccione match the ( $^{234}\text{U}/^{238}\text{U}$ ) variations obtained in the Var sediment routing system (Fig. 5.10), despite possible incoherence due to the chronology based on their own stratigraphy. The low ( $^{234}\text{U}/^{238}\text{U}$ ) values representative of long sediment residence time during the main GI correspond to the high abundance of the temperate forest taxa, indicative of maximum extension of the temperate forest at Lagaccione and in the western Mediterranean region as a whole. The presence of this kind of temperate forest indicates that precipitation rates were elevated during the major GI, which is supported by the precipitation gradient from the region (see Sánchez Goñi et al. 2002). Therefore, it is interesting to note that despite the high precipitation rates during the major GI, the sediment residence time are long (this study) and the turbiditic flows are almost absent (Bonneau et al. 2014). Yet, the opposite would be expected: higher precipitation rate would have enhanced erosion and thus favored flood events resulting in more turbiditic accumulation during these major GI. In the Var basin, the precipitation rate is influenced by the sea surface temperature (SST). The increase of the SST induces extreme events of precipitations. Figure 5.11 shows that when the SST are higher, the ( $^{234}\text{U}/^{238}\text{U}$ ) is lower, which suggests longer residence time. From the above comparison with pollen information and SST, we assume that this expectation is compensated for by the vegetation cover: the increase of the temperate forest stabilized the soil enhancing the soil production and therefore increasing sediment residence time (low ( $^{234}\text{U}/^{238}\text{U}$ )), which also explains the absence of floods.

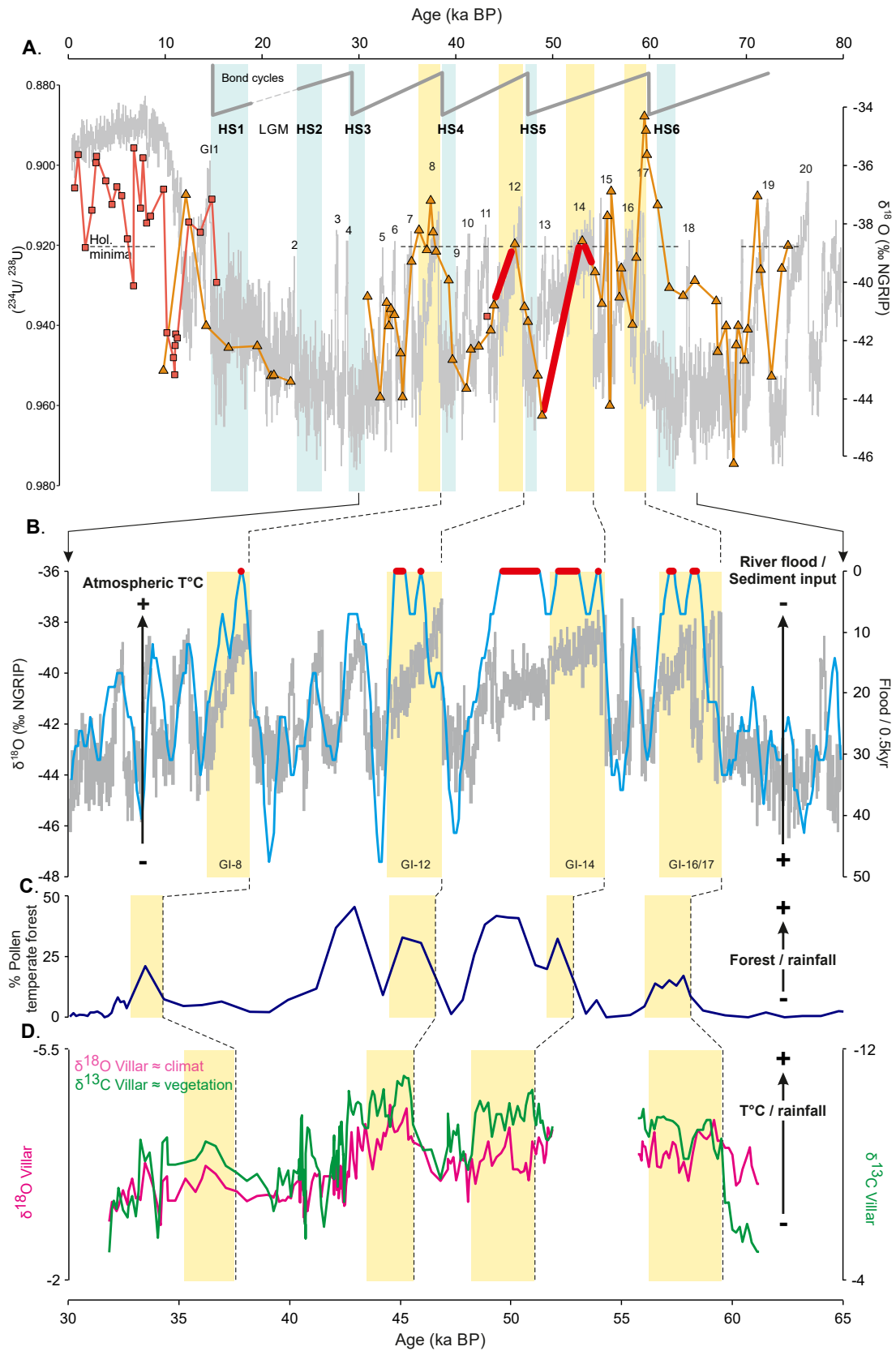


Figure 5.10 –  $(^{234}\text{U}/^{238}\text{U})$  compared to climatic and vegetation parameters with: A. reverse  $(^{234}\text{U}/^{238}\text{U})$  variations from the Var basin concordant with the major  $\delta^{18}\text{O}$  NGRIP variation; B. flood accumulation for the Var basin; C. percentage of pollen from temperate forest from the Lagacionne site (Fletcher et al. 2010b); D.  $\delta^{18}\text{O}$  and  $\delta^{13}\text{C}$  from the villar cave (Genty et al. 2003).

The obtained correlation between ( $^{234}\text{U}/^{238}\text{U}$ ) from the Var basin and the regional values of palyno data from Fletcher et al. (2010a) promotes the idea of an ‘invasion’ of temperate forests in the upper parts of the basin (Tinee and Vesubie sub-catchments) during the majors GI. Thus, the vegetation cover likely compensates completely the denudation effect of the precipitation, which is required for the development of this temperate forest. Conversely, during the cold and arid period, the vegetation was composed of grassland and steppe (Fletcher et al. 2010a).

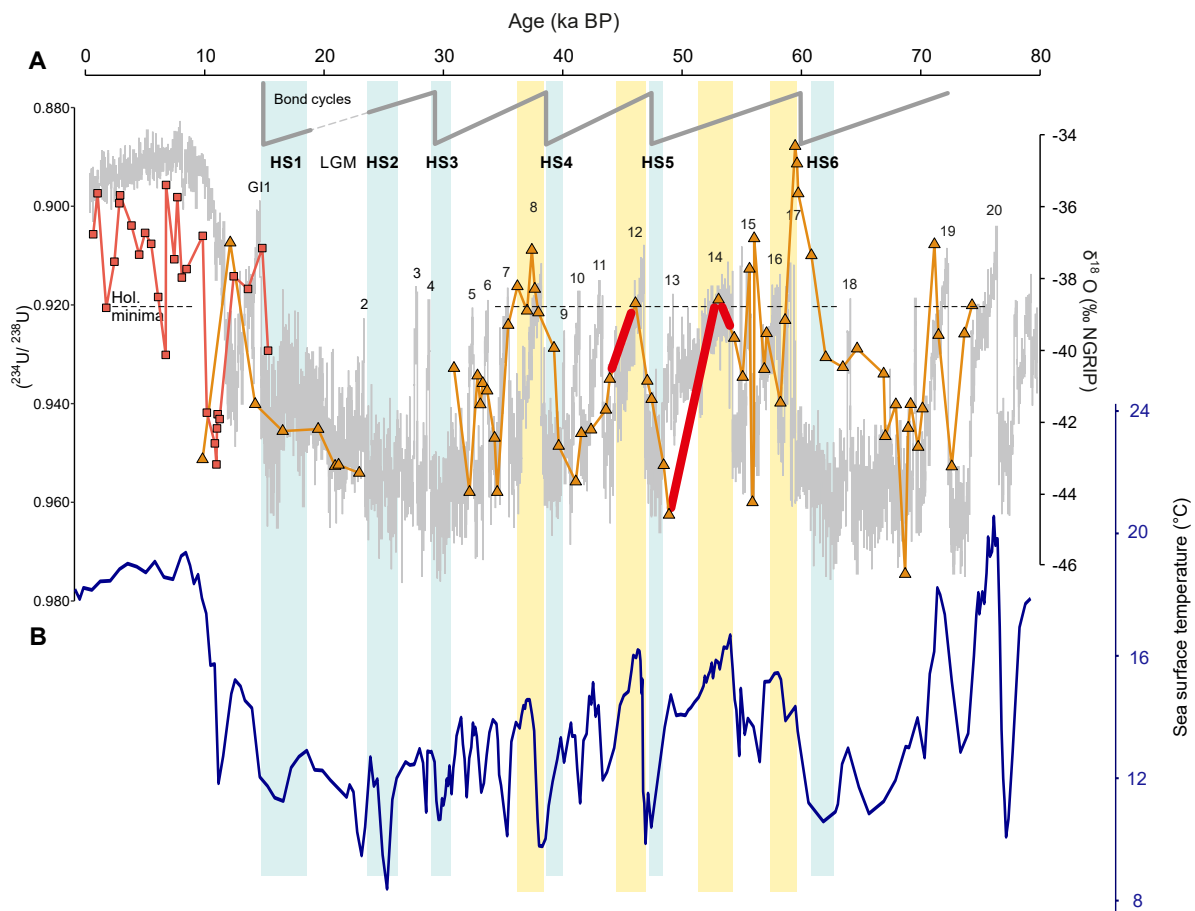


Figure 5.11 – A. reverse ( $^{234}\text{U}/^{238}\text{U}$ ) variations from the Var basin concordant with the major  $\delta^{18}\text{O}$  NGRIPP variation; B. Sea surface temperature (°C) from the ODP977 (Martrat et al. 2004).

An interesting point has been underlined by Fletcher et al. (2010a): in the latitudes above  $40^\circ\text{N}$  (thus including the Var basin), the development of the forest was stronger during GI-14 and 12 than either GI-16-17 or 8. It is particularly visible in the Lagacionne and Lago Grande di Moticchio series in Italia. These extensive forest growths are concordant with the decrease of  $\delta^{13}\text{C}$  and  $\delta^{18}\text{O}$  data of the speleothems from the Villar cave (Périgord, France; see Genty et al., 2003 for further details). It indicates that the period of precipitation and vegetation cover increased in Villar are similar of the forest development around the Mediterranean. It also explained the turbiditic flows and the ( $^{234}\text{U}/^{238}\text{U}$ )

variations: during both GI -14 and 12 there is an absence of overflow in the Var basin. The forest extension in the Var basin stabilized the soil and reduced denudation. It led to a reduction of sediment flow and a limitation in the turbiditic accumulation. Hence the basin is completely transport limited, which increased the sediment residence time (low  $(^{234}\text{U}/^{238}\text{U})$ ). Note that because of the absence of sediment transfer during these two major GI -14 and 12, there is no turbidite material to measure  $(^{234}\text{U}/^{238}\text{U})$  which explain the lack of data for these events.

### 5.2.5 Conclusion

The paleo variation of  $(^{234}\text{U}/^{238}\text{U})$  in the Var basin, and the associated sediment residence time, show first a variation between Holocene (long sediment residence time; low  $(^{234}\text{U}/^{238}\text{U})$ ) and the last Glacial maximum (rapid sediment residence time;  $(^{234}\text{U}/^{238}\text{U})$  close to 1). This long-term variation can be explained by the presence of LGM glaciers in the Alps that promote erosion, enhancing the sediment transfer to the deposition zone. A second scale variation is identified in  $(^{234}\text{U}/^{238}\text{U})$  during the last glacial period, with  $(^{234}\text{U}/^{238}\text{U})$  and therefore sediment residence time variation following the Bond cycle. This  $(^{234}\text{U}/^{238}\text{U})$  variation cannot be fully explained by glaciers because of their absence in the Var catchment during the MIS 3. On the other hand, a comparison between  $(^{234}\text{U}/^{238}\text{U})$  and the percentage of pollen from temperate forest (Laggaccione, Italia) suggests that the increase of temperate forest in the region during the warmer event (GI) promote the soil stabilization. Hence it increases the sediment residence time. In the major GI events, soil stabilization is such that there is no more turbidites and the highest sediment residence time. Thus, this observed cyclicality following short-term climatic variation is an indicator that land-sea signals can be transmitted and preserved in turbiditic deposits.

In the future, rainfall is expected to be high but erratic with heavy flooding due to global warming. According to our data, this is not necessarily synonymous of high denudation rates and seaward sediment transfer as commonly accepted (e.g. Kober et al. 2007). Indeed, the dense vegetation cover under wet climate conditions could counterbalance the erosive effect of rainfall events as evidenced by the residence times of paleo-sediments. Despite improvements in land cover during the last decades in the Var basin, urbanisation still greatly impacts the landscape. Human control of the landscape affect greatly soils, which are in consequence generally less prone to adsorb the precipitation water, creating river floods. This situation could deteriorate in light of the increase in extreme rainfall in the French Mediterranean (Ribes et al. 2019), which is already visible with the autumn floods of this year (e.g. Alex tempete - 3 October 2020).



# CONCLUSIONS AND PERSPECTIVES

---

## Rationale and objectives of this thesis

The interaction between tectonics, climate and weathering are known to control the evolution of landscape morphology over geological timescales. Tectonic processes result in mountain building, which in turn promotes erosion, weathering and soil formation. Soils are eroded at different rates depending on the efficiency of sediment routing systems, resulting in the transfer of sediments to depositional areas. Those systems where soil denudation is greater than soil production are called *weathering-limited*, while those characterized higher soil production relative to sediment export are referred to as *transport-limited*.

In source-to-sink systems, the variation of one or multiple controlling factors such as e.g. climate, weathering, tectonic, or morphology, induces an environmental signal (i.e. disturbance) in the sediment cycle, from production to deposition. This disturbance can be abrupt (i.e. earthquake) or occurring over long timescale (i.e. glacial - interglacial cyclicity). The system then needs to adapt and evolves towards a new equilibrium that creates a change in the sedimentary cycle (e.g. nature of sediments; sediment production, etc.). These variations can propagate into the sediment routing system as an environmental signal, which can be stored and preserved in the depositional zone. In the case where the sediment as well as the environmental signals are rapidly transported from source to sink (i.e. without temporary storage along the path), the system is referred to as *reactive*.

However, major limitations in the transmission of these environmental signals exist. For instance, the storage of sediments in floodplains can buffer or attenuate any change in sedimentary fluxes. Such limitations can result in discrepancies between any given environmental change and its recording in the sedimentary depositional zone. As a result, the extent to which environmental signals are buffered or transferred downstream river systems and be efficiently preserved in the sedimentary record remains a matter of debate. The sediment residence time, as the time elapsed between the generation of the sediment grains in the source areas and the time of deposition in the sedimentary record, is a measure that provide useful information about environmental signals in watersheds and their propagation through time.

Over the last decades, the uranium series have been used to estimate sediment residence time through the so-called comminution age method. Previous work highlighted the great potential of this approach by demonstrating strong correlations between sediment residence time and long-term climate changes. Nevertheless, the interpretation of sediment

residence time is currently limited by the lack of information on the spatial distribution of sedimentary ( $^{234}\text{U}/^{238}\text{U}$ ) in catchments, and on the extent to which the preferential  $^{234}\text{U}$  loss may be affected by factors such as the lithology, the morphology of the catchment, etc.

In this study, we aimed at improving our understanding on  $^{234}\text{U}$ - $^{238}\text{U}$  fractionation in river sediments. To this purpose, we first investigated the large-scale spatial distribution of sedimentary ( $^{234}\text{U}/^{238}\text{U}$ ) ratios at the Earth's surface, through the analysis of various sediment samples from many rivers worldwide (Chapter 3). In a second part, we then focused on the detailed spatial distribution of  $^{234}\text{U}$ - $^{238}\text{U}$  fractionation inside a small mountainous catchment, to refine our understanding of the use of ( $^{234}\text{U}/^{238}\text{U}$ ) to quantify erosion and transfer processes (Chapter 4). This latter part was followed by the application of U isotopes to nearby marine sedimentary records, in order to infer how erosion and transfer times may have changed in the past due to climate change (Chapter 5). Our main results are synthesized here after.

## The variation of U-fractionation

The first part of this thesis focused on studying the spatial distribution of ( $^{234}\text{U}/^{238}\text{U}$ ) in world river sediments to assess the main parameters (e.g. grain size, lithology, climate, weathering, catchment size) controlling U isotope fractionation in watersheds. For this purpose, a series of 64 modern sediment samples from various rivers was analyzed. The same sediments had been previously analyzed for other geochemical tracers (Bayon et al. 2015, 2016, 2018, 2020, Bindeman et al. 2019), demonstrating interesting relationships between weathering proxies and various external parameters (e.g. climate, lithology, weathering regime). The new U isotope data acquired during the course of this PhD thesis represents the first large scale investigation of ( $^{234}\text{U}/^{238}\text{U}$ ) in world river sediments. This work, presented in detail in Chapter 3, has been published in *Geochimica et Cosmochimica Acta* in September 2020.

The measurement of ( $^{234}\text{U}/^{238}\text{U}$ ) in two separate size fractions (clay:  $<4\ \mu\text{m}$  and silt:  $4-63\ \mu\text{m}$ ) revealed an interesting size-dependent U isotopic fractionation, showing that the clay size fractions derived from small crystalline basins commonly exhibited ( $^{234}\text{U}/^{238}\text{U}$ )  $>1$ . This finding was not expected as analyzes were conducted on the detrital part of the grains (i.e. the non-detrital part has been previously leached), which is supposed to be under the secular equilibrium. Because our leaching protocol ensures a quantitative removal of all non-detrital components (carbonates, iron oxides, organic compounds), we are confident that these results truly reflect the particular U isotopic composition of clay minerals in many crystalline catchments, highlighting the importance of yet unidentified secondary processes that result in the preferential gain of  $^{234}\text{U}$  in secondary weathering

products.

The comparison of measured sedimentary ( $^{234}\text{U}/^{238}\text{U}$ ) in river sediments with environmental parameters (e.g. lithology, weathering, morphology) did not highlight a strong control on the fractionation of  $^{234}\text{U}$  over  $^{238}\text{U}$  of any of these factors. However, I showed that ( $^{234}\text{U}/^{238}\text{U}$ ) displayed an inverse relationship with the size of the catchment area, pointing towards an increase in the sediment residence time associated with decreasing  $^{234}\text{U}/^{238}\text{U}$  ratios in river sediments, as the storage capacity along the sediment routing system increases.

A multi-analysis approach including all the parameters investigated in the global survey of U isotopes indicates that the observed ( $^{234}\text{U}/^{238}\text{U}$ ) variability in river sediments can be accounted for at about 70-80% by environmental factors (i.e climatic, weathering, depth to bedrock, catchment size and maximum elevation and lithology). Note however that the obtained p-values were not statistically significant, suggesting that this finding, despite its importance, should be treated with caution. Nevertheless, it shows two interesting points: 1. the fractionation of ( $^{234}\text{U}/^{238}\text{U}$ ) at the Earth surface is dependent of a multiple of factors (e.g. soil thickness, precipitation, lithology, *etc.*), reflecting the complexity of sedimentary systems and the intercorrelation of many influential parameters; 2. the higher degree of correlation observed between ( $^{234}\text{U}/^{238}\text{U}$ ) in clay size fractions with the environmental factors implies that this size fraction might be more prone to adequately reflect environmental changes, compared to silt-size fractions. Overall, the large scale survey of ( $^{234}\text{U}/^{238}\text{U}$ ) in world river sediments emphasizes the great potential of U isotopes for investigating the influence of environmental signals on Earth surface processes.

## **Spatial variation of the sediment residence time in a mountainous river basin**

A regional investigation of the spatial variability of sediment residence times within a reactive sediment routing system was conducted in the Var River basin, a small mountainous catchments in the French Southern Alps. For this purpose, ( $^{234}\text{U}/^{238}\text{U}$ ) was measured in a series of river sediment samples collected along the Var River and its tributaries. A publication is currently under preparation, which should be submitted to Earth and Planetary Science Letters before the end of 2020.

As shown in Chapter 4, the observed variability of ( $^{234}\text{U}/^{238}\text{U}$ ) across the Var basin reflects differences in the weathering regime in different parts of the watershed. We show that in those sub-catchment areas dominated by kinetically-limited weathering regime

(e.g. Tinée and Vésubie sub-catchment), characteristic of the high topographic regions of the basin, soils do not develop, limiting the time required for ( $^{234}\text{U}/^{238}\text{U}$ ) to fractionate. As a result, the estimated sediment residence times in these areas are low (generally  $<200$  ka). In contrast, in those low elevation regions of the basin (e.g. Var and Esteron sub-catchment), characterized by transport-limited weathering conditions, the weathering profile is more developed, leading to an increase in the sediment residence time ( $>300$  ka).

In order to validate these findings based on U isotopes, we used a second approach to infer regolith residence times. This approach makes use of existing data on the spatial distribution of soil thickness, combined with  $^{10}\text{Be}$  denudation rates. We show that a good correlation exists between the sediment residence times inferred from U isotopes and those using the approach described above. This finding underlines the fact that the residence times estimated with U isotopes mostly reflect the time spent in the soil, namely regolith residence time, at least in reactive sediment routing systems.

Finally, we pointed out the influence of the morphology on the regolith residence time in the Var basin, demonstrating lower regolith residence time in high elevation regions than in flatter areas. We also showed that a direct correlation exists between the slope, and to a less extent the curvature, and the regolith residence time inferred with U isotopes, hence supporting the idea that obtained regolith residence times could be used as a proxy for morphology in addition to tracing weathering.

## **Linking paleo-sediment residence time to paleo-erosional processes**

On the basis of the results of the spatial analysis of sedimentary residence times across the Var River basin (Chapter 4), we moved to the deep-sea depositional area of the same Var routing system, focusing on long sediment cores with the aim to reconstruct the evolution of past sediment residence time. A publication is currently in preparation with the aim to submit in the near future.

A great variability of ( $^{234}\text{U}/^{238}\text{U}$ ) and corresponding sediment residence time is observed over the studied time interval. Sediment residence time ranges from 38.2 to 135.4 kyr. To understand the variability of sediment residence time based on U isotopes, we compared the obtained results with the climatic variation. The variation of ( $^{234}\text{U}/^{238}\text{U}$ ) over the last 75ka first indicated an evolution at glacial-interglacial timescale, i.e. between the Last Glacial Period (that ended ca. 11,700 years ago) and the Holocene. We show that during the Last Glacial Period and the Last Glacial Maximum (ca. 26-29 ka) in particular,

sediment residence time were significantly lower ( $(^{234}\text{U}/^{238}\text{U})$  closer to 1) than during the Holocene ( $(^{234}\text{U}/^{238}\text{U}) < 1$ ).

Superimposed to the glacial-interglacial variability of sediment residence time; the detailed study of  $(^{234}\text{U}/^{238}\text{U})$  variations revealed a ‘cyclicality’ that follows the millennial-scale glacial climate variability (well-expressed in the Marine Isotope Stage 3, ca. 57-29 ka). Indeed, during the warm but wet climatic phases, i.e. the major Greenland Interstadials of the last glacial: (GI-8,12,14,15,17 and 19), our results reveal that the sediment residence time was particularly long ( $(^{234}\text{U}/^{238}\text{U}) < 1$ ), reaching values close to those found for the Holocene. Conversely during the cold and dry Heinrich stadials, the sediment residence time significantly decreased to LGM values, i.e.  $(^{234}\text{U}/^{238}\text{U})$  close to 1. These results document for the first time the variability of sediment residence time over the millennial-scale climatic variability (well-expressed in the Marine Isotope Stage 3, ca. 57-29 ka), and especially the so-called Bond cyclicality.

The observed differences in the degree of U isotopic fractionation that accompanies the alternation of short-lived cold and warm events mostly likely reflect differences in the erosional regime, notably induced by the presence of glaciers in the southern Alps during the last glacial period, which are known to act as highly efficient erosive agents. Enhanced erosive processes during these periods most likely limited soil development, thus sediments were exported down to the system more rapidly. In comparison with the sediment residence time variability observed at the glacial-interglacial timescale, the short-term glacial cyclicality cannot be explained by glacial-induced erosion alone. Indeed, it has been shown recently that  $^{10}\text{Be}$  derived denudation rates were stable throughout the Marine Isotopic Stage 3 (Mariotti et al. 2021). Furthermore, the extent of glacier coverage was reduced in the Var basin at that time (Mariotti et al. 2021).

On this basis, we investigated the potential control of the vegetation cover on the sediment residence time by comparing our U isotope data to nearby high-resolution palynological records from the Italian Alps that cover the same period of time. This comparison showed that the sediment residence time derived from U isotopes varied in pair with the variation of pollen percentage. During the warm / wet interstadials (e.g. GI-8,12,14,16-17), pollen data suggest that temperate forests were at their maximal extension in the northern Italy region. Widespread forest cover at these times coincided with periods characterized by long sediment residence time. This relationship can be explained by the effect of the vegetation on the stabilization of soils, increasing the time spent by the sediment within the soil profile. As a result, sedimentary fluxes decreased drastically during these short-lived warm events, in agreement with evidence for the absence of turbidites deposited in the Var Sedimentary Ridge during these same periods. Conversely, during the cold and dry periods, the temperate forest cover decreased, with opposite effect on soil stabilization. As a consequence, the sediment was more easily exported out of the catchment, resulting

in lower sediment residence times.

This investigation, in addition to demonstrating for the first time a short-term variability in residence times and thus climate-related erosion processes, underlines the importance of vegetation cover. It points out the complexity of the sediment routing-system with multiple interactions between parameters such as weathering, climate, and vegetation. This also underlines the natural regulation of Earth surface processes: with the increase in rainfall during the same periods, intense erosion could have been expected. However, the situation was opposite, because the vegetation cover that developed during these warm millennial events acted as a shield protecting soils from the erosion due to intense rainfall episodes. In the near future, higher precipitation levels are expected in the Mediterranean basin (Polade et al., 2017), most likely resulting in an intensification of the frequency of these so-called "Mediterranean episodes", which correspond to episodes of heavy rainfall (e.g. the Storm Alex, which hit south-eastern France in October 2020). This could have important consequences if vegetation does not have time to adapt to these climatic changes.

Overall, the work carried out during this thesis has above all highlighted the utility of using an interdisciplinary approach in the study of sedimentary systems.

## Perspectives

The results obtained in this thesis further demonstrate the value of U isotopes for source-to-sink studies. They also re-emphasize the benefits of studying sediment transfer times and provide many perspectives for future studies. These perspectives can be separated in two groups: one of them is to pursue the development of the method aiming at quantifying sediment residence times; the second group is to go further in the application of the sediment residence time.

### Perspectives to improve the estimation of sediment residence time

The work carried out on modern river sediments has brought unexpected findings, including the observation of  $(^{234}\text{U}/^{238}\text{U}) > 1$  in a number of clay-size fractions derived from crystalline basins. In theory, such high U activity ratios above secular equilibrium should not be found in sediments, considering the particular behavior of U isotopes during Earth surface processes. While these results questioned the reliability of our leaching protocol, the few experimental tests carried out did not point out any particular deficiencies in this respect. Furthermore, the  $^{234}\text{U}/^{238}\text{U}$  values falling above secular equilibrium in the two studies focusing on modern sediments (Chapters 3 & 4) shared similarities: in both cases, the high  $(^{234}\text{U}/^{238}\text{U})$  values were generally encountered in small river basins draining crys-

talline rocks. As such, it would be interesting to further investigate what may result in the preferential  $^{234}\text{U}$  incorporation in clays formed in these environments. For this purpose, a large scale ( $^{234}\text{U}/^{238}\text{U}$ ) survey of unweathered pristine bedrocks, including a great diversity of lithology, could be conducted. It would be interesting to focus particularly on crystalline basements as our results shows that the preferential  $^{234}\text{U}$  gain occurs in clay fractions derived from old crystalline basins. The method protocol could then be adapted to this enrichment in  $^{234}\text{U}$  to infer more precise sediment residence time.

In this thesis, we compared the sediment residence time (calculated with uranium isotopes) with an alternative method to estimate regolith residence time based on the soil thickness and the denudation rate. Both approaches yield similar residence times. As soil thickness can be difficult to estimate correctly, it could be interesting to develop a model combining U isotopes and denudation rates (as inferred from  $^{10}\text{Be}$  isotope for example) to infer soil thickness variation between sub-catchment. This approach could be conducted in small monolithological basins, characterized by distinctive weathering regimes, such as the Tinée (weathering-limited) and the Esteron (transport-limited) sub-catchments of the Var basin, for which ( $^{234}\text{U}/^{238}\text{U}$ ) could be measured in bedrocks, soils and sediments.

### **Perspectives to go further in the application of sediment residence time studies**

Our investigation of paleo sediment residence times revealed the presumed importance of the vegetation on the soil thickness and therefore on weathering processes. One interesting future perspective would be to investigate whether similar short-term co-cyclicity also occurred in other small mountainous glaciated catchments during the Last Glacial Period, elsewhere in the Mediterranean region (e.g. Corsica) or in other regions characterized by high denudation rates (e.g. New Zealand).

The anthropisation of the Earth's surface induced a non-natural vegetation cover evolution and deforestation. In order to quantify the impact of human activity on weathering processes, an interesting approach would be to study the recent to modern evolution of the Var basin, which is a small and anthropized sediment routing system. With a precise and very fine sampling strategy focusing on Late Holocene deposits it could revealed and quantified the human impact on the sedimentary cycle. For this purpose, sediments cores obtained during the ENVAR-1-6 campaigns and already described in detailed by Mas et al. (2010) could be studied. The quantification of the anthropic influence could be revealed with sediment residence time based on U isotopes, in comparison with sediment residence time variation obtained for the last 75 ka, i.e. before the anthropisation of the basin.

Finally, in the light of the extreme rainfall event that recently hit south-eastern France (and in particular the Var River basin), a collaborative investigation led by P-H Blard and

co-workers has been set up to sample suspended river particulates on a regular weekly-to-monthly basis in order to assess the short-term response of denudation rates. One exciting perspective would be to take advantage of this forthcoming project to investigate the impact of such extreme rainfall event on measured sedimentary ( $^{234}\text{U}/^{238}\text{U}$ ) ratios. Such a study would allow us to test the efficiency of U isotopes for monitoring short-term environmental changes. Should these results be promising, the use of U isotopes combined with provenance information inferred from Nd isotopes could provide in future studies an unique means for detecting shifts in erosional patterns following extreme climate events.

# CONCLUSIONS ET PERSPECTIVES

---

## Rappel des objectifs de la thèse

Il est connu que l'interaction entre les processus tectoniques, climatiques et d'altération contrôle l'évolution de la morphologie du paysage sur des échelles de temps géologiques. L'activité tectonique favorise la formation de reliefs, qui eux même intensifient les mécanismes d'érosion. Les systèmes sédimentaires où le taux de dénudation sont plus important que le taux de production de sol sont dits *limités par l'altération*. Au contraire ceux qui sont caractérisés par une production de sol plus élevée que le taux de dénudations sont dits *limités par le transport*.

Dans les systèmes sédimentaires, la variation d'un ou de plusieurs facteurs environnementaux tels que le climat, la météorologie, la tectonique ou la morphologie, induit un signal environnemental (c'est-à-dire une perturbation) dans le cycle des sédiments, de la production au dépôt. Cette perturbation peut être instantanée (par exemple un tremblement de terre) ou se produire sur une longue période (par exemple la cyclicité glaciaire - interglaciaire). Le système doit alors s'adapter et évoluer vers un nouvel équilibre qui induit un changement dans le cycle sédimentaire (par exemple, la nature des sédiments ; la production de sédiments, etc.). Ces variations peuvent se propager dans le système sédimentaire sous la forme d'un signal environnemental. Il peut alors être stocké et préservé dans la zone de dépôt. Dans le cas où les sédiments et ainsi les signaux environnementaux sont rapidement transportés de la source au puits (c'est-à-dire sans stockage temporaire le long du chemin), le système est dit *réactif*. Toutefois, l'étude de ces signaux environnementaux présente des limites importantes. Par exemple, le stockage temporaire de sédiments dans le système peut atténuer ou faire disparaître tout changement de production sédimentaires. Ces stockages peuvent induire des écarts temporels entre la création du signal environnemental donné et son enregistrement dans la zone de dépôt sédimentaire finale . Ainsi le signal peut être accentué, tamponné ou bien tout simplement effacé des archives sédimentaires. Leur bonne conservation et interprétation restent par conséquent sujet à débat. Le temps de résidence sédimentaire, c'est-à-dire le temps écoulé entre la formation du sédiment dans la zone d'altération et le moment du dépôt final, est une information utile dans l'analyse des signaux environnementaux.

Au cours des dernières décennies, les séries isotopiques de l'uranium ont été utilisées pour estimer le temps résidence sédimentaire par la méthode dite de l'âge de comminution. Des travaux antérieurs ont mis en évidence le potentiel de cette approche en présentant de

fortes corrélations entre le temps de résidence sédimentaire et les variations climatiques à long terme. Néanmoins, l'interprétation des variations de temps de résidence sédimentaire est actuellement limitée par le manque d'informations les variations des rapports ( $^{234}\text{U}/^{238}\text{U}$ ) dans les sédiments ainsi que sur l'influence des facteurs tels que la lithologie, la morphologie du bassin versant, *etc.* dans le fractionnement isotopique de l'uranium.

L'objectif de cette thèse est dans un premier temps d'étudier les variations du rapport ( $^{234}\text{U}/^{238}\text{U}$ ) dans les sédiments à la surface de la Terre. Pour cela des sédiments provenant de nombreux cours d'eau du monde entier (chapitre 3) sont analysés. Ensuite, l'intérêt s'est porté sur la distribution spatiale du fractionnement  $^{234}\text{U}$ - $^{238}\text{U}$  à l'intérieur d'un petit bassin versant montagneux. L'objectif est d'affiner notre compréhension de l'utilisation de ( $^{234}\text{U}/^{238}\text{U}$ ) pour quantifier les processus d'érosion et de transfert (chapitre 4). Cette dernière partie est suivie par l'application de cette méthode aux enregistrements sédimentaires marins. Le but est d'étudier l'évolution passée des processus d'érosion et des temps de transfert en fonction des variations climatiques (chapitre 5). Les principaux résultats obtenus durant cette thèse sont synthétisés ci-après.

## La distribution spatiale de ( $^{234}\text{U}/^{238}\text{U}$ )

La première partie de cette thèse porte sur l'étude de la répartition spatiale des rapports ( $^{234}\text{U}/^{238}\text{U}$ ) dans les sédiments fluviaux mondiaux. L'objectif est d'évaluer les principaux paramètres (par exemple, la taille des grains, la lithologie, le climat, l'altération, la taille des bassins versants) qui contrôlent le fractionnement des isotopes U dans les bassins versants. Dans ce contexte, une série de 64 échantillons de sédiments modernes provenant de diverses rivières a été analysée. Ces mêmes sédiments ont été précédemment étudiés avec d'autres traceurs géochimiques (Bayon et al. 2015, 2016, 2018, 2020, Bindeman et al. 2019). Ces travaux antérieurs ont permis de démontrer des relations intéressantes entre l'altération et divers paramètres externes (par exemple le climat, la lithologie, les régimes d'altération). Les nouvelles données isotopiques en uranium (U) acquises au cours de cette thèse représentent la première étude à grande échelle sur le rapport ( $^{234}\text{U}/^{238}\text{U}$ ) dans des sédiments fluviaux mondiaux. Les résultats, présentés en détail dans le chapitre 3, ont été publiés dans *Geochimica et Cosmochimica Acta* en septembre 2020.

La mesure de ( $^{234}\text{U}/^{238}\text{U}$ ) dans deux fractions de tailles distinctes (argile:  $<4 \mu\text{m}$  et silt:  $4\text{-}63 \mu\text{m}$ ) a montré un lien entre la fraction granulométrique et ( $^{234}\text{U}/^{238}\text{U}$ ). En effet, les fractions argileuses provenant de petits bassins cristallins présentent couramment des rapports ( $^{234}\text{U}/^{238}\text{U}$ )  $>1$ . Cette découverte est inattendue du fait que les mesures ont été effectuées dans la partie détritique des grains (i.e. la partie non détritique ayant été préalablement lessivée). Cette fraction est supposée être inférieure à l'équilibre séculaire

compte tenue des propriétés de la série isotopique de l'uranium. Comme le protocole de lessivage appliqué assure l'élimination de tous les composants non détritiques (carbonates, oxydes de fer, matière organique), ces résultats reflètent la composition isotopique en uranium distinctive des minéraux argileux dans de nombreux bassins versants cristallins. Cela souligne l'importance de processus d'altération pas encore identifiés qui permettraient un gain préférentiel de  $^{234}\text{U}$  dans les fractions argileuses.

La comparaison des mesures ( $^{234}\text{U}/^{238}\text{U}$ ) dans les sédiments fluviaux en fonction des paramètres environnementaux (par exemple la lithologie, l'altération, la morphologie) a mis en évidence l'absence de contrôle unique de l'un de ces facteurs sur le fractionnement  $^{234}\text{U}$ - $^{238}\text{U}$ . Toutefois, il a été montré que le rapport ( $^{234}\text{U}/^{238}\text{U}$ ) présentait une relation inverse avec la taille du bassin versant. Cela indique une augmentation du temps de résidence sédimentaire associée à une diminution des rapports ( $^{234}\text{U}/^{238}\text{U}$ ) dans les sédiments fluviaux, traduisant l'augmentation de la capacité de stockage temporaire en fonction de la taille des bassins versants.

Une approche multi-analyse incluant tous les paramètres étudiés dans l'étude mondiale des isotopes U indique que la variabilité observée ( $^{234}\text{U}/^{238}\text{U}$ ) dans les sédiments fluviaux peut être expliquée à environ 70-80% par des facteurs environnementaux (c'est-à-dire le climat, l'altération, la profondeur du substratum rocheux, la taille du bassin versant et l'altitude maximale et la lithologie). Il convient toutefois de noter que les valeurs-p obtenues ne sont pas statistiquement significatives. Ainsi, malgré son importance, cette constatation doit être traitée avec prudence. Néanmoins, cela montre deux points intéressants : 1. le fractionnement de  $^{234}\text{U}$ - $^{238}\text{U}$  à la surface de la Terre dépend de multiples facteurs (par exemple l'épaisseur du sol, les précipitations, la lithologie, etc.). Cela reflète la complexité des systèmes sédimentaires et l'intercorrélation de nombreux paramètres influents ; 2. les corrélations observées entre le rapport ( $^{234}\text{U}/^{238}\text{U}$ ) et les facteurs environnementaux sont plus élevées dans les fractions argileuses. Cette taille de grains seraient susceptible de refléter avec plus d'exactitude les changements environnementaux, par rapport aux fractions silteuses. Dans l'ensemble, l'étude à grande échelle des rapports ( $^{234}\text{U}/^{238}\text{U}$ ) dans les sédiments fluviaux mondiaux souligne le grand potentiel des isotopes U pour étudier les signaux environnementaux reflétant les processus à la surface de la Terre.

## Variation spatiale du temps de résidence sédimentaire dans un bassin montagneux

Une étude régionale portant sur la variabilité spatiale des temps de résidence sédimentaire dans un système réactifs a été menée dans le bassin du Var. C'est un petit bassin versant montagneux dans les Alpes du Sud françaises. À cette fin, le rapport ( $^{234}\text{U}/^{238}\text{U}$ ) a été mesuré dans une série d'échantillons de sédiments fluviaux prélevés le long du Var et de ses affluents. Une publication est actuellement en cours de préparation, et devrait être soumise à *Earth and Planetary Science Letters* pour la fin de l'année 2020.

Comme reporté dans le chapitre 4, la variabilité observée du rapport ( $^{234}\text{U}/^{238}\text{U}$ ) dans le bassin du Var reflète les différences de régime d'altération dans les différentes parties du bassin versant. Nous montrons que dans les sous-bassins dominés par un régime d'altération dit limité (par exemple le sous-bassin de la Tinée et de la Vésubie), caractéristiques des régions d'altitudes élevées, le rapport ( $^{234}\text{U}/^{238}\text{U}$ ) est élevé. Cela est causé par l'absence ou la quasi-absence de sol dans ses région, ce qui limite le fractionnement du rapport ( $^{234}\text{U}/^{238}\text{U}$ ). En conséquence, les temps de résidence sédimentaire estimés dans ces zones sont faibles (généralement  $<200$  kyr). En revanche, dans les régions de faible altitude (par exemple le sous-bassin du Var et de l'Esteron), où le développement des sols est plus important, le rapport ( $^{234}\text{U}/^{238}\text{U}$ ) est plus faible. Le temps de résidence sédimentaire y est plus élevé ( $>300$  kyr).

Afin de valider ces résultats obtenus par les mesures des isotopes d'uranium, nous avons utilisé une deuxième approche pour déduire les temps de résidence des régolithes. Cette approche novatrice utilise les estimations existantes de la répartition de l'épaisseur du sol, combinées aux taux de dénudation. Nous montrons qu'il existe une corrélation entre les temps de résidence sédimentaire déduits des isotopes d'U et ceux en utilisant l'approche décrite ci-dessus. Cette constatation souligne le fait que le temps de résidence estimés avec les isotopes U reflètent principalement le temps passé dans le sol, à savoir le temps de résidence dans le régolithe, au moins dans les systèmes sédimentaires réactifs.

Enfin, nous avons souligné l'influence de la morphologie du bassin sur le temps de résidence dans le régolithe dans le bassin du Var. Nous présentons des temps de résidence plus courts dans les régions de haute altitude que dans des zones de plaines. Nous avons également montré qu'il existe une corrélation directe entre la pente, et dans une moindre mesure la courbure des pentes, et le temps de résidence déduit avec les isotopes U. Cela suggère que les temps de résidence obtenus pourraient être utilisés comme un substitut pour étudier la morphologie en plus du régime d'altération.

## Lier les temps de résidence aux événements passés

Sur la base des résultats de l'analyse spatiale des temps de résidence sédimentaire dans le bassin du Var (chapitre 4), nous nous sommes intéressés à l'évolution temporelle des temps de résidence. Pour cela, nous avons étudié des sédiments marins issus de carotte sédimentaires prélevées dans le système sédimentaire du Var. Une publication est actuellement en préparation dans le but d'une soumission printemps 2021.

On observe une grande variabilité des rapports ( $^{234}\text{U}/^{238}\text{U}$ ) et ainsi du temps de résidence sédimentaire sur l'intervalle de temps étudié. Le temps de résidence sédimentaire varie entre 38,2 et 135,4 kyr. Dans l'objectif de comprendre la variabilité du temps de résidence sédimentaire déduits par les isotopes U, nous avons comparé les résultats obtenus avec les variations climatiques passées. Les variations de ( $^{234}\text{U}/^{238}\text{U}$ ) sur les derniers 75 ka présentent premièrement une évolution à l'échelle de temps glaciaire-interglaciaire, c'est-à-dire entre la dernière période glaciaire (qui s'est terminée il y a environ 11 700 ans) et l'Holocène. Nous montrons que durant la dernière période glaciaire et en particulier au dernier maximum glaciaire (ca. 26-29 ka), les temps de résidence sédimentaires ont été sensiblement plus faibles ( $^{234}\text{U}/^{238}\text{U}$  plus proche de 1) que pendant l'Holocène ( $^{234}\text{U}/^{238}\text{U} < 1$ ).

Ensuite, une étude plus détaillée des variations ( $^{234}\text{U}/^{238}\text{U}$ ) a révélé une "cyclicité" qui suit la variabilité du climat à l'échelle du millénaire glaciaire (bien exprimée dans MIS (Marine Isotope Stage) 3, à environ 57-29 ka). En effet, pendant les phases climatiques chaudes mais humides, c'est-à-dire les principaux interstades du Groenland durant la dernière période glaciaire : (GI-8,12,14,15,17 et 19), nos résultats révèlent que les temps de résidence sédimentaires ont été particulièrement longs (avec  $^{234}\text{U}/^{238}\text{U} < 1$ ). Les valeurs atteignent des valeurs proches de celles mesurées pour la période Holocène. Inversement, lors des stades de Heinrich, froids et secs, les temps de résidence sédimentaires sont courts. Ces résultats documentent pour la première fois la variabilité du temps de résidence sédimentaire à l'échelle du millénaire et de la variabilité climatique, et surtout la cyclicité dite de Bond.

Les évolutions observées dans le degré de fractionnement entre  $^{234}\text{U}$  et  $^{238}\text{U}$  qui accompagne l'alternance d'événements climatiques froids et chauds de courtes durées reflètent probablement des variations des agents d'érosion. Parmi les agents d'érosion, la présence de glaciers dans les Alpes du Sud pendant la dernière période glaciaire sont connus pour agir comme des agents érosifs très efficaces. Les processus d'érosion durant la dernière période glaciaire ont très probablement limité le développement des sols, les sédiments ont été exportés hors du bassin versant plus rapidement. Contrairement à la variabilité glaciaire-interglaciaire des temps de résidence sédimentaire qui peut être expliquée par

la présence de glacier dans la région, la cyclicité à plus faible échelle ne peut s'expliquer par la seule érosion induite par les glaciers. En effet, il a été démontré récemment que les taux de dénudation dérivés du  $^{10}\text{Be}$  étaient stables dans l'ensemble du MIS 3 (Mariotti et al. 2021), contrairement au temps de résidence sédimentaire. En outre, l'étendue de la couverture glaciaire était réduite dans le bassin du Var à cette époque (Mariotti et al. 2021).

Sur cette base, nous avons étudié le contrôle potentiel de la couverture végétale sur le temps de résidence sédimentaire. Pour cela nous avons comparés les variations des rapports ( $^{234}\text{U}/^{238}\text{U}$ ) aux enregistrements palynologiques à haute résolution des Alpes italiennes qui couvrent la même période. Cette comparaison a montré que les temps de résidence sédimentaire estimés à partir des isotopes de U variaient en concordance avec la variation du pourcentage de pollen des forêts tempérées. Pendant les stades chauds / humides (par exemple GI-8,12,14,16-17), les données polliniques suggèrent que les forêts tempérées étaient à leurs extensions maximales dans la région du nord de l'Italie. La couverture forestière élargie durant ces périodes coïncide avec les périodes caractérisées par un temps de résidence élevé. Cette relation peut s'expliquer par l'effet de la végétation sur la stabilisation des sols, augmentant le temps passé par les sédiments dans le profil d'altération. En conséquence, les flux sédimentaires ont diminué de façon drastique pendant ces événements chauds de courte durée. Cela est en accord avec les absences d'accumulation de turbidites déposées dans le domaine marin du système sédimentaire du Var pendant ces mêmes périodes. À l'inverse, pendant les périodes froides et sèches, la couverture forestière tempérée a diminué, avec un effet inverse sur la stabilisation des sols. En conséquence, les sédiments ont été plus facilement exportés hors du bassin versant, ce qui a entraîné une réduction des temps de résidence sédimentaire.

Cette étude, en plus de démontrer pour la première fois une variabilité à court terme des temps de résidence sédimentaire et donc les processus d'érosion liés au climat, souligne l'importance de la couverture végétale. Cela illustre la complexité du système sédimentaire avec de multiples interactions entre des paramètres tels que l'altération, le climat et la végétation. Les résultats montrent également la régulation naturelle des processus à la surface de la Terre. Durant les périodes d'intenses précipitations, des phénomènes d'érosion accrues seraient attendus. Hors l'inverse est montré avec le développement de la couverture végétale pendant ces événements millénaires qui a agi en protecteur des sols face à l'érosion. Dans un avenir proche, des niveaux de précipitations plus élevés sont attendus dans le bassin méditerranéen (Polade et al., 2017). Cela se traduira très probablement par une intensification de la fréquence de ces "épisodes méditerranéens", qui correspondent à des épisodes de fortes précipitations (par exemple la tempête Alex, qui a frappé le sud-est de la France en octobre 2020). Cela pourrait engendrer des conséquences importantes si la végétation n'a pas le temps de s'adapter à ces changements.

Dans l'ensemble, les travaux réalisés au cours de cette thèse ont aussi mis en évidence l'utilité d'approches interdisciplinaires dans l'étude des systèmes sédimentaires.

## Perspectives

Les résultats obtenus dans le cadre de cette thèse démontrent encore une fois l'intérêt des isotopes de l'U pour les études des systèmes sédimentaires. Ils soulignent également à nouveau les avantages de l'étude des temps de transfert des sédiments et offrent de nombreuses perspectives pour les études futures. Ces perspectives peuvent être séparées en deux groupes : l'un d'eux est de poursuivre le développement de la méthode visant à quantifier les temps de résidence sédimentaire ; le second groupe est d'aller plus loin dans l'application de cette méthode.

### **Perspectives pour améliorer l'estimation du temps de résidence sédimentaire**

Les travaux effectués sur les sédiments fluviaux modernes ont permis de faire des découvertes inattendues, notamment l'observation de  $(^{234}\text{U}/^{238}\text{U}) > 1$  dans un certain nombre de fractions argileuses provenant de bassins cristallins. En théorie, des rapports d'activité en uranium aussi élevés ( $> 1$ ) ne devraient pas être découverts dans les parties détritiques des sédiments. Bien que ces résultats puissent remettre en question la fiabilité de notre protocole de lessivage, les quelques tests expérimentaux réalisés n'ont pas mis en évidence de lacunes particulières à cet égard. En outre, les valeurs de  $(^{234}\text{U}/^{238}\text{U})$  dépassant l'équilibre séculaire dans les deux études portant sur les sédiments modernes (chapitres 3 et 4) présentaient des similitudes. Dans les deux cas, les valeurs élevées  $(^{234}\text{U}/^{238}\text{U})$  étaient généralement rencontrées dans de petits bassins fluviaux drainant des roches cristallines. Il serait donc intéressant d'étudier plus en détail ce qui peut résulter de l'incorporation préférentielle de  $^{234}\text{U}$  dans les argiles formées dans ces environnements. À cette fin, une étude à grande échelle  $(^{234}\text{U}/^{238}\text{U})$  des roches vierges non altérées, y compris une grande diversité de la lithologie, pourrait être menée. L'objectif serait de se concentrer en particulier sur des sous-sols cristallins, car nos résultats montrent que le gain préférentiel de  $^{234}\text{U}$  se produit dans les parties argileuses dérivées d'anciens bassins cristallins. Le protocole de la méthode pourrait alors être adapté à cet enrichissement en  $^{234}\text{U}$  pour en déduire des temps de résidences sédimentaires plus précis.

Dans cette thèse, nous avons comparé les temps de résidence sédimentaires avec des temps de résidence dans le régolithe. Ceux-ci ont été déterminés par une approche utilisant l'épaisseur du sol et le taux de dénudation. Les deux approches donnent une concordance des durées obtenues. Comme l'épaisseur des sols peut être difficile à estimer correctement, il pourrait être intéressant de développer un modèle en combinant les isotopes d'uranium

et les taux de pour déduire la variation de l'épaisseur du sol entre les sous-bassins versants. Cette approche pourrait être menée dans de petits bassins mono-lithologiques, caractérisés par des régimes d'altération particuliers. Ainsi les sous-bassins de la Tinée (dont le régime est dit limité par l'altération) et de l'Esteron (dont le régime est dit limité par le transport) dans le bassin du Var, pour lequel ( $^{234}\text{U}/^{238}\text{U}$ ) pourrait être mesuré dans les roches, les sols et les sédiments seraient de bons exemples.

### **Perspectives pour aller plus loin dans l'application de la méthode d'estimation des temps de résidence sédimentaire**

Notre enquête sur les paléo-variations des temps de résidence sédimentaire a révélé l'importance présumée de la végétation sur l'épaisseur du sol et donc sur les processus d'altération. Une perspective future intéressante serait d'étudier si une co-cyclicité à court terme similaire s'est également produite dans d'autres petits bassins glaciaires montagneux pendant la dernière période glaciaire, ailleurs dans la région méditerranéenne (par exemple en Corse) ou dans d'autres régions caractérisées par un taux de dénudation élevé (par exemple en Nouvelle-Zélande).

L'anthropisation de la surface de la Terre a induit une évolution du couvert végétal non naturel et la déforestation. Afin de quantifier l'impact de l'activité humaine sur l'altération climatique une approche intéressante consisterait à étudier l'évolution récente à moderne dans le bassin du Var, qui est un petit système sédimentaire anthropisé. Avec une stratégie d'échantillonnage très fine et axée sur les dépôts de l'Holocène tardif, cela pourrait révéler et quantifier l'impact anthropique sur le cycle sédimentaire. À cette fin, des carottes de sédiments obtenus lors des campagnes ENVAR-1-6 et déjà décrits en détail par Mas et al. (2010) pourraient être étudiés. La quantification de l'influence anthropique pourrait être révélée avec un temps de séjour dans les sédiments basé sur les isotopes U, en comparaison avec la résidence dans les sédiments variation temporelle obtenue pour les 75 derniers ka, c'est-à-dire avant l'anthropisation du bassin.

Enfin, au regard des événements extrêmes qui ont récemment frappés le sud-est de la France (et en particulier le bassin du Var), une étude est menée par P-H Blard et ses collaborateurs. Ils échantillonnent les sédiments de rivières sur une base régulière, de semaines en mois, afin d'évaluer la réponse à court terme des taux de dénudation face à ces événements climatiques. Un apport intéressant serait de mesurer les variations du rapport d'activité de l'uranium dans ces mêmes sédiments pour déterminer l'impact à très court terme de ces précipitations sur les temps de transfert mesurés. Une telle étude nous permettrait de tester l'efficacité des isotopes U pour l'évolution des changements environnementaux à court terme. Si ces résultats sont prometteurs, l'utilisation des isotopes U combinés avec les informations sur la provenance déduites des isotopes Nd pourrait fournir dans de futures études un moyen unique de détecter les changements dans les schémas d'érosion à la suite d'événements climatiques extrêmes.

# APPENDIX

Table A2.1 – Location of sediments from world rivers

River	Country	Latitude	Longitude	Sampling Environment
Adour	France	43.49	-1.47	River
Amazon	Brazil	3.10	-49.50	Sub Delta
Betsiboka	Madagascar	-15.52	45.72	River
Blackwater	Ireland	54.51	-6.58	River
Brantas	Indonesia	-7.44	112.46	River
Chao Phraya	Thailand	13.57	100.58	Delta
Churchill	Canada	58.97	-94.10	River
Clarence	Australia	-29.43	153.25	River
Danube	Romania	45.06	29.62	River
Don	Russia	47.29	39.10	River
Dordogne	France	45.03	-0.59	River
Elbe	Germany	53.54	9.81	River
Elorn	France	48.40	-4.38	Estuary
Fitzroy river	Australia	-17.73	123.64	River
Fly	PNG	-8.67	144.00	Sub Delta
Fortescue river	Australia	-21.29	116.14	River
Foyle	Ireland	54.76	-7.45	River
Fraser	Canada	49.16	-123.37	Sub Delta
Ganges	Bangladesh	23.17	90.47	River
Gascogne	Australia	-29.83	113.77	River
Glenariff	Ireland	55.02	-6.11	River
Jamata	Nigeria	6.13	6.76	Estuary
Kymijoki	Finland	60.46	26.91	Estuary
Lee	Ireland	51.88	-8.27	River
Loire	France	47.28	-1.90	River
Lough Erne	Ireland	54.30	-7.64	River
Lower Bann	Ireland	54.86	-6.48	River

*continued on next page*

*continued from previous page*

<b>River</b>	<b>Country</b>	<b>Latitude</b>	<b>Longitude</b>	<b>Sampling Environment</b>
Lule	Norway	65.68	21.82	River
MacKenzie	Canada	69.26	-137.29	Sub Delta
Mae Klong	Thailand	13.43	99.95	River
Maine	Ireland	54.75	-6.32	River
Mayenne	France	47.50	-0.55	River
Mekong	Cambodia	10.96	105.06	Delta
Mississippi	USA	28.93	-89.49	Sub Delta
Moyola	Ireland	54.75	-6.52	River
Murchison	Australia	-27.83	114.69	River
Nalon	Spain	43.56	-6.07	River
Narva	Estonia	59.54	27.58	Estuary
Nelson river	Canada	57.39	-91.80	River
Niger	Nigeria	3.20	6.68	Sub Delta
Nile	Egypt	32.51	30.38	Margin
Northern Dvina	Russia	65.09	39.00	Estuary
Orinoco	Venezuela	7.65	-66.18	River
Pamisos	Greece	37.02	22.02	River
Red River	Vietnam	20.26	106.52	Delta
Rhine	Netherlands	51.91	4.48	Estuary
Rio Aro	Venezuela	7.39	-64.01	River
Rio Caroni	Venezuela	8.33	-62.71	River
Rio Caura	Venezuela	7.58	-64.94	River
Ropotamo	Bulgaria	42.32	27.75	River
Sefid Rud	Iran	37.47	49.94	River
Sepik river	PNG	-3.13	142.78	River
Severn	UK	51.49	-2.78	River
Shannon	Eire	52.69	-8.91	Estuary
Six Mile	Ireland	54.70	-6.15	River
Spercheios	Ireland	54.93	-7.81	River
Swilly	Ireland	54.93	-7.81	River
Thames	Sweden	63.72	20.27	River
Ume	Sweden	63.72	20.27	Estuary
Upper River Bann	Ireland	54.38	-6.33	River
Vanuatu	Vanuatu	-17.76	168.38	River

*continued on next page*

*continued from previous page*

<b>River</b>	<b>Country</b>	<b>Latitude</b>	<b>Longitude</b>	<b>Sampling Environment</b>
<b>Vistula</b>	Poland	54.65	19.28	Gulf
<b>Yangtze</b>	China	31.62	121.01	Estuary
<b>Yellow River</b>	China	37.80	118.91	Delta

Table A2.2 – Location of sediments from Var River

River	Sample	Latitude	Longitude	Sampling date
Esteron	BV-EST-05	43.8488	6.73097	17/09/2012
Esteron	BV-EST-04	43.85345	6.93178	11/06/2011
Esteron	BV-RIO-01	43.867	6.9502	11/06/2011
Esteron	BV-EST-03	43.87228	7.00653	11/06/2011
Esteron	BV-EST-01	43.82372	7.18433	11/06/2011
Tinee	BV-TIN-05	44.24993	6.9347	19/09/2012
Tinee	BV-TIN-03	44.18457	7.05117	12/06/2011
Tinee	BV-TIN-04	44.18387	7.0537	12/06/2011
Tinee	BV-NEG-01	44.15057	7.23703	15/06/2011
Tinee	BV-MOL-01	44.13028	7.10143	12/06/2011
Tinee	BV-TIN-02b	44.12828	7.09752	12/06/2011
Tinee	BV-TIN-07	44.04542	7.12812	19/09/2012
Var	BV-COU-02	43.9764	6.65273	18/09/2012
Var	BV-VAR-08	44.08825	6.8527	18/09/2012
Var	BV-VAR-03	43.95488	6.896	11/06/2011
Var	BV-CIA-03	44.01085	6.9834	18/09/2012
Var	BV-VAR-04	43.94568	7.01217	11/06/2011
Var	BV-VAR-11	43.88597	7.18953	19/09/2012
Var	BV-VAR-01	43.83663	7.19112	11/06/2011
Var	BV-VAR-15	43.78567	7.21615	21/09/2012
Var	BV-VAR-06	43.66652	7.19698	12/06/2011
Vesubie	BV-VES-03	44.06628	7.256	13/06/2011
Vesubie	BV-VES-02	44.0025	7.31	13/06/2011
Vesubie	BV-GUA-01	44.00157	7.31092	13/06/2011
Vesubie	BV-VES-04	43.97645	7.3151	13/06/2011
Vesubie	BV-VES-01	43.85983	7.1988	12/06/2011

Table A2.3 – Information on sediments from the core ESSK08-CS01

Core	Sample	Size fraction	Depth-top	Depth-bottom	Age (ka)
ESSK08-CS01	CS01_1	clay	350	352	9.8
ESSK08-CS01	CS01_2	silt	352	355	9.8
ESSK08-CS01	CS01_3	silt	803	807	19.7
ESSK08-CS01	CS01_4	clay	948	949	20.9

Table A2.4 – Information on sediments from the core KESC9-14

Core	Sample	Size fraction	Depth-top	Depth-bottom	Age (ka)
KESC9-14	KESC9_1	Undifferentiated	5	6	0.65
KESC9-14	KESC9_2	Undifferentiated	74	75	1.01
KESC9-14	KESC9_3	Undifferentiated	128	129	1.74
KESC9-14	KESC9_4	Undifferentiated	159	160	2.42
KESC9-14	KESC9_5	Undifferentiated	188	189	2.84
KESC9-14	KESC9_6	Undifferentiated	204	205	2.90
KESC9-14	KESC9_7	Undifferentiated	243	244	3.85
KESC9-14	KESC9_9	Undifferentiated	287	288	4.50
KESC9-14	KESC9_10	Undifferentiated	306	307	5.00
KESC9-14	KESC9_11	Undifferentiated	325	326	5.50
KESC9-14	KESC9_12	Undifferentiated	344	345	6.09
KESC9-14	KESC9_13	Undifferentiated	363	364	6.75
KESC9-14	KESC9_14	Undifferentiated	384	385	7.44
KESC9-14	KESC9_15	Undifferentiated	398	399	7.69
KESC9-14	KESC9_16	Undifferentiated	412	413	8.07
KESC9-14	KESC9_17	Undifferentiated	419	420	8.47
KESC9-14	KESC9_19	Undifferentiated	443	444	9.82
KESC9-14	KESC9_20	Undifferentiated	449	450	10.16
KESC9-14	KESC9_21	Undifferentiated	479	480	10.83
KESC9-14	KESC9_22	Undifferentiated	491	492	10.97
KESC9-14	KESC9_23	Undifferentiated	497	498	11.01
KESC9-14	KESC9_24	Undifferentiated	504	505	11.06
KESC9-14	KESC9_25	Undifferentiated	513	514	11.23
KESC9-14	KESC9_26	Undifferentiated	557	558	12.41
KESC9-14	KESC9_27	Undifferentiated	601	602	13.61
KESC9-14	KESC9_28	Undifferentiated	647	648	14.80
KESC9-14	KESC9_29	Undifferentiated	666	667	15.29

Table A2.5 – Information on sediments from the core ESK08-CS13

Core	Sample	Size fraction	Depth-top	Depth-bottom	Age (ka)
ESSK08-CS13	CS13_1	silt	92	93	6.72
ESSK08-CS13	CS13_2	clay	268	269	12.12
ESSK08-CS13	CS13_3	clay	336	338	14.21
ESSK08-CS13	CS13_5	clay	438	440	16.51
ESSK08-CS13	CS13_6	silt	440	442	16.51
ESSK08-CS13	CS13_7	clay	603	605	19.48
ESSK08-CS13	CS13_8	silt	610	615	19.48
ESSK08-CS13	CS13_9	clay	722	723	21.19
ESSK08-CS13	CS13_12	clay	816	818	22.92
ESSK08-CS13	CS13_13	silt	949	951	27.06
ESSK08-CS13	CS13_14	clay	1048	1050	30.85
ESSK08-CS13	CS13_15	silt	1050	1053	30.85
ESSK08-CS13	CS13_114	clay	1074	1075	32.15
ESSK08-CS13	CS13_115	silt	1075	1076	32.15
ESSK08-CS13	CS13_116	clay	1108	1109	32.82
ESSK08-CS13	CS13_117	silt	1109	1110	32.82
ESSK08-CS13	CS13_118	clay	1114	1115	33.06
ESSK08-CS13	CS13_119	silt	1115	1116	33.06
ESSK08-CS13	CS13_120	clay	1118.5	1119	33.26
ESSK08-CS13	CS13_121	silt	1119	1120	33.26
ESSK08-CS13	CS13_123	clay	1123	1124	33.63
ESSK08-CS13	CS13_122	silt	1122	1123	33.63
ESSK08-CS13	CS13_124	clay	1136.5	1137	34.25
ESSK08-CS13	CS13_125	silt	1137	1138	34.25
ESSK08-CS13	CS13_126	clay	1139.5	1140	34.47
ESSK08-CS13	CS13_127	silt	1140	1140.5	34.47
ESSK08-CS13	CS13_128	clay	1164	1164.5	35.39
ESSK08-CS13	CS13_129	silt	1164.5	1165.5	35.39
ESSK08-CS13	CS13_130	clay	1178	1179	36.16
ESSK08-CS13	CS13_131	silt	1179	1180	36.16
ESSK08-CS13	CS13_133	clay	1201	1202	36.97
ESSK08-CS13	CS13_132	silt	1200	1201	36.97
ESSK08-CS13	CS13_135	clay	1208.5	1209.5	37.37
ESSK08-CS13	CS13_134	silt	1207.5	1208.5	37.37

*continued on next page*

*continued from previous page*

<b>Core</b>	<b>Sample</b>	<b>Size fraction</b>	<b>Depth-top</b>	<b>Depth-bottom</b>	<b>Age (ka)</b>
ESSK08-CS13	CS13_136	clay	1215.5	1216.5	37.62
ESSK08-CS13	CS13_137	silt	1216.5	1217.5	37.62
ESSK08-CS13	CS13_138	clay	1222	1222.5	37.92
ESSK08-CS13	CS13_139	silt	1222.5	1223.5	37.92
ESSK08-CS13	CS13_29	silt	1245	1246	38.84
ESSK08-CS13	CS13_30	clay	1256	1257	39.22
ESSK08-CS13	CS13_31	silt	1257	1258	39.26
ESSK08-CS13	CS13_32	clay	1267	1268	39.62
ESSK08-CS13	CS13_37	clay	1303	1304	41.05
ESSK08-CS13	CS13_39	clay	1318	1319	41.51
ESSK08-CS13	CS13_41	clay	1339	1340	42.33
ESSK08-CS13	CS13_42	silt	1340	1341	42.39
ESSK08-CS13	CS13_18	silt	1358	1362	43.18
ESSK08-CS13	CS13_43	clay	1368	1369	43.57
ESSK08-CS13	CS13_44	silt	1371	1372	43.66
ESSK08-CS13	CS13_45	clay	1378	1379	43.89
ESSK08-CS13	CS13_47	clay	1423	1424	46.04
ESSK08-CS13	CS13_49	clay	1444	1445	47.04
ESSK08-CS13	CS13_50	silt	1445	1446	47.07
ESSK08-CS13	CS13_51	clay	1456	1457	47.40
ESSK08-CS13	CS13_52	silt	1457	1458	47.43
ESSK08-CS13	CS13_53	clay	1490	1491	48.41
ESSK08-CS13	CS13_54	silt	1491	1492	48.44
ESSK08-CS13	CS13_55	clay	1505	1506	48.85
ESSK08-CS13	CS13_19	clay	1561	1562	53.00
ESSK08-CS13	CS13_60	clay	1594	1594.5	54.31
ESSK08-CS13	CS13_59	silt	1593	1593.5	54.31
ESSK08-CS13	CS13_61	clay	1614	1615	55.02
ESSK08-CS13	CS13_62	silt	1615	1616	55.02
ESSK08-CS13	CS13_63	clay	1630.5	1631.5	55.59
ESSK08-CS13	CS13_21	clay	1633	1636	55.59
ESSK08-CS13	CS13_64	silt	1634	1635	55.59
ESSK08-CS13	CS13_65	clay	1652	1653	55.98
ESSK08-CS13	CS13_66	silt	1656	1656.5	55.98
ESSK08-CS13	CS13_68	clay	1676	1677	56.83

*continued on next page*

*continued from previous page*

<b>Core</b>	<b>Sample</b>	<b>Size fraction</b>	<b>Depth-top</b>	<b>Depth-bottom</b>	<b>Age (ka)</b>
ESSK08-CS13	CS13_67	silt	1674	1675	56.83
ESSK08-CS13	CS13_69	clay	1682.5	1683.5	57.02
ESSK08-CS13	CS13_71	clay	1712.5	1713.5	58.18
ESSK08-CS13	CS13_70	silt	1711.5	1712.5	58.18
ESSK08-CS13	CS13_72	clay	1722.5	1723.5	58.57
ESSK08-CS13	CS13_73	silt	1727	1728	58.57
ESSK08-CS13	CS13_74	clay	1762.5	1763.5	59.41
ESSK08-CS13	CS13_75	silt	1763.5	1764	59.41
ESSK08-CS13	CS13_76	clay	1767.5	1768	59.57
ESSK08-CS13	CS13_77	silt	1769	1770	59.57
ESSK08-CS13	CS13_78	clay	1770.5	1771	59.67
ESSK08-CS13	CS13_79	silt	1771	1772	59.67
ESSK08-CS13	CS13_80	clay	1806.5	1807	60.77
ESSK08-CS13	CS13_81	silt	1807	1808	60.77
ESSK08-CS13	CS13_82	clay	1843.5	1844	61.97
ESSK08-CS13	CS13_83	silt	1848	1849	61.97
ESSK08-CS13	CS13_84	clay	1888.5	1889	63.40
ESSK08-CS13	CS13_85	silt	1889	1889.5	63.40
ESSK08-CS13	CS13_86	clay	1920	1922	64.60
ESSK08-CS13	CS13_87	silt	1924	1925	64.60
ESSK08-CS13	CS13_90	clay	1992	1993	66.82
ESSK08-CS13	CS13_91	silt	1993	1993.5	66.82
ESSK08-CS13	CS13_92	clay	1997.5	1998	66.96
ESSK08-CS13	CS13_93	silt	1998	1998.5	66.96
ESSK08-CS13	CS13_96	clay	2042	2043	67.84
ESSK08-CS13	CS13_94	silt	2019.5	2020.5	67.84
ESSK08-CS13	CS13_95	clay	2021	2022	68.62
ESSK08-CS13	CS13_97	silt	2044	2045	68.62
ESSK08-CS13	CS13_98	clay	2050.5	2051.5	68.87
ESSK08-CS13	CS13_100	clay	2056.5	2057	69.08
ESSK08-CS13	CS13_99	silt	2055.5	2056.5	69.08
ESSK08-CS13	CS13_102	clay	2075	2076	69.71
ESSK08-CS13	CS13_101	silt	2074	2075	69.71
ESSK08-CS13	CS13_103	clay	2083.5	2084	70.07
ESSK08-CS13	CS13_104	silt	2086	2087	70.07

*continued on next page*

*continued from previous page*

<b>Core</b>	<b>Sample</b>	<b>Size fraction</b>	<b>Depth-top</b>	<b>Depth-bottom</b>	<b>Age (ka)</b>
ESSK08-CS13	CS13_105	clay	2112.5	2113.5	71.07
ESSK08-CS13	CS13_106	clay	2121.5	2122.5	71.41
ESSK08-CS13	CS13_107	silt	2126	2127	71.41
ESSK08-CS13	CS13_108	clay	2151.5	2152	72.52
ESSK08-CS13	CS13_109	silt	2155.5	2156.5	72.52
ESSK08-CS13	CS13_111	clay	2180	2181	73.58
ESSK08-CS13	CS13_26	silt	2188	2190	73.58
ESSK08-CS13	CS13_112	clay	2204	2204.5	74.22

Table A2.6 – Values of the measured standards

Standard	U (ppm)	2SD	( <sup>234</sup> U/ <sup>238</sup> U)	2SD	Date
BHVO-2	0.43	0.02	1.025	0.002	14/12/2017
BHVO-2	0.44	0.04	1.000	0.003	14/12/2017
BHVO-2	0.43	0.02	1.007	0.003	07/03/2018
BHVO-2	0.41	0.03	1.000	0.005	07/03/2018
BHVO-2	0.41	0.02	1.001	0.005	28/05/2018
BHVO-2	0.43	0.02	1.010	0.002	28/05/2018
BHVO-2	0.41	0.02	1.013	0.004	24/07/2018
BHVO-2	0.42	0.02	1.006	0.003	06/08/2018
BHVO-2	0.43	0.02	1.013	0.004	06/08/2018
<b>Mean</b>	<b>0.42</b>	<b>0.02</b>	<b>1.008</b>	<b>0.016</b>	
<b>Reference value</b>	<b>0.42</b>	<b>0.29</b>	<b>1.000</b>	<b>0.001</b>	
W-2	0.50	0.13	0.982	0.004	14/12/2017
W-2	0.50	0.03	0.986	0.004	14/12/2017
W-2	0.47	0.24	0.988	0.003	14/12/2017
W-2	0.50	0.02	1.005	0.002	07/03/2018
W-2	0.49	0.03	0.993	0.002	28/05/2018
<b>Mean</b>	<b>0.49</b>	<b>0.02</b>	<b>0.991</b>	<b>0.020</b>	
<b>Reference value</b>	<b>0.53</b>	<b>0.19</b>	<b>1.001</b>	<b>0.001</b>	
QLO-01	1.96	0.01	1.004	0.004	11/10/2019
QLO-01	1.88	0.04	1.004	0.004	26/02/2020
QLO-01	1.91	0.03	1.003	0.004	27/02/2020
QLO-01	1.90	0.01	0.999	0.004	7/03/2020
QLO-01	2.02	0.01	1.005	0.006	23/03/2020
QLO-01	2.00	0.02	1.005	0.003	24/03/2020
<b>Mean</b>	<b>1.95</b>	<b>0.11</b>	<b>1.003</b>	<b>0.004</b>	
<b>Reference value</b>	<b>1.90</b>	<b>0.12</b>	<b>1.000</b>	<b>0.001</b>	

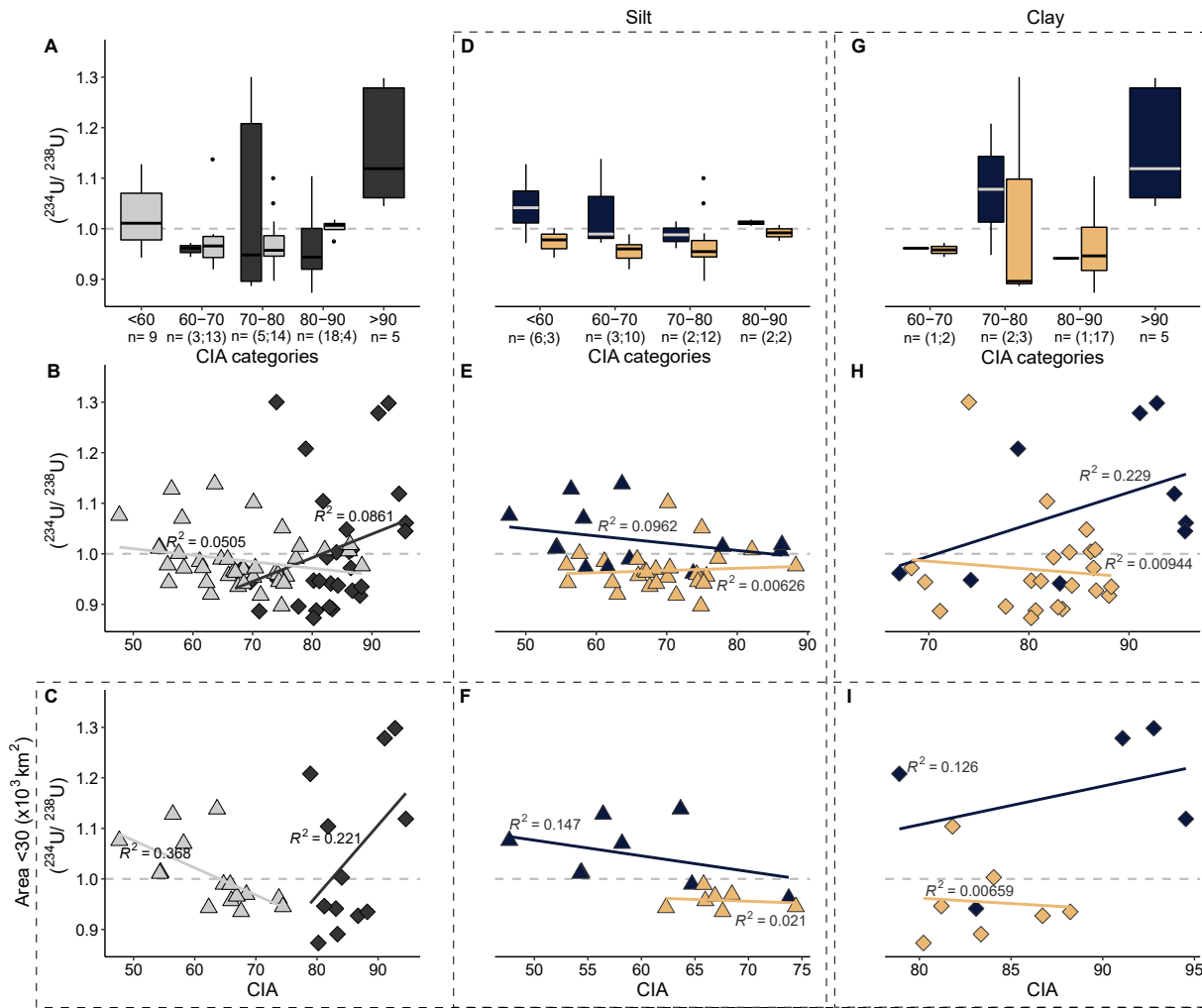


Figure A3.1

Relationships between  $(^{234}\text{U}/^{238}\text{U})$  and the chemical index of alteration (CIA)(A) as categories or (B) as continuous values (C) and in small area ( $<30 \times 10^3 \text{ km}^2$ ) in silt ( $n=40$ , light grey) and clay ( $n=34$ , dark grey) size fraction fractions ; depending on two lithology groups (blue for igneous & metamorphic rocks and beige for sedimentary and mixed lithologies) in respectively silt and clay size fractions (D)(G) as categories or (E)(H) as continuous values and (F)(I) in small area ( $<30 \times 10^3 \text{ km}^2$ ).

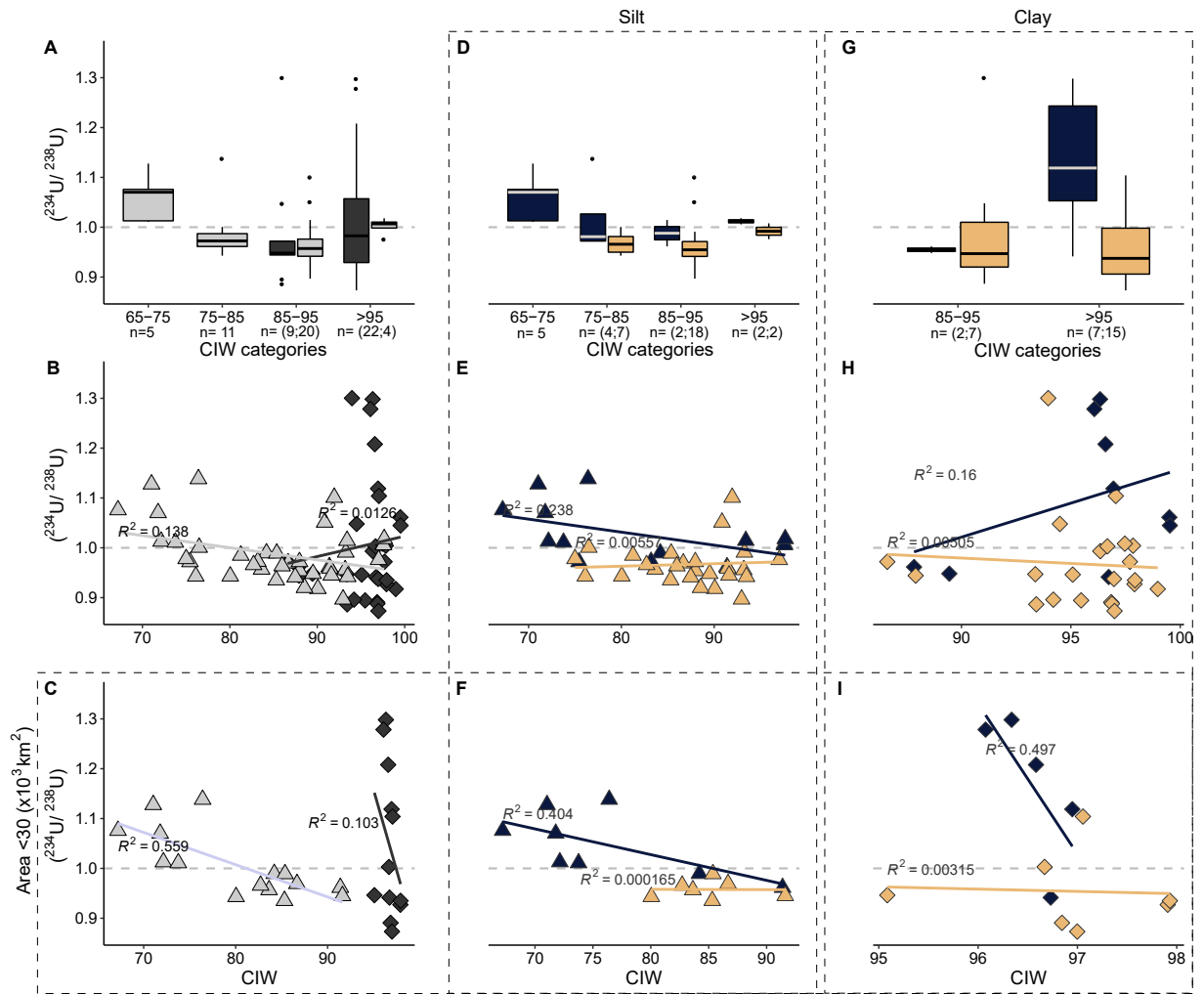


Figure A3.2

Relationships between  $(^{234}\text{U}/^{238}\text{U})$  and the chemical index of weathering (CIW)(A) as categories or (B) as continuous values (C) and in small area  $(^{234}\text{U}/^{238}\text{U})$  in silt ( $n=40$ , light grey) and clay ( $n=34$ , dark grey) size fraction fractions ; depending on two lithology groups ( blue for igneous metamorphic rocks and beige for sedimentary and mixed lithologies) in respectively silt and clay size fractions (D)(G) as categories or (E)(H) as continuous values and (F)(I) in small area  $(^{234}\text{U}/^{238}\text{U})$ .

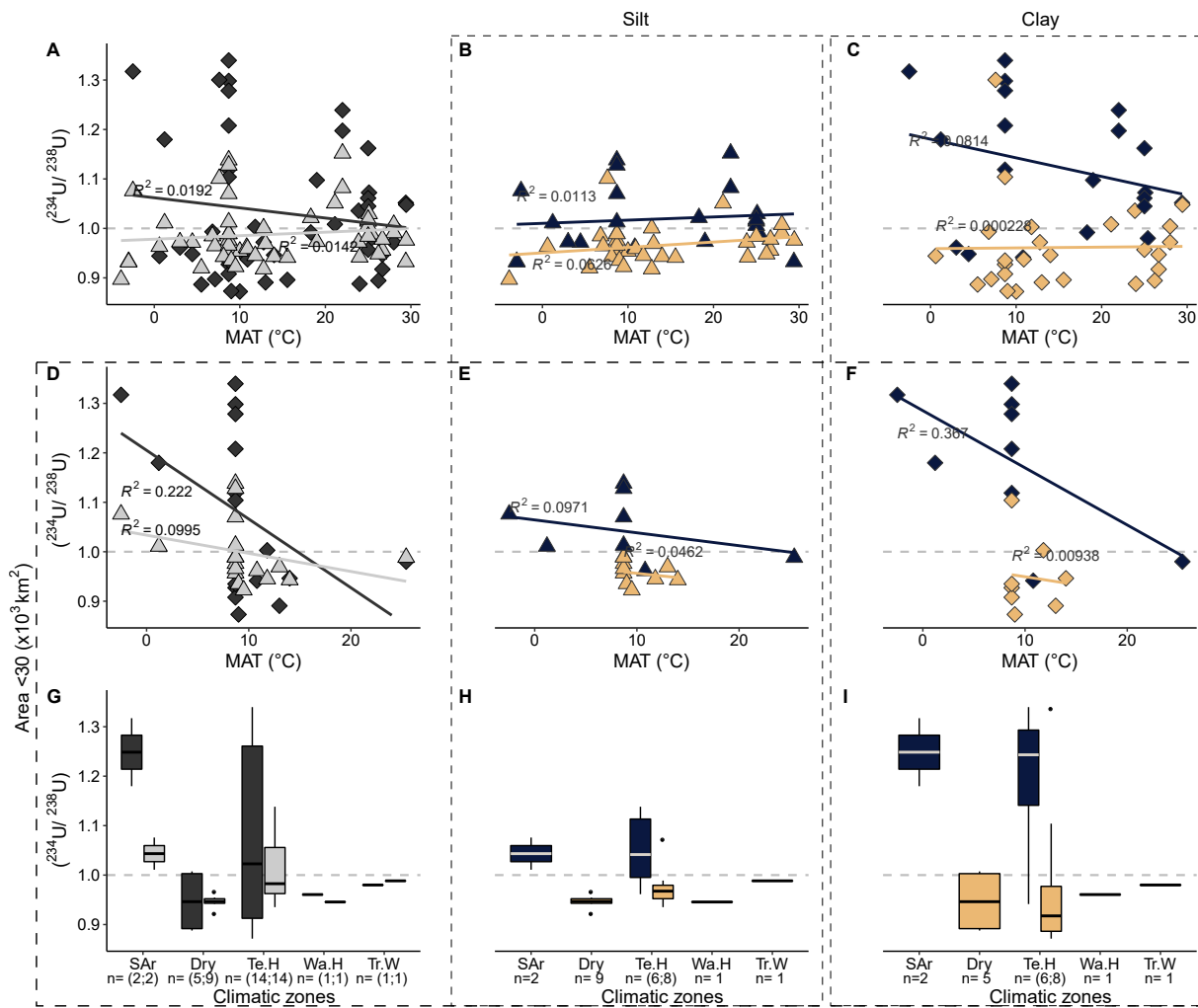


Figure A3.3

$(^{234}\text{U}/^{238}\text{U})$  activity ratios as a function of Mean Annual Temperature (MAT) of the catchment depending on (A) grain size fractions (silt :light grey and clay: dark grey) ; lithology (blue for igneous & metamorphic rocks and beige for sedimentary and mixed lithologies) in (B) silt and (C) in clay size fraction for all the studied river and in the same way for sediment from small catchments (D).(E) and (F) respectively ;  $(^{234}\text{U}/^{238}\text{U})$  activity ratios as function of (A) climatic zones as explained in Fig. 4 for sediments from small catchment groups depending on (G) grains size fraction (silt - light grey and clay - dark grey) and lithologies (blue for igneous metamorphic rocks and beige for sedimentary and mixed lithologies) in (H) silt and (I) clay.

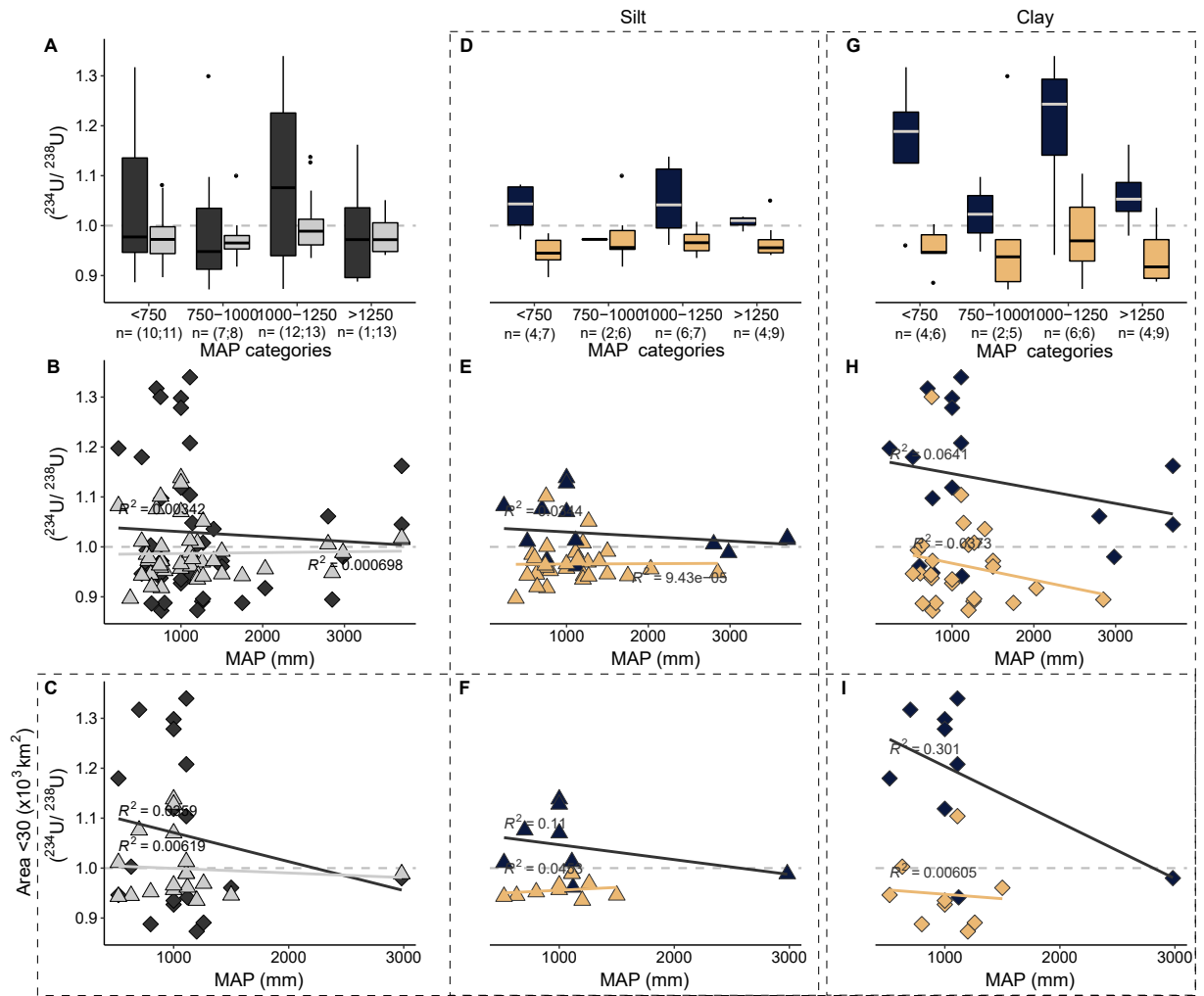


Figure A3.4

$(^{234}\text{U}/^{238}\text{U})$  activity ratios grouped based on grain size (silt :light grey and clay: dark grey) as a function of Mean Annual Precipitation (MAP) (A) as categories. (B) for all the studied sediments, (C) for sediments from small catchments (Area  $<30 \times 10^3 \text{ km}^2$ ); grouped based on two lithological categories (blue for igneous & metamorphic rocks and beige for sedimentary and mixed lithologies) in silt size fraction (D) as categories. (E) for all the studied sediments. (F) for sediments from small catchments (Area  $<30 \times 10^3 \text{ km}^2$ ); and in clay size fraction respectively (G). (H) and (I).

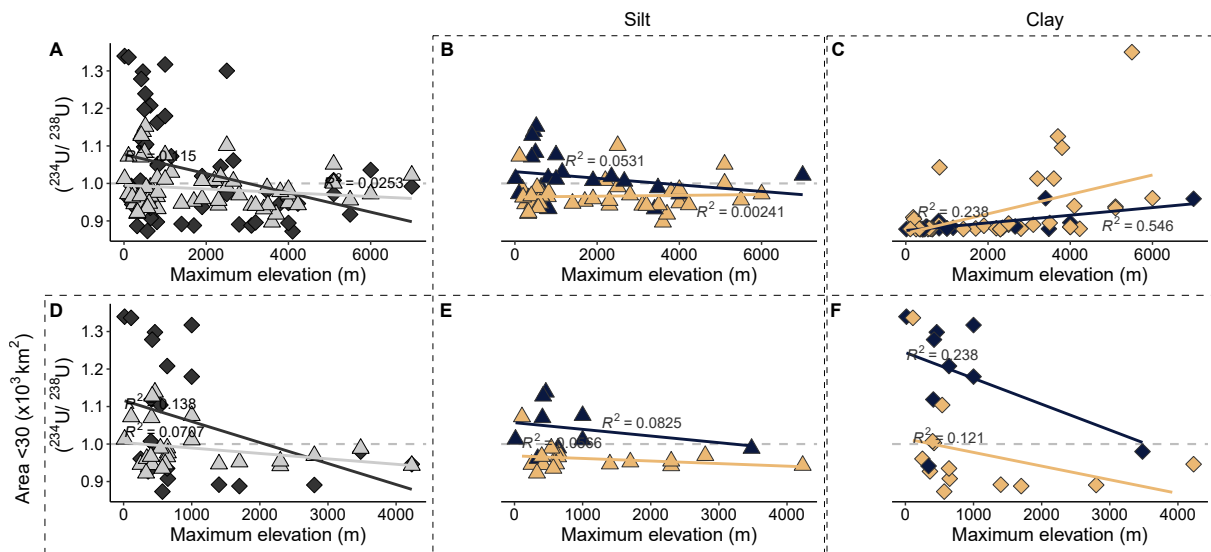


Figure A3.5

$(^{234}\text{U}/^{238}\text{U})$  activity ratios as a function of maximum elevation of the basin depending on (A) grain size fractions (silt :light grey and clay: dark grey) ; lithology (blue for igneous & metamorphic rocks and beige for sedimentary and mixed lithologies) in (B) silt and (C) in clay size fraction for all the studied river and in the same way for sediment from small catchments (D),(E) and (F) respectively.

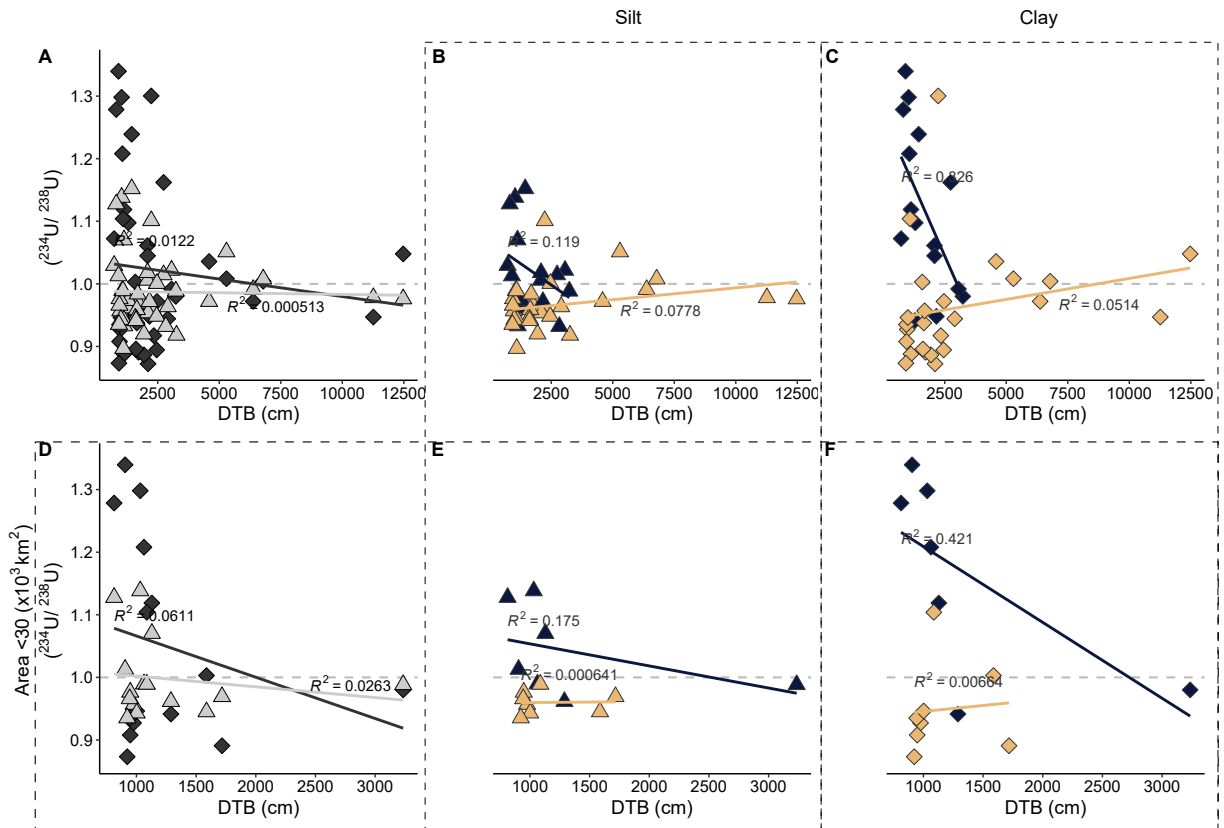


Figure A3.6

$(^{234}\text{U}/^{238}\text{U})$  activity ratios as a function of Depth To Bedrock (DTB) of the basin depending on (A) grain size fractions (silt :light grey and clay: dark grey) ; lithology (blue for igneous metamorphic rocks and beige for sedimentary and mixed lithologies) in (B) silt and (C) in clay size fraction for all the studied river and in the same way for sediment from small catchments (D),(E) and (F) respectively

Sample name	U (ppm)	2SD	( <sup>234</sup> U/ <sup>238</sup> U)	2SD	S	T <sub>res</sub>
CS01_1	2.70	0.01	0.951	0.003	24.8	84
CS01_2	5.40	0.01	0.956	0.003	14	72
CS01_3	3.71	0.01	0.968	0.003	11.5	64
CS01_4	2.37	0.01	0.953	0.005		72

Sample name	U (ppm)	2SE.U	( <sup>234</sup> U/ <sup>238</sup> U)	2SD	S	T <sub>res</sub>
KESC9_1	3.83	0.01	0.906	0.002		125
KESC9_2	3.29	0.01	0.897	0.003	21	128
KESC9_3	3.88	0.01	0.921	0.002		111
KESC9_4	3.56	0.01	0.911	0.003		115
KESC9_5	3.97	0.01	0.899	0.003		123
KESC9_6	4.24	0.01	0.898	0.003		133
KESC9_7	3.20	0.01	0.904	0.004		128
KESC9_9	2.98	0.01	0.910	0.003		115
KESC9_10	3.62	0.01	0.905	0.003	17	124
KESC9_11	3.92	0.01	0.908	0.002		121
KESC9_12	3.76	0.01	0.918	0.003		116
KESC9_13	3.07	0.01	0.896	0.003		134
KESC9_14	3.38	0.01	0.911	0.003		117
KESC9_15	3.37	0.01	0.898	0.003	18	129
KESC9_16	3.43	0.01	0.914	0.003		112
KESC9_17	3.30	0.01	0.913	0.003		120
KESC9_19	3.69	0.01	0.906	0.004		121
KESC9_20	4.11	0.01	0.942	0.002	14	88
KESC9_21	4.78	0.01	0.948	0.004		77
KESC9_22	4.89	0.01	0.952	0.003		78
KESC9_23	4.00	0.01	0.945	0.004		80
KESC9_24	4.01	0.01	0.942	0.003		92
KESC9_25	5.28	0.01	0.943	0.003		82
KESC9_26	5.59	0.01	0.914	0.002		108
KESC9_27	3.59	0.01	0.917	0.004		108
KESC9_28	3.89	0.01	0.908	0.004		118
KESC9_29	3.48	0.01	0.929	0.003	12	96

Table A5.1 – U concentration, ( $^{234}\text{U}/^{238}\text{U}$ ), Specific surface area and sediment residence time for the ESSK08-CS13 samples.

Sample name	U (ppm)	2SD	( $^{234}\text{U}/^{238}\text{U}$ )	2SD	S	$T_{res}$
CS13_1	4.05	0.01	0.930	0.002		99
CS13_2	1.19	0.00	0.907	0.004	12.4	119
CS13_3	3.00	0.01	0.940	0.004		87
CS13_5	3.50	0.01	0.946	0.004	10.9	77
CS13_6	3.63	0.01	0.955	0.003	7.6	75
CS13_7	2.65	0.01	0.945	0.004		81
CS13_8	5.00	0.01	0.945	0.003		84
CS13_9	2.60	0.01	0.952	0.004		70
CS13_12	2.68	0.01	0.954	0.004	11.7	79
CS13_13	3.86	0.01	0.964	0.004	14.6	61
CS13_14	3.01	0.01	0.933	0.003	18.2	92
CS13_15	2.47	0.01	0.945	0.005		76
CS13_114	1.85	0.01	0.958	0.004		68
CS13_115	1.77	0.01	0.942	0.004		80
CS13_116	2.01	0.01	0.934	0.004	25	93
CS13_117	0.65	0.01	0.960	0.003		66
CS13_118	1.04	0.01	0.940	0.003		84
CS13_119	1.12	0.01	0.972	0.003	21	54
CS13_120	1.99	0.01	0.936	0.005		93
CS13_121	2.84	0.01	0.939	0.007		84
CS13_123	4.00	0.01	0.937	0.002		83
CS13_122	3.39	0.01	0.959	0.003		66
CS13_124	3.23	0.01	0.947	0.003		69
CS13_125	2.94	0.01	0.943	0.004		85
CS13_126	3.36	0.01	0.958	0.002		67
CS13_127	3.41	0.01	0.948	0.003		75
CS13_128	0.05	0.01	0.924	0.004		93
CS13_129	2.59	0.01	0.956	0.004		68
CS13_130	2.93	0.01	0.916	0.005		109
CS13_131	3.49	0.01	0.910	0.003		113
CS13_133	3.54	0.01	0.921	0.002		104
CS13_132	2.64	0.01	0.916	0.003		105
CS13_135	2.65	0.01	0.909	0.004	18	117

*continued on next page*

continued from previous page

Sample name	U (ppm)	2SD	( <sup>234</sup> U/ <sup>238</sup> U)	2SD	S	T <sub>res</sub>
CS13_134	3.11	0.01	0.906	0.004		123
CS13_136	3.56	0.01	0.917	0.002		109
CS13_137	2.59	0.01	0.915	0.003		113
CS13_138	3.51	0.01	0.922	0.004		98
CS13_139	3.37	0.01	0.904	0.003	17	124
CS13_29	2.74	0.01	0.955	0.005		64
CS13_30	2.72	0.01	0.929	0.004		98
CS13_31	2.15	0.01	0.948	0.004		75
CS13_32	2.50	0.01	0.949	0.004		73
CS13_37	2.40	0.01	0.956	0.005	14	65
CS13_39	2.94	0.01	0.946	0.003		80
CS13_41	2.34	0.01	0.945	0.005		72
CS13_42	2.39	0.01	0.987	0.006	9	38
CS13_18	2.40	0.01	0.938	0.004		85
CS13_43	3.34	0.01	0.941	0.004		80
CS13_44	2.48	0.01	0.979	0.004		48
CS13_45	2.00	0.01	0.935	0.006		82
CS13_47	2.28	0.01	0.920	0.005	16	107
CS13_49	2.57	0.01	0.935	0.004	13.2	86
CS13_50	2.31	0.00	0.971	0.004	6.9	51
CS13_51	2.60	0.01	0.939	0.005		85
CS13_52	2.86	0.01	0.942	0.004		76
CS13_53	2.58	0.01	0.952	0.005		70
CS13_54	2.24	0.01	0.953	0.005	18.2	70
CS13_55	2.34	0.00	0.963	0.004	14.0	57
CS13_19	3.11	0.01	0.919	0.004		105
CS13_60	2.61	0.00	0.927	0.003		96
CS13_59	2.52	0.01	0.926	0.004		91
CS13_61	3.31	0.00	0.935	0.003		84
CS13_62	2.43	0.01	0.938	0.004		87
CS13_63	1.98	0.00	0.913	0.004		112
CS13_21	2.33	0.00	0.960	0.005		57
CS13_64	2.35	0.01	0.939	0.004		86
CS13_65	2.73	0.01	0.907	0.004		117
CS13_66	2.59	0.01	0.935	0.003		91

continued on next page

*continued from previous page*

<b>Sample name</b>	<b>U (ppm)</b>	<b>2SD</b>	<b>(<sup>234</sup>U/<sup>238</sup>U)</b>	<b>2SD</b>	<b>S</b>	<b>T<sub>res</sub></b>
CS13_68		0.00	0.933	0.004		82
CS13_67	2.46	0.01	0.917	0.004		103
CS13_69	2.64	0.01	0.926	0.004		91
CS13_71	2.72	0.01	0.940	0.004		78
CS13_70	2.52	0.01	0.925	0.004		91
CS13_72	2.72	0.01	0.923	0.005		93
CS13_73	2.95	0.01	0.943	0.004		77
CS13_74	2.46	0.01	0.888	0.003	17	135
CS13_75	3.56	0.01	0.947	0.008	6.2	61
CS13_76	3.94	0.01	0.891	0.002		130
CS13_77	2.99	0.01	0.907	0.003	9.5	112
CS13_78	3.05	0.01	0.897	0.003		123
CS13_79	2.86	0.01	0.922	0.003		97
CS13_80	3.57	0.01	0.910	0.005		117
CS13_81	4.06	0.01	0.949	0.003		64
CS13_82	2.60	0.01	0.931	0.004		86
CS13_83	3.60	0.01	0.940	0.004		78
CS13_84	3.29	0.01	0.933	0.004		85
CS13_85	3.83	0.01	0.948	0.003		73
CS13_86	3.40	0.01	0.929	0.003	13	83
CS13_87	3.14	0.01	0.927	0.004	14	98
CS13_90	2.66	0.01	0.934	0.003		85
CS13_91	4.14	0.01	0.966	0.002		48
CS13_92	2.88	0.01	0.947	0.004		74
CS13_93	2.99	0.01	0.955	0.004		56
CS13_96	2.36	0.01	0.940	0.004		74
CS13_94	3.67	0.01	0.976	0.003	5.7	42
CS13_95	3.59	0.01	0.975	0.003	38	40
CS13_97	3.25	0.01	0.943	0.004		70
CS13_98	3.07	0.01	0.945	0.004		76
CS13_100	2.80	0.01	0.940	0.004		80
CS13_99	3.13	0.01	0.946	0.004		75
CS13_102	3.18	0.01	0.949	0.003		68
CS13_101	3.95	0.01	0.952	0.003		60
CS13_103	2.95	0.01	0.941	0.004		76

*continued on next page*

*continued from previous page*

<b>Sample name</b>	<b>U (ppm)</b>	<b>2SD</b>	<b>(<sup>234</sup>U/<sup>238</sup>U)</b>	<b>2SD</b>	<b>S</b>	<b>T<sub>res</sub></b>
CS13_104	2.91	0.01	0.925	0.005		92
CS13_105	3.87	0.01	0.908	0.004		109
CS13_106	3.45	0.01	0.926	0.005		85
CS13_107	3.22	0.01	0.950	0.003	13	64
CS13_108	3.65	0.01	0.953	0.003		65
CS13_109	3.41	0.01	0.929	0.005		82
CS13_111	2.91	0.01	0.926	0.004		89
CS13_26	2.45	0.00	0.951	0.002	13	67
CS13_112	3.57	0.01	0.920	0.005	20	96

# BIBLIOGRAPHY

---

- Ackerer, J., Chabaux, F., Van der Woerd, J., Viville, D., Pelt, E., Kali, E., Lerouge, C., Ackerer, P., di Chiara Roupert, R. & Négrel, P. (2016), 'Regolith evolution on the millennial timescale from combined U–Th–Ra isotopes and in situ cosmogenic  $^{10}\text{Be}$  analysis in a weathering profile (Strengbach catchment, France)', *Earth and Planetary Science Letters* **453**, 33–43.
- Adloff, J. P. & Roessler, K. (1991), 'Recoil and Transmutation Effects in the Migration Behaviour of Actinides', *Radiochimica Acta* **52-53**(1), 269–274.
- Ahnert, F. (1967), 'The role of the equilibrium concept in the interpretation of landforms of fluvial erosion and deposition.', *L'évolution des Versants* pp. 23–41.
- Ahnert, F. (1970), 'Functional relationships between denudation, relief, and uplift in large, mid-latitude drainage basins', *American Journal of Science* **268**(3), 243–263.
- Ahnert, F. (1976), 'Brief description of a comprehensive three-dimensional process-response model of landform development.', *Geographic Institute* **25**, 29–49.
- Ahnert, F. (1994), 'Equilibrium, scale and inheritance in geomorphology', *Geomorphology* **11**(2), 125–140.
- Allen, J. R. M., Brandt, U., Brauer, A., Hubberten, H.-W., Huntley, B., Keller, J., Kraml, M., Mackensen, A., Mingram, J., Negendank, J., Nowaczyk, N., Oberhänsli, H., Watts, W., Wulf, S. & Zolitschka, B. (1999), 'Rapid environmental changes in southern Europe during the last glacial period', *Nature* **400**(6746), 740–743.
- Allen, P. A. (1997), *Earth Surface Processes*.
- Allen, P. A. (2008a), 'From landscapes into geological history', *Nature* **451**(7176), 274–276.
- Allen, P. A. (2008b), 'Time scales of tectonic landscapes and their sediment routing systems', *Geological Society, London, Special Publications* **296**(1), 7–28.
- Allen, P. & Heller, P. L. (2012), Dispersal and Preservation of Tectonically Generated Alluvial Gravels in Sedimentary Basins, *in* 'Tectonics of Sedimentary Basins', John Wiley & Sons, Ltd, chapter 6, pp. 111–130.
- Ames, L., McGarrah, J., Walker, B. & Salter, P. (1983), 'Uranium and radium sorption on amorphous ferric oxyhydroxide', *Chemical Geology* **40**(1), 135–148.

- Amorosi, A., Maselli, V. & Trincardi, F. (2016), 'Onshore to offshore anatomy of a late Quaternary source-to-sink system (Po Plain–Adriatic Sea, Italy)', *Earth-Science Reviews* **153**, 212–237.
- Amundson, R., Richter, D. D., Humphreys, G. S., Jobbagy, E. G. & Gaillardet, J. (2007), 'Coupling between Biota and Earth Materials in the Critical Zone', *Elements* **3**(5), 327–332.
- Andersen, M. B., Erel, Y. & Bourdon, B. (2009), 'Experimental evidence for  $^{234}\text{U}$ – $^{238}\text{U}$  fractionation during granite weathering with implications for  $^{234}\text{U}/^{238}\text{U}$  in natural waters', *Geochimica et Cosmochimica Acta* **73**(14), 4124–4141.
- Anderson, R. F. (1982), 'Concentration, vertical flux, and remineralization of particulate uranium in seawater', *Geochimica et Cosmochimica Acta* **46**(7), 1293–1299.
- Anderson, R. S. & Anderson, S. P. (2010), *Geomorphology: The Mechanics and Chemistry of Landscapes*, Cambridge University Press.
- Anderson, R. S. & Humphrey, N. F. (1989), 'Interaction of weathering and transport processes in the evolution of arid landscapes.', pp. 349–361.
- Anderson, S. P. (2005), 'Glaciers show direct linkage between erosion rate and chemical weathering fluxes', *Geomorphology* **67**(1), 147–157.
- Anderson, S. P., Blum, J., Brantley, S. L., Chadwick, O., Chorover, J., Derry, L. A., Drever, J. I., Hering, J. G., Kirchner, J. W., Kump, L. R., Richter, D. & White, A. E. (2004), 'Proposed initiative would study Earth's weathering engine', *Eos, Transactions American Geophysical Union* **85**(28), 265–269.
- Anderson, S. P., Dietrich, W. E. & Brimhall, G. H. (2002), 'Weathering profiles, mass-balance analysis, and rates of solute loss: Linkages between weathering and erosion in a small, steep catchment', *GSA Bulletin* **114**(9), 1143–1158.
- Anderson, S. P., von Blanckenburg, F. & White, A. F. (2007), 'Physical and Chemical Controls on the Critical Zone', *Elements* **3**(5), 315–319.
- Andersson, P. S., Porcelli, D., Gustafsson, Ö., Ingri, J. & Wasserburg, G. J. (2001), 'The importance of colloids for the behavior of uranium isotopes in the low-salinity zone of a stable estuary - ScienceDirect', *Geochimica et Cosmochimica Acta* **65**(1), 13–25.
- Andersson, P. S., Porcelli, D., Wasserburg, G. J. & Ingri, J. (1998), 'Particle Transport of  $^{234}\text{U}$ – $^{238}\text{U}$  in the Kalix River and in the Baltic Sea', *Geochimica et Cosmochimica Acta* **62**(3), 385–392.

- Anthony, E. J. (1995), 'Impacts géomorphologiques côtiers des aménagements du Var et de son delta, Côte d'Azur, France', *Hommes et Terres du Nord* **1**(1), 73–81.
- Anthony, E. J. & Julian, M. (1999), 'Source-to-sink sediment transfers, environmental engineering and hazard mitigation in the steep Var River catchment, French Riviera, southeastern France', *Geomorphology* **31**(1), 337–354.
- Armitage, J. J., Dunkley Jones, T., Duller, R. A., Whittaker, A. C. & Allen, P. A. (2013), 'Temporal buffering of climate-driven sediment flux cycles by transient catchment response', *Earth and Planetary Science Letters* **369-370**, 200–210.
- Armstrong, A. (1976), 'A three-dimensional simulation of slope forms', *Z. Geomorphol. Suppl.* **25**, 20–28.
- Arribas, J. & Tortosa, A. (2003), 'Detrital modes in sedimenticlastic sands from low-order streams in the Iberian Range, Spain: The potential for sand generation by different sedimentary rocks', *Sedimentary Geology* **159**(3), 275–303.
- Baker, P. A., Seltzer, G. O., Fritz, S. C., Dunbar, R. B., Grove, M. J., Tapia, P. M., Cross, S. L., Rowe, H. D. & Broda, J. P. (2001), 'The History of South American Tropical Precipitation for the Past 25,000 Years', *Science* **291**(5504), 640–643.
- Bateman, H. (1910), 'The solution of a system of differential equations occurring in the theory of radio-active transformations', *Proc. Cambridge Phil. Soc.*, 1910 **15**, 423–427.
- Bates, R. & Jackson, J. (1987), 'Glossary of Geology, third edition', *American Geological Institute* .
- Bayon, G., Burton, K. W., Soulet, G., Vigier, N., Dennielou, B., Etoubleau, J., Ponzevera, E., German, C. R. & Nesbitt, R. W. (2009), 'Hf and Nd isotopes in marine sediments: Constraints on global silicate weathering', *Earth and Planetary Science Letters* **277**(3), 318–326.
- Bayon, G., Delvigne, C., Ponzevera, E., Borges, A. V., Darchambeau, F., De Deckker, P., Lambert, T., Monin, L., Toucanne, S. & André, L. (2018), 'The silicon isotopic composition of fine-grained river sediments and its relation to climate and lithology', *Geochimica et Cosmochimica Acta* **229**, 147–161.
- Bayon, G., Dennielou, B., Etoubleau, J., Ponzevera, E., Toucanne, S. & Bermell, S. (2012), 'Intensifying Weathering and Land Use in Iron Age Central Africa', *Science* **335**(6073), 1219–1222.
- Bayon, G., German, C. R., Boella, R. M., Milton, J. A., Taylor, R. N. & Nesbitt, R. W. (2002), 'An improved method for extracting marine sediment fractions and its application to Sr and Nd isotopic analysis', *Chemical Geology* **187**(3), 179–199.

- Bayon, G., Lambert, T., Vigier, N., De Deckker, P., Freslon, N., Jang, K., Larkin, C. S., Piotrowski, A. M., Tachikawa, K., Thollon, M. & Tipper, E. T. (2020), 'Rare earth element and neodymium isotope tracing of sedimentary rock weathering', *Chemical Geology* **553**, 119794.
- Bayon, G., Skonieczny, C., Delvigne, C., Toucanne, S., Bermell, S., Ponzevera, E. & André, L. (2016), 'Environmental Hf–Nd isotopic decoupling in World river clays', *Earth and Planetary Science Letters* **438**, 25–36.
- Bayon, G., Toucanne, S., Skonieczny, C., André, L., Bermell, S., Cheron, S., Dennielou, B., Etoubleau, J., Freslon, N., Gauchery, T., Germain, Y., Jorry, S. J., Ménot, G., Monin, L., Ponzevera, E., Rouget, M. L., Tachikawa, K. & Barrat, J. A. (2015), 'Rare earth elements and neodymium isotopes in world river sediments revisited', *Geochimica et Cosmochimica Acta* **170**, 17–38.
- Beaudouin, C., Jouet, G., Suc, J.-P., Berné, S. & Escarguel, G. (2007), 'Vegetation dynamics in southern France during the last 30kyBP in the light of marine palynology', *Quaternary Science Reviews* **26**(7), 1037–1054.
- Beny, F., Toucanne, S., Skonieczny, C., Bayon, G. & Ziegler, M. (2018), 'Geochemical provenance of sediments from the northern East China Sea document a gradual migration of the Asian Monsoon belt over the past 400,000 years', *Quaternary Science Reviews* **190**, 161–175.
- Berger, A. (1988), 'Milankovitch Theory and climate', *Reviews of Geophysics* **26**(4), 624–657.
- Berner, R. A. (1990), 'Atmospheric Carbon Dioxide Levels Over Phanerozoic Time', *Science* **249**(4975), 1382–1386.
- Bigot-Cormier, F., Braucher, R., Bourlès, D., Guglielmi, Y., Dubar, M. & Stéphan, J. F. (2005), 'Chronological constraints on processes leading to large active landslides', *Earth and Planetary Science Letters* **235**(1), 141–150.
- Bindeman, I. N., Bayon, G. & Palandri, J. (2019), 'Triple oxygen isotope investigation of fine-grained sediments from major world's rivers: Insights into weathering processes and global fluxes into the hydrosphere', *Earth and Planetary Science Letters* **528**, 115851.
- Binnie, S. A., Phillips, W. M., Summerfield, M. A. & Fifield, L. K. (2007), 'Tectonic uplift, threshold hillslopes, and denudation rates in a developing mountain range', *Geology* **35**(8), 743–746.

- Blanco, P., Tomé, F. V. & Lozano, J. C. (2004), 'Sequential extraction for radionuclide fractionation in soil samples: A comparative study', *Applied Radiation and Isotopes* **61**(2), 345–350.
- Blum, M. D. & Törnqvist, T. E. (2000), 'Fluvial responses to climate and sea-level change: A review and look forward', *Sedimentology* **47**(s1), 2–48.
- Blum, M., Rogers, K., Gleason, J., Najman, Y., Cruz, J. & Fox, L. (2018), 'Allogenic and Autogenic Signals in the Stratigraphic Record of the Deep-Sea Bengal Fan', *Scientific Reports* **8**(1), 7973.
- Bluth, G. J. S. & Kump, L. R. (1994), 'Lithologic and climatologic controls of river chemistry', *Geochimica et Cosmochimica Acta* **58**(10), 2341–2359.
- Boch, R., Spötl, C. & Frisia, S. (2011), 'Origin and palaeoenvironmental significance of lamination in stalagmites from Katerloch Cave, Austria', *Sedimentology* **58**(2), 508–531.
- Bond, G., Broecker, W., Johnsen, S., McManus, J., Labeyrie, L., Jouzel, J. & Bonani, G. (1993), 'Correlations between climate records from North Atlantic sediments and Greenland ice', *Nature* **365**(6442), 143–147.
- Bonneau, L. (2014), Impact Des Oscillations Climatiques Rapides Du Dernier Cycle Glaciaire Sur l'érosion et Les Transferts Sédimentaires Dans Le Sud Des Alpes (SE France) Millennial-Scale Response of a Western Mediterranean River to Late Quaternary Climate Changes : A View from the Deep Sea Geochemical Evidences for Response of Erosion and Sediment Transfers to Rapid Climate Change and Glaciation, SW Alps, France, These de doctorat, Paris 6. Sous la direction de Laurent Emmanuel et de Catherine Pierre. Soutenue le 10-12-2014, à Paris 6 , dans le cadre de École doctorale Géosciences, ressources naturelles et environnement (Paris) .
- Bonneau, L., Jorry, S. J., Toucanne, S., Silva Jacinto, R. & Emmanuel, L. (2014), 'Millennial-Scale Response of a Western Mediterranean River to Late Quaternary Climate Changes: A View from the Deep Sea', *The Journal of Geology* **122**(6), 687–703.
- Bonneau, L., Toucanne, S., Bayon, G., Jorry, S. J., Emmanuel, L. & Silva Jacinto, R. (2017), 'Glacial erosion dynamics in a small mountainous watershed (Southern French Alps): A source-to-sink approach', *Earth and Planetary Science Letters* **458**, 366–379.
- Bosia, C. (2016), Les Séries Radioactives de l'uranium Dans Les Sédiments de La Gandak (Himalaya) : De La Roche Total Aux Analyses in Situ Sur Les Minéraux Séparés, Thesis, Strasbourg.

- Bosia, C., Chabaux, F., Pelt, E., Cogez, A., Stille, P., Deloule, E. & France-Lanord, C. (2018), 'U-series disequilibria in minerals from Gandak River sediments (Himalaya)', *Chemical Geology* **477**, 22–34.
- Bourdon, B., Bureau, S., Andersen, M. B., Pili, E. & Hubert, A. (2009), 'Weathering rates from top to bottom in a carbonate environment', *Chemical Geology* **258**(3), 275–287.
- Bourdon, B. & Sims, K. W. W. (2003), 'U-series Constraints on Intraplate Basaltic Magmatism', *Reviews in Mineralogy and Geochemistry* **52**(1), 215–254.
- Bourdon, B., Turner, S., Henderson, G. M. & Lundstrom, C. C. (2003), 'Introduction to U-series Geochemistry', *Reviews in Mineralogy and Geochemistry* **52**(1), 1–21.
- Bracken, L. J., Turnbull, L., Wainwright, J. & Bogaart, P. (2015), 'Sediment connectivity: A framework for understanding sediment transfer at multiple scales', *Earth Surface Processes and Landforms* **40**(2), 177–188.
- Brantley, S. L., Goldhaber, M. B. & Ragnarsdottir, K. V. (2007), 'Crossing Disciplines and Scales to Understand the Critical Zone', *Elements* **3**(5), 307–314.
- Broecker, W. S. (1998), 'Paleocean circulation during the Last Deglaciation: A bipolar seesaw?', *Paleoceanography* **13**(2), 119–121.
- Broecker, W. S., Thurber, D. L., Goddard, J., Ku, T.-l., Matthews, R. K. & Mesolella, K. J. (1968), 'Milankovitch Hypothesis Supported by Precise Dating of Coral Reefs and Deep-Sea Sediments', *Science* **159**(3812), 297–300.
- Brown, A. G., Carey, C., Erkens, G., Fuchs, M., Hoffmann, T., Macaire, J.-J., Moldenhauer, K.-M. & Walling, D. E. (2009), 'From sedimentary records to sediment budgets: Multiple approaches to catchment sediment flux', *Geomorphology* **108**(1), 35–47.
- Brunauer, s., Emmett, P. & Teller, E. (1938), 'Adsorption of gases in multimolecular layers.', *Journal of the American Chemical Society* **60**, 309–319.
- Brunsdon, D. & Thornes, J. B. (1979), 'Landscape Sensitivity and Change', *Transactions of the Institute of British Geographers* **4**(4), 463–484.
- Bull, W. B. (1991), 'Geomorphic responses to climatic change'.
- Buoncristiani, J. F. & Campy, M. (2004), 'Expansion and retreat of the Jura ice sheet (France) during the last glacial maximum', *Sedimentary Geology* **165**(3), 253–264.
- Burbank, D. W. & Anderson, R. S. (2011), *Tectonic Geomorphology*, John Wiley & Sons.

- Burbank, D. W., Leland, J., Fielding, E., Anderson, R. S., Brozovic, N., Reid, M. R. & Duncan, C. (1996), 'Bedrock incision, rock uplift and threshold hillslopes in the northwestern Himalayas', *Nature* **379**(6565), 505–510.
- Cacho, I., Grimalt, J. O., Pelejero, C., Canals, M., Sierro, F. J., Flores, J. A. & Shackleton, N. (1999), 'Dansgaard-Oeschger and Heinrich event imprints in Alboran Sea paleotemperatures', *Paleoceanography* **14**(6), 698–705.
- Calvès, G., Toucanne, S., Jouet, G., Charrier, S., Thereau, E., Etoubleau, J., Marsset, T., Droz, L., Bez, M., Abreu, V., Jorry, S., Mulder, T. & Lericolais, G. (2013), 'Inferring denudation variations from the sediment record; an example of the last glacial cycle record of the Golo Basin and watershed, East Corsica, western Mediterranean sea', *Basin Research* **25**(2), 197–218.
- Campos, B., Aguilar-Carrillo, J., Algarra, M., Gonçalves, M. A., Rodríguez-Castellón, E., Esteves da Silva, J. C. G. & Bobos, I. (2013), 'Adsorption of uranyl ions on kaolinite, montmorillonite, humic acid and composite clay material', *Applied Clay Science* **85**, 53–63.
- Capron, E., Landais, A., Chappellaz, J., Schilt, A., Buiron, D., Dahl-Jensen, D., Johnsen, S. J., Jouzel, J., Lemieux-Dudon, B., Loulergue, L., Leuenberger, M., Masson-Delmotte, V., Meyer, H., Oerter, H. & Stenni, B. (2010), 'Millennial and sub-millennial scale climatic variations recorded in polar ice cores over the last glacial period', *Climate of the Past* **6**(3), 345–365.
- Caracciolo, L. (2020), 'Sediment generation and sediment routing systems from a quantitative provenance analysis perspective: Review, application and future development', *Earth-Science Reviews* **209**, 103226.
- Caracciolo, L., Tolosana-Delgado, R., Le Pera, E., von Eynatten, H., Arribas, J. & Tarquini, S. (2012), 'Influence of granitoid textural parameters on sediment composition: Implications for sediment generation', *Sedimentary Geology* **280**, 93–107.
- Carl, C. (1987), 'Investigations of U series disequilibria as a means to study the transport mechanism of uranium in sandstone samples during weathering', *Uranium* **3**(2-4), 285–305.
- Carretier, S., Guerit, L., Harries, R., Regard, V., Maffre, P. & Bonnet, S. (2020), 'The distribution of sediment residence times at the foot of mountains and its implications for proxies recorded in sedimentary basins', *Earth and Planetary Science Letters* **546**, 116448.
- Carson, M. A. & Kirkby, M. J. (1972), 'Hillslope form and process', *Cambridge University Press* p. 475pp.

- Casson, B., Delacourt, C., Baratoux, D. & Allemand, P. (2003), ‘Seventeen years of the “La Clapière” landslide evolution analysed from ortho-rectified aerial photographs’, *Engineering Geology* **68**(1), 123–139.
- Castelltort, S. & Van Den Driessche, J. (2003), ‘How plausible are high-frequency sediment supply-driven cycles in the stratigraphic record?’, *Sedimentary Geology* **157**(1), 3–13.
- Catani, F., Segoni, S. & Falorni, G. (2010), ‘An empirical geomorphology-based approach to the spatial prediction of soil thickness at catchment scale’, *Water Resources Research* **46**(5).
- Chabaux, F., Blaes, E., Granet, M., Roupert, R. d. C. & Stille, P. (2012), ‘Determination of transfer time for sediments in alluvial plains using  $^{238}\text{U}$ - $^{234}\text{U}$ - $^{230}\text{Th}$  disequilibria: The case of the Ganges river system’, *Comptes Rendus Geoscience* **344**(11), 688–703.
- Chabaux, F., Blaes, E., Stille, P., di Chiara Roupert, R., Pelt, E., Dosseto, A., Ma, L., Buss, H. L. & Brantley, S. L. (2013), ‘Regolith formation rate from U-series nuclides: Implications from the study of a spheroidal weathering profile in the Rio Icacos watershed (Puerto Rico)’, *Geochimica et Cosmochimica Acta* **100**, 73–95.
- Chabaux, F., Bourdon, B. & Riotte, J. (2008), Chapter 3 U-Series Geochemistry in Weathering Profiles, River Waters and Lakes, in S. Krishnaswami & J. K. Cochran, eds, ‘Radioactivity in the Environment’, Vol. 13 of *U-Th Series Nuclides in Aquatic Systems*, Elsevier, pp. 49–104.
- Chabaux, F., Dequincey, O., Lévêque, J.-J., Leprun, J.-C., Clauer, N., Riotte, J. & Paquet, H. (2003a), ‘Tracing and dating recent chemical transfers in weathering profiles by trace-element geochemistry and  $^{238}\text{U}$ - $^{234}\text{U}$ - $^{230}\text{Th}$  disequilibria: The example of the Kaya lateritic toposequence (Burkina-Faso)’, *Comptes Rendus Geoscience* **335**(16), 1219–1231.
- Chabaux, F., Granet, M., Pelt, E., France-Lanord, C. & Galy, V. (2006), ‘ $^{238}\text{U}$ - $^{234}\text{U}$ - $^{230}\text{Th}$  disequilibria and timescale of sedimentary transfers in rivers: Clues from the Gangetic plain rivers’, *Journal of Geochemical Exploration* **88**(1), 373–375.
- Chabaux, F., Ma, L., Stille, P., Pelt, E., Granet, M., Lemarchand, D., Roupert, R. d. C. & Brantley, S. L. (2011), ‘Determination of chemical weathering rates from U series nuclides in soils and weathering profiles: Principles, applications and limitations’, *Applied Geochemistry* **26**, S20–S23.
- Chabaux, F., Riotte, J. & Dequincey, O. (2003b), 13. U-Th-Ra Fractionation During Weathering and River Transport, in ‘Uranium-Series Geochemistry’, Vol. 52, De Gruyter, Berlin, Boston.

- Cheng, H., Edwards, R. L., Hoff, J., Gallup, C. D., Richards, D. A. & Asmerom, Y. (2000), 'The half-lives of uranium-234 and thorium-230', *Chemical Geology* **169**(1), 17–33.
- Chorover, J., Kretzschmar, R., Garcia-Pichel, F. & Sparks, D. L. (2007), 'Soil Biogeochemical Processes within the Critical Zone', *Elements* **3**(5), 321–326.
- Church, M. & Ryder, J. M. (1972), 'Paraglacial Sedimentation: A Consideration of Fluvial Processes Conditioned by Glaciation', *GSA Bulletin* **83**(10), 3059–3072.
- Ciobanu, M., Rabineau, M., Droz, L., Révillon, S., Ghiglione, J. F., Dennielou, B., Jorry, S. J., Kallmeyer, J., Etoubleau, J., Pignet, P., Crassous, P., Vandenabeele-Trambouze, O., Laugier, J., Guegan, M., Godfroy, A. & Alain, K. (2012), 'Sedimentological imprint on subseafloor microbial communities in Western Mediterranean Sea Quaternary sediments', *Biogeosciences* **9**, 3491–3512.
- Clark, C. D., Hughes, A. L. C., Greenwood, S. L., Jordan, C. & Sejrup, H. P. (2012b), 'Pattern and timing of retreat of the last British-Irish Ice Sheet', *Quaternary Science Reviews* **44**, 112–146.
- Clark, P. U., Dyke, A. S., Shakun, J. D., Carlson, A. E., Clark, J., Wohlfarth, B., Mitrovica, J. X., Hostetler, S. W. & McCabe, A. M. (2009), 'The Last Glacial Maximum', *Science* **325**(5941), 710–714.
- Clark, P. U., Shakun, J. D., Baker, P. A., Bartlein, P. J., Brewer, S., Brook, E., Carlson, A. E., Cheng, H., Kaufman, D. S., Liu, Z., Marchitto, T. M., Mix, A. C., Morrill, C., Otto-Bliesner, B. L., Pahnke, K., Russell, J. M., Whitlock, C., Adkins, J. F., Blois, J. L., Clark, J., Colman, S. M., Curry, W. B., Flower, B. P., He, F., Johnson, T. C., Lynch-Stieglitz, J., Markgraf, V., McManus, J., Mitrovica, J. X., Moreno, P. I. & Williams, J. W. (2012), 'Global climate evolution during the last deglaciation', *Proceedings of the National Academy of Sciences* **109**(19), E1134–E1142.
- Clift, P. D., Hodges, K. V., Heslop, D., Hannigan, R., Van Long, H. & Calves, G. (2008), 'Correlation of Himalayan exhumation rates and Asian monsoon intensity', *Nature Geoscience* **1**(12), 875–880.
- Clift, P. D., Lee, J. I., Hildebrand, P., Shimizu, N., Layne, G. D., Blusztajn, J., Blum, J. D., Garzanti, E. & Khan, A. A. (2002), 'Nd and Pb isotope variability in the Indus River System: Implications for sediment provenance and crustal heterogeneity in the Western Himalaya', *Earth and Planetary Science Letters* **200**(Issues 1–2), 91–106.
- Clift, P. D., Wan, S. & Blusztajn, J. (2014), 'Reconstructing chemical weathering, physical erosion and monsoon intensity since 25Ma in the northern South China Sea: A review of competing proxies', *Earth-Science Reviews* **130**, 86–102.

- Cochran, J. K. (1992), ‘The oceanic chemistry of the uranium- and thorium-series nuclides’, *Uranium-series disequilibrium: applications to earth, marine, and environmental sciences. 2. ed.*
- Cogez, A., Meynadier, L., Allègre, C., Limmois, D., Herman, F. & Gaillardet, J. (2015), ‘Constraints on the role of tectonic and climate on erosion revealed by two time series analysis of marine cores around New Zealand’, *Earth and Planetary Science Letters* **410**, 174–185.
- Columbu, A., Chiarini, V., Waele, J. D., Drysdale, R., Woodhead, J., Hellstrom, J. & Forti, P. (2017), ‘Late quaternary speleogenesis and landscape evolution in the northern Apennine evaporite areas’, *Earth Surface Processes and Landforms* **42**(10), 1447–1459.
- Combourieu-Nebout, N., Peyron, O., Dormoy, I., Desprat, S., Célia, B., Kotthoff, U. & Marret, F. (2010), ‘West Mediterranean rapid climatic variability during the last 25 000 years from high resolution vegetation record (ODP site 976, Alboran Sea)’.
- Combourieu-Nebout, N., Turon, J. L., Zahn, R., Capotondi, L., Londeix, L. & Pahnke, K. (2002), ‘Enhanced aridity and atmospheric high-pressure stability over the western Mediterranean during the North Atlantic cold events of the past 50 k.y.’, *Geology* **30**(10), 863–866.
- Condie, K. C. (1993), ‘Chemical composition and evolution of the upper continental crust: Contrasting results from surface samples and shales’, *Chemical Geology* **104**(1), 1–37.
- Condomines, M., Gauthier, P.-J. & Sigmarsson, O. (2003), ‘Timescales of Magma Chamber Processes and Dating of Young Volcanic Rocks’, *Reviews in Mineralogy and Geochemistry* **52**(1), 125–174.
- Corenblit, D. & Steiger, J. (2009), ‘Vegetation as a major conductor of geomorphic changes on the Earth surface: Toward evolutionary geomorphology’, *Earth Surface Processes and Landforms* **34**(6), 891–896.
- Costa, A., Molnar, P., Stutenbecker, L., Bakker, M., Silva, T. A., Schlunegger, F., Lane, S. N., Loizeau, J.-L. & Girardclos, S. (2018), ‘Temperature signal in suspended sediment export from an Alpine catchment’, *Hydrology and Earth System Sciences* **22**(1), 509–528.
- Covault, J. A., Craddock, W. H., Romans, B. W., Fildani, A. & Gosai, M. (2013), ‘Spatial and Temporal Variations in Landscape Evolution: Historic and Longer-Term Sediment Flux through Global Catchments’, *The Journal of Geology* **121**(1), 35–56.

- Covault, J. A. & Graham, S. A. (2010), 'Submarine fans at all sea-level stands: Tectonomorphologic and climatic controls on terrigenous sediment delivery to the deep sea', *Geology* **38**(10), 939–942.
- Covault, J. A., Romans, B. W., Graham, S. A., Fildani, A. & Hilley, G. E. (2011), 'Terrestrial source to deep-sea sink sediment budgets at high and low sea levels: Insights from tectonically active Southern California', *Geology* **39**(7), 619–622.
- Cox, N. J. (1980), 'On the relationship between bedrock lowering and regolith thickness', *Earth Surface Processes* **5**(3), 271–274.
- Crowley, T. J. (1992), 'North Atlantic Deep Water cools the southern hemisphere', *Paleoceanography* **7**(4), 489–497.
- Culling, W. E. H. (1960), 'Analytical Theory of Erosion', *The Journal of Geology* **68**(3), 336–344.
- Cunningham, S. A., Kanzow, T., Rayner, D., Baringer, M. O., Johns, W. E., Marotzke, J., Longworth, H. R., Grant, E. M., Hirschi, J. J.-M., Beal, L. M., Meinen, C. S. & Bryden, H. L. (2007), 'Temporal Variability of the Atlantic Meridional Overturning Circulation at 26.5°N', *Science* **317**(5840), 935–938.
- Dahlkamp, F. J. (1993), 'Geology of the uranium deposits'.
- Dan, G., Sultan, N. & Savoye, B. (2007), 'The 1979 Nice harbour catastrophe revisited: Trigger mechanism inferred from geotechnical measurements and numerical modelling', *Marine Geology* **245**(1), 40–64.
- Dansgaard, W., Johnsen, S. J., Clausen, H. B., Dahl-Jensen, D., Gundestrup, N. S., Hammer, C. U., Hvidberg, C. S., Steffensen, J. P., Sveinbjörnsdottir, A. E., Jouzel, J. & Bond, G. (1993), 'Evidence for general instability of past climate from a 250-kyr ice-core record', *Nature* **364**(6434), 218–220.
- Davis, W. M. (1892), 'The convex profil of bad land divided.', *Science* **ns-20**(508), 245–245.
- Davis, W. M. (1899), 'The Geographical Cycle', *The Geographical Journal* **14**(5), 481–504.
- de Vente, J., Poesen, J., Arabkhedri, M. & Verstraeten, G. (2007), 'The sediment delivery problem revisited', *Progress in Physical Geography: Earth and Environment* **31**(2), 155–178.
- Dearing, J. A. & Jones, R. T. (2003), 'Coupling temporal and spatial dimensions of global sediment flux through lake and marine sediment records', *Global and Planetary Change* **39**(1), 147–168.

- Dearlove, J. P. L., Longworth, G., Ivanovich, M., Kim, J. I., Delakowitz, B. & Zeh, P. (1991), 'A Study of Groundwater-Colloids and their Geochemical Interactions with Natural Radionuclides in Gorleben Aquifer Systems', *Radiochimica Acta* **52-53**(1), 83–90.
- Dempster, M., Dunlop, P., Scheib, A. & Cooper, M. (2013), 'Principal component analysis of the geochemistry of soil developed on till in Northern Ireland', *Journal of Maps* **9**(3), 373–389.
- Denton, G. H. & Karlén, W. (1973), 'Holocene climatic variations—Their pattern and possible cause', *Quaternary Research* **3**(2), 155–205.
- DePaolo, D. J., Lee, V. E., Christensen, J. N. & Maher, K. (2012), 'Uranium comminution ages: Sediment transport and deposition time scales', *Comptes Rendus Geoscience* **344**(11), 678–687.
- DePaolo, D. J., Maher, K., Christensen, J. N. & McManus, J. (2006), 'Sediment transport time measured with U-series isotopes: Results from ODP North Atlantic drift site 984', *Earth and Planetary Science Letters* **248**(1), 394–410.
- Dequincey, O., Chabaux, F., Clauer, N., Liewig, N. & Muller, J.-P. (1999), 'Dating of weathering profiles by radioactive disequilibria: Contribution of the study of authigenic mineral fractions', *Comptes Rendus de l'Académie des Sciences - Series IIA - Earth and Planetary Science* **328**(10), 679–685.
- Dequincey, O., Chabaux, F., Clauer, N., Sigmarsson, O., Liewig, N. & Leprun, J. C. (2002), 'Chemical mobilizations in laterites: Evidence from trace elements and  $^{238}\text{U}$ - $^{234}\text{U}$ - $^{230}\text{Th}$  disequilibria', *Geochimica et Cosmochimica Acta* **66**(7), 1197–1210.
- Dietrich, W. E., Reiss, R., Hsu, M.-L. & Montgomery, D. R. (1995), 'A process-based model for colluvial soil depth and shallow landsliding using digital elevation data', *Hydrological Processes* **9**(3-4), 383–400.
- Dixon, J. L., Heimsath, A. M. & Amundson, R. (2009), 'The critical role of climate and saprolite weathering in landscape evolution', *Earth Surface Processes and Landforms* **34**(11), 1507–1521.
- Dixon, J. L., von Blanckenburg, F., Stüwe, K. & Christl, M. (2016), 'Glaciation's topographic control on Holocene erosion at the eastern edge of the Alps', *Earth Surface Dynamics* **4**(4), 895–909.
- Donnini, M., Marchesini, I. & Zucchini, A. (2020), 'Geo-LiM: A new geo-lithological map for Central Europe (Germany, France, Switzerland, Austria, Slovenia, and Northern

- Italy) as a tool for the estimation of atmospheric CO<sub>2</sub> consumption', *Journal of Maps* **16**(2), 43–55.
- Dosseto, A., Bourdon, B., Gaillardet, J., Allègre, C. J. & Filizola, N. (2006a), 'Time scale and conditions of weathering under tropical climate: Study of the Amazon basin with U-series', *Geochimica et Cosmochimica Acta* **70**(1), 71–89.
- Dosseto, A., Bourdon, B., Gaillardet, J., Maurice-Bourgoin, L. & Allègre, C. J. (2006b), 'Weathering and transport of sediments in the Bolivian Andes: Time constraints from uranium-series isotopes', *Earth and Planetary Science Letters* **248**(3), 759–771.
- Dosseto, A., Bourdon, B. & Turner, S. P. (2008a), 'Uranium-series isotopes in river materials: Insights into the timescales of erosion and sediment transport', *Earth and Planetary Science Letters* **265**(1), 1–17.
- Dosseto, A., Buss, H. L. & Chabaux, F. (2014), 'Age and weathering rate of sediments in small catchments: The role of hillslope erosion', *Geochimica et Cosmochimica Acta* **132**, 238–258.
- Dosseto, A., Buss, H. L. & Suresh, P. O. (2012), 'Rapid regolith formation over volcanic bedrock and implications for landscape evolution', *Earth and Planetary Science Letters* **337–338**, 47–55.
- Dosseto, A., Hesse, P. P., Maher, K., Fryirs, K. & Turner, S. (2010), 'Climatic and vegetation control on sediment dynamics during the last glacial cycle', *Geology* **38**(5), 395–398.
- Dosseto, A. & Schaller, M. (2016), 'The erosion response to Quaternary climate change quantified using uranium isotopes and in situ-produced cosmogenic nuclides', *Earth-Science Reviews* **155**, 60–81.
- Dosseto, A., Turner, S. P. & Chappell, J. (2008b), 'The evolution of weathering profiles through time: New insights from uranium-series isotopes', *Earth and Planetary Science Letters* **274**(3), 359–371.
- Dosseto, A., Vigier, N., Joannes-Boyau, R., Moffat, I., Singh, T. & Srivastava, P. (2015), 'Rapid response of silicate weathering rates to climate change in the Himalaya', *Faculty of Science, Medicine and Health - Papers: part A* pp. 10–19.
- Dou, Y., Yang, S., Shi, X., Clift, P. D., Liu, S., Liu, J., Li, C., Bi, L. & Zhao, Y. (2016), 'Provenance weathering and erosion records in southern Okinawa Trough sediments since 28ka: Geochemical and Sr–Nd–Pb isotopic evidences', *Chemical Geology* **425**, 93–109.
- Drever, J. I. (1994), 'The effect of land plants on weathering rates of silicate minerals', *Geochimica et Cosmochimica Acta* **58**(10), 2325–2332.

- Dubar, M. & Anthony, E. J. (1995), ‘Holocene Environmental Change and River-Mouth Sedimentation in the Baie des Anges, French Riviera’, *Quaternary Research* **43**(3), 329–343.
- Dupré, B., Viers, J., Dandurand, J.-L., Polve, M., Bénézech, P., Vervier, P. & Braun, J.-J. (1999), ‘Major and trace elements associated with colloids in organic-rich river waters: Ultrafiltration of natural and spiked solutions’, *Chemical Geology* **160**(1), 63–80.
- Edwards, R. L., Chen, J. & Wasserburg, G. (1986), ‘ $^{238}\text{U}$ - $^{234}\text{U}$ - $^{230}\text{Th}$ - $^{232}\text{Th}$  systematics and the precise measurement of time over the past 500,000 years’, *Earth and Planetary Science Letters* **81**(87), 175–192.
- Edwards, R. L., Gallup, C. D. & Cheng, H. (2003), ‘Uranium-series Dating of Marine and Lacustrine Carbonates’, *Reviews in Mineralogy and Geochemistry* **52**(1), 363–405.
- Egli, M., Dahms, D. & Norton, K. (2014), ‘Soil formation rates on silicate parent material in alpine environments: Different approaches—different results?’, *Geoderma* **213**, 320–333.
- Egli, M., Mirabella, A. & Sartori, G. (2008), ‘The role of climate and vegetation in weathering and clay mineral formation in late Quaternary soils of the Swiss and Italian Alps’, *Geomorphology* **102**(3), 307–324.
- Ehlers, J. & Gibbard, P. L. (2007), ‘The extent and chronology of Cenozoic Global Glaciation’, *Quaternary International* **164-165**, 6–20.
- El Bedoui, S., Guglielmi, Y., Lebourg, T. & Pérez, J.-L. (2009), ‘Deep-seated failure propagation in a fractured rock slope over 10,000 years: The La Clapière slope, the south-eastern French Alps’, *Geomorphology* **105**(3), 232–238.
- Fairbanks, R. (1989), ‘A 17,000-year glacio-eustatic sea level record: Influence of glacial melting rates on the Younger Dryas event and deep-ocean circulation’, p. 6.
- Ferrier, K. L. & Kirchner, J. W. (2008), ‘Effects of physical erosion on chemical denudation rates: A numerical modeling study of soil-mantled hillslopes’, *Earth and Planetary Science Letters* **272**(3), 591–599.
- Fierens, R., Droz, L., Toucanne, S., Raison, F., Jouet, G., Babonneau, N., Miramontes, E., Landurain, S. & Jorry, S. J. (2019), ‘Late Quaternary geomorphology and sedimentary processes in the Zambezi turbidite system (Mozambique Channel)’, *Geomorphology* **334**, 1–28.
- Fleischer, R. L. (1980), ‘Isotopic Disequilibrium of Uranium: Alpha-Recoil Damage and Preferential Solution Effects’, *Science* **207**(4434), 979–981.

- Fleischer, R. L. (1982), 'Nature of alpha-recoil damage: Evidence from preferential solution effects', *Nuclear Tracks and Radiation Measurements (1982)* **6**(1), 35–42.
- Fleischer, R. L. (1988), 'Alpha-recoil damage: Relation to isotopic disequilibrium and leaching of radionuclides', *Geochimica et Cosmochimica Acta* **52**(6), 1459–1466.
- Fleischer, R. L. & Raabe, O. G. (1978), 'Recoiling alpha-emitting nuclei. Mechanisms for uranium-series disequilibrium', *Geochimica et Cosmochimica Acta* **42**(7), 973–978.
- Fletcher, W. J. & Goñi, M. F. S. (2008), 'Orbital- and sub-orbital-scale climate impacts on vegetation of the western Mediterranean basin over the last 48,000 yr', *Quaternary Research* **70**(3), 451–464.
- Fletcher, W. J., Sánchez Goñi, M. F., Allen, J. R. M., Cheddadi, R., Combourieu-Nebout, N., Huntley, B., Lawson, I., Londeix, L., Magri, D., Margari, V., Müller, U. C., Naughton, F., Novenko, E., Roucoux, K. & Tzedakis, P. C. (2010a), 'Millennial-scale variability during the last glacial in vegetation records from Europe', *Quaternary Science Reviews* **29**(21), 2839–2864.
- Fletcher, W. J., Sanchez Goñi, M. F., Peyron, O. & Dormoy, I. (2010b), 'Abrupt climate changes of the last deglaciation detected in a Western Mediterranean forest record', *Climate of the Past* **6**(2), 245–264.
- Foster, G. L. & Vance, D. (2006), 'Negligible glacial–interglacial variation in continental chemical weathering rates', *Nature* **444**(7121), 918–921.
- Francke, A., Carney, S., Wilcox, P. & Dosseto, A. (2018), 'Sample preparation for determination of comminution ages in lacustrine and marine sediments', *Chemical Geology* **479**, 123–135.
- Francke, A., Dosseto, A., Just, J., Wagner, B. & Jones, B. G. (2020), 'Assessment of the controls on (234U/238U) activity ratios recorded in detrital lacustrine sediments', *Chemical Geology* **550**, 119698.
- Francke, A., Dosseto, A., Panagiotopoulos, K., Leicher, N., Lacey, J. H., Kyriakou, S., Wagner, B., Zanchetta, G., Kouli, K. & Leng, M. J. (2019), 'Sediment residence time reveals Holocene shift from climatic to vegetation control on catchment erosion in the Balkans', *Global and Planetary Change* **177**, 186–200.
- Frenzel, B. (n.d.), 'Über einen frühen letzteiszeitlichen Vorstoß des Rheingletschers in das deutsche Alpenvorland', p. 24.
- Freslon, N., Bayon, G., Toucanne, S., Bermell, S., Bollinger, C., Chéron, S., Etoubleau, J., Germain, Y., Khripounoff, A., Ponzevera, E. & Rouget, M.-L. (2014), 'Rare earth

- elements and neodymium isotopes in sedimentary organic matter', *Geochimica et Cosmochimica Acta* **140**, 177–198.
- Gabet, E. J. (2000), 'Gopher bioturbation: Field evidence for non-linear hillslope diffusion', *Earth Surface Processes and Landforms* **25**(13), 1419–1428.
- Gaillardet, J., Dupre, B., Allegre, C. J. & Négrel, P. (1997), 'Chemical and physical denudation in the Amazon River Basin', *Chemical Geology* **142**(3), 141–173.
- Gaillardet, J., Dupré, B., Louvat, P. & Allègre, C. J. (1999), 'Global silicate weathering and CO<sub>2</sub> consumption rates deduced from the chemistry of large rivers', *Chemical Geology* **159**(1), 3–30.
- Gasse, F. (2000), 'Hydrological changes in the African tropics since the Last Glacial Maximum', *Quaternary Science Reviews* **19**(1), 189–211.
- Genty, D., Blamart, D., Ouahdi, R., Gilmour, M., Baker, A., Jouzel, J. & Van-Exter, S. (2003), 'Precise dating of Dansgaard–Oeschger climate oscillations in western Europe from stalagmite data', *Nature* **421**(6925), 833–837.
- Gilbert, G. K. (1877), 'Report on the Geology of the Henry Mountains.'
- Gilbert, G. K. (1909), 'The Convexity of Hilltops', *The Journal of Geology* **17**(4), 344–350.
- Godard, V., Ollivier, V., Bellier, O., Miramont, C., Shabanian, E., Fleury, J., Benedetti, L. & Guillou, V. (2016), 'Weathering-limited hillslope evolution in carbonate landscapes', *Earth and Planetary Science Letters* **446**, 10–20.
- Goldstein, S. J. & Jacobsen, S. B. (1987), 'The Nd and Sr isotopic systematics of river-water dissolved material: Implications for the sources of Nd and Sr in seawater', *Chemical Geology: Isotope Geoscience section* **66**(3), 245–272.
- Goldstein, S. L. & Hemming, S. R. (2003), 'Long-lived Isotopic Tracers in Oceanography, Paleoceanography, and Ice-sheet Dynamics', *Treatise on Geochemistry* **6**, 625.
- Goldstein, S. L., O'Nions, R. K. & Hamilton, P. J. (1984), 'A Sm-Nd isotopic study of atmospheric dusts and particulates from major river systems', *Earth and Planetary Science Letters* **70**(2), 221–236.
- Granet, M., Chabaux, F., Stille, P., Dosseto, A., France-Lanord, C. & Blaes, E. (2010), 'U-series disequilibria in suspended river sediments and implication for sediment transfer time in alluvial plains: The case of the Himalayan rivers', *Geochimica et Cosmochimica Acta* **74**(10), 2851–2865.

- Granet, M., Chabaux, F., Stille, P., France-Lanord, C. & Pelt, E. (2007), 'Time-scales of sedimentary transfer and weathering processes from U-series nuclides: Clues from the Himalayan rivers', *Earth and Planetary Science Letters* **261**(3), 389–406.
- Guillevic, M., Bazin, L., Landais, A., Kindler, P., Orsi, A., Masson-Delmotte, V., Blunier, T., Buchardt, S. L., Capron, E., Leuenberger, M., Martinerie, P., Prié, F. & Vinther, B. M. (2013), 'Spatial gradients of temperature, accumulation and delta18O-ice in Greenland over a series of Dansgaard-Oeschger events', *Climate of the past* **9**(3), 1029–1051.
- Hallet, B., Hunter, L. & Bogen, J. (1996), 'Rates of erosion and sediment evacuation by glaciers: A review of field data and their implications', *Global and Planetary Change* **12**(1-4), 213–235.
- Handley, H. K., Turner, S., Afonso, J. C., Dosseto, A. & Cohen, T. (2013a), 'Sediment residence times constrained by uranium-series isotopes: A critical appraisal of the comminution approach', *Geochimica et Cosmochimica Acta* **103**, 245–262.
- Handley, H. K., Turner, S. P., Dosseto, A., Haberlah, D. & Afonso, J. C. (2013b), 'Considerations for U-series dating of sediments: Insights from the Flinders Ranges, South Australia', *Chemical Geology* **340**, 40–48.
- Harnois, L. (1988), 'The CIW index: A new chemical index of weathering', *Sedimentary Geology* **55**, 319–322.
- Harvey, A. M. (2002), 'Effective timescales of coupling within fluvial systems', *Geomorphology* **44**(3), 175–201.
- Hashimoto, T., Aoyagi, Y., Kudo, H. & Sotobayashi, T. (1985), 'Range calculation of alpha-recoil atoms in some minerals using LSS-theory', *Journal of Radioanalytical and Nuclear Chemistry* **90**(2), 415–438.
- Hawkesworth, C. J., Turner, S. P., McDermott, F., Peate, D. W. & van Calsteren, P. (1997), 'U-Th Isotopes in Arc Magmas: Implications for Element Transfer from the Subducted Crust', *Science* **276**(5312), 551–555.
- Hayes, A., Kucera, M., Kallel, N., Saffi, L. & Rohling, E. J. (2005), 'Glacial Mediterranean sea surface temperatures based on planktonic foraminiferal assemblages', *Quaternary Science Reviews* **24**(7), 999–1016.
- Heimsath, A. M., Chappell, J., Dietrich, W. E., Nishiizumi, K. & Finkel, R. C. (2000), 'Soil production on a retreating escarpment in southeastern Australia', *Geology* **28**(9), 787–790.

- Heimsath, A. M., Chappell, J., Dietrich, W. E., Nishiizumi, K. & Finkel, R. C. (2001a), ‘Late Quaternary erosion in southeastern Australia: A field example using cosmogenic nuclides’, *Quaternary International* **83-85**, 169–185.
- Heimsath, A. M., Dietrich, W. E., Nishiizumi, K. & Finkel, R. C. (1997), ‘The soil production function and landscape equilibrium’, *Nature* **388**(6640), 358–361.
- Heimsath, A. M., Dietrich, W. E., Nishiizumi, K. & Finkel, R. C. (2001b), ‘Stochastic processes of soil production and transport: Erosion rates, topographic variation and cosmogenic nuclides in the Oregon Coast Range’, *Earth Surface Processes and Landforms* **26**(5), 531–552.
- Heimsath, A. M., Dietrich, W., Nishiizumi, K. & Finkel, R. C. (1999), ‘Cosmogenic nuclides, topography, and the spatial variation of soil depth’, *Geomorphology* **27**(1), 151–172.
- Heimsath, A. M., Furbish, D. J. & Dietrich, W. E. (2005), ‘The illusion of diffusion: Field evidence for depth-dependent sediment transport’, *Geology* **33**(12), 949–952.
- Heinrich, H. (1988), ‘Origin and consequences of cyclic ice rafting in the Northeast Atlantic Ocean during the past 130,000 years’, *Quaternary Research* **29**(2), 142–152.
- Helgeson, H. C., Murphy, W. M. & Aagaard, P. (1984), ‘Thermodynamic and kinetic constraints on reaction rates among minerals and aqueous solutions. II. Rate constants, effective surface area, and the hydrolysis of feldspar’, *Geochimica et Cosmochimica Acta* **48**(12), 2405–2432.
- Henderson, G. M. & Anderson, R. F. (2003), ‘The U-series Toolbox for Paleoceanography’, *Reviews in Mineralogy and Geochemistry* **52**(1), 493–531.
- Hengl, T., Mendes de Jesus, J., Heuvelink, G. B. M., Ruiperez Gonzalez, M., Kilibarda, M., Blagotić, A., Shangguan, W., Wright, M. N., Geng, X., Bauer-Marschallinger, B., Guevara, M. A., Vargas, R., MacMillan, R. A., Batjes, N. H., Leenaars, J. G. B., Ribeiro, E., Wheeler, I., Mantel, S. & Kempen, B. (2017), ‘SoilGrids250m: Global gridded soil information based on machine learning’, *PLOS ONE* **12**(2), e0169748.
- Herman, F. & Champagnac, J.-D. (2016), ‘Plio-Pleistocene increase of erosion rates in mountain belts in response to climate change’, *Terra Nova* **28**(1), 2–10.
- Hinderer, M. (2001), ‘Late Quaternary denudation of the Alps, valley and lake fillings and modern river loads’, *Geodinamica Acta* **14**(4), 231–263.

- Hippe, K., Kober, F., Zeilinger, G., Ivy-Ochs, S., Maden, C., Wacker, L., Kubik, P. W. & Wieler, R. (2012), 'Quantifying denudation rates and sediment storage on the eastern Altiplano, Bolivia, using cosmogenic  $^{10}\text{Be}$ ,  $^{26}\text{Al}$ , and in situ  $^{14}\text{C}$ ', *Geomorphology* **179**, 58–70.
- Holland, H. D. (1978), 'Weathering and other near-surface reactions.'
- Holmgren, K., Lee-Thorp, J. A., Cooper, G. R. J., Lundblad, K., Partridge, T. C., Scott, L., Sithaldeen, R., Siep Talma, A. & Tyson, P. D. (2003), 'Persistent millennial-scale climatic variability over the past 25,000 years in Southern Africa', *Quaternary Science Reviews* **22**(21), 2311–2326.
- Hovius, N. (1998), 'Controls on Sediment Supply by Large Rivers.'
- Hovius, N., Stark, C. P. & Allen, P. A. (1997), 'Sediment flux from a mountain belt derived by landslide mapping', *Geology* **25**(3), 231–234.
- Howard, A. D. (1997), 'Badland Morphology and Evolution: Interpretation Using a Simulation Model', *Earth Surface Processes and Landforms* **22**(3), 211–227.
- Hsi, C.-k. D. & Langmuir, D. (1985), 'Adsorption of uranyl onto ferric oxyhydroxides: Application of the surface complexation site-binding model', *Geochimica et Cosmochimica Acta* **49**(9), 1931–1941.
- Huber, C., Leuenberger, M., Spahni, R., Flückiger, J., Schwander, J., Stocker, T. F., Johnsen, S., Landais, A. & Jouzel, J. (2006), 'Isotope calibrated Greenland temperature record over Marine Isotope Stage 3 and its relation to  $\text{CH}_4$ ', *Earth and Planetary Science Letters* **243**(3), 504–519.
- Humphreys, G. S. & Wilkinson, M. T. (2007), 'The soil production function: A brief history and its rediscovery', *Geoderma* **139**(1), 73–78.
- Ivory, S. J., McGlue, M. M., Ellis, G. S., Lézine, A.-M., Cohen, A. S. & Vincens, A. (2014), 'Vegetation Controls on Weathering Intensity during the Last Deglacial Transition in Southeast Africa', *PLOS ONE* **9**(11), e112855.
- Ivy-Ochs, S., Kerschner, H., Reuther, A., Preusser, F., Heine, K., Maisch, M., Kubik, P. W. & Schlüchter, C. (2008), 'Chronology of the last glacial cycle in the European Alps', *Journal of Quaternary Science* **23**(6-7), 559–573.
- Ivy-Ochs, S., Schäfer, J., Kubik, P. W., Synal, H.-A. & Schlüchter, C. (2004), 'Timing of deglaciation on the northern Alpine foreland (Switzerland)', *Eclogae Geologicae Helveticae* **97**(1), 47–55.

- Jackson, M. L. & Sherman, G. D. (1953), Chemical Weathering of Minerals in Soils, *in* A. G. Norman, ed., ‘Advances in Agronomy’, Vol. 5, Academic Press, pp. 219–318.
- Jaffey, A. H., Flynn, K. F., Glendenin, L. E., Bentley, W. C. & Essling, A. M. (1971), ‘Precision Measurement of Half-Lives and Specific Activities of  $^{235}\text{U}$  and  $^{238}\text{U}$ ’, *Physical Review C* **4**(5), 1889–1906.
- Jalali, B., Sicre, M.-A., Klein, V., Schmidt, S., Maselli, V., Lirer, F., Bassetti, M.-A., Toucanne, S., Jorry, S. J., Insinga, D. D., Petrosino, P. & Châles, F. (2018), ‘Deltaic and Coastal Sediments as Recorders of Mediterranean Regional Climate and Human Impact Over the Past Three Millennia’, *Paleoceanography and Paleoclimatology* **33**(6), 579–593.
- Jerolmack, D. J. & Paola, C. (2010), ‘Shredding of environmental signals by sediment transport’, *Geophysical Research Letters* **37**(19).
- Johnsen, S. J., Clausen, H. B., Dansgaard, W., Fuhrer, K., Gundestrup, N., Hammer, C. U., Iversen, P., Jouzel, J., Stauffer, B. & Steffensen, J. P. (1992), ‘Irregular glacial interstadials recorded in a new Greenland ice core’, *Nature* **359**(6393), 311–313.
- Johnsson, M. J. & Basu, A. (1993), *Processes Controlling the Composition of Clastic Sediments*, Geological Society of America.
- Jorda, M., Rosique, T. & Évin, J. (2000), ‘Données nouvelles sur l’âge du dernier maximum glaciaire dans les Alpes méridionales françaises’, *Comptes Rendus de l’Académie des Sciences - Series IIA - Earth and Planetary Science* **331**(3), 187–193.
- Jorry, S. J., Jégou, I., Emmanuel, L., Silva Jacinto, R. & Savoye, B. (2011), ‘Turbiditic levee deposition in response to climate changes: The Var Sedimentary Ridge (Ligurian Sea)’, *Marine Geology* **279**(1), 148–161.
- Juilleret, J., Dondeyne, S. & Hissler, C. (2014), *What about the Regolith, the Saprolite and the Bedrock? Proposals for Classifying the Subsolium in WRB*.
- Julian, M. (1977), ‘Une carte géomorphologique des Alpes Maritimes franco-italiennes au 1/200 000e en couleurs. Présentation succincte’, *Méditerranée* **28**(1), 45–53.
- Julian, M. & Anthony, E. (1996), ‘Aspects of landslide activity in the Mercantour Massif and the French Riviera, southeastern France’, *Geomorphology* **15**(3), 275–289.
- Kerckhove, C. & Montjuvent, G. (1979), ‘Carte géologique de la France à 1/250 000. Feuille de Gap (35).’.
- Kigoshi, K. (1971), ‘Alpha-Recoil Thorium-234: Dissolution into Water and the Uranium-234/Uranium-238 Disequilibrium in Nature’, *Science* **173**(3991), 47–48.

- Kindler, P., Guillevic, M., Baumgartner, M. F., Schwander, J., Landais, A. & Leuenberger, M. (2014), 'Temperature reconstruction from 10 to 120 kyr b2k from the NGRIP ice core', *Climate of the past* **10**(2), 887–902.
- Kirkby, M. J. (1971), 'Hillslope process-response models based on the continuity equation.', *Institute of British Geographers Special Publication* **3**, 15–30.
- Kirkby, M. J. (1976), 'Deterministic continuous slope models.', *Z. Geomorphol. Suppl.* **25**, 1–19.
- Kober, F., Ivy-Ochs, S., Schlunegger, F., Baur, H., Kubik, P. W. & Wieler, R. (2007), 'Denudation rates and a topography-driven rainfall threshold in northern Chile: Multiple cosmogenic nuclide data and sediment yield budgets', *Geomorphology* **83**(1), 97–120.
- Kolodny, Y., Torfstein, A., Weiss-Sarusi, K., Zakon, Y. & Halicz, L. (2017), '238U-235U-234U fractionation between tetravalent and hexavalent uranium in seafloor phosphorites', *Chemical Geology* **451**, 1–8.
- Koppes, M. N. & Montgomery, D. R. (2009), 'The relative efficacy of fluvial and glacial erosion over modern to orogenic timescales', *Nature Geoscience* **2**(9), 644–647.
- Kronfeld, J., Godfrey-Smith, D. I., Johannessen, D. & Zentilli, M. (2004), 'Uranium series isotopes in the Avon Valley, Nova Scotia', *Journal of Environmental Radioactivity* **73**(3), 335–352.
- Kuhlemann, J., Frisch, W., Székely, B., Dunkl, I. & Kázmér, M. (2002), 'Post-collisional sediment budget history of the Alps: Tectonic versus climatic control', *International Journal of Earth Sciences* **91**(5), 818–837.
- Lambeck, K. & Chappell, J. (2001), 'Sea Level Change Through the Last Glacial Cycle', *Science* **292**(5517), 679–686.
- Landais, A., Barnola, J. M., Masson-Delmotte, V., Jouzel, J., Chappellaz, J., Caillon, N., Huber, C., Leuenberger, M. & Johnsen, S. J. (2004), 'A continuous record of temperature evolution over a sequence of Dansgaard-Oeschger events during Marine Isotopic Stage 4 (76 to 62 kyr BP)', *Geophysical Research Letters* **31**(22).
- Landais, A., Masson-Delmotte, V., Jouzel, J., Raynaud, D., Johnsen, S., Huber, C., Leuenberger, M., Schwander, J. & Minster, B. (2006), 'The glacial inception as recorded in the NorthGRIP Greenland ice core: Timing, structure and associated abrupt temperature', *Climate Dynamics* **26**(2-3), 273 à 284.
- Landstroem, O. & Tullborg, E.-L. (2001), Effects of glacial/post-glacial weathering compared with hydrothermal alteration - implications for matrix diffusion. Results from

- drillcore studies in porphyritic quartz monzodiorite from Aespoe SE Sweden, Technical Report SKB-R-01-37, Swedish Nuclear Fuel and Waste Management Co.
- Lane, P., Donnelly, J. P., Woodruff, J. D. & Hawkes, A. D. (2011), ‘A decadal-resolved paleohurricane record archived in the late Holocene sediments of a Florida sinkhole’, *Marine Geology* **287**(1), 14–30.
- Langmuir, D. (1978), ‘Uranium solution-mineral equilibria at low temperatures with applications to sedimentary ore deposits’, *Geochimica et Cosmochimica Acta* **42**(6, Part A), 547–569.
- Langmuir, D. & Herman, J. S. (1980), ‘The mobility of thorium in natural waters at low temperatures’, *Geochimica et Cosmochimica Acta* **44**(11), 1753–1766.
- Langmuir, I. (1918), ‘The adsorption of gases on planes surfaces of glass, mica, and platinum.’, *Journal of the American Chemical Society* **40**(9), 1361–1403.
- Larsen, I. J. & Montgomery, D. R. (2012), ‘Landslide erosion coupled to tectonics and river incision’, *Nature Geoscience* **5**(7), 468–473.
- Latham, A. G. & Schwarcz, H. P. (1987), ‘On the possibility of determining rates of removal of uranium from crystalline igneous rocks using U-series disequilibria—1: A U-leach model, and its applicability to whole-rock data’, *Applied Geochemistry* **2**(1), 55–65.
- Lee, S. Y. & Baik, M. H. (2009), ‘Uranium and other trace elements’ distribution in Korean granite: Implications for the influence of iron oxides on uranium migration - ProQuest’, **31**(3), 413–420.
- Lee, V. E. (2009), Radiogenic Isotope Geochemistry and the Evolution of the Earth’s Surface and Interior, PhD thesis, University of California, Berkeley.
- Lee, V. E., DePaolo, D. J. & Christensen, J. N. (2010), ‘Uranium-series comminution ages of continental sediments: Case study of a Pleistocene alluvial fan’, *Earth and Planetary Science Letters* **296**(3), 244–254.
- Lefort, O. (2008), ‘ESSDIV cruise, Pourquoi pas ? R/V’.
- Lerman, A. (1988), Weathering Rates and Major Transport Processes an Introduction, *in* A. Lerman & M. Meybeck, eds, ‘Physical and Chemical Weathering in Geochemical Cycles’, NATO ASI Series, Springer Netherlands, Dordrecht, pp. 1–10.
- Lewis, S. L. & Maslin, M. A. (2015), ‘Defining the Anthropocene’, *Nature* **519**(7542), 171–180.

- Li, C., Francois, R., Yang, S., Barling, J., Darfeuil, S., Luo, Y. & Weis, D. (2016a), ‘Constraining the transport time of lithogenic sediments to the Okinawa Trough (East China Sea)’, *Chemical Geology* **445**, 199–207.
- Li, C., Yang, S., Zhao, J.-x., Dosseto, A., Bi, L. & Clark, T. R. (2016b), ‘The time scale of river sediment source-to-sink processes in East Asia’, *Chemical Geology* **446**, 138–146.
- Li, L., Liu, X., Li, T., Li, L., Zhao, L., Ji, J., Chen, J. & Li, G. (2017), ‘Uranium comminution age tested by the eolian deposits on the Chinese Loess Plateau’, *Earth and Planetary Science Letters* **467**, 64–71.
- Lin, G.-W., Chen, H., Hovius, N., Horng, M.-J., Dadson, S., Meunier, P. & Lines, M. (2008), ‘Effects of earthquake and cyclone sequencing on landsliding and fluvial sediment transfer in a mountain catchment’, *Earth Surface Processes and Landforms* **33**(9), 1354–1373.
- Liu, Z., Zhu, J., Rosenthal, Y., Zhang, X., Otto-Bliesner, B. L., Timmermann, A., Smith, R. S., Lohmann, G., Zheng, W. & Timm, O. E. (2014), ‘The Holocene temperature conundrum’, *Proceedings of the National Academy of Sciences* **111**(34), E3501–E3505.
- Löbmann, M. T., Geitner, C., Wellstein, C. & Zerbe, S. (2020), ‘The influence of herbaceous vegetation on slope stability – A review’, *Earth-Science Reviews* **209**, 103328.
- Lucas, Y. (2001), ‘The Role of Plants in Controlling Rates and Products of Weathering: Importance of Biological Pumping’, *Annual Review of Earth and Planetary Sciences* **29**(1), 135–163.
- Luo, S., Ku, T.-L., Roback, R., Murrell, M. & McLing, T. L. (2000), ‘In-situ radionuclide transport and preferential groundwater flows at INEEL (Idaho): Decay-series disequilibrium studies’, *Geochimica et Cosmochimica Acta* **64**(5), 867–881.
- Lupker, M., Blard, P.-H., Lavé, J., France-Lanord, C., Leanni, L., Puchol, N., Charreau, J. & Bourlès, D. (2012), ‘<sup>10</sup>Be-derived Himalayan denudation rates and sediment budgets in the Ganga basin’, *Earth and Planetary Science Letters* **333–334**, 146–156.
- Ma, L., Chabaux, F., Pelt, E., Blaes, E., Jin, L. & Brantley, S. (2010), ‘Regolith production rates calculated with uranium-series isotopes at Susquehanna/Shale Hills Critical Zone Observatory’, *Earth and Planetary Science Letters* **297**(1), 211–225.
- Macklin, M. G., Lewin, J. & Woodward, J. C. (2012), ‘The fluvial record of climate change’, *Philosophical Transactions of the Royal Society A: Mathematical, Physical and Engineering Sciences* **370**(1966), 2143–2172.

- Magny, M. (2004), 'Fluctuations du niveau des lacs dans le Jura, les Préalpes françaises du Nord et le Plateau suisse, et variabilité du climat pendant l'Holocène', *Méditerranée* **102**(1), 61–70.
- Maher, K., DePaolo, D. J. & Lin, J. C.-F. (2004), 'Rates of silicate dissolution in deep-sea sediment: In situ measurement using  $^{234}\text{U}/^{238}\text{U}$  of pore fluids', *Geochimica et Cosmochimica Acta* **68**(22), 4629–4648.
- Maher, K., Steefel, C. I., DePaolo, D. J. & Viani, B. E. (2006), 'The mineral dissolution rate conundrum: Insights from reactive transport modeling of U isotopes and pore fluid chemistry in marine sediments', *Geochimica et Cosmochimica Acta* **70**(2), 337–363.
- Mahowald, N., Kohfeld, K., Hansson, M., Balkanski, Y., Harrison, S. P., Prentice, I. C., Schulz, M. & Rodhe, H. (1999), 'Dust sources and deposition during the last glacial maximum and current climate: A comparison of model results with paleodata from ice cores and marine sediments', *Journal of Geophysical Research: Atmospheres* **104**(D13), 15895–15916.
- Marc, O., Hovius, N., Meunier, P., Uchida, T. & Hayashi, S. (2015), 'Transient changes of landslide rates after earthquakes', *Geology* **43**(10), 883–886.
- Marcott, S. A., Shakun, J. D., Clark, P. U. & Mix, A. C. (2013), 'A Reconstruction of Regional and Global Temperature for the Past 11,300 Years', *Science* **339**(6124), 1198–1201.
- Mariotti, A. (2020), Impact du dernier cycle glaciaire interglaciaire sur la dénudation dans les Alpes Maritimes Françaises, PhD thesis, Université de Lorraine.
- Mariotti, A., Blard, P.-H., Charreau, J., Petit, C., Molliex, S. & Bourles, D. (2019), 'Denudation systematics inferred from in situ cosmogenic  $^{10}\text{Be}$  concentrations in fine (50-100 Mm) and medium (100-250 Mm) sediments of the Var River basin, southern French Alps', *Earth Surface Dynamics* **7**(4), 1059–1074.
- Mariotti, A., Blard, P.-H., Charreau, J., Toucanne, S., Jorry, S. J., Molliex, S., Bourlès, D. L., Aumaître, G. & Keddadouche, K. (2021), 'Nonlinear forcing of climate on mountain denudation during glaciations', *Nature Geoscience* **14**(1), 16–22.
- Martin, A. N., Dosseto, A. & Kinsley, L. P. J. (2015), 'Evaluating the removal of non-detrital matter from soils and sediment using uranium isotopes', *Chemical Geology* **396**, 124–133.
- Martin, A. N., Dosseto, A., May, J.-H., Jansen, J. D., Kinsley, L. P. J. & Chivas, A. R. (2019), 'Sediment residence times in catchments draining to the Gulf of Carpentaria,

- northern Australia, inferred by uranium comminution dating', *Geochimica et Cosmochimica Acta* **244**, 264–291.
- Martrat, B., Grimalt, J. O., Lopez-Martinez, C., Cacho, I., Sierro, F. J., Flores, J. A., Zahn, R., Canals, M., Curtis, J. H. & Hodell, D. A. (2004), 'Abrupt Temperature Changes in the Western Mediterranean over the Past 250,000 Years', *Science* **306**(5702), 1762–1765.
- Mas, V., Mulder, T., Dennielou, B., Schmidt, S., Khripounoff, A. & Savoye, B. (2010), 'Multiscale spatio-temporal variability of sedimentary deposits in the Var turbidite system (North-Western Mediterranean Sea)', *Marine Geology* **275**(1), 37–52.
- Mathieu, D., Bernat, M. & Nahon, D. (1995), 'Short-lived U and Th isotope distribution in a tropical laterite derived from granite (Pitinga river basin, Amazonia, Brazil): Application to assessment of weathering rate', *Earth and Planetary Science Letters* **136**(3-4), 703–714.
- Mayewski, P. A., Rohling, E. E., Curt Stager, J., Karlén, W., Maasch, K. A., David Meeker, L., Meyerson, E. A., Gasse, F., van Kreveld, S., Holmgren, K., Lee-Thorp, J., Rosqvist, G., Rack, F., Staubwasser, M., Schneider, R. R. & Steig, E. J. (2004), 'Holocene climate variability', *Quaternary Research* **62**(3), 243–255.
- McKean, J. A., Dietrich, W. E., Finkel, R. C., Southon, J. R. & Caffee, M. W. (1993), 'Quantification of soil production and downslope creep rates from cosmogenic  $^{10}\text{Be}$  accumulations on a hillslope profile', *Geology* **21**(4), 343–346.
- McKenzie, D. (1985), ' $^{230}\text{Th}/^{238}\text{U}$  disequilibrium and the melting processes beneath ridge axes', *Earth and Planetary Science Letters* **72**(2), 149–157.
- McLennan, S. M. (2001), 'Relationships between the trace element composition of sedimentary rocks and upper continental crust', *Geochemistry, Geophysics, Geosystems* **2**(4).
- Megumi, K. & Mamuro, T. (1977), 'Concentration of uranium series nuclides in soil particles in relation to their size', *Journal of Geophysical Research (1896-1977)* **82**(2), 353–356.
- Mesolella, K. J., Matthews, R. K., Broecker, W. S. & Thurber, D. L. (1969), 'The Astronomical Theory of Climatic Change: Barbados Data', *The Journal of Geology* **77**(3), 250–274.
- Meybeck, M. (1987), 'Global chemical weathering of surficial rocks estimated from river dissolved loads', *American Journal of Science* **287**(5), 401–428.

- Migeon, S., Mulder, T., Savoye, B. & Sage, F. (2012), 'Hydrodynamic processes, velocity structure and stratification in natural turbidity currents: Results inferred from field data in the Var Turbidite System', *Sedimentary Geology* **245-246**, 48–62.
- Migeon, S., Savoye, B., Zanella, E., Mulder, T., Faugères, J. C. & Weber, O. (2001), 'Detailed seismic-reflection and sedimentary study of turbidite sediment waves on the Var Sedimentary Ridge (SE France): Significance for sediment transport and deposition and for the mechanisms of sediment-wave construction', *Marine and Petroleum Geology* **18**(2), 179–208.
- Milliman, J. D. & Farnsworth, K. L. (2013), *River Discharge to the Coastal Ocean: A Global Synthesis*, Cambridge University Press.
- Milliman, J. D., Lin, S. W., Kao, S. J., Liu, J. P., Liu, C. S., Chiu, J. K. & Lin, Y. C. (2007), 'Short-term changes in seafloor character due to flood-derived hyperpycnal discharge: Typhoon Mindulle, Taiwan, July 2004', *Geology* **35**(9), 779–782.
- Milliman, J. D. & Meade, R. H. (1983), 'World-Wide Delivery of River Sediment to the Oceans', *The Journal of Geology* **91**(1), 1–21.
- Milliman, J. D. & Syvitski, J. P. M. (1992), 'Geomorphic/Tectonic Control of Sediment Discharge to the Ocean: The Importance of Small Mountainous Rivers', *The Journal of Geology* **100**(5), 525–544.
- Millot, R., Gaillardet, J., Dupré, B. & Allègre, C. J. (2002), 'The global control of silicate weathering rates and the coupling with physical erosion: New insights from rivers of the Canadian Shield', *Earth and Planetary Science Letters* **196**(1), 83–98.
- Minasny, B. & McBratney, A. B. (2006), 'Mechanistic soil–landscape modelling as an approach to developing pedogenetic classifications', *Geoderma* **133**(1), 138–149.
- Miramontes, E., Penven, P., Fierens, R., Droz, L., Toucanne, S., Jorry, S. J., Jouet, G., Pastor, L., Silva Jacinto, R., Gaillot, A., Giraudeau, J. & Raison, F. (2019), 'The influence of bottom currents on the Zambezi Valley morphology (Mozambique Channel, SW Indian Ocean): In situ current observations and hydrodynamic modelling', *Marine Geology* **410**, 42–55.
- Molina, A., Govers, G., Cisneros, F. & Vanacker, V. (2009), 'Vegetation and topographic controls on sediment deposition and storage on gully beds in a degraded mountain area', *Earth Surface Processes and Landforms* **34**(6), 755–767.
- Molnar, P. & England, P. (1990), 'Late Cenozoic uplift of mountain ranges and global climate change: Chicken or egg?', *Nature* **346**(6279), 29–34.

- Monaghan, M. C., McKean, J., Dietrich, W. & Klein, J. (1992), '10Be chronometry of bedrock-to-soil conversion rates', *Earth and Planetary Science Letters* **111**(2), 483–492.
- Monegato, G., Ravazzi, C., Donegana, M., Pini, R., Calderoni, G. & Wick, L. (2007), 'Evidence of a two-fold glacial advance during the last glacial maximum in the Tagliamento end moraine system (eastern Alps)', *Quaternary Research* **68**(2), 284–302.
- Montgomery, D. R. & Brandon, M. T. (2002), 'Topographic controls on erosion rates in tectonically active mountain ranges', *Earth and Planetary Science Letters* **201**(3), 481–489.
- Montgomery, D. R. & Dietrich, W. E. (1995), 'Hydrologic Processes in a Low-Gradient Source Area', *Water Resources Research* **31**(1), 1–10.
- Moore, G. W. K., Renfrew, I. A. & Pickart, R. S. (2012), 'Spatial distribution of air-sea heat fluxes over the sub-polar North Atlantic Ocean', *Geophysical Research Letters* **39**(18).
- Moreira-Nordemann, L. M. (1980), 'Use of  $^{234}\text{U}/^{238}\text{U}$  disequilibrium in measuring chemical weathering rate of rocks', [http://dx.doi.org/10.1016/0016-7037\(80\)90180-5](http://dx.doi.org/10.1016/0016-7037(80)90180-5).
- Muhs, D. R., Kennedy, G. L. & Rockwell, T. K. (1994), 'Uranium-Series Ages of Marine Terrace Corals from the Pacific Coast of North America and Implications for Last-Interglacial Sea Level History', *Quaternary Research* **42**(1), 72–87.
- Mulder, T., Migeon, S., Savoye, B. & Faugeres J.-C. (2001), 'Inversely graded turbidite sequences in the deep Mediterranean: A record of deposits from flood-generated turbidity currents?', *Geo-Marine Letters* **21**(2).
- Mulder, T., Savoye, B., Piper, D. J. W. & Syvitski, J. P. M. (1998), 'The Var submarine sedimentary system: Understanding Holocene sediment delivery processes and their importance to the geological record', *Geological Society, London, Special Publications* **129**(1), 145–166.
- Mulder, T., Savoye, B. & Syvitski, J. P. M. (1997), 'Numerical modelling of a mid-sized gravity flow: The 1979 Nice turbidity current (dynamics, processes, sediment budget and seafloor impact)', *Sedimentology* **44**(2), 305–326.
- Murphy, W. M. & Shock, E. L. (1999), 'Environmental aqueous geochemistry of actinides', *Reviews in Mineralogy and Geochemistry* **38**, 221–253.
- Muto, T. & Steel, R. J. (1992), 'Retreat of the front in a prograding delta', *Geology* **20**(11), 967–970.

- National Research Council Committee on Basic Research Opportunities in the Earth Sciences (2001), *Basic Research Opportunities in Earth Sciences*, National Academies Press, Washington, DC.
- Négrel, P., Allègre, C. J., Dupré, B. & Lewin, E. (1993), ‘Erosion sources determined by inversion of major and trace element ratios and strontium isotopic ratios in river water: The Congo Basin case’, *Earth and Planetary Science Letters* **120**(1), 59–76.
- Neimark, A. V. (1990), ‘Calculating Surface Fractal Dimensions of Adsorbents’, *Adsorption Science & Technology* **7**(4), 210–219.
- Nesbitt, H. W., Fedo, C. M. & Young, G. M. (1997), ‘Quartz and Feldspar Stability, Steady and Non-steady-State Weathering, and Petrogenesis of Siliciclastic Sands and Muds’, *The Journal of Geology* **105**(2), 173–192.
- Nesbitt, H. W. & Young, G. M. (1982), ‘Early Proterozoic climates and plate motions inferred from major element chemistry of lutites’, *Nature* **299**(5885), 715–717.
- Newman, S., Macdougall, J. D. & Finkel, R. C. (1984), ‘<sup>230</sup>Th–<sup>238</sup>U disequilibrium in island arcs: Evidence from the Aleutians and the Marianas’, *Nature* **308**(5956), 268–270.
- Ortu, E., Peyron, O., Bordon, A., de Beaulieu, J. L., Siniscalco, C. & Caramiello, R. (2008), ‘Lateglacial and Holocene climate oscillations in the South-western Alps: An attempt at quantitative reconstruction’, *Quaternary International* **190**(1), 71–88.
- Osmond, J. K. & Ivanovich, M. (1992), ‘Uranium-series mobilization and surface hydrology’, *Uranium-series disequilibrium: applications to earth, marine, and environmental sciences. 2. ed.*
- Pabalan, R. T., Bertetti, F. P., Prikryl, J. D. & Turner, D. R. (1996), ‘Uranium (VI) sorption onto selected mineral surfaces: Key geochemical parameters’, (CONF-960376-).
- Palumbo, L., Hetzel, R., Tao, M. & Li, X. (2010), ‘Topographic and lithologic control on catchment-wide denudation rates derived from cosmogenic <sup>10</sup>Be in two mountain ranges at the margin of NE Tibet’, *Geomorphology* **117**(1), 130–142.
- Parsons, D. R., Best, J. L., Lane, S. N., Orfeo, O., Hardy, R. J. & Kostaschuk, R. (2007), ‘Form roughness and the absence of secondary flow in a large confluence–difffluence, Rio Paraná, Argentina’, *Earth Surface Processes and Landforms* **32**(1), 155–162.
- Patton, N. R., Lohse, K. A., Godsey, S. E., Crosby, B. T. & Seyfried, M. S. (2018), ‘Predicting soil thickness on soil mantled hillslopes’, *Nature Communications* **9**(1), 3329.

- Pedersen, V. K. & Egholm, D. L. (2013), 'Glaciations in response to climate variations preconditioned by evolving topography', *Nature* **493**(7431), 206–210.
- Peizhen, Z., Molnar, P. & Downs, W. R. (2001), 'Increased sedimentation rates and grain sizes 2–4 Myr ago due to the influence of climate change on erosion rates', *Nature* **410**(6831), 891–897.
- Pelletier, J. D. & Rasmussen, C. (2009), 'Geomorphically based predictive mapping of soil thickness in upland watersheds', *Water Resources Research* **45**(9).
- Pelt, E., Chabaux, F., Innocent, C., Navarre-Sitchler, A. K., Sak, P. B. & Brantley, S. L. (2008), 'Uranium–thorium chronometry of weathering rinds: Rock alteration rate and paleo-isotopic record of weathering fluids', *Earth and Planetary Science Letters* **276**(1), 98–105.
- Pelt, E., Chabaux, F., Stille, P., Innocent, C., Ghaleb, B., Gérard, M. & Guntzer, F. (2013), 'Atmospheric dust contribution to the budget of U-series nuclides in soils from the Mount Cameroon volcano', *Chemical Geology* **341**, 147–157.
- Phillips, C. B. & Jerolmack, D. J. (2016), 'Self-organization of river channels as a critical filter on climate signals', *Science* **352**(6286), 694–697.
- Phillips, J. (2003), 'Alluvial storage and the long-term stability of sediment yields', *Basin Research* **15**(2), 153–163.
- Piper, D. J. W. & Savoye, B. (1993), 'Processes of late Quaternary turbidity current flow and deposition on the Var deep-sea fan, north-west Mediterranean Sea', *Sedimentology* **40**(3), 557–582.
- Plater, A. J., Dugdale, R. E. & Ivanovich, M. (1988), 'The application of uranium series disequilibrium concepts to sediment yield determination', *Earth Surface Processes and Landforms* **13**(2), 171–182.
- Plater, A. J., Ivanovich, M. & Dugdale, R. E. (1992), 'Uranium series disequilibrium in river sediments and waters: The significance of anomalous activity ratios', *Applied Geochemistry* **7**(2), 101–110.
- Pogge von Strandmann, P. A. E., Burton, K. W., James, R. H., van Calsteren, P., Gíslason, S. R. & Mokadem, F. (2006), 'Riverine behaviour of uranium and lithium isotopes in an actively glaciated basaltic terrain', *Earth and Planetary Science Letters* **251**(1), 134–147.
- Porcelli, D., Andersson, P. S., Baskaran, M. & Wasserburg, G. J. (2001), 'Transport of U- and Th-series nuclides in a Baltic shield watershed and the Baltic sea', *Geochimica et Cosmochimica Acta* **65**(15), 2439–2459.

- Porcelli, D., Andersson, P. S., Wasserburg, G. J., Ingri, J. & Baskaran, M. (1997), 'The importance of colloids and mires for the transport of uranium isotopes through the Kalix River watershed and Baltic Sea', *Geochimica et Cosmochimica Acta* **61**(19), 4095–4113.
- Prentice, I. C., Sykes, M. T., Lautenschlager, M., Harrison, S. P., Denissenko, O. & Bartlein, P. J. (1993), 'Modelling Global Vegetation Patterns and Terrestrial Carbon Storage at the Last Glacial Maximum', *Global Ecology and Biogeography Letters* **3**(3), 67–76.
- Preston, N. & Schmidt, J. (2003), Modelling sediment fluxes at large spatial and temporal scales, *in* A. Lang, R. Dikau & K. Hennrich, eds, 'Long Term Hillslope and Fluvial System Modelling: Concepts and Case Studies from the Rhine River Catchment', Lecture Notes in Earth Sciences, Springer, Berlin, Heidelberg, pp. 53–72.
- Preusser, F., Geyh, M. A. & Schlüchter, C. (2003), 'Timing of Late Pleistocene climate change in lowland Switzerland', *Quaternary Science Reviews* **22**(14), 1435–1445.
- Rai, D. & Lindsay, W. L. (1975), 'A Thermodynamic Model for Predicting the Formation, Stability, and Weathering of Common Soil Minerals', *Soil Science Society of America Journal* **39**(5), 991–996.
- Railsback, L. B., Gibbard, P. L., Head, M. J., Voarintsoa, N. R. G. & Toucanne, S. (2015), 'An optimized scheme of lettered marine isotope substages for the last 1.0 million years, and the climatostratigraphic nature of isotope stages and substages', *Quaternary Science Reviews* **111**, 94–106.
- Ramstein, G., Kageyama, M., Guiot, J., Wu, H., Hély, C., Krinner, G. & Brewer, S. (2007), 'How cold was Europe at the Last Glacial Maximum? A synthesis of the progress achieved since the first PMIP model-data comparison', *Climate of the Past* **3**(2), 331–339.
- Rasmussen, S. O., Andersen, K. K., Svensson, A. M., Steffensen, J. P., Vinther, B. M., Clausen, H. B., Siggaard-Andersen, M.-L., Johnsen, S. J., Larsen, L. B., Dahl-Jensen, D., Bigler, M., Röthlisberger, R., Fischer, H., Goto-Azuma, K., Hansson, M. E. & Ruth, U. (2006), 'A new Greenland ice core chronology for the last glacial termination', *Journal of Geophysical Research: Atmospheres* **111**(D6).
- Raymo, M. E. & Ruddiman, W. F. (1992), 'Tectonic forcing of late Cenozoic climate.', *Nature* **359**(6391), 117–122.
- Reinhardt, L., Jerolmack, D., Cardinale, B. J., Vanacker, V. & Wright, J. (2010), 'Dynamic interactions of life and its landscape: Feedbacks at the interface of geomorphology and ecology', *Earth Surface Processes and Landforms* **35**(1), 78–101.

- Reitner, J. (2005), Quartärgeologie Und Landschaftsentwicklung Im Raum Kitzbühel – St. Johann i. T. – Hopfgarten (Nordtirol) Vom Riss Bis In Das Würm-Spätglazial (MIS 6-2), PhD thesis.
- Reneau, S. L. & Dietrich, W. E. (1991), ‘Erosion rates in the southern oregon coast range: Evidence for an equilibrium between hillslope erosion and sediment yield’, *Earth Surface Processes and Landforms* **16**(4), 307–322.
- Reneau, S. L., Dietrich, W. E., Rubin, M., Donahue, D. J. & Jull, A. J. T. (1989), ‘Analysis of Hillslope Erosion Rates Using Dated Colluvial Deposits’, *The Journal of Geology* **97**(1), 45–63.
- Retallack, G. (1984), ‘Completeness of the Rock and Fossil Record: Some Estimates Using Fossil Soils.’, *Paleobiology* **10**(1), 59–78.
- Ribes, A., Thao, S., Vautard, R., Dubuisson, B., Somot, S., Colin, J., Planton, S. & Soubeyroux, J.-M. (2019), ‘Observed increase in extreme daily rainfall in the French Mediterranean’, *Climate Dynamics* **52**(1), 1095–1114.
- Richter, D. D., Eppes, M.-C., Austin, J. C., Bacon, A. R., Billings, S. A., Brecheisen, Z., Ferguson, T. A., Markewitz, D., Pachon, J., Schroeder, P. A. & Wade, A. M. (2020), ‘Soil production and the soil geomorphology legacy of Grove Karl Gilbert’, *Soil Science Society of America Journal* **84**(1), 1–20.
- Richter, S. & Goldberg, S. A. (2003), ‘Improved techniques for high accuracy isotope ratio measurements of nuclear materials using thermal ionization mass spectrometry’, *International Journal of Mass Spectrometry* **229**(3), 181–197.
- Riebe, C. S., Kirchner, J. W. & Finkel, R. C. (2004), ‘Erosional and climatic effects on long-term chemical weathering rates in granitic landscapes spanning diverse climate regimes’, *Earth and Planetary Science Letters* **224**(3), 547–562.
- Riebe, C. S., Kirchner, J. W., Granger, D. E. & Finkel, R. C. (2001), ‘Strong tectonic and weak climatic control of long-term chemical weathering rates’, *Geology* **29**(6), 511–514.
- Riebe, C. S., Sklar, L. S., Lukens, C. E. & Shuster, D. L. (2015), ‘Climate and topography control the size and flux of sediment produced on steep mountain slopes’, *Proceedings of the National Academy of Sciences* **112**(51), 15574–15579.
- Rihs, S., Prunier, J., Thien, B., Lemarchand, D., Pierret, M.-C. & Chabaux, F. (2011), ‘Using short-lived nuclides of the U- and Th-series to probe the kinetics of colloid migration in forested soils’, *Geochimica et Cosmochimica Acta* **75**(23), 7707–7724.

- Riotte, J., Chabaux, F., Benedetti, M., Dia, A., Gérard, M., Boulègue, J. & Etamé, J. (2003), ‘Uranium colloidal transport and origin of the  $^{234}\text{U}$ – $^{238}\text{U}$  fractionation in surface waters: New insights from Mount Cameroon’, *Chemical Geology* **202**(3), 365–381.
- Robinson, L. F., Henderson, G. M., Hall, L. & Matthews, I. (2004), ‘Climatic Control of Riverine and Seawater Uranium-Isotope Ratios’, *Science* **305**(5685), 851–854.
- Roering, J. J., Kirchner, J. W. & Dietrich, W. E. (2001), ‘Hillslope evolution by nonlinear, slope-dependent transport: Steady state morphology and equilibrium adjustment timescales’, *Journal of Geophysical Research: Solid Earth* **106**(B8), 16499–16513.
- Roering, J. J., Marshall, J., Booth, A. M., Mort, M. & Jin, Q. (2010), ‘Evidence for biotic controls on topography and soil production’, *Earth and Planetary Science Letters* **298**(1), 183–190.
- Romans, B. W., Castelltort, S., Covault, J. A., Fildani, A. & Walsh, J. P. (2016), ‘Environmental signal propagation in sedimentary systems across timescales’, *Earth-Science Reviews* **153**, 7–29.
- Rosholt, J. N. (1983), ‘Isotopic composition of uranium and thorium in crystalline rocks’, *Journal of Geophysical Research: Solid Earth* **88**(B9), 7315–7330.
- Rosholt, J. N., Doe, B. R. & Tatsumoto, M. (1966), ‘Evolution of the Isotopic Composition of Uranium and Thorium in Soil Profiles’, *GSA Bulletin* **77**(9), 987–1004.
- Rothacker, L., Dosseto, A., Francke, A., Chivas, A. R., Vigier, N., Kotarba-Morley, A. M. & Menozzi, D. (2018), ‘Impact of climate change and human activity on soil landscapes over the past 12,300 years’, *Scientific Reports* **8**(1), 247.
- Rouire, J., Autran, A., Prost, A., Rossi, J. & Rosset, C. (1980), ‘Carte géologique de la France à 1/250 000, feuille de Nice (40)’.  
*Carte géologique de la France*, 1/250 000, feuille de Nice (40).
- Ruddiman, W. F. (2001), ‘Earth’s climate: Past and future.’, *Macmillan* .
- Russell, R. D. (1955), ‘Effects of Transportation on Sedimentary Particles’.
- Sage, L. (1976), *La Sédimentation à l’embouchure d’un Fleuve Cotier Méditerranéen: Le Var*.
- Sánchez Goñi, M., Cacho, I., Turon, J., Guiot, J., Sierro, F., Peypouquet, J., Grimalt, J. & Shackleton, N. (2002), ‘Synchronicity between marine and terrestrial responses to millennial scale climatic variability during the last glacial period in the Mediterranean region’, *Climate Dynamics* **19**(1), 95–105.

- Sanchez Goni, M. F. & Harrison, S. P. (2010), 'Millennial-scale climate variability and vegetation changes during the last glacial: Concepts and terminology', *Quaternary Science Reviews* **29**(21-22), 2823–2827.
- Sandercock, P. J. & Hooke, J. M. (2011), 'Vegetation effects on sediment connectivity and processes in an ephemeral channel in SE Spain', *Journal of Arid Environments* **75**(3), 239–254.
- Sarin, M. M., Krishnaswami, S., Somayajulu, B. L. K. & Moore, W. S. (1990), 'Chemistry of uranium, thorium, and radium isotopes in the Ganga-Brahmaputra river system: Weathering processes and fluxes to the Bay of Bengal', *Geochimica et Cosmochimica Acta* **54**(5), 1387–1396.
- Sarnthein, M. (1978), 'Sand deserts during glacial maximum and climatic optimum', *Nature* **272**(5648), 43–46.
- Schluechter, C., Maisch, M., Suter, J., Fitze, P., Keller, W. A., Burga, C. & Wynistorf, E. (1987), 'Das Schieferkohlenprofil von Gossau (Kt. Zürich) und seine stratigraphische Stellung innerhalb der letzten Eiszeit', [/paper/Das-Schieferkohlenprofil-von-Gossau-\(Kt.-Z%C3%BCrich\)-Schluechter-Maisch/1b78ee7517dc81e9be224c3ff512113d523a2302](#).
- Schoeneich, P. (1998), 'Corrélation du dernier maximum glaciaire et de la déglaciation alpine avec l'enregistrement isotopique du Groenland [Correlation of the alpine LGM and déglaciation with the Greenland isotopic record.]', *Quaternaire* **9**(3), 203–215.
- Schumm, S. A. (1977), *The Fluvial System*, Vol. 338, Wiley, New York.
- Selby, M. J. (1993), *Hillslope Materials and Processes*, Oxford University Press.
- Semkow, T. M. (1991), 'Fractal model of radon emanation from solids', *Physical Review Letters* **66**(23), 3012–3015.
- Shangguan, W., Hengl, T., de Jesus, J. M., Yuan, H. & Dai, Y. (2017), 'Mapping the global depth to bedrock for land surface modeling', *Journal of Advances in Modeling Earth Systems* **9**(1), 65–88.
- Sharp, W. D., Ludwig, K. R., Chadwick, O. A., Amundson, R. & Glaser, L. L. (2003), 'Dating fluvial terraces by  $^{230}\text{Th}/\text{U}$  on pedogenic carbonate, Wind River Basin, Wyoming', *Quaternary Research* **59**(2), 139–150.
- Siddall, M., Rohling, E. J., Almogi-Labin, A., Hemleben, C., Meischner, D., Schmelzer, I. & Smeed, D. A. (2003), 'Sea-level fluctuations during the last glacial cycle', *Nature* **423**(6942), 853–858.

- Simpson, G. & Castelltort, S. (2012), 'Model shows that rivers transmit high-frequency climate cycles to the sedimentary record', *Geology* **40**(12), 1131–1134.
- Sims, K. W. W., Gill, J. B., Dosseto, A., Hoffmann, D. L., Lundstrom, C. C., Williams, R. W., Ball, L., Tollstrup, D., Turner, S., Prytulak, J., Glessner, J. J. G., Standish, J. J. & Elliott, T. (2008), 'An Inter-Laboratory Assessment of the Thorium Isotopic Composition of Synthetic and Rock Reference Materials', *Geostandards and Geoanalytical Research* **32**(1), 65–91.
- Sims, R., Lawless, T. A., Alexander, J. L., Bennett, D. G. & Read, D. (1996), 'Uranium migration through intact sandstone: Effect of pollutant concentration and the reversibility of uptake', *Journal of Contaminant Hydrology* **21**(1), 215–228.
- Sing, K. S. W. (1985), 'Reporting physisorption data for gas/solid systems with special reference to the determination of surface area and porosity (Recommendations 1984)', *Pure and Applied Chemistry* **57**(4), 603–619.
- Slaymaker, O. (2003), 'The sediment budget as conceptual framework and management tool', *Hydrobiologia* (494), 71–82.
- Small, E. E., Anderson, R. S. & Hancock, G. S. (1999), 'Estimates of the rate of regolith production using  $^{10}\text{Be}$  and  $^{26}\text{Al}$  from an alpine hillslope', *Geomorphology* **27**(1), 131–150.
- Sømme, T. O., Helland-Hansen, W., Martinsen, O. J. & Thurmond, J. B. (2009), 'Relationships between morphological and sedimentological parameters in source-to-sink systems: A basis for predicting semi-quantitative characteristics in subsurface systems', *Basin Research* **21**(4), 361–387.
- Spötl, C., Holzkämper, S. & Mangini, A. (2007), 31. The last and the penultimate interglacial as recorded by speleothems from a climatically sensitive high-elevation cave site in the alps, *in* F. Sirocko, M. Claussen, M. F. Sánchez Goñi & T. Litt, eds, 'Developments in Quaternary Sciences', Vol. 7 of *The Climate of Past Interglacials*, Elsevier, pp. 471–491.
- Stallard, R. F. (1985), River Chemistry, Geology, Geomorphology, and Soils in the Amazon and Orinoco Basins, *in* J. I. Drever, ed., 'The Chemistry of Weathering', Nato ASI Series, Springer Netherlands, Dordrecht, pp. 293–316.
- Stallard, R. F. (1988), Weathering and Erosion in the Humid Tropics, *in* A. Lerman & M. Meybeck, eds, 'Physical and Chemical Weathering in Geochemical Cycles', NATO ASI Series, Springer Netherlands, Dordrecht, pp. 225–246.

- Stallard, R. F. & Edmond, J. M. (1983), 'Geochemistry of the Amazon: 2. The influence of geology and weathering environment on the dissolved load', *Journal of Geophysical Research: Oceans* **88**(C14), 9671–9688.
- Steiger, R. H. & Jager, E. (1978), 'Subcommission on Geochronology: Convention on the Use of Decay Constants in Geochronology and Cosmochronology', **116**, 67–71.
- Stocker, T. F. & Schmittner, A. (1997), 'Influence of CO<sub>2</sub> emission rates on the stability of the thermohaline circulation', *Nature* **388**(6645), 862–865.
- Suchet, P. A., Probst, J.-L. & Ludwig, W. (2003), 'Worldwide distribution of continental rock lithology: Implications for the atmospheric/soil CO<sub>2</sub> uptake by continental weathering and alkalinity river transport to the oceans', *Global Biogeochemical Cycles* **17**(2).
- Summerfield, M. A. & Hulton, N. J. (1994), 'Natural controls of fluvial denudation rates in major world drainage basins', *Journal of Geophysical Research: Solid Earth* **99**(B7), 13871–13883.
- Suresh, P. O., Dosseto, A., Handley, H. K. & Hesse, P. P. (2014), 'Assessment of a sequential phase extraction procedure for uranium-series isotope analysis of soils and sediments', *Applied Radiation and Isotopes* **83**, 47–55.
- Suresh, P. O., Dosseto, A., Hesse, P. P. & Handley, H. K. (2013), 'Soil formation rates determined from Uranium-series isotope disequilibria in soil profiles from the southeastern Australian highlands', *Earth and Planetary Science Letters* **379**, 26–37.
- Svensson, A., Andersen, K. K., Bigler, M., Clausen, H. B., Dahl-Jensen, D., Davies, S. M., Johnsen, S. J., Muscheler, R., Rasmussen, S. O., Röthlisberger, R., Peder Steffensen, J. & Vinther, B. M. (2006), 'The Greenland Ice Core Chronology 2005, 15–42ka. Part 2: Comparison to other records', *Quaternary Science Reviews* **25**(23), 3258–3267.
- Swift, D. A., Nienow, P. W., Spedding, N. & Hoey, T. B. (2002), 'Geomorphic implications of subglacial drainage configuration: Rates of basal sediment evacuation controlled by seasonal drainage system evolution', *Sedimentary Geology* **149**(1), 5–19.
- Syvitski, J. P. M. & Kettner, A. (2011), 'Sediment flux and the Anthropocene', *Philosophical Transactions of the Royal Society A: Mathematical, Physical and Engineering Sciences* **369**(1938), 957–975.
- Syvitski, J. P. M., Kettner, A. J., Correggiari, A. & Nelson, B. W. (2005), 'Distributary channels and their impact on sediment dispersal', *Marine Geology* **222–223**, 75–94.

- Syvitski, J. P. M. & Milliman, J. D. (2007), 'Geology, Geography, and Humans Battle for Dominance over the Delivery of Fluvial Sediment to the Coastal Ocean', *The Journal of Geology* **115**(1), 1–19.
- Syvitski, J. P. M., Peckham, S. D., Hilberman, R. & Mulder, T. (2003), 'Predicting the terrestrial flux of sediment to the global ocean: A planetary perspective', *Sedimentary Geology* **162**(1), 5–24.
- Syvitski, J. P. M. & Saito, Y. (2007), 'Morphodynamics of deltas under the influence of humans', *Global and Planetary Change* **57**(3), 261–282.
- Taylor, S. R. & McLennan, S. M. (1995), 'The geochemical evolution of the continental crust', *Reviews of Geophysics* **33**(2), 241–265.
- Thollon, M., Bayon, G., Toucanne, S., Trinquier, A., Germain, Y. & Dosseto, A. (2020), 'The distribution of ( $^{234}\text{U}/^{238}\text{U}$ ) activity ratios in river sediments', *Geochimica et Cosmochimica Acta* **290**, 216–234.
- Tinner, W. & Kaltenrieder, P. (2005), 'Rapid responses of high-mountain vegetation to early Holocene environmental changes in the Swiss Alps'.
- Tofelde, S., Savi, S., Wickert, A. D., Bufe, A. & Schildgen, T. F. (2019), 'Alluvial channel response to environmental perturbations: Fill-terrace formation and sediment-signal disruption', *Earth Surface Dynamics* **7**(2), 609–631.
- Trimble, S. W. (1983), 'A sediment budget for Coon Creek basin in the Driftless Area, Wisconsin, 1853-1977', *American Journal of Science* **283**(5), 454–474.
- Tucker, G. E. & Slingerland, R. (1997), 'Drainage basin responses to climate change', *Water Resources Research* **33**(8), 2031–2047.
- Turnbull, L., Wainwright, J. & Brazier, R. E. (2008), 'A conceptual framework for understanding semi-arid land degradation: Ecohydrological interactions across multiple-space and time scales', *Ecohydrology* **1**(1), 23–34.
- Vail, P. R., Jr, R. M. M. & Iii, S. T. (1977), 'Seismic Stratigraphy and Global Changes of Sea Level: Part 4. Global Cycles of Relative Changes of Sea Level.: Section 2. Application of Seismic Reflection Configuration to Stratigraphic Interpretation', **165**, 83–97.
- van Breemen, N. & Buurman, P. (2002), *Soil Formation*, Springer Science & Business Media.
- Van der Zwan, C. J. (2002), 'The impact of Milankovitch-scale climatic forcing on sediment supply', *Sedimentary Geology* **147**(3), 271–294.

- Vanacker, V., Bellin, N., Molina, A. & Kubik, P. W. (2014), ‘Erosion regulation as a function of human disturbances to vegetation cover: A conceptual model’, *Landscape Ecology* **29**(2), 293–309.
- Vance, D., Teagle, D. A. H. & Foster, G. L. (2009), ‘Variable Quaternary chemical weathering fluxes and imbalances in marine geochemical budgets’, *Nature* **458**(7237), 493–496.
- Vigier, N., Bourdon, B., Lewin, E., Dupré, B., Turner, S., Chakrapani, G. J., van Calsteren, P. & Allègre, C. J. (2005), ‘Mobility of U-series nuclides during basalt weathering: An example from the Deccan Traps (India)’, *Chemical Geology* **219**(1), 69–91.
- Vigier, N., Bourdon, B., Turner, S. & Allègre, C. J. (2001), ‘Erosion timescales derived from U-decay series measurements in rivers’, *Earth and Planetary Science Letters* **193**(3), 549–563.
- Vigier, N., Burton, K. W., Gislason, S. R., Rogers, N. W., Duchene, S., Thomas, L., Hodge, E. & Schaefer, B. (2006), ‘The relationship between riverine U-series disequilibria and erosion rates in a basaltic terrain’, *Earth and Planetary Science Letters* **249**(3), 258–273.
- von Blanckenburg, F. (2006), ‘The control mechanisms of erosion and weathering at basin scale from cosmogenic nuclides in river sediment’, *Earth and Planetary Science Letters* **242**(3), 224–239.
- von Blanckenburg, F., Bouchez, J., Ibarra, D. E. & Maher, K. (2015), ‘Stable runoff and weathering fluxes into the oceans over Quaternary climate cycles’, *Nature Geoscience* **8**(7), 538–542.
- von Eynatten, H. & Dunkl, I. (2012), ‘Assessing the sediment factory: The role of single grain analysis’, *Earth-Science Reviews* **115**(1), 97–120.
- Walker, J. C. G., Hays, P. B. & Kasting, J. F. (1981), ‘A negative feedback mechanism for the long-term stabilization of Earth’s surface temperature’, *Journal of Geophysical Research: Oceans* **86**(C10), 9776–9782.
- Walling, D. E. & Webb, B. (1996), *Erosion and Sediment Yield: Global and Regional Perspectives : Proceedings of an International Symposium Held at Exeter, UK, from 15 to 19 July 1996*, IAHS.
- Wanner, H., Beer, J., Bütikofer, J., Crowley, T. J., Cubasch, U., Flückiger, J., Goosse, H., Grosjean, M., Joos, F., Kaplan, J. O., Küttel, M., Müller, S. A., Prentice, I. C., Solomina, O., Stocker, T. F., Tarasov, P., Wagner, M. & Widmann, M. (2008), ‘Mid- to Late Holocene climate change: An overview’, *Quaternary Science Reviews* **27**(19), 1791–1828.

- Watkins, S. E., Whittaker, A. C., Bell, R. E., McNeill, L. C., Gawthorpe, R. L., Brooke, S. A. & Nixon, C. W. (2019), 'Are landscapes buffered to high-frequency climate change? A comparison of sediment fluxes and depositional volumes in the Corinth Rift, central Greece, over the past 130 k.y.', *GSA Bulletin* **131**(3-4), 372–388.
- Weltje, G. J. & von Eynatten, H. (2004), 'Quantitative provenance analysis of sediments: Review and outlook', *Sedimentary Geology* **171**(1), 1–11.
- West, A. J. (2012), 'Thickness of the chemical weathering zone and implications for erosional and climatic drivers of weathering and for carbon-cycle feedbacks', *Geology* **40**(9), 811–814.
- West, A. J., Galy, A. & Bickle, M. (2005), 'Tectonic and climatic controls on silicate weathering', *Earth and Planetary Science Letters* **235**(1), 211–228.
- West, A. J., Hetzel, R., Li, G., Jin, Z., Zhang, F., Hilton, R. G. & Densmore, A. L. (2014), 'Dilution of  $^{10}\text{Be}$  in detrital quartz by earthquake-induced landslides: Implications for determining denudation rates and potential to provide insights into landslide sediment dynamics', *Earth and Planetary Science Letters* **396**, 143–153.
- Whipple, K. X. & Tucker, G. E. (1999), 'Dynamics of the stream-power river incision model: Implications for height limits of mountain ranges, landscape response timescales, and research needs', *Journal of Geophysical Research: Solid Earth* **104**(B8), 17661–17674.
- Whitchurch, A. L., Carter, A., Sinclair, H. D., Duller, R. A., Whittaker, A. C. & Allen, P. A. (2011), 'Sediment routing system evolution within a diachronously uplifting orogen: Insights from detrital zircon thermochronological analyses from the South-Central Pyrenees', *American Journal of Science* **311**(5), 442–482.
- White, A. F. & Blum, A. (1995), Effects of climate on chemical weathering in watersheds.
- Wiel, M. J. V. D. & Coulthard, T. J. (2010), 'Self-organized criticality in river basins: Challenging sedimentary records of environmental change', *Geology* **38**(1), 87–90.
- Wilkinson, B. H. & McElroy, B. J. (2007), 'The impact of humans on continental erosion and sedimentation', *GSA Bulletin* **119**(1-2), 140–156.
- Wilkinson, M. T., Chappell, J., Humphreys, G. S., Fifield, K., Smith, B. & Hesse, P. (2005), 'Soil production in heath and forest, Blue Mountains, Australia: Influence of lithology and palaeoclimate', *Earth Surface Processes and Landforms* **30**(8), 923–934.
- Willenbring, J. K. & Jerolmack, D. J. (2016), 'The null hypothesis: Globally steady rates of erosion, weathering fluxes and shelf sediment accumulation during Late Cenozoic mountain uplift and glaciation', *Terra Nova* **28**(1), 11–18.

- Willgoose, G., Bras, R. L. & Rodriguez-Iturbe, I. (2008), 'A physical explanation of an observed link area-slope relationship', *Water Resources Research* pp. 1697–1702.
- Williams, R. W. & Gill, J. B. (1989), 'Effects of partial melting on the uranium decay series', *Geochimica et Cosmochimica Acta* **53**(7), 1607–1619.
- Wittmann, H., von Blanckenburg, F., Guyot, J. L., Maurice, L. & Kubik, P. W. (2009), 'From source to sink: Preserving the cosmogenic  $^{10}\text{Be}$ -derived denudation rate signal of the Bolivian Andes in sediment of the Beni and Mamoré foreland basins', *Earth and Planetary Science Letters* **288**(3), 463–474.
- Woerther, P. (2008), 'ESSCAR-9 cruise, Le Suroît R/V'.
- Wu, H., Guiot, J., Brewer, S. & Guo, Z. (2007), 'Climatic changes in Eurasia and Africa at the last glacial maximum and mid-Holocene: Reconstruction from pollen data using inverse vegetation modelling', *Climate Dynamics* **29**(2), 211–229.
- Yang, H. F., Yang, S. L., Xu, K. H., Milliman, J. D., Wang, H., Yang, Z., Chen, Z. & Zhang, C. Y. (2018), 'Human impacts on sediment in the Yangtze River: A review and new perspectives', *Global and Planetary Change* **162**, 8–17.
- Yokoyama, Y., Lambeck, K., De Deckker, P., Johnston, P. & Fifield, L. K. (2000), 'Timing of the Last Glacial Maximum from observed sea-level minima', *Nature* **406**(6797), 713–716.
- Yoo, K. & Mudd, S. M. (2008), 'Toward process-based modeling of geochemical soil formation across diverse landforms: A new mathematical framework', *Geoderma* **146**(1), 248–260.
- Zanchetta, G., Drysdale, R. N., Hellstrom, J. C., Fallick, A. E., Isola, I., Gagan, M. K. & Pareschi, M. T. (2007), 'Enhanced rainfall in the Western Mediterranean during deposition of sapropel S1: Stalagmite evidence from Corchia cave (Central Italy)', *Quaternary Science Reviews* **26**(3), 279–286.



**Titre : Evolution des temps de transfert sédimentaire océan-continent au regard de la variabilité climatique quaternaire : Apports des isotopes de l'Uranium.**

**Mots clés :** Rapport d'activité de l'uranium, érosion, temps de résidence, variation climatique.

**Résumé :** Comprendre les liens qui lient érosion continentale et variations climatiques est un enjeu majeur pour appréhender l'évolution des paysages et des flux sédimentaires à l'océan, en particulier dans le contexte actuel de réchauffement global. Dans ce but, le présent travail s'est focalisé sur la reconstruction des variations des temps de résidence sédimentaire qui permettent, par extension, d'évaluer les variations de l'érosion dans les systèmes continentaux. Ces temps de résidences sont estimés à partir du rapport d'activité de l'uranium ( $^{234}\text{U}/^{238}\text{U}$ ). Premièrement, les rapports ( $^{234}\text{U}/^{238}\text{U}$ ) ont été mesurés dans des sédiments de rivières mondiales afin d'améliorer la compréhension de l'outil au regard des paramètres environnementaux. Cette approche a montré que seul l'approche multi-paramètres en le climat, l'altération et la morphologie permet d'estimer convenablement le ratio ( $^{234}\text{U}/^{238}\text{U}$ ), témoignant de son évolution en fonction des interactions environnementales.

Ensuite, la variabilité spatiale du temps de résidence sédimentaire au sein d'un unique bassin versant (Var, France) a été étudiée. Des temps de résidence rapide sont obtenus pour les sous-bassins au régime d'altération dit limité par l'altération alors que les sous-bassins au régime d'altération dit limité par le transport montrent des temps de résidence plus long. Enfin, la variation temporelle du temps de résidence sédimentaires du système Var a été reconstruite pour les 75 000 dernières années. En complément d'une variation du temps de résidence sédimentaire glaciaire-interglaciaire, expliquée par les fluctuations des glaciers alpins qui favorisent l'érosion, une seconde et plus fine cyclicité glaciaire a été identifiée à l'échelle millénaire. Ces variations de temps de résidence sédimentaire ont été attribuées à l'évolution rapide de la couverture végétale pendant les variations climatiques relatives à la variabilité climatique dite de Dansgaard-Oeschger.

**Title: Uranium isotopes as proxies for investigating land-to-sea sediment transfer response to Late Quaternary climate changes**

**Keywords:** Uranium activity ratio, erosion, residence time, climate change.

**Abstract:** Studying how catchment erosion has responded to past climate change can help us better understand not only how landscape evolution and source-to-sink processes operate, but also predict the consequences of future climate change on soil resource availability and sediment discharge to the ocean. In this context, the aim of this PhD was to focus on the sediment residence times variation to assess past erosion as a function of climatic variations. The sediment residence times are calculated based on the uranium activity ratio ( $^{234}\text{U}/^{238}\text{U}$ ). First, ( $^{234}\text{U}/^{238}\text{U}$ ) was determined in a numerous of world rivers sediments improve the comprehension of this ratio depending on environmental parameters. Only a multi-parameters approach can properly predict the ( $^{234}\text{U}/^{238}\text{U}$ ) in sediments, attesting the possibility to use ( $^{234}\text{U}/^{238}\text{U}$ ) to study environmental interactions

within the basin. Then, the spatial variability of sediment residence times was studied inside a mountainous catchment (Var, France). Low sediment residence times have been obtained for the sub-catchments considered as transport-limited, while the longer sediment residence times were found in sediments from weathering limited sub-catchments. Finally, the temporal variation of sediment residence times over the last 75,000 years was studied. It revealed a variation of sediment residence times between glacial and interglacial period, which can be explain by the presence of LGM glaciers in the Alps, enhancing the erosion. A second and finest cyclicity of sediment residence times was identified on a millennium scale during the last glacial period following the Bond cycle. These sediment residence times variations were attributed to the rapid evolution of the vegetation cover during the so-called Dansgaard-Oeschger climatic variability.